2022-12-01

Reprocessing Groundwater Resistivity Surveys In The Lower Mesilla Basin, New Mexico, And Texas

Leslie Bernal
University of Texas at El Paso

REPROCESSING GROUNDWATER RESISTIVITY SURVEYS IN THE LOWER MESILLA BASIN, NEW MEXICO, AND TEXAS

LESLIE ALEJANDRA BERNAL LOPEZ

Master's Program in Geophysics

APPROVED:

Diane I. Doser, Ph.D., Co-Chair

Marianne Karplus, Ph.D. Co-Chair

Aaron A. Velasco, Ph.D.

Ivonne Santiago, Ph.D., P.E.

Stephen L. Crites, Jr., Ph.D.
Dean of the Graduate School

Dedication

To my grandparents, and only parents I had, Mariano Bernal, and Antonia Lopez. Thank you.

REPROCESSING GROUNDWATER RESISTIVITY SURVEYS IN THE LOWER MESILLA BASIN, NEW MEXICO, AND TEXAS

by

LESLIE ALEJANDRA BERNAL LOPEZ, B.S.

THESIS

Presented to the Faculty of the Graduate School of

The University of Texas at El Paso

in Partial Fulfillment

of the Requirements

for the Degree of

MASTER OF SCIENCE

Department of Earth, Environmental and Resource Sciences

THE UNIVERSITY OF TEXAS AT EL PASO

December, 2022

Acknowledgments

This work would not have been done without the help of my advisor, Dr. Diane Doser. Thank you for your help and understanding, and for believing in me even after going through life-changing situations. You were always there giving me your support and I will never forget that. I would also like to thank all my professors and the Geology Department staff, including Dr. Kubicki, for being an amazing team, and encouraging me to keep going because quitting was never an option. I would like to thank Dr. Velasco for his advice and sometimes for just listening to my concerns, which will always be appreciated. And I especially need to thank Annette Veilleux, because she has been extremely nice and helpful since the beginning, when everything was new to me, and always offered me her help when I needed it the most. Thanks to Carlos Montana for always being available to help me out with "computer stuff". And of course, I need to thank my friends Manuel Moncada and Juan Ochoa for convincing me to join the program and for helping me to adapt to life in a new country. Thank you to UTEP for giving me the support and resources I needed to complete this program. Thank you to CONACYT and ConTEX, for the scholarship awarded which has been extremely helpful to continue my studies. And finally, thank you to my fiancée, Eric Staib, for always believing in me, being there, and supporting me no matter what.

Abstract

The Mesilla Basin is part of the Rio Grande Basin System. Its northern boundary is defined by the Doña Ana Mountains in New Mexico and to the south by Sierra San Blas, Sierra Almirez, and Sierra La Candelaria in Mexico, where the basin changes its name to Conejos-Médanos. It supplies water for irrigation and public use to the cities of Las Cruces, NM, El Paso, TX, and Ciudad Juárez, Mexico. The southern part of the basin in the U.S. territory, known as the Lower Mesilla Basin, is bounded to the east by the Franklin Mountains, to the west by the Potrillo Mountains, and to the south by the international border. In 1973 the U.S. Geological Survey (USGS) made a series of resistivity soundings to estimate and delineate the portion of the basin containing fresh groundwater. They used automated software to obtain results, but no interpretation was made. In 1996, the soundings were re-interpreted as part of a different research project that produced profiles that fit the observed data; however, these profiles do not fit the known geological features of the area. The cross-sections presented have low resistivity values (3 to 10 ohm-m), at depths within the bedrock that would require bedrock porosities of over 30%. These results are concerning since other studies use this data as part of an analysis of how fast fresh groundwater is being depleted within the basin. This thesis reprocesses the 1973 resistivity sounding data using available water well logs, geologic cross-sections, and gravity modeling studies to help develop subsurface resistivity models consistent with geologic information. This study was able to identify some of the issues present in previous interpretations: (1) the attempt to match soundings at depths beyond resolution of electrode spacing; (2) in soundings located close to rock bodies, extremely high resistivities caused the electrical current to flow sideways rather than deeper into the ground as sounding spacing was increased; (3) there are several topographic changes and fault systems affecting some of the soundings that can cause lateral (2-D) anomalies. These issues were found to explain why low resistivity values were present in some sounding interpretations at depths where low values are not likely. Correcting them gives us a more confident interpretation.

Table of Contents

List of Tables

List of Figures

Chapter 1: Introduction

The cities of El Paso, TX, and Ciudad Juárez, Mexico, located in the Chihuahuan Desert, have been dealing with water scarcity plus population growth for the last 30 years. Despite being next to the Rio Grande and having access to two aquifers, the Hueco Bolson and the Mesilla Basin (Figure 1), the region has a history of drought and water supply problems. For instance, the Rio Grande water is only available in the summer and 75% of it goes to agriculture (International Boundary and Water Commission, n.d.). As a result, for nearly a century the Hueco Bolson has been the major source of drinking water for both cities (Chavez, 2000) (Figure 2). A dramatic increase in population in the last 40 years (Table 1) has caused problems such as large drops in groundwater level, deterioration of water quality due to intrusion of brackish water, and land subsidence (Sheng, 2013).

Table 1. Population growth in the last 40 years.

City	1980	2020	% Increase
El Paso	425,259 [1]	649,275 [2]	59.6%
Ciudad Juárez	678,815 [1]	1,512,450 [3]	132.9%

Source: 1. Chavez (2000), 2. U.S. Census Bureau (2020), 3. SCITEL INEGI (2020).

As a consequence, the Hueco Bolson has been widely studied through the years, and in 1991, an aggressive conservation plan was implemented by El Paso Water authorities. This plan adopted practices such as water restriction times, rates where the price increases as water consumption increases, aquifer recharge (only for the Hueco Bolson), wastewater management, educational programs for the population, and a redistribution of the water production (Figure 3), among others (El Paso Water, 2019). The Hueco Bolson contains a large amount of brackish water that was unusable, but after the creation of the Kay Bailey Hutchison (KBH) Desalination

Plant, the largest inland desalination plant in the world, this water gets filtered, creating a new supply of 27.5 million gallons of fresh water per day (El Paso Water, 2018a). This is one of the most successful projects from the conservation plan, which has already yielded results. Figure 4 shows how the water consumption per capita has decreased by 42% from 1977 to 2017 (El Paso Water, 2019), and Figure 5 reflects how the water levels in the Hueco Bolson are recovering (Bruun et al., 2016) after the production dropped down from 80,000 acre-feet per year in the 1980s to 40,000 acre-feet per year in 2010 (El Paso Water, 2018b).

The Mesilla Basin provides a smaller percentage of water for Texas and Mexico due to its location and size. It is bounded to the north by the Doña Ana Mountains, to the east by the Franklin Mountains, to the west by the Potrillo Mountains, and to the south by Sierra San Blas, Sierra Almirez, and Sierra La Candelaria. The southern part of the basin in the U.S. territory is known as the Lower Mesilla Basin and is bounded to the south by the international border. The portion of the Lower Mesilla Basin next to the river is called the Lower Mesilla Valley and is the primary region of study of this thesis (Figure 6). Only a small portion of this aquifer is located within Texas limits. The Canutillo well field is located within this area and is the one that provides water from the Mesilla Basin to the city of El Paso. The highest percentage of groundwater extraction from this aquifer in the United States occurs in the city of Las Cruces, NM, and on a smaller scale, from farms within the state. The situation for Mexico is problematic; the aquifer is located 40 km west of Ciudad Juárez, with the Sierra de Juárez located in between. In 2006, the city of Juárez built the Conejos-Médanos aqueduct, a piping project designed to bring water to the city across the mountains. In 2010, Ciudad Juárez began draining about 24 million cubic meters of water annually from the Mesilla Basin, almost as much as the 27 million cubic meters Las Cruces consumes on an annual basis (Villagran, 2017a). This change is

reflected by the depletion of water wells on local farms in New Mexico with farmers along the border needing to drill deeper for water (Villagran, 2017b).

Another dilemma for the Lower Mesilla Basin is brackish water. As a shallow aquifer, it contains a larger percentage of dissolved solids when compared to the Hueco Bolson. Water-rock interactions with intrusive bodies such as Cristo Rey, and limestones from the western Franklin Mountains foothills, are the main cause of this problem (Hawley and Lozinsky, 1992). The variations in bedrock type and depth and water salinity make the aquifer hard to map.

To better understand the Lower Mesilla aquifer structure, a resistivity survey was conducted by Zohdy et al. (1976) from the United States Geological Survey (USGS) in cooperation with the Texas Water Development Board (Figure 7). Preliminary modeling of these data was conducted by Zohdy et al. (1976) but no geological or hydrological interpretations were made. In 1996 Al-Garni re-processed the 65 Schlumberger resistivity soundings using updated software, and as a result, he obtained 6 cross-sections and 8 color maps. Al-Garni did not relate the new results to other available geological, hydrological or geophysical constraints (e.g., well cuttings, water well levels well logs, gravity data). The original Schlumberger sounding curves are described as of "good quality" by Al-Garni, with only a few of them being affected by lateral geologic inhomogeneities and man-made objects. According to Zohdy et al. (1994), the only way to fit soundings affected by inhomogeneities, is to create a 2-D horizontally layered model. And, in the case of measurements severely distorted by man-made objects, the best option is to discard them from the survey. Although Al-Garni identified a few bad-quality soundings, he processed them in the same manner as the good-quality ones, making no changes.

When creating the cross-sections, Al-Garni proposed a relationship between resistivity values and material compositions, summarized in Table 2.

Table 2. Resistivity interpretations (Al-Garni, 1996).

Resistivity values (Ωm)	Proposed materials
150 - 300 Ωm	Dry alluvial fan deposits of sand, gravel, and cobbles.
70 - 150 Ωm	Sedimentary deposits of coarse sand and gravel saturated with fresh water.
30 - 70 Ωm	Basin fill deposits composed of sand and gravel mixed with some clay and probably saturated with fresh water.
10 - 30 Ωm	Sedimentary deposits with a medium percentage of clay mixed with sand and gravel and saturated with fresh water.
3 - 10 Ωm	Sedimentary deposits with a very high percentage of clay saturated with fresh water or sand and gravel deposits saturated with brackish to saline water.

While these resistivity values for materials are reasonable, there are a few things to consider:

1) Resistivity values larger than 300 Ωm were not noted in his models, although the basin's basement is composed of low porosity igneous and sedimentary rocks that should have resistivities higher than 300 Ωm. A good example of a sedimentary rock found in the Mesilla Basin is limestone. The estimated resistivity value for a fractured limestone with 11% water saturation is around 600 Ωm (Telford et al., 1990). Besides the basin basement, there are a few soundings located at the foot of the Franklin Mountains, that should also have limestone close to the surface.
2) According to water well records (e.g., Hawley and Kennedy, 2004) and gravity modeling (Hiebing et al., 2018), the maximum depth to bedrock in the study area is around 320 m. Below that point, fractured igneous and sedimentary rocks are found.

The resistivity values assigned to these rocks by Al-Garni (3 to 10 Ωm) are substantially below expected values for bedrock at this depth.

3) The resistivity cross-sections show resolution of structure to maximum depths of 500 to 1000 m. In general, the depth of penetration for resistivity soundings is 1/3 to 1/5 of the current electrode spacing (Bernard, 2003). For the 1 km current electrode spacings used in this study, this would give a penetration depth of only about 200 to 300 m.
4) Only one of the interpretations (see Table 2), includes the possibility of brackish water. This portion of the basin is primarily replenished by underflow from local sources that are predominantly brackish (Hawley, 2016).
5) Some of the soundings cross features like fault zones or changes in surface topography and the 1-D assumptions used in the interpretations are likely not valid for these soundings.

Taking these observations into account, we concluded that this survey needs to be reprocessed based on the geophysical, geochemical, and hydrological information that has been gathered in the last 26 years.

For this thesis, I will analyze the soundings using different software developed by Baker (2019). The main advantage of using this software is that it allows results to be adjusted/constrained by water well data. Thus higher resistivity values can be assigned to the deepest layers (bedrock) that reflect the known geology of the basin.

GEOLOGIC SETTING

The sediments and groundwater geochemistry of the southern Mesilla Basin are influenced by the rocks surrounding the valley as well as its basement structure. The earliest

sediments were deposited during the Tertiary, giving origin to the basin as we know it during the Lower Quaternary. Of particular importance are rocks of the Franklin Mountains that border the valley on the east, Cristo Rey and the Sierra de Juárez that border the valley on the south and the Potrillo Mountains and recent volcanic features to the west. The basement of the Mesilla Valley region is composed of rocks of the Mazatzal province, formed by accretion of the crust to southern Laurentia at ~ 1.65 Ga (Karlstrom et al., 2004).

In our study area, we find younger Precambrian formations (~1.1-1.2 Gya) in the central Franklin Mountains. These are either metamorphosed sedimentary rocks (Castner Marble, Lanoria Quartzite) or igneous rocks of several sorts (Red Bluff Granite, Thunderbird Group) (Cornell, 1996). Erosion was the dominant process in the area from the time of formation of Precambrian rocks of the Thunderbird Group (953 Ma) (Thomann, 1980) until deposition of the Bliss formation began (Latest Cambrian to Early Ordovician) (Chenoweth, 2015). This erosional interval lasted for about 0.5 Ga (Cornell, 1996).

Roughly 100 million years ago, uplift of the Chihuahua trough brought the El Paso region above sea level during Late Cretaceous time, a situation that has persisted to the present (Cornell, 1996). About 75 million years ago, the North American Plate began to collide with the oceanic Farallon Plate. This collision generated compressional stresses throughout western North America and a major mountain building event, the Laramide Orogeny, began (Cornell, 1996). It was a major compressional, but non-volcanic event due to the shallow angle of subduction. Uplift of the Rocky Mountains, the Colorado Plateau, and the Basin and Range Province took place during this orogeny (Cornell, 1996). The end of the Laramide Orogeny came in the Eocene. In the Mesilla Valley area, three distinct aspects of the Laramide Orogeny are evident.

Laramide Orogeny

The first phase of the Laramide Orogeny began with the Franklin Mountains (75 Ma); they are a tilted fault block range composed of a core of Precambrian rocks overlain by Paleozoic sedimentary rocks. The trend of the range is controlled by north/south reverse faults (Cornell, 1996). The range was squeezed and tilted as it was uplifted, and the eastern side rose faster than the western side. Uplift on the eastern fault system amounts to 30,000 feet (9,150 m), while uplift on the western fault system totals about 10,000 feet (3,050 m) (Cornell, 1996).

During the second phase, on the Mexican side, deformation intensely folded and faulted Cretaceous sedimentary rocks, forming the Sierra de Juárez (Swift, 1973) (50 Ma). Since the youngest rocks are 100 million years old, thrusting could not have begun earlier than that.

The third phase of Laramide deformation is marked by the emplacement of andesites in the Lower Mesilla Basin (Cornell, 1996) at ~ 47 Ma (Hoffer, 1970). Geophysical studies have suggested that a segment of the Farallon Plate was subducted at a lower-than-normal angle so that the subducted slab did not get deep enough to melt the Farallon plate until it was much further inland than normal (Cornell, 1996). Andesite emplacement occurred within the Sierra de Juárez as well as other localities. Since the andesite is not deformed in the Sierra, it must have been emplaced after thrusting, folding, and faulting of the Sierra. In the case of plutons, the andesite has been exhumed by subsequent erosion (Cornell, 1996). The Campus Andesite is the largest of the plutons, the Muleros Andesite forms the core of Cristo Rey, and numerous smaller andesite bodies are found including the Coronado, Three Sisters, and Vado andesites (Cornell, 1996). These andesites are similar in mineralogy, suggesting that they were derived from a common magma source at about the same time.

In southern New Mexico 29 Ma ago, extension began in the Rio Grande rift to the east, and the Basin and Range province to the west. These provinces merge to form an interconnected zone of extension, although the existence, location, and nature of the boundary between the two provinces are uncertain (Ricketts et al., 2021). The early phase of extension in the Rio Grande rift occurred during the latter part of a major phase of mostly Oligocene volcanism (Morgan et al., 1986). Low angle faulting and broad shallow basins formed along the trend of the central rift. Faulting was either planar or curved. This combination of large strains on closely spaced faults produced highly rotated strata (Morgan et al., 1986).

The second phase of extension occurred primarily in the late Miocene (10–5 Ma) with minor extension continuing to the present (Morgan et al., 1986). It was characterized by apparently synchronous, high-angle faulting giving large vertical strains with relatively minor lateral strain (5–20%) which produced the modern Rio Grande rift morphology. The extension direction was approximately E-W, consistent with the contemporary regional stress field (Morgan et al., 1986).

The late phase of extension in the Rio Grande rift followed a mid-Miocene lull in magmatism that lasted 7 Ma (Morgan et al., 1986). In the central Rio Grande rift this phase of extension produced narrow elongate fault bounded basins along the locus of the earlier shallow broad basin. In contrast to the earlier phase of extension, faulting during the late phase resulted in much less tilted and rotated strata (Morgan et al., 1986). Renewed uplift during Miocene and Pliocene time has brought the land to its present elevation and downcutting by rivers has carved the current topography of the Rockies and the Colorado Plateau (Cornell, 1996).

The Santa Fe group

The Santa Fe Group is composed of Tertiary to Quaternary basin-filling deposits, that constitute the Lower Mesilla Valley aquifer system. This formation was deposited during fluvial inundation of the bolsons (Stuart and Willingham, 1984) on top of igneous and sedimentary basement rocks. It is comprised of a thick sequence of alluvial, eolian, and lacustrine sediments, deposited in intermontane basins of the Rio Grande rift during an interval of about 25 million years starting in the late Oligocene (Hawley and Lozinsky, 1992).

In southern New Mexico, the Santa Fe group is usually divided into three formations: lower, middle, and upper lithostratigraphic units. The lower Santa Fe Group is dominated by fine-grained, basin-floor sediments that intertwine with alluvial fan deposits. It ranges in age from about 25 to 10 Ma (Hawley and Kennedy, 2004). Lower Santa Fe eolian sediments also form thick sheets and lenticular bodies that are interbedded with both basin-floor and piedmont-slope deposits in the southern part of the Mesilla Basin (Hawley and Kennedy, 2004).

The middle Santa Fe Group was deposited between 10 and 4 Ma when rift tectonism was most active, and filling of subbasins adjacent to the major boundary fault zones (Jornada, Mesilla Valley, East Robledo) was accelerated (Hawley and Kennedy, 2004). Alternating beds of clean sand, silty sand, and silt-clay mixtures are the dominant lithofacies in much of the central basin area. Eolian sediments also continued to accumulate in the eastern basin area, but the thickest buried dune sequences appear to be confined to the lower Santa Fe Group (Hawley and Kennedy, 2004).

The major upper Santa Fe formation in the Hueco-Mesilla-Jornada Basin region is also known as the Camp Rice formation (Hawley and Kennedy, 2004). It is composed of a thick sequence of fluvial sand and pebbly sand deposited by the ancestral Rio Grande during an

interval of 2 to 3 million years. However, because of complex river-channel shifts (influenced by both tectonism and climatic factors) during basin-floor aggradation, fine-grained (slack-water) facies are also locally present (Hawley and Kennedy, 2004).

Post-Santa Fe deposits include inset valley fill of the ancestral Rio Grande and tributary arroyos that forms terraces bordering the modern floodplain, and river and arroyo alluvium that has been deposited since the last major episode of valley incision in late Pleistocene time (Hawley and Lozinsky, 1992).

PREVIOUS STUDIES

Although a considerable amount of geological, geochemical, and geophysical research has been conducted in the Lower Mesilla Basin, only two resistivity surveys have been made in the area. The first one, which is also the focus of this thesis, was published as a preliminary report by Zohdy et al. (1976). It contains a location map and 65 Schlumberger sounding curves. They used an average current electrode spacing of about 1 km, recording measurements at each point along the line. Current electrode spacings for some soundings were as large as 2 km, and the smallest one was around 300 m. This work only shows the processed soundings, but no interpretation was made at the time. It was not until twenty years later, that Al-Garni (1996), reprocessed this dataset using an automatic interpretation program developed by Zohdy and Bisdorf (1989).

Another resistivity survey in the area was conducted by Arunshankar (1993), and it took a different approach. His thesis focused on the use of resistivity measurements to estimate salinity changes over time. He spaced the current electrodes at 200 m and took several measurements over time at each point. While different in focus, Arunshankar's research has been a useful tool to evaluate the area and compare results for several locations in the valley.

Additionally, a small resistivity survey made by Imana (2002), was conducted along Artcraft Road from the river west to Upper Valley Road before Artcraft was opened to traffic. Imana's work focused on delineating shallow geologic features, such as faults, river channels, and other sediment depositional variations in the Mesilla Basin.

Besides resistivity, other geophysical studies have been made in the Mesilla Basin and surroundings. Hiebing (2016) completed a gravity survey to identify faults that might be related to sources of salinity in the lower Mesilla Basin and the adjacent Rio Grande (Figure 8). Cervantes (2018) conducted another gravity survey to determine the structural and stratigraphic controls of the lower Mesilla basin with a specific focus on attempting to better locate the position of the Mesilla Valley fault system. These two surveys added to the UTEP regional gravity dataset.

The USGS released a Scientific Investigations Report (Teeple, 2017), assessing the groundwater resources in the Mesilla Basin using geophysical surveys and geochemistry analyses. The geophysical techniques used include helicopter frequency domain electromagnetic surveys (HFEM), DC Resistivity, and time-domain electromagnetic soundings (TDEM) (Figure 9). The only concern here is that for the DC Resistivity, Teeple (2017) used the survey data collected by Zohdy et al. (1976), and the interpretations made by Al-Garni (1996), to identify areas of low resistivity. The USGS report states that low bulk resistivities could be associated with sediments having either a large number of clayey deposits or high concentration of dissolved solids in the pore water (Teeple, 2017). This is unlikely the case because as we will see further in this thesis most of the soundings showing these low resistivity values were at depths that should be well within the bedrock. The geochemical data analyzed by Teeple (2017) included groundwater samples for physicochemical properties, major ions, trace elements,

nutrients, pesticides, and environmental tracers. Based on these data, an upwelling of groundwater from a deep saline source in the Sierra de Juárez area was suggested (Teeple, 2017).

The most recent geophysical work was a gradient self-potential logging survey taken in the Mesilla basin by Ikard et al. (2021). In this research, they were able to identify the gaining and losing reaches of the Rio Grande in the Mesilla Valley. They found a mild surface water gain for 22 km downstream from the Mesilla Diversion Dam, and a losing condition for the final 18 km of the survey (Ikard, 2021), where only the last 8 km were located inside our study area. The survey incorporated the resistivity data from Teeple (2017) to assist in the interpretation of results, noting resistivity values of less than 10 ohm-m appeared south of Anthony, NM (Ikard, 2021). Ultimately, the issue of other researchers using the same outdated resistivity interpretations will not change until there is a new interpretation made, which is the focus of this thesis.

Additional important constraints to the modeling I conducted were provided by hydrologic and geochemical studies. Hawley and Kennedy's (2004) hydrogeologic cross-sections are of utmost importance for the interpretation of resistivity in this thesis. Kubicki et al., (2021) used a geochemical approach to define sources of groundwater salinity in the study area, and Garcia et al. (2020) combined two isotope tracers to identify and quantify solute sources in the Rio Grande River in the lower Mesilla Basin.

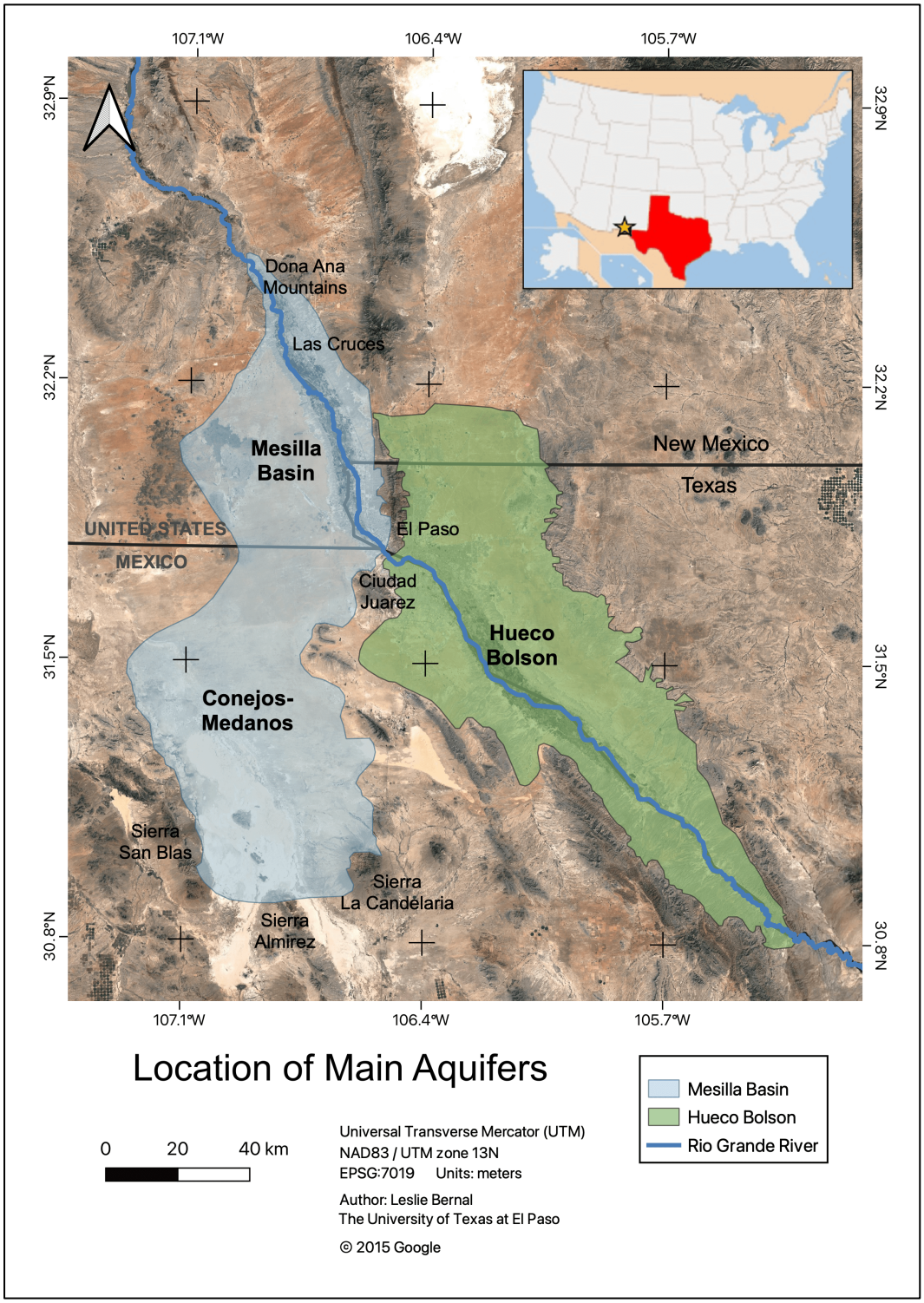

Figure 1. Location of Main Aquifers.
This map shows the Mesilla Basin/Conejos-Médanos (light blue) and the Hueco Bolson (green) aquifers. The locations of El Paso, TX, Las Cruces, NM, and Ciudad Juárez, Mexico, along with the Rio Grande River (blue line) are indicated. Modified from Sheng (2013).

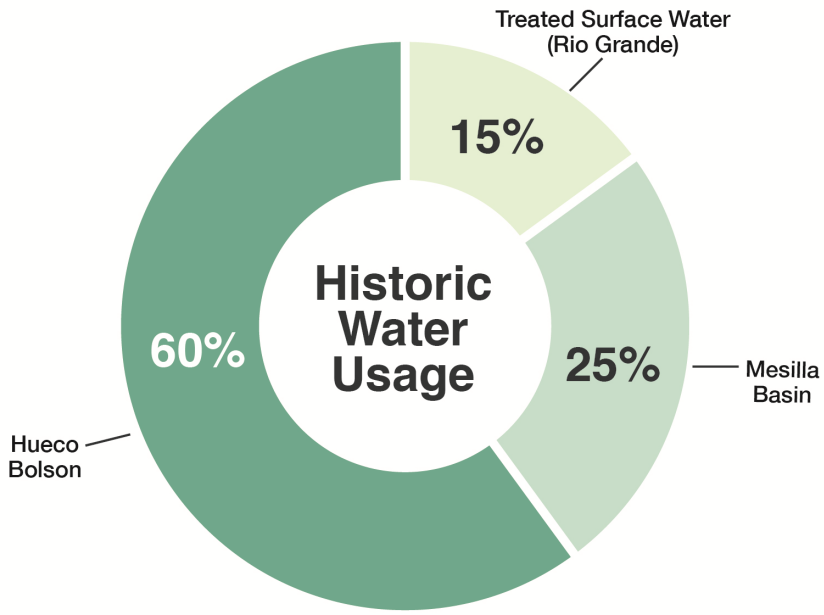

Figure 2. Historic Water Usage.
For nearly a century the Hueco Bolson has been the major source of drinking water for El Paso and Ciudad Juárez. Data from Chavez, (2000).

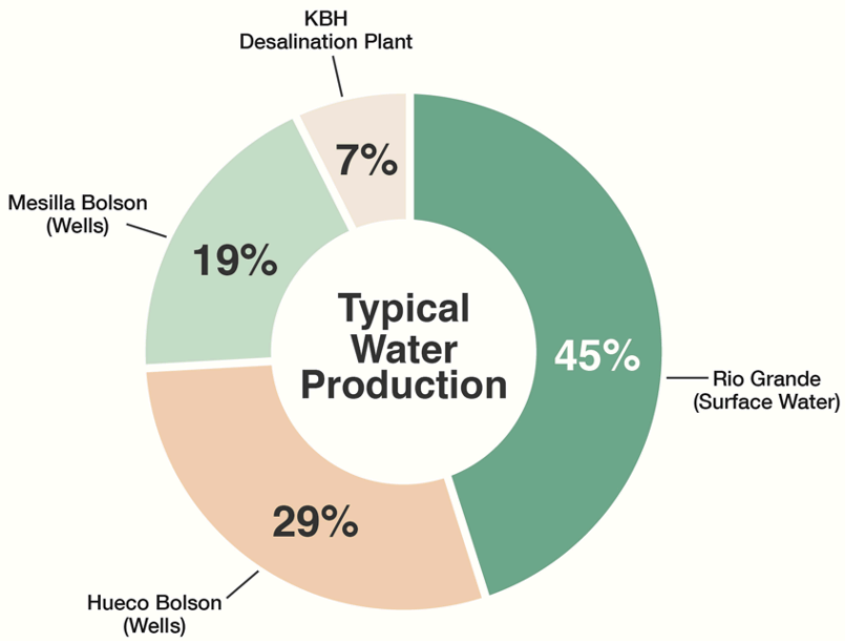

Water Source	Water Production in m^3/yr
Rio Grande	172,709,412
Hueco Bolson	111,301,621
Mesilla Basin	72,921,751
KBH Desalination Plant	26,865,908

Figure 3. Typical Water Production in 2018.
Values vary each year. As of 2022, droughts have affected the Rio Grande flow and the City of El Paso only obtained 16% (27,633,506 m3/yr) of its regular water supply from the river (Pskowski, 2022). Data from El Paso Water (personal communication, November 9, 2022).

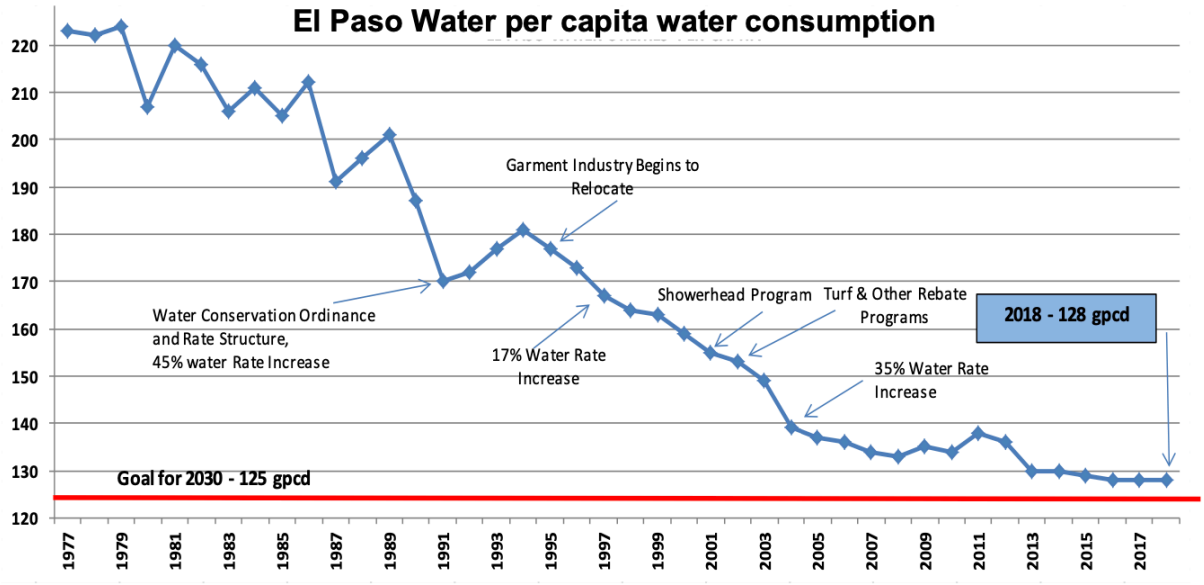

Figure 4. Water Consumption Per Capita in El Paso, TX.
In the last 45 years, water consumption has decreased by 42% thanks to the water conservation measures. Source: El Paso Water (2019).

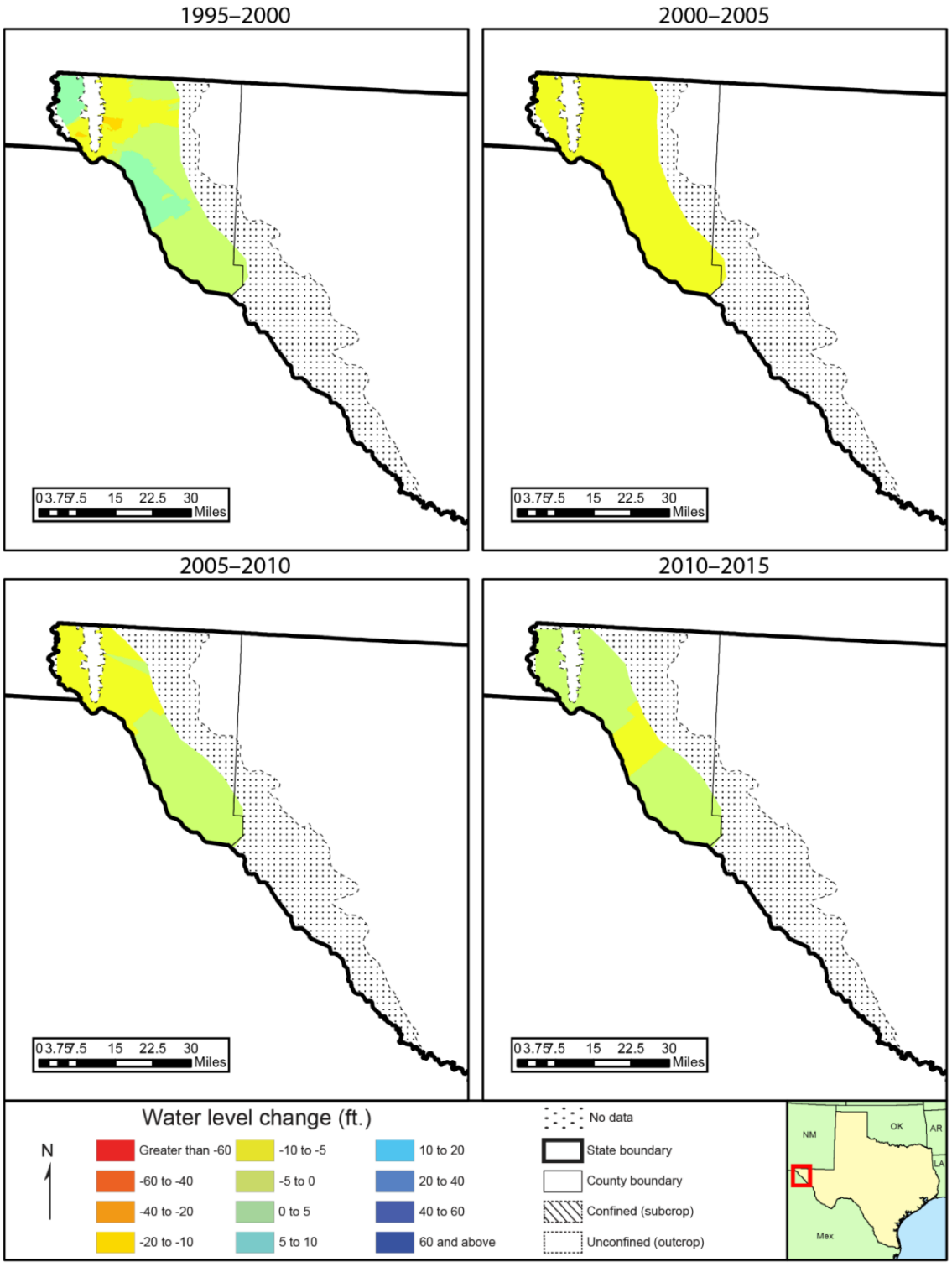

Figure 5. Water Level Changes in the Hueco Bolson - Mesilla Aquifer from 1995 to 2015. Thanks to the measures implemented from the water conservation plan, the aquifers are not at high risk anymore. Source: Bruun et al., (2016).

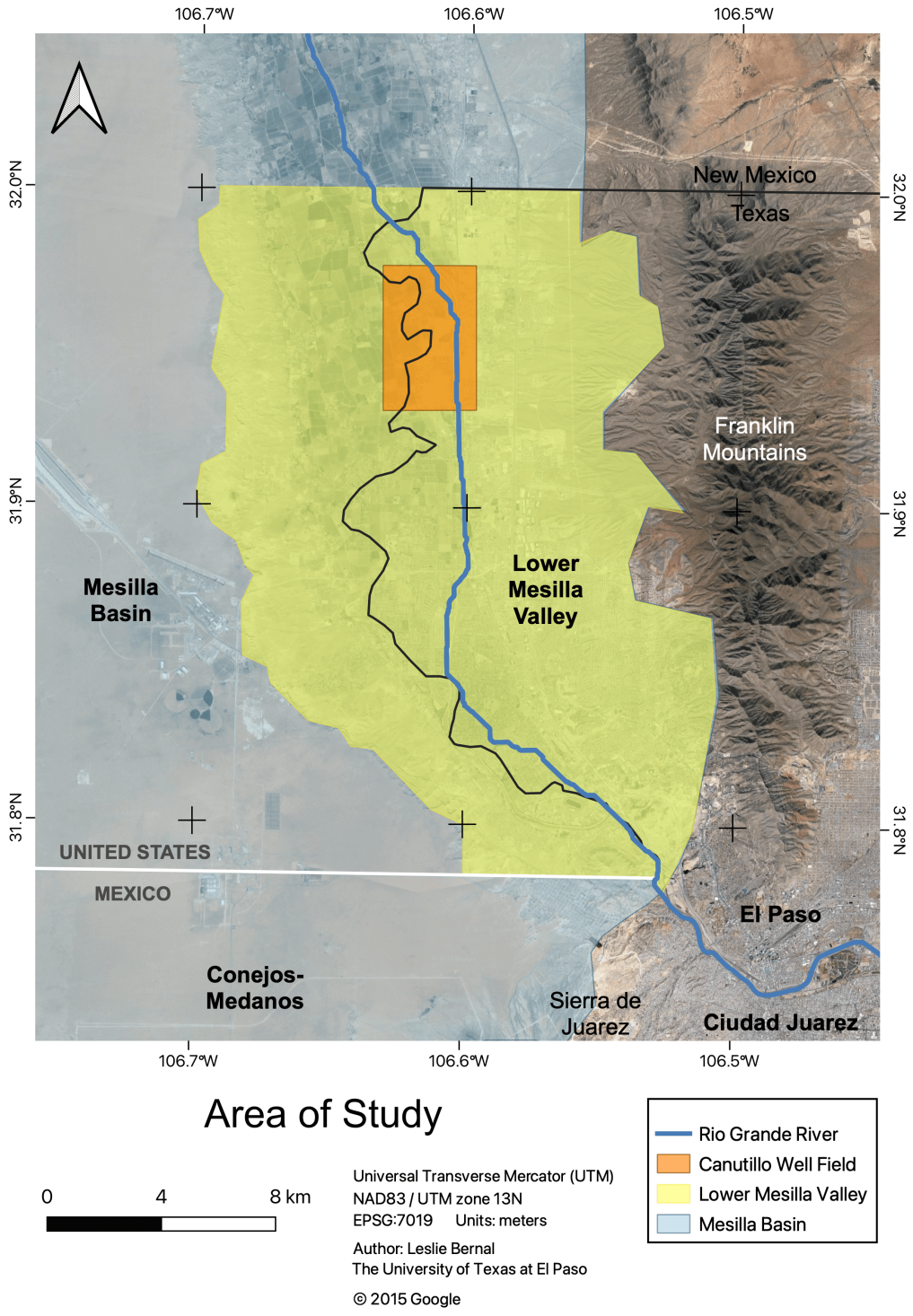

Figure 6. Area of Study.
The Lower Mesilla Valley (yellow) is located between El Paso, TX, and Dona Ana County, NM. El Paso Water production wells in the Mesilla Basin are located within the Canutillo Well Field and are categorized as shallow, intermediate, and deep wells (Chavez, 2000).

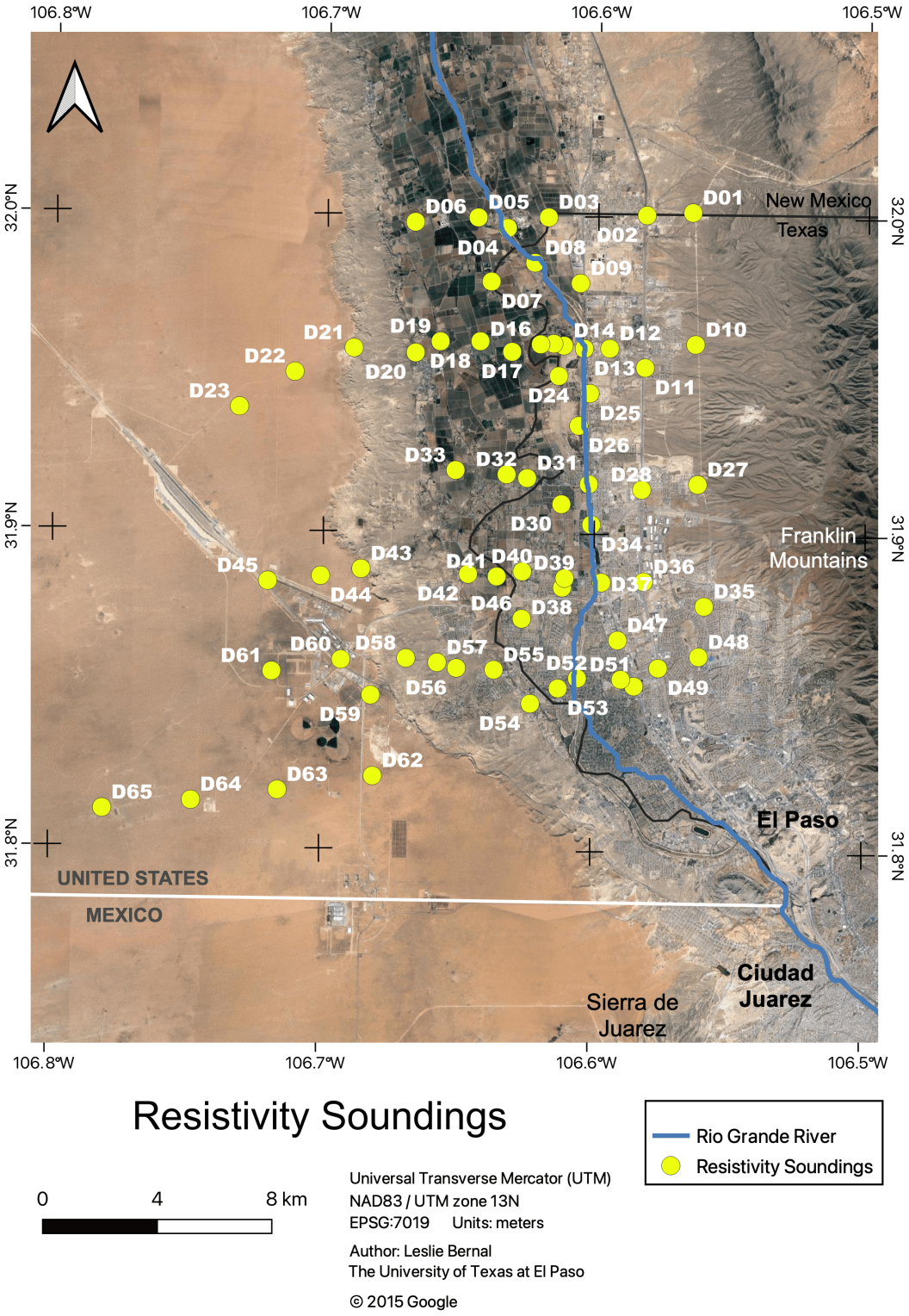

Figure 7. Resistivity Soundings.
This survey was taken in 1973 by the USGS in cooperation with the Texas Water Development Board to try to delineate the groundwater system.

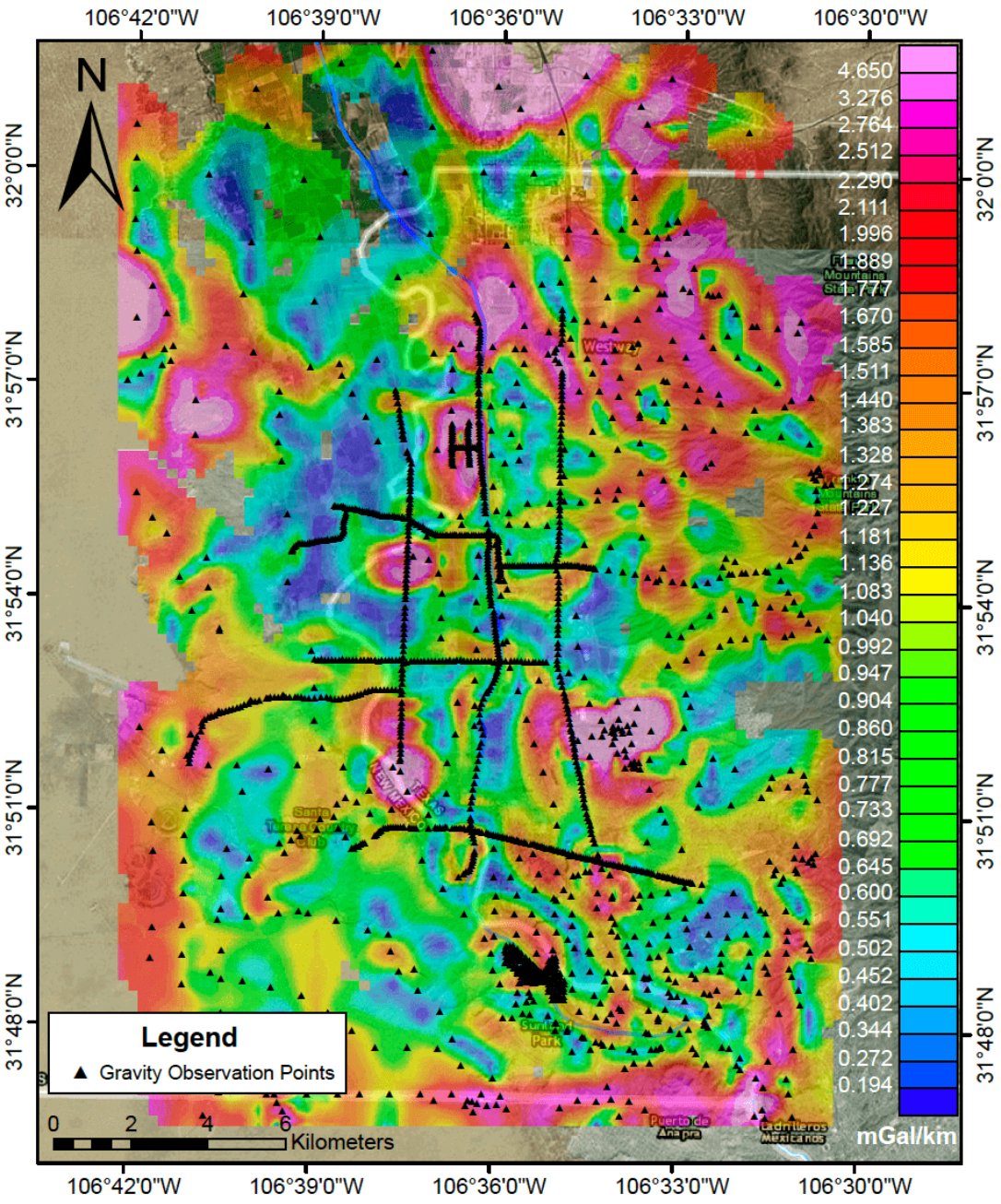

Figure 8. Gravity Studies Made in the Area.
This map shows the residual Bouguer gravity anomaly in the study area. Source: Hiebing (2016).

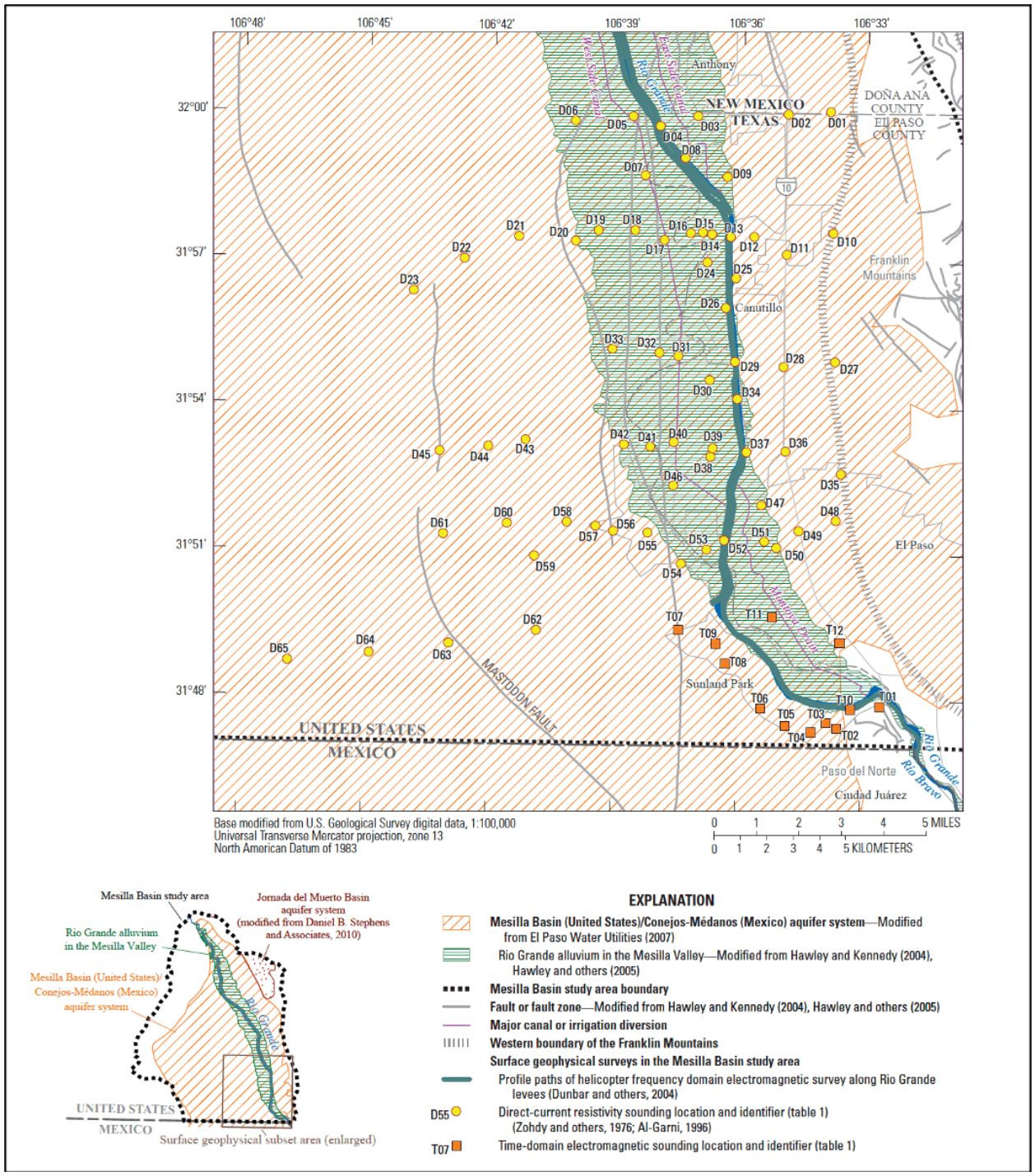

Figure 9. Previous Geophysical Studies.
This map shows other geophysical studies made in the study area, such as Helicopter Frequency Domain Electromagnetic (HFEM), and Time Domain Electromagnetics (TDEM). Source: Teeple (2017).

Chapter 2: Methods

The resistance of a material R can be calculated using Ohm's law:

$$R = \frac{\Delta V}{I}$$

where ΔV is the voltage or potential difference, and I is the current. The direct current I is introduced into the ground by two-point electrodes A and B. Then the potential difference is measured between two-point electrodes M and N (Figure 10).

To measure the apparent resistivity $\bar{\rho}$ of the subsurface, we need to multiply the resistance by a geometric factor K that depends on the kind of array being used (Zohdy et al., 1974):

$$\bar{\rho} = K\frac{\Delta V}{I}$$

The electric current path depends on the variation of the electrical resistivity or its reciprocal, the conductivity. Currents flow through good conductors, for example, a formation saturated with water or fine-grained sediments, especially clays. On the other hand, currents flow around resistors, for example, limestone (Figure 11) or coarse grained, dry sediment.

The array used to collect this survey is the Schlumberger array (Figure 12). Apparent resistivity for this array is given by:

$$\bar{\rho} = \pi\frac{\left(\frac{\overline{AB}}{2}\right)^2 - \left(\frac{\overline{MN}}{2}\right)^2}{\overline{MN}}\frac{\Delta V}{I}$$

where $\overline{AB}$ is the distance between current electrodes A and B, and $\overline{MN}$ is the distance between potential electrodes M and N. If $\overline{MN} \to 0$, then the above equation can be written as:

$$\bar{\rho_s} = \pi\left(\frac{\overline{AB}}{2}\right)^2\frac{E}{I}$$

where $E = \lim_{\overline{MN}\to 0} \frac{\Delta V}{\overline{MN}}$ = Electric Field, and the Schlumberger apparent resistivity $\overline{\rho_s}$ is a function of a single distance variable $(\overline{AB}/2)$ (Zohdy et al., 1974). The equation for $\overline{\rho_s}$ can be used provided that $\overline{AB} \geq 5\overline{MN}$ (Zohdy et al., 1974).

SURVEY

The equipment needed to perform a Vertical Electrical Resistivity survey (VES), consists of a power source, electrode cables, the resistivity equipment, tape measure, hammer, and metal stakes. We do not have the specifications of what equipment was used in this survey, but here I describe the general process to take a resistivity survey. Once you arrive to the exact location, lay out the tape measure to mark the spacing between the potential electrodes (MN). Set up the resistivity equipment and the power source close to the center of the array. Start hammering two metal stakes (electrodes) in the ground (these will be your potential electrodes). Then lay out the tape measure to mark your distance between current electrodes (AB) and hammer the last two electrodes into the ground (these will be your current electrodes). Connect the electrode cables to the stakes and to the resistivity equipment. Run a quick test to check that all is connected right. Start measuring. According to the Schlumberger array, the potential electrodes will remain fixed, while the current electrodes will be moved apart. Eventually, the current electrodes will be too far away from the potential electrodes to adequately measure the potential, so the spacing between potential electrodes (MN) will be increased and then the spacing between current electrodes can continue to be increased. Figure 12 shows an example of the array set up. The spacings used in the surveys of Zohdy et al. (1976) can be found in Table 3.

Table 3. AB/2 and MN spacings used by Zohdy et al. (1976).

AB/2 in ft	MN in ft
6.8	0.5
10.0	2.0
14.6	2.0
21.5	2.0
31.5	2.0
45.0	20.0
68.0	20.0
100.0	20.0
146.0	60.0
215.0	60.0
315.0	60.0
450.0	200.0
680.0	200.0
1000.0	200.0
1460.0	200.0
2150.0	200.0
3150.0	200.0
4300.0	200.0

DATA AND PROCESSING

There are 65 Schlumberger resistivity soundings (Figure 13) that needed to be reprocessed. The model interpretation was aided by the following datasets:

- Water well databases within Texas and New Mexico (Figure 14). They contain valuable information such as water level, temperature, geochemistry, and drilling reports.
- Geological cross-sections from Hawley and Kennedy (2004): profiles I – I' (Figure 17), J – J'(Figure 18), K – K'(Figure 19), NW – SE (Figure 20).
- Gravity maps and models from Hiebing (2016) (Figure 21), and Cervantes (2018).

To process the resistivity data, a software package developed by Baker (2019) was used (Figure 22). It applies a 1-D modeling technique based on Keller and

Frischknecht (1966), called logarithmic curve matching. This method uses two types of resistivity curves: a field curve, which is a plot of apparent resistivity as a function of electrode spacing obtained in a field survey, and a curve computed from theoretically derived expressions (Keller and Frischknecht, 1966). The field curve should have the same shape as the computed one, and both are plotted to the same logarithmic scales. Then, they can be compared directly by superposition (Keller and Frischknecht, 1966). Baker's method allows the user to include measurement uncertainty estimates when matching the observed to theoretical curves during either forward modeling or inversion. The inversion method also allows the user to put uncertainties on the theoretical model resistivities and depths to help constrain solutions to models based on available geologic information.

To be able to use Baker's (2019) software, the following information is required:

- MN_sp: Distance between potential electrodes in meters.
- R_Meas: Apparent resistivity at MN_sp (ohm-m).
- R_SD: Standard Deviation of measured apparent resistivity (ohm-m).
- R_Est: Estimated resistivity from structure (calculated).
- Array: Electrode array geometry W-Wenner, S-Schlumberger, D-Dipole-dipole, P-Price.
- AB/2: One-half of the current electrode spacing (meters).
- Thicknesses and resistivities of different units plus their correspondent uncertainties.

The only information needed from the original report of Zohdy et al. (1976) was the measured apparent resistivity values, the MN values, and the AB/2 values. As the figures in the report were hard to read, I took this information from the tables in Al-Garni's thesis (1996), as he uses the exact same data set for his analysis.

The AB/2 spacings were measured in feet to approximate the rate of six logarithmically equally spaced points per decade. Such unusual electrode spacings were neither used before nor after this survey (Zohdy to Al-Garni, oral communication, 1996). The reason for using this rate is based on the coefficients of the old software used to process these data; the curve needed to be digitized at the logarithmic electrode spacing $AB/2$ interval of $\frac{\left(\frac{AB}{2}\right)_{i+1}}{\left(\frac{AB}{2}\right)_{i}} = e^{\ln\left(\frac{10}{6}\right)} \cong 1.4678$, where i is the ith point on the curve (Zohdy, 1973). This interval specifies six logarithmically equally spaced points per logarithmic cycle.

The MN spacing needs to be 1/5 or less of the AB distance, according to the Schlumberger model. Table 2 gives the MN and AB/2 values used by Zohdy et al. (1976). In most soundings, we used a Standard Deviation of 5 ohm-m (R_SD) since we did not have the field measurements to evaluate data repeatability. This value was changed if the resistivity values were small (e.g., less than 5 ohm-m), because the lower bounds would then give negative resistivity values. The R_Est is the calculated resistivity based on a given 1-D layered Earth model (the best model that matches the observations and other geological constraints). These values in the input file are initially set to 1 and then updated by the software for a given layered Earth model. The thickness and resistivities of different units are added to a different section of the software and are part of the geological model.

To start processing, the next steps were followed:

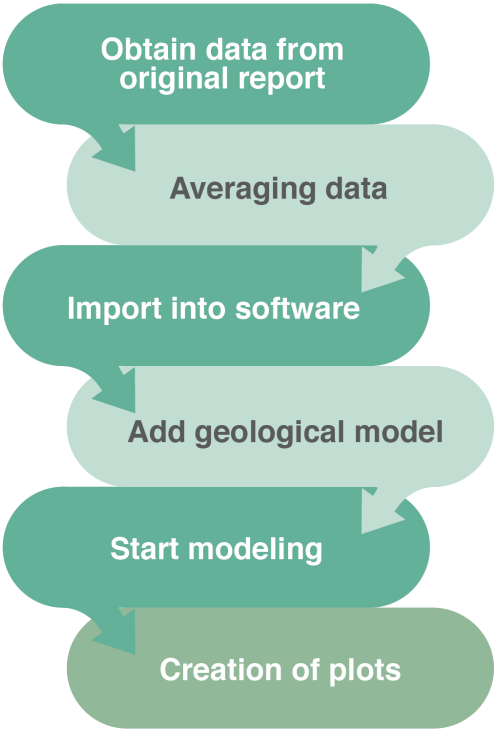

Obtain data from the original report

All the resistivity values used in this work were taken from Al-Garni's thesis (1996). An excel worksheet was created with three columns: apparent resistivity values, MN, and AB/2 values, both converted from ft to m.

Averaging data

When the survey was conducted, if there was a change of apparent resistivity values of more than 5% when the MN spacing changed, additional measurements were taken, so that the two segments of the curve would overlap by two points instead of one. Instead of keeping both values for the same MN spacing, we took the average.

Import into software

Once the six columns of information were ready in the excel spreadsheet, the header lines were deleted, and the file was saved as a CSV document that could be imported into the software. Appendix 4 shows an example of the data format required by the software.

Add geological model

This is one of the most important parts of the process. To create the geological model, water well information (from a well near the sounding) is used, such as lithology, water level, and water quality. The location of the wells is also important, considering their elevation and their proximity to the Rio Grande. In the state of Texas, well reports were found in the Texas Water Development Board database (2022), with some of the wells going as far back as 1936. More recent reports (from the 2000s) can be found in the Texas Commission on Environmental Quality database (2022). In the state of New Mexico, we obtained a complete database from the New Mexico Water Rights Reporting System (2022) that includes water table and well depth. Figure 23 shows how many wells were used in this thesis, and how many had valuable information, as well as their location with respect to the study area. In addition to the well information, hydrogeologic profiles from Hawley and Kennedy (2004) were extremely helpful in characterizing the geological models. The software also requires that every geological formation has a correspondent resistivity value and a thickness. These values can be approximate, and there is room to add as many layers as needed.

A different geological model was created for every resistivity sounding. Some of the geological models may have similarities with each other because of the proximity between soundings, but in the end, the results ended up varying considerably.

Start modeling

Once all parameters are entered, we run the program. Two graph areas are displayed; the one on the left shows the observed apparent resistivity, upper and lower bounds related to the standard deviation, and the computed apparent resistivity from the expected structure (Figure

22). The other graph on the right shows the expected resistivity structure of the region (Baker, 2019).

The modeling of a sounding progresses as follows: First, a computed apparent resistivity is generated and compared to the measured apparent resistivity. The computed curve is based on a geologic model derived from well drilling reports, geological cross-sections, well logs, and other geophysical and geochemical reports. Second, the model is varied until a good match (as low of RMS as possible) is obtained between the observed and calculated apparent resistivities. In most cases, I stopped the process once I got a model that fit the observed data within the uncertainties of the resistivity. Other times I kept iterating until I got the lowest rms without severely modifying the known geology. Table 4 shows resistivity values associated to rocks found in this basin:

Table 4. Resistivity values of common rocks.
Modified from Saad and Mohamad, (2012).

Material	Ohm-m
Alluvium	10 - 800
Sand	60 – 1,000
Clay	1 - 100
Groundwater (fresh)	10 - 100
Limestone	50 - $4x10^3$
Granite	5,000 – 1,000,000

Creation of plots

Once a reasonable fit is found between the observed and calculated resistivities for a sounding, two customized plots per sounding are created to show more detail. These plots are generated in R software, with code written using the ggplot2 package (Appendix 5). The first

shows the observed and predicted apparent resistivities, and the other shows the resistivity versus depth structure.

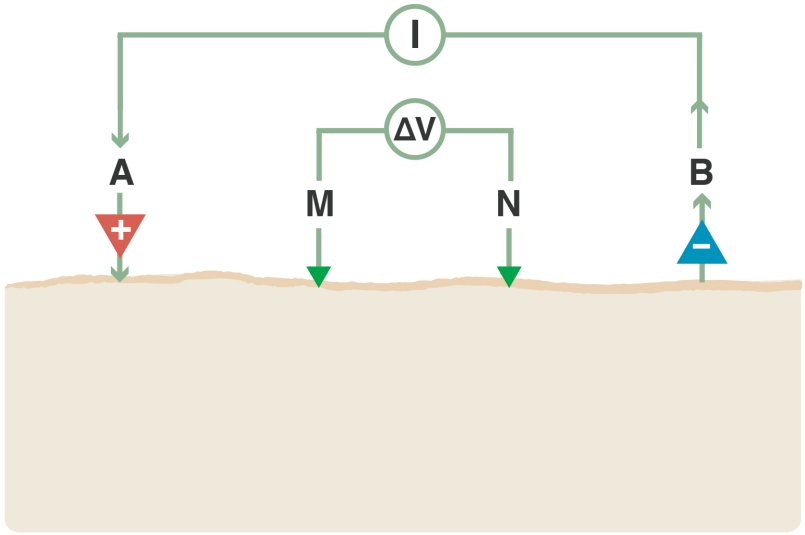

Figure 10. Resistivity Method.
Example of resistivity array where the electrical current travels between electrodes A and B, and the potential difference is measured by electrodes M and N.

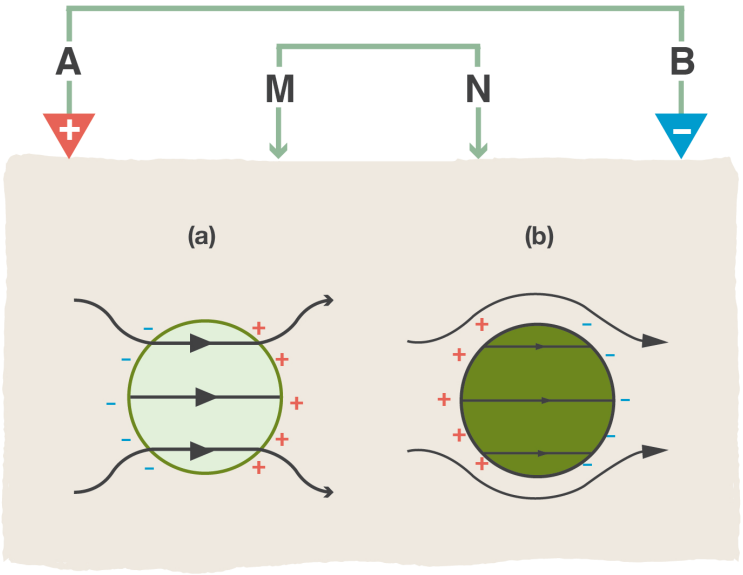

Figure 11. Resistivity Paths.
Once the electrical current is injected into the ground, it will travel along the path of least resistance. If a material has a high conductivity (low resistivity) (example a), current will be deflected toward the object, for example, sand saturated with water. If the material has a low conductivity (high resistivity) (example b), then the current will try to avoid going through it, for example, limestone.

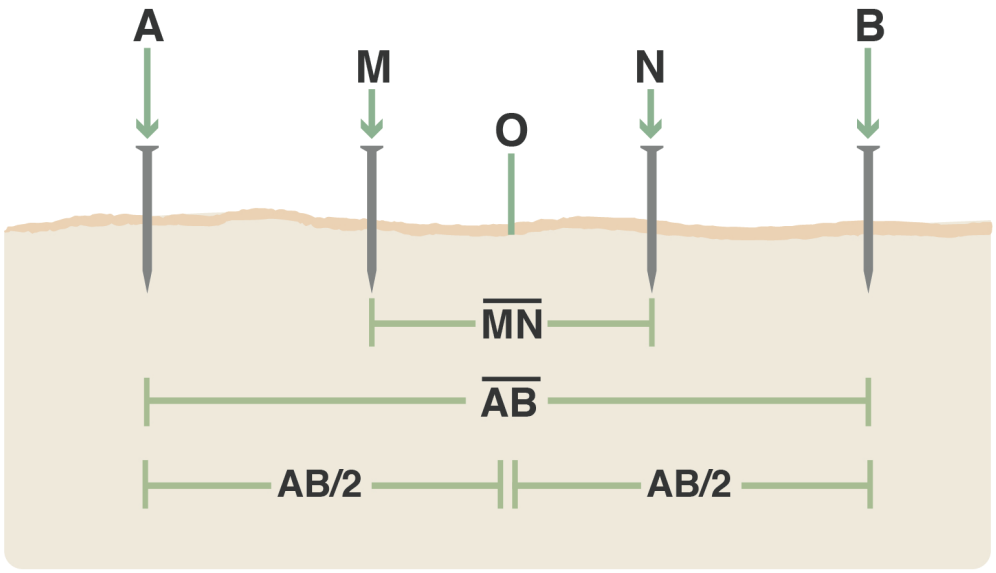

Figure 12. Schlumberger Array.
This array consists of fixing the potential electrodes MN, and moving the current electrodes AB. The MN spacing will change in intervals out to a maximum of 1/5 the AB spacing.

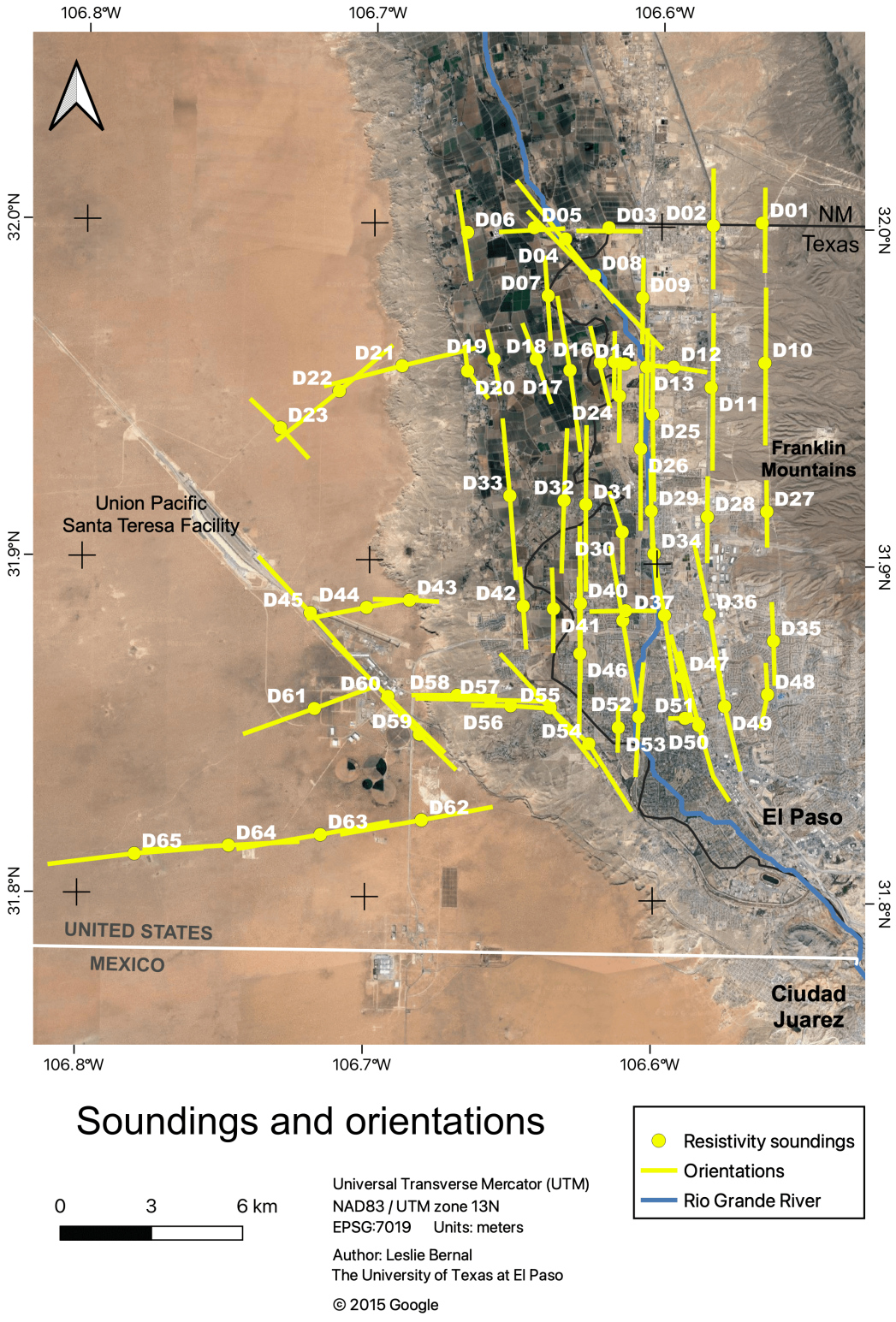

Figure 13. Soundings and Orientations.
This map shows the resistivity soundings with their orientations and lengths. This information can be found with more detail in Appendix 1.

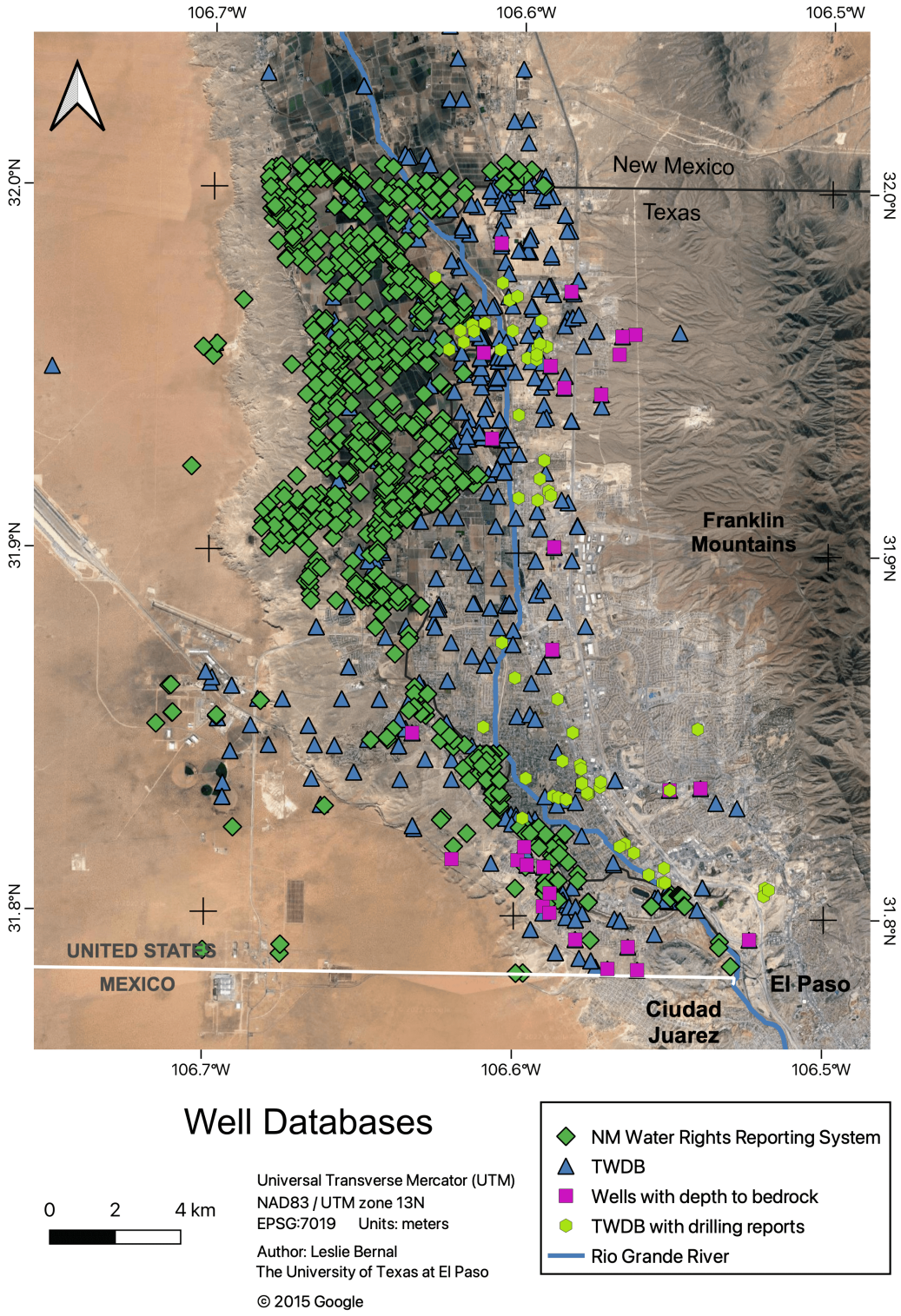

Figure 14. Well Databases.
These are most of the water wells located in the study area.

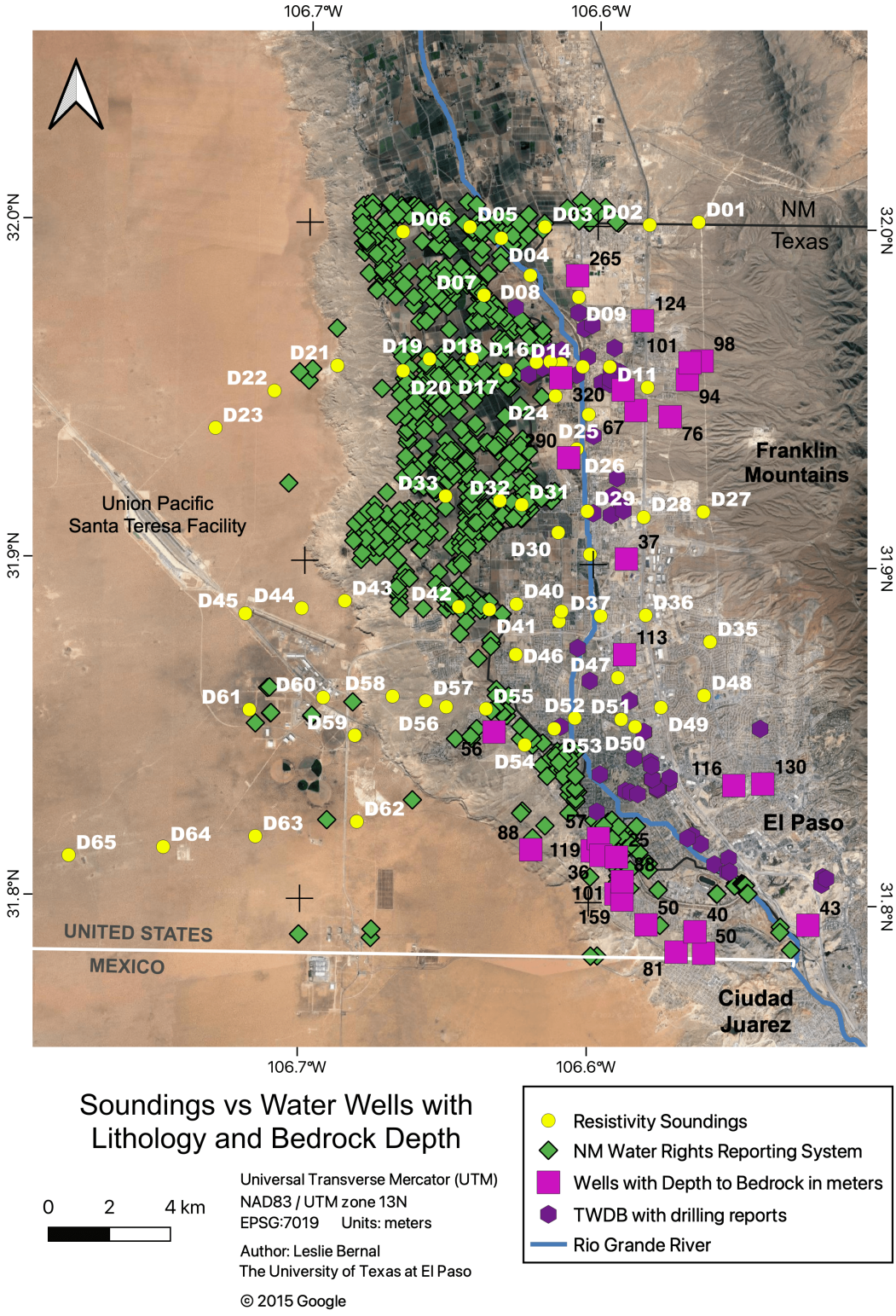

Figure 15. Soundings, Water Wells with Lithology, and Bedrock Depths in meters. This map shows the resistivity soundings with the water wells that include lithology or drilling reports, plus the wells that have depth to bedrock information.

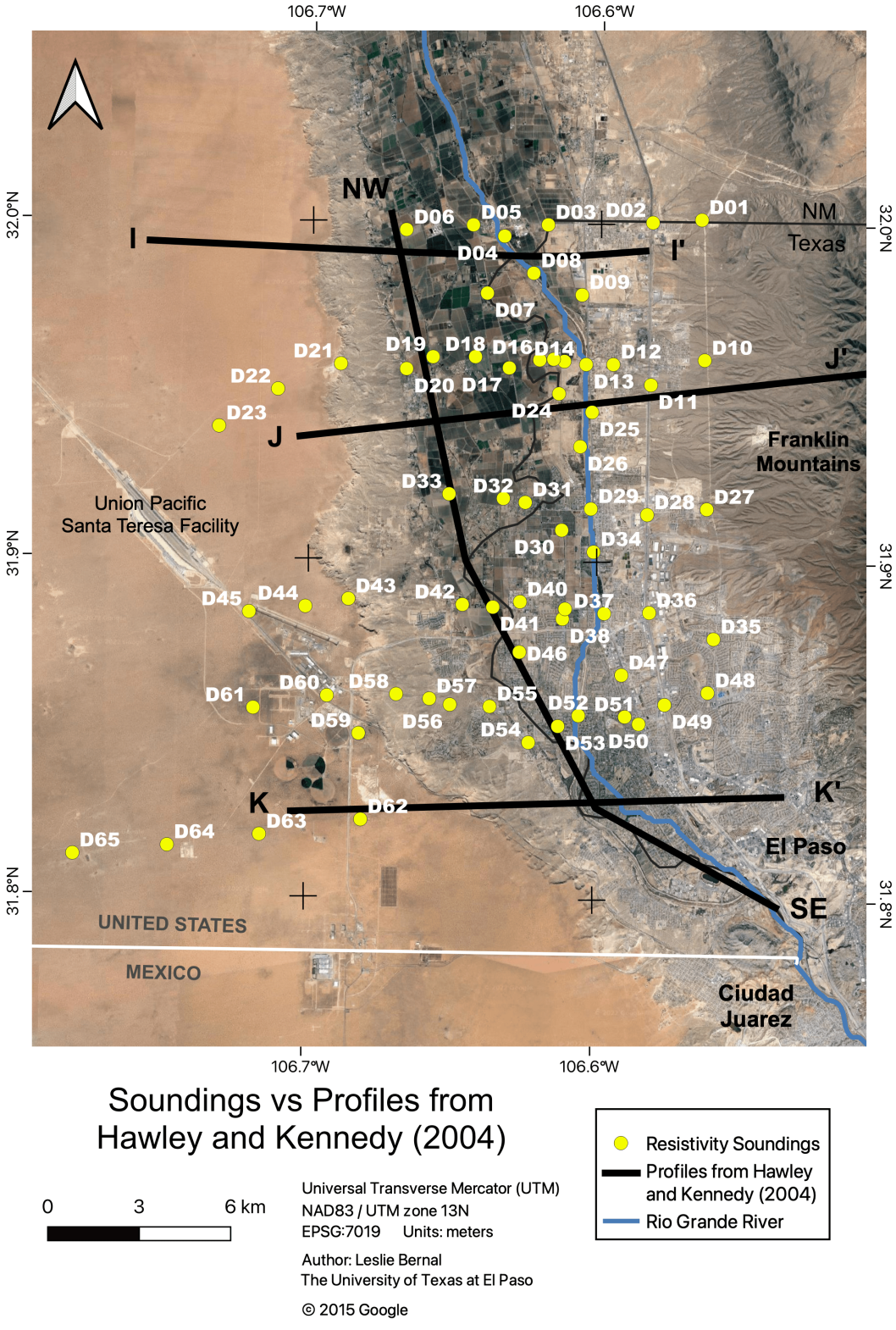

Figure 16. Soundings vs Profiles from Hawley and Kennedy (2004).
This map shows Hawley and Kennedy geological profiles, along with the resistivity soundings. These profiles were extremely helpful in defining the structure of the models.

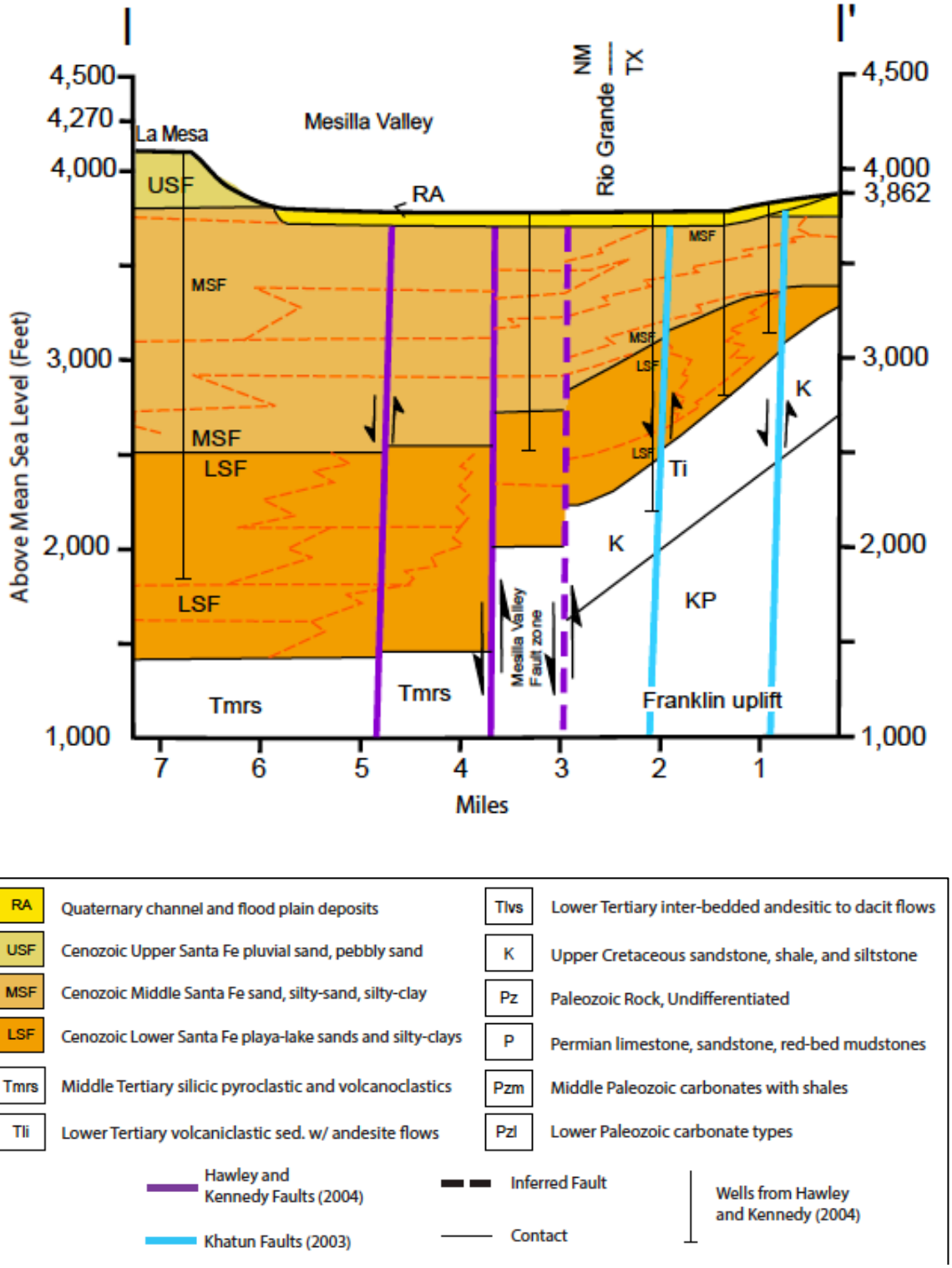

Figure 17. Profile I – I'.
Example of profile used in this analysis from Hawley and Kennedy (2004), and Khatun (2003). Modified by Hiebing (2016).

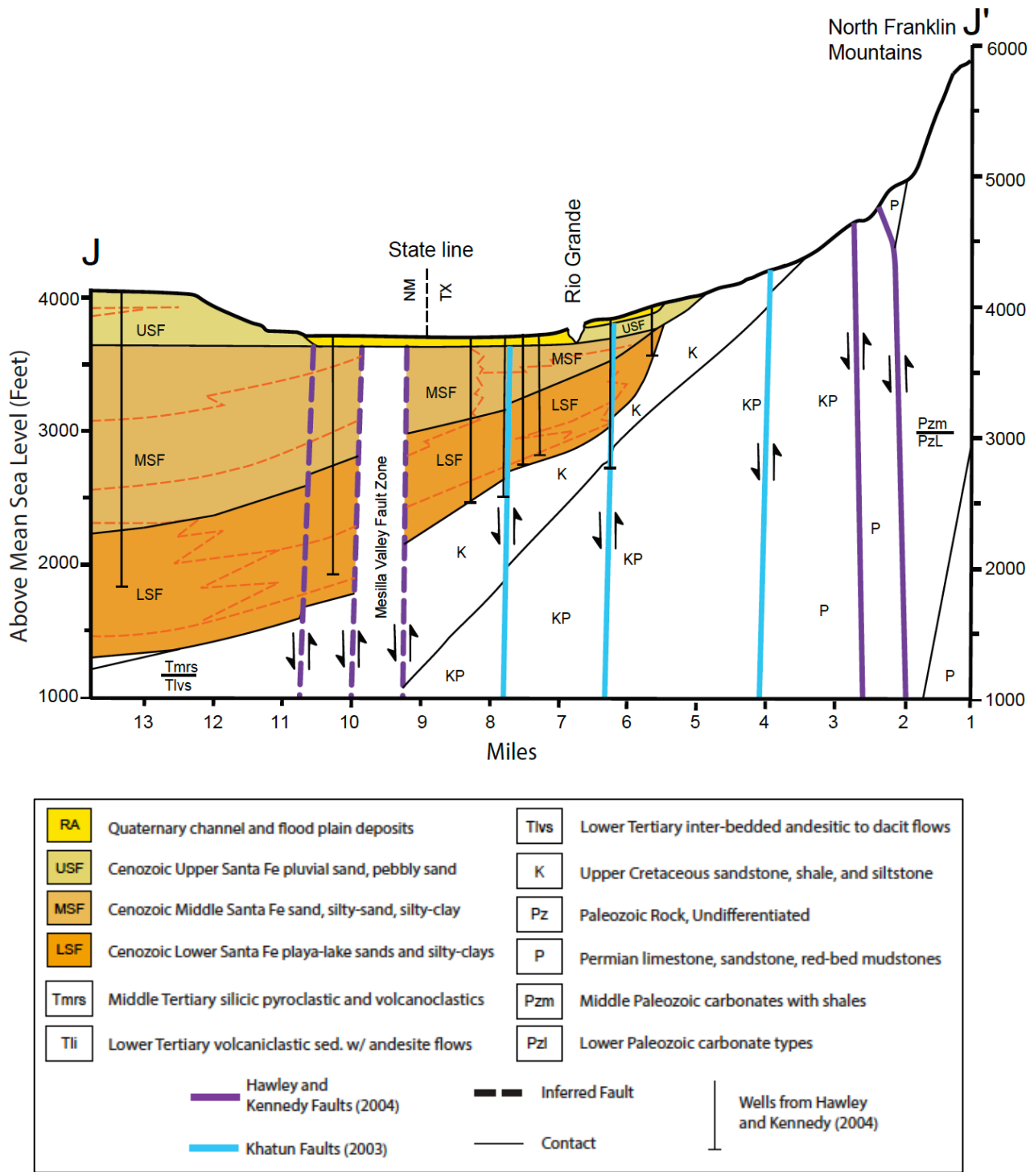

Figure 18. Profile J – J'.
Example of profile used in this analysis from Hawley and Kennedy (2004), and Khatun (2003). Modified by Hiebing (2016).

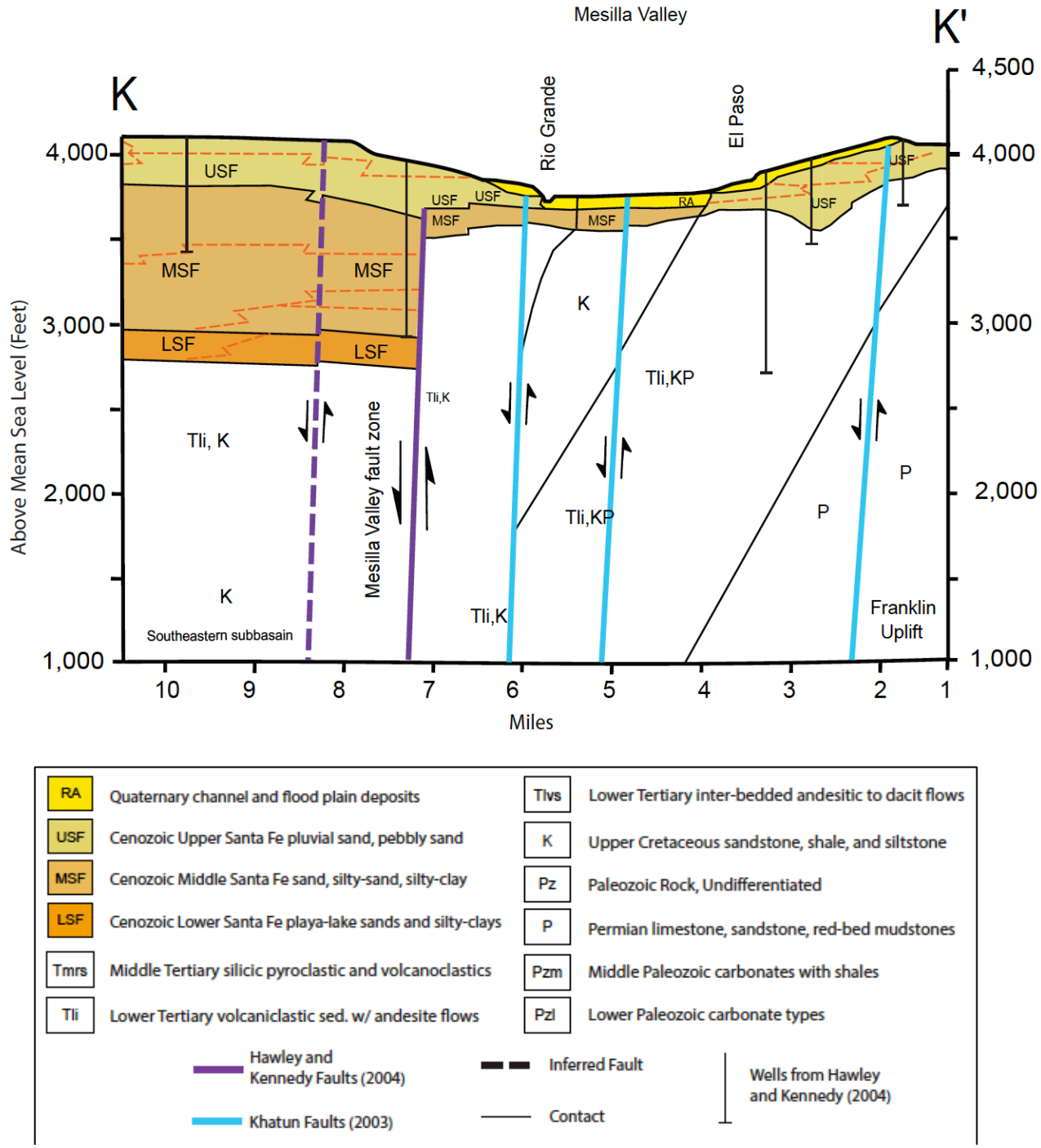

Figure 19. Profile K – K'.
Example of profile used in this analysis from Hawley and Kennedy (2004), and Khatun (2003). Modified by Hiebing (2016).

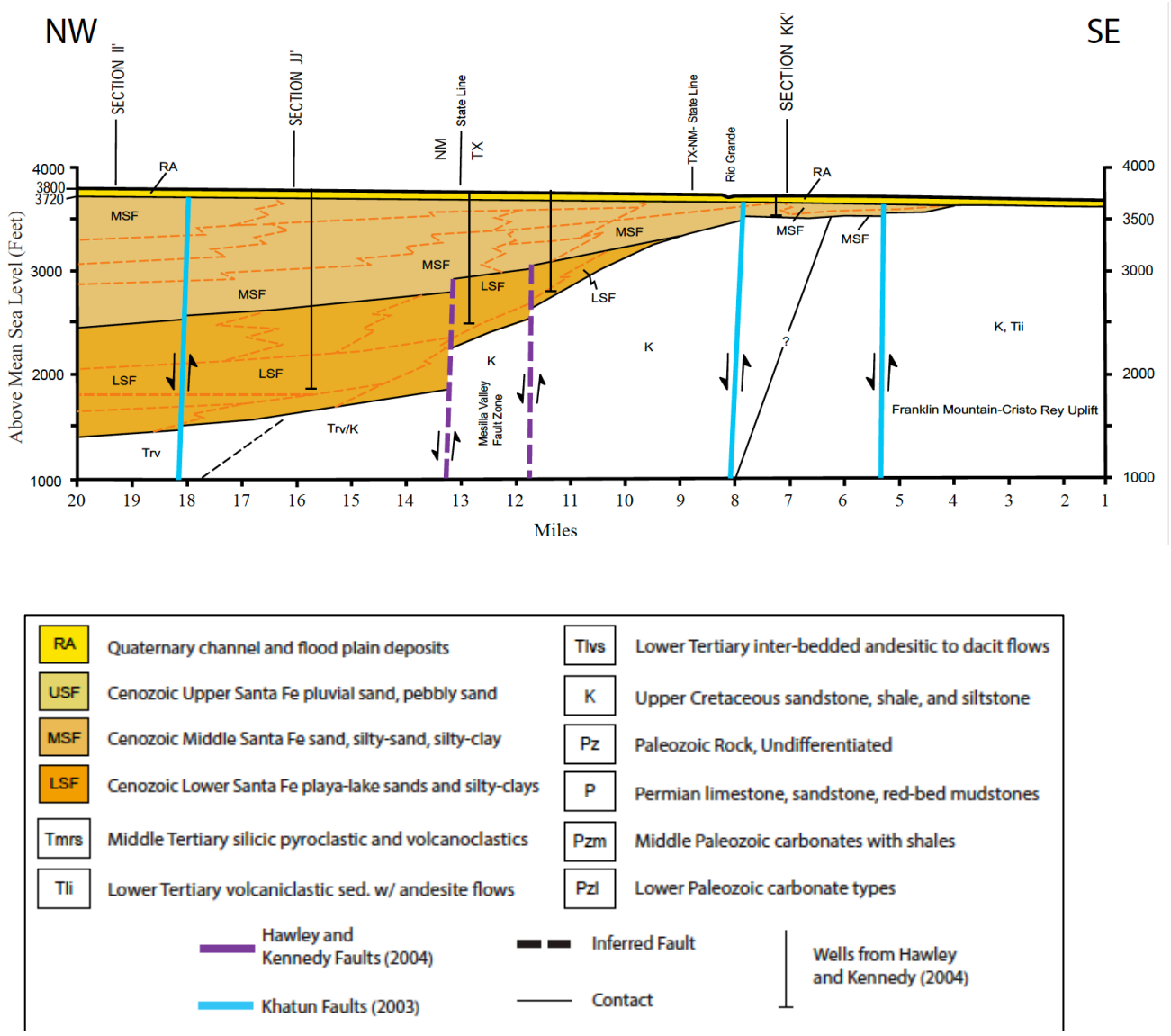

Figure 20. Profile NW – SE.
Example of profile used in this analysis from Hawley and Kennedy (2004), and Khatun (2003). Modified by Hiebing (2016).

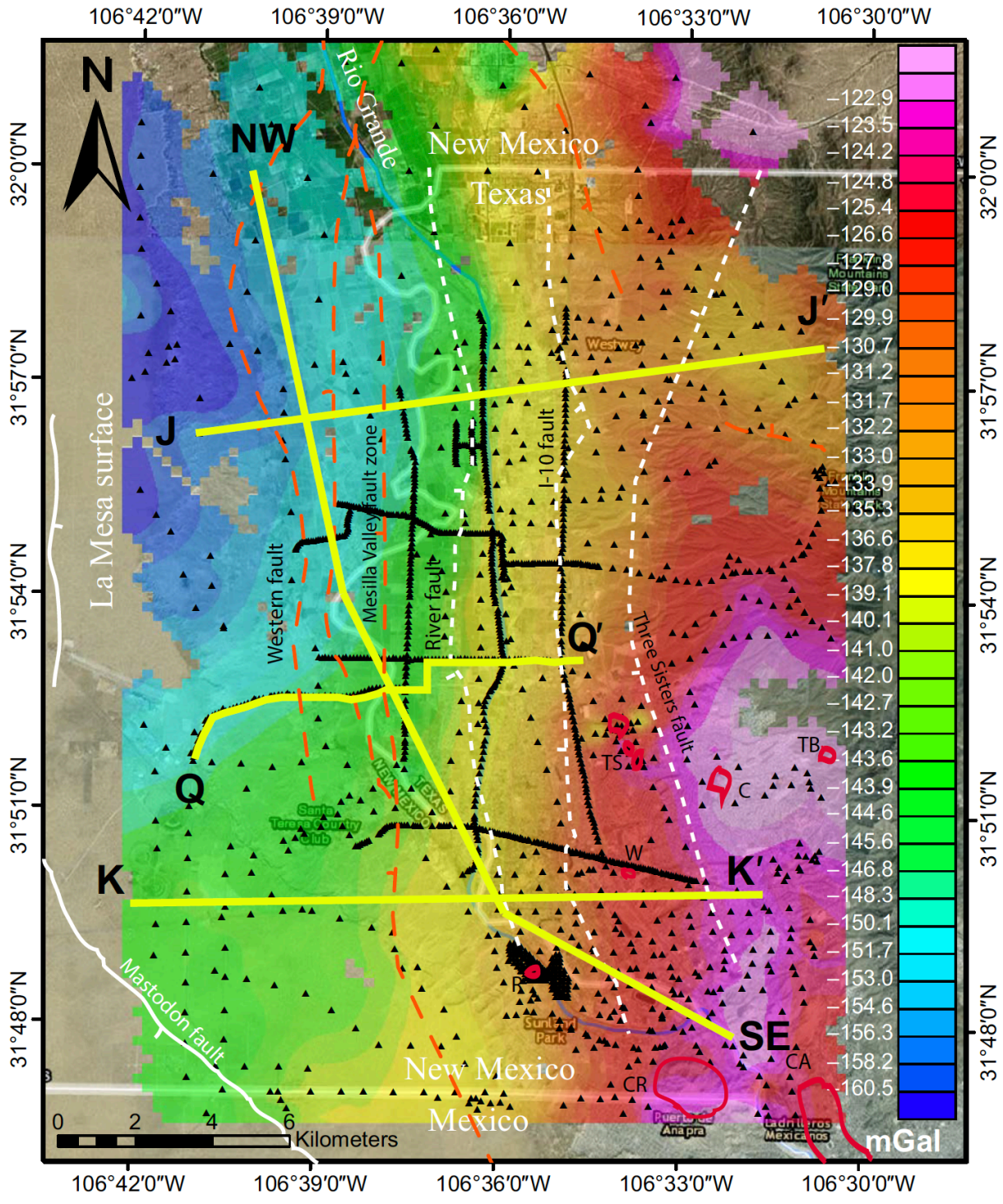

Figure 21. Q - Q' Profile.
Locations of gravity profiles modeled by Hiebing et al., (2018). All profiles, except Q-Q' follow portions of profiles of Hawley and Kennedy (2004).

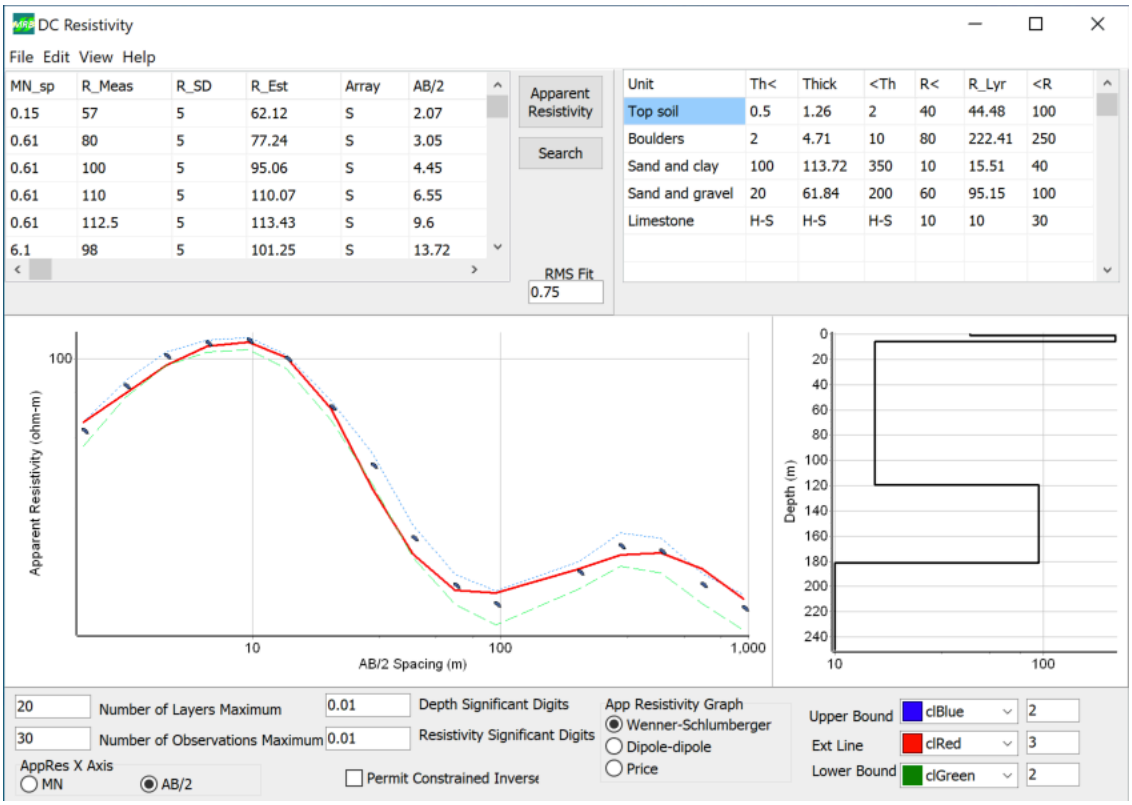

Figure 22. Software Processing Example.
This figure shows an example of the processing of Sounding 15. In the left plot dots are observed data, red line is predicted data, green and blue lines are data uncertainties. Plot at right shows resistivity model as a function of depth.

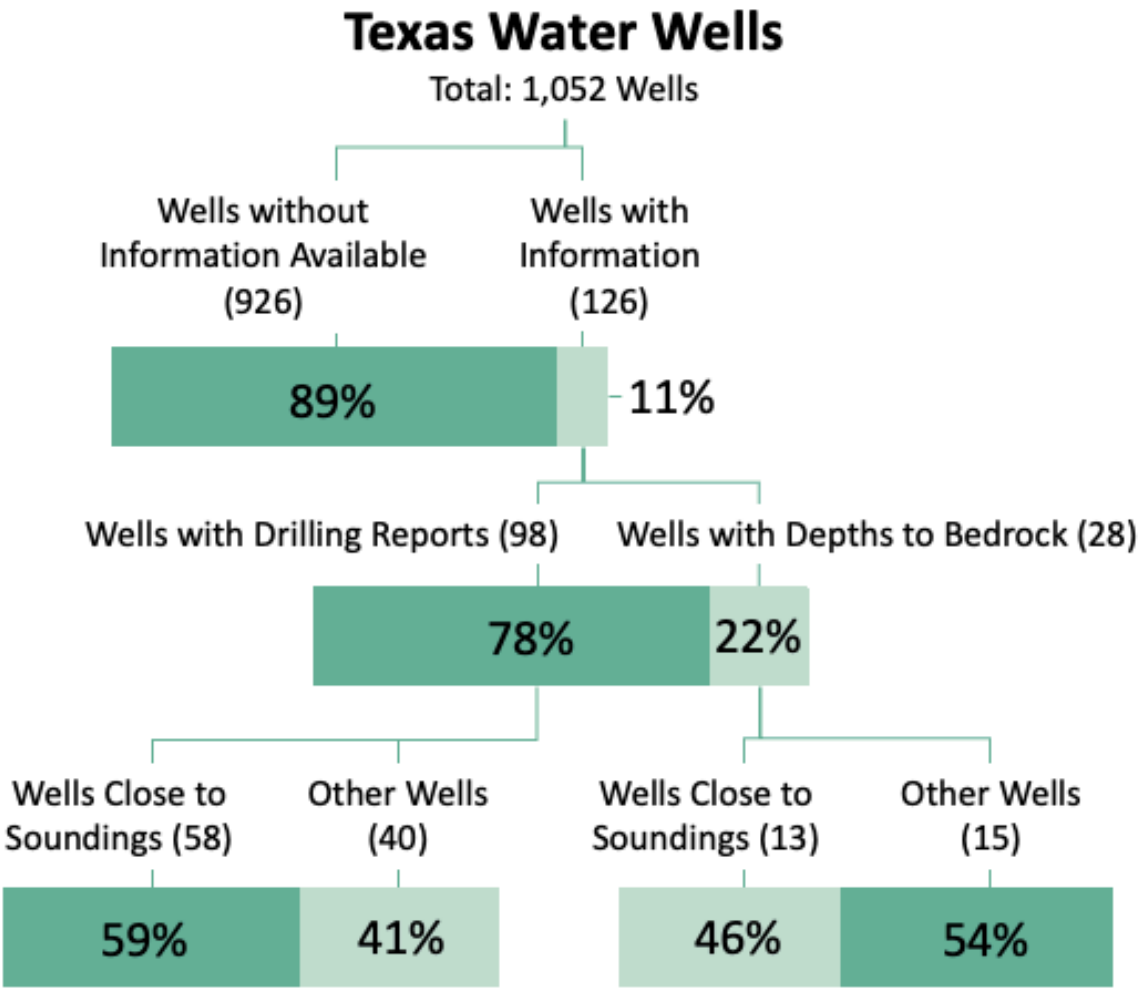

Figure 23. Statistics for Texas Water Wells.
This graph shows the percentages of wells used in this thesis.

Chapter 3: Results

Two different models were created for most soundings. One model matched the geological information available from the area. The second model represented the best fit to the observed data, but in most cases, did not give a geologically plausible fit. These second models were called "Not Accurate" or NA, to differentiate them from the accurate model. This issue provided insight into the depths of resolution for a sounding and aided in determining if the original data could be influenced by 2-D effects (e.g., crossing fault zones).

The soundings represented by length and orientation are shown in Figure 13, and their exact locations can be found in Appendix 1. Plots of the two models obtained for each sounding can be found in Appendix 2, and the notes for each sounding (such as stratigraphy from closest well or cross section) are found in Appendix 3. Note that Figure 24 indicates several soundings (13, 16, 25, 26, 30, 31, 35, 36, 38, 39, 41, 45, 50, 51, 53, 54, 55, 61, 62, 63, and 64) are located near faults or folds and some soundings (12, 21, 43, 56, 57, and 58) were recorded along significant changes in topography (Figure 25).

The results were grouped into 4 different regions.

1. FOOTHILLS OF THE FRANKLIN MOUNTAINS

The soundings in this area (1, 2, 10, 11, 12, 27, 28, 35, 36, 48, and 49) are located between Doniphan Drive and the Franklin Mountains (Figure 26). Bedrock is shallow (2 to 5 m) east of I-10 and increases in depth (up to 130 m) from I-10 west to Doniphan Drive. Water well information indicates that the depth to the water table changes from 35 m on the east to 1 m near Doniphan Drive.

Sounding 1 (Figure 27) is located in the Franklin Mountains foothills, 1.6 km east of I-10. It is one of the closest soundings to the mountains with bedrock expected very near the

surface (< 5m), which is why there are no wells drilled in the area. High apparent resistivity values (> 200 ohm-m) are observed at shallow spacings (< 50 m), but the problem comes when they drop to values < 50 ohm-m at spacings > 50 m. Given we expect massive, non-porous bedrock extending from the surface to great depths (e.g., Hiebing et al., 2018), these low apparent resistivities are not geologically feasible. It is possible that the very high resistivity of the bedrock causes the current to flow laterally at shallow depths rather than to penetrate deeper into the subsurface.

Sounding 12 (Figure 28) shows the same problem (extremely low (< 20 ohm-m) apparent resistivities at spacings > 200 m) but there are different circumstances related to it. It was recorded with an east-west orientation (Figure 25), that follows a significant change in topography, and it is intersected by a fault (Figure 26). Wells around the area show the water table between 28-30 m. These details would be able to explain the inaccuracy of the model. Soundings 35 and 36 are intersected by faults as well (Figure 24).

Sounding 48 poses a special case (Figure 29). As can be seen in Figure 29, the apparent resistivity values keep oscillating in value as well as decreasing with increasing spacing. This is caused by the fact that a part of the sounding was recorded in the vicinity of the complicated 3-D structure of the Three Sisters Andesite outcrop, and the other part continued into the alluvium, parallel to Resler Drive.

2. SOUNDINGS WITHIN THE RIVER VALLEY

These sounding locations in this area (3, 4, 5, 6, 7, 8, 9, 13, 14, 15, 16, 17, 18, 19, 20, 24, 25, 26, 29, 30, 31, 32, 33, 34, 37, 38, 39, 40, 41, and 42) range from roughly Doniphan Drive to the east edge of La Mesa surface and north of Artcraft Road (Figure 30). Based on

water well and other geophysical information, the depth to bedrock is about 200 to 300 m here.

The Mesilla fault is probably located at the western edge of this region, but its location is not well known. Elevated temperatures in water wells located near the suspected Mesilla fault trace indicate the fault might serve as a conduit for deeper (sub-Santa Fe group) water (Hiebing et al., 2018).

The city of El Paso pumps water from this region (Canutillo Well Field), specifically from these three different units: the shallow, the intermediate, and the deep aquifers, that can be differentiated by water table depth, lithology, and groundwater quality. The shallow aquifer does not exceed 30 m in depth and includes the Rio Grande alluvium (Cliett, 1969). The intermediate aquifer is hydrologically similar to the shallow aquifer, with groundwater quality changes being the only characteristic separating the two zones (Cliett, 1969). The deep aquifer (lower Santa Fe group) is about 150 m depth and is hydraulically separated from the other two. Groundwater quality is good in the deep aquifer in the area that covers Anthony to Canutillo (Witcher et al., 2004). To the south of Canutillo the deep aquifer quality is poorer than in the intermediate aquifer, varying from fresh to saline, with salinity increasing in the southern part of the valley (Cliett, 1969).

The deepest aquifer is unusually fined-grained, with well log information indicating resistivities of 12-15 ohm-m. This makes it difficult to use resistivity information alone to determine water salinity changes within the aquifer (Arunshankar, 1993).

As described above, soundings in this region are difficult to model, so we had to refer to drilling reports. Sounding 9, for example, showed a complicated pattern that we attributed to a lateral inhomogeneity (Figure 31). After studying a few drilling reports from wells

located in the area, we found out that there was a layer of clay likely responsible for the observed low apparent resistivity values. Once this information was incorporated into the model, we obtained a good fit. The drilling reports observed a layer of conglomerate and limestone at about 300 m depth, but this was not detected in the observed apparent resistivity data.

Sounding 13 is located next to the Rio Grande River (Figure 32). It is intersected by a fault and the water table is found at 6 and 18 m depth. A drilling report indicates that there is a layer of gravel between 5 and 40 m that is reflected in the higher apparent resistivities observed between spacings of 10 and 100 m (Figure 32). The rest of the well report indicated interbedded sands and clays at depth.

The only sounding of my study that was not reprocessed is Sounding 14. The sounding curve is strongly distorted and according to Al-Garni (1996), this same level of distortion has been observed before, when a wired mesh was buried near the sounding origin.

Sounding 25 is a good example of apparent resistivities found in the Doniphan Drive area. There is a lot of near-surface clay along this road, and it is known to present drainage problems after it rains. Drilling reports show clay layers with only one sand and gravel layer located between 5 and 10 m of depth. After incorporating this information into our resistivity model, we obtained an accurate fit (Figure 33).

Soundings 13, 16, 25, 30, 31, 39, and 41 are intersected by faults (Figure 24) but none of the region's soundings are affected by topographical changes.

3. SOUNDINGS IN THE SOUTHERN MESILLA VALLEY

These soundings (46, 47, 50, 51 fix, 52, 53, 54, 55, 56, 57, and 58) are located south of Artcraft Road (Figure 34). The bedrock is near the surface (less than 30 m) in a few areas, and the influence of igneous intrusives in the bedrock that are related to the Campus Andesite volcanism is significant. Water salinities exceed 2,000 ppm in this region and the levels of other minerals (such as As), are also high (Hiebing et al., 2018). The water table here is found at between 3 and 80 m depth.

Soundings 47 and 50 (Figures 34, 35 and 36) were recorded parallel to each other 150 m apart with the same orientation. Their apparent resistivities look similar and both show a high resistivity structure (70 to 75 ohm-m) at the same depth (220 - 250 m), with resistivity values decreasing after that.

Sounding 51 is located between Doniphan Drive and the Rio Grande River with an East-West orientation (Figure 37). This is the only sounding covering a specific area known for groundwater with a high salinity index. There is a water reservoir 100 m north, and a canal 100 m to the south of the sounding. The sounding was difficult to model due to the low apparent resistivity values observed and resistivity structure can only be resolved to about 200 m depth. Note that there are high in apparent resistivities observed in the last four measurements, making it consistent with the geology.

Soundings 54 and 55 (Appendix 2) were recorded close to each other (Figure 39), and so both models look similar with high resistivities (47 to 90 ohm-m) in the northwest. Modeling suggests that I am unable to resolve structures at greater than 50-60 m depth.

Soundings 56, 57, and 58 extend from the river valley to the La Mesa surface, crossing a change in topography of around 55 m. Sounding 58 is best matched by a shallow

(4 m depth) resistive layer (160 ohm-m) but because of its location, it is not likely it is bedrock (Figure 38). Soundings 50, 51, 53, 54, and 55 are intersected by faults (Figure 24).

4. LA MESA SURFACE

The La Mesa region includes soundings 21, 22, 23, 43, 44, 45, 59, 60, 61, 62, 63, 64, and 65 (Figure 39). In this area, water is found at about 100 m depth. Bedrock is found at about 400 m depth (Hiebing et al, 2018). Some of the soundings in this region cross faults (45, 62, 63, and 64) (Figure 24) or significant changes in topography (21 and 43) (Figure 39).

Soundings 21 and 22 appear different even though they were recorded close to each other, but both are best modeled with a resistive layer (170 to 340 ohm-m) in the first 10 m depth (Figures 40 and 41). Sounding 23 is also close to 21 and 22 but recorded perpendicular to the others and is best modeled with the high resistivity layer (Figure 42). The same high resistivity pattern is seen in the interpretations of soundings 43, 44, and 45. Soundings 43 and 44 are close to each other (Figure 39) and recorded with the same orientation while 45 is perpendicular to them (Figures 43, 44, and 45). Soundings 62, 63, 64, and 65 look very similar and are best modeled by high resistivity values (Appendix 2).

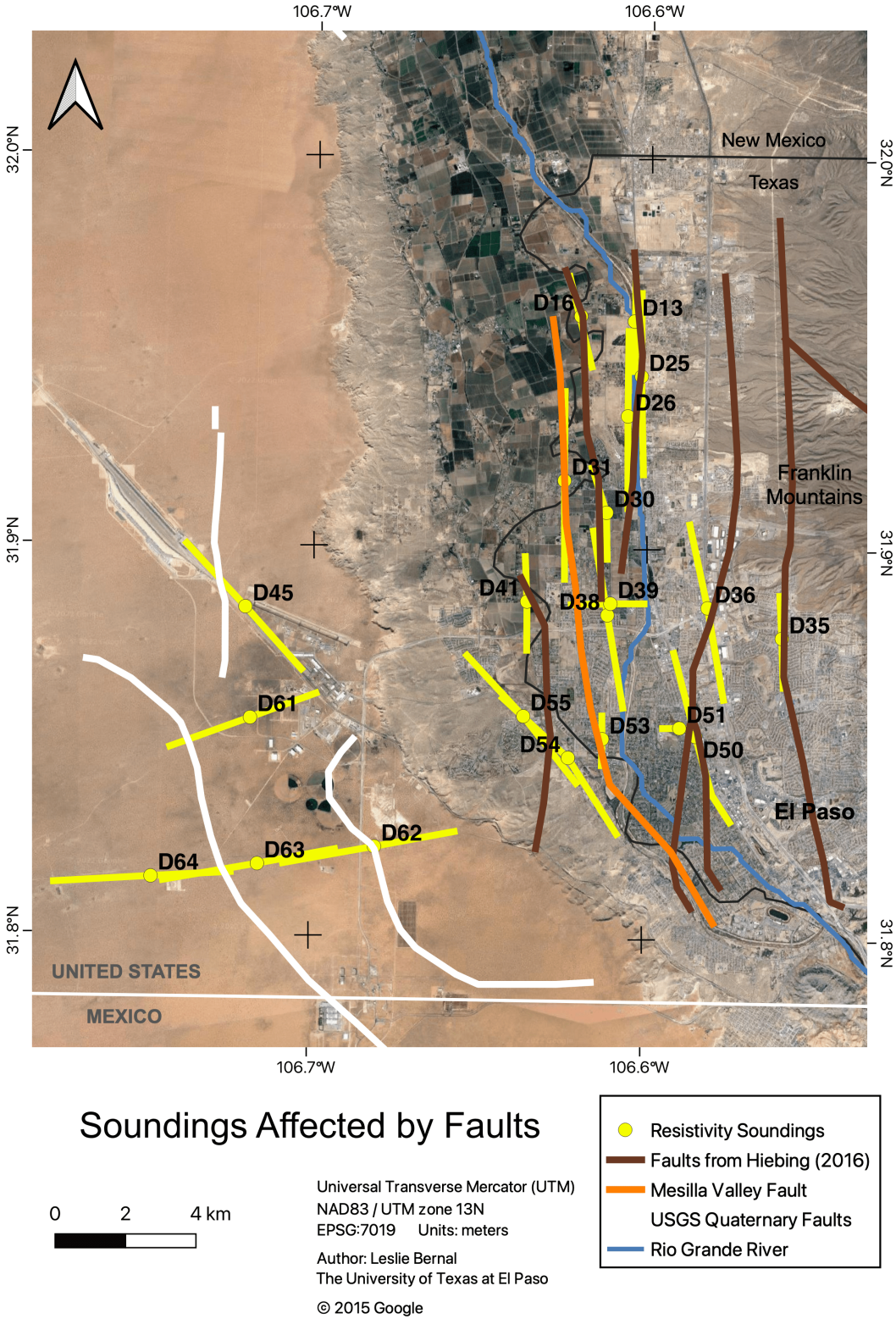

Figure 24. Soundings Affected by Faults.
This map shows all the soundings affected by mapped or suspected faults.

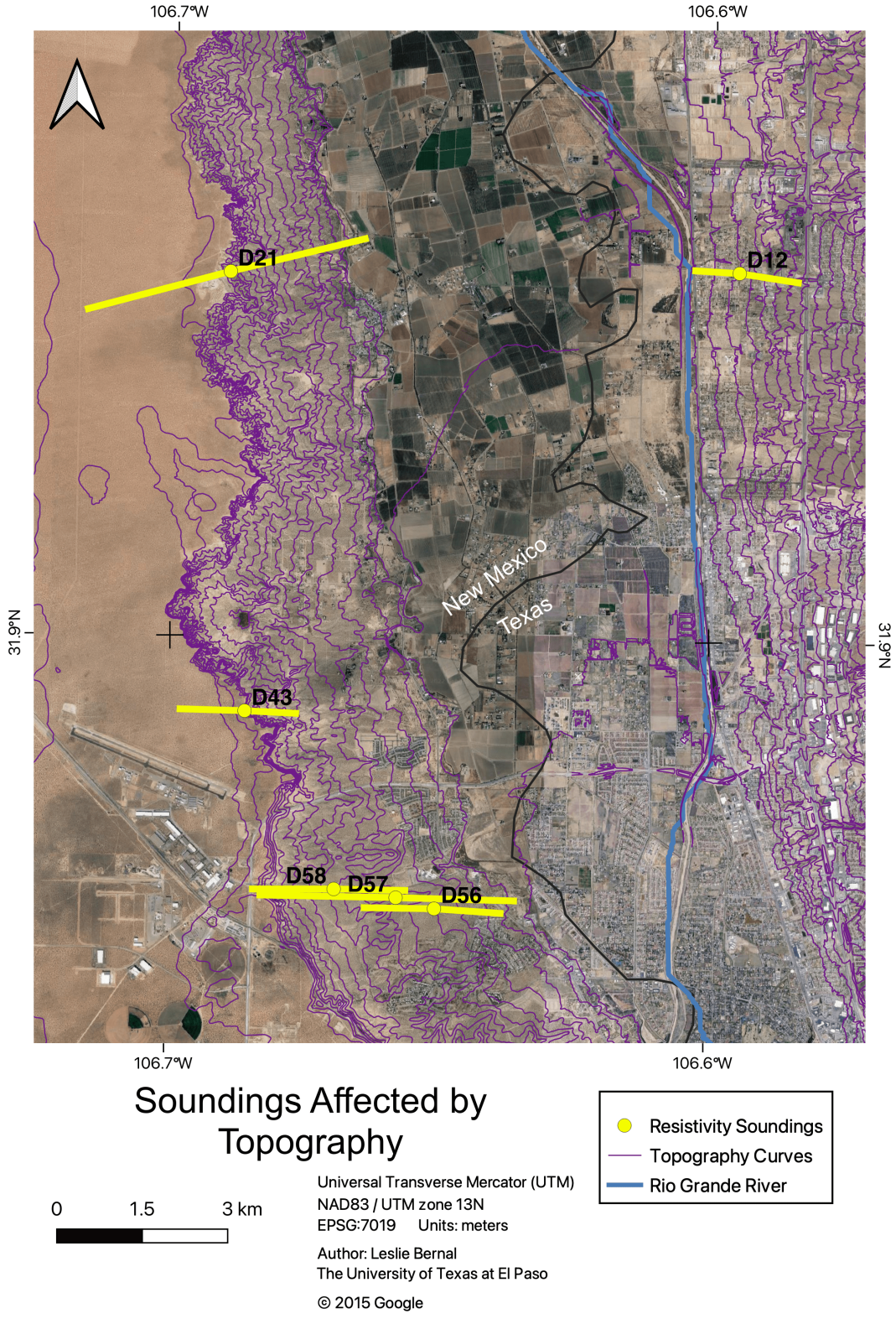

Figure 25. Soundings Affected by Topography.
This map shows all the soundings affected by large changes in topography (from 5 to 100 m).

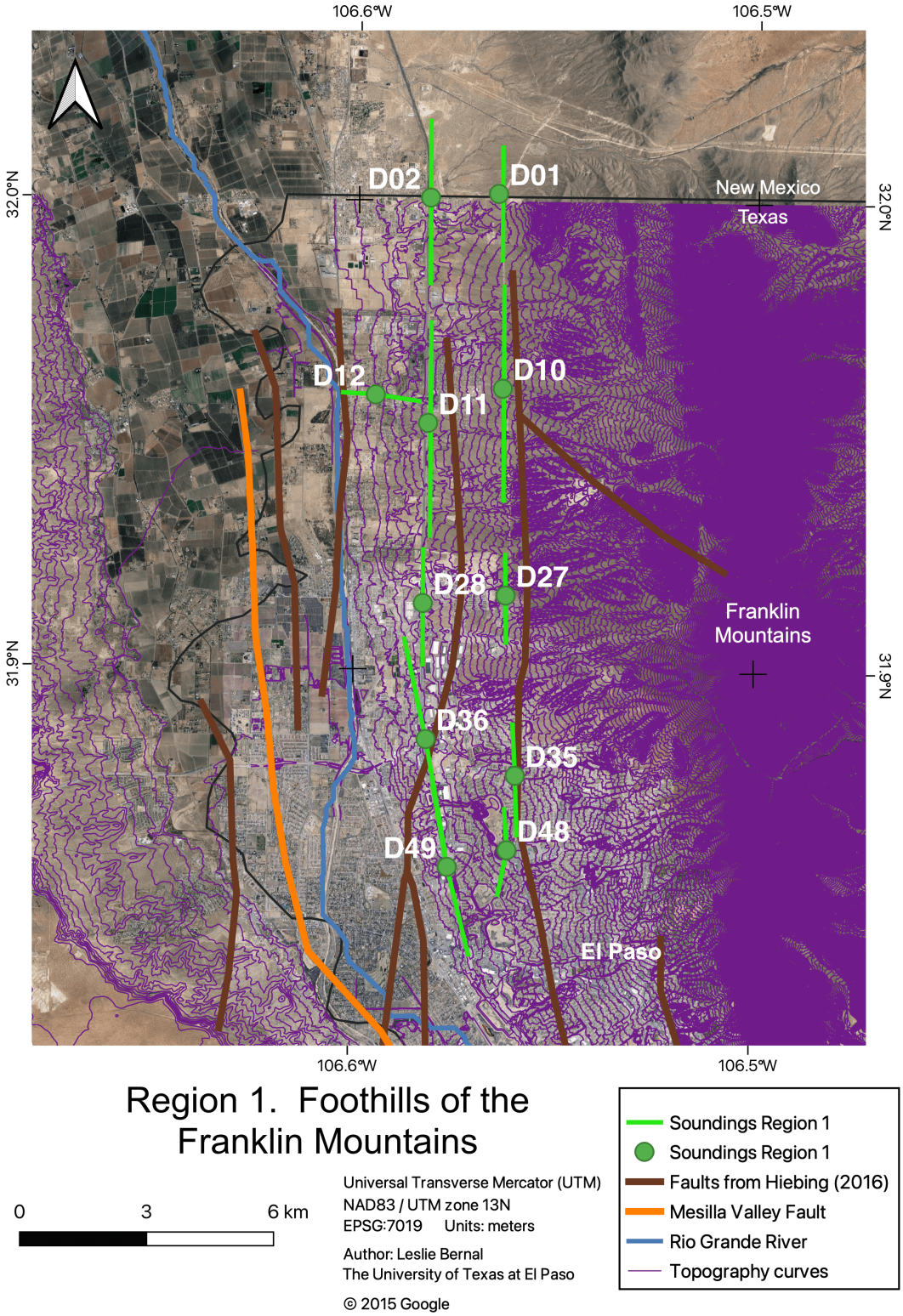

Figure 26. Region 1 - Foothills of the Franklin Mountains.
This figure shows the soundings belonging to Group 1, which are located the closest to the Franklin Mountains.

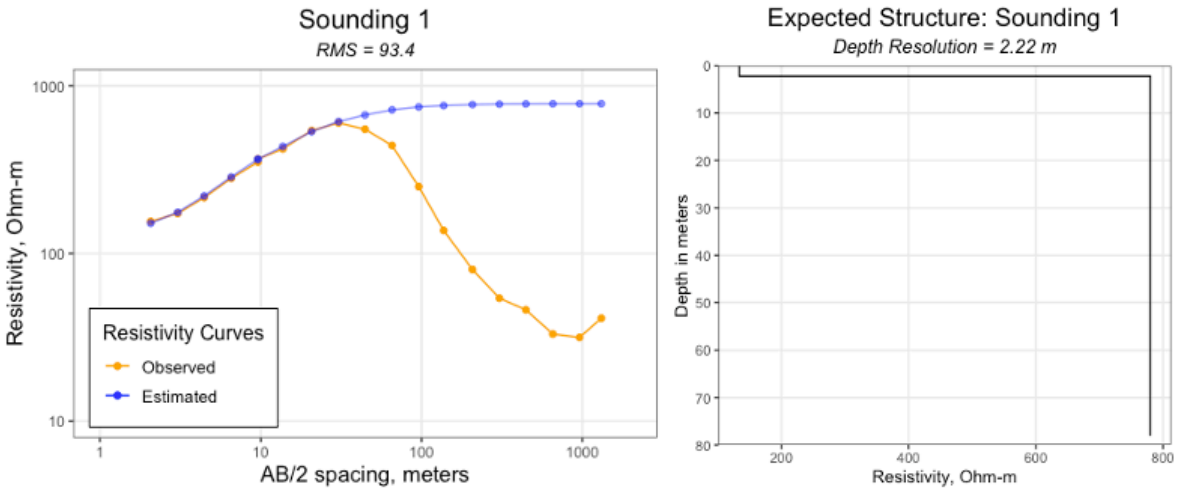

Figure 27. Sounding 1 (left) with Resistivity-Depth Structure (right).

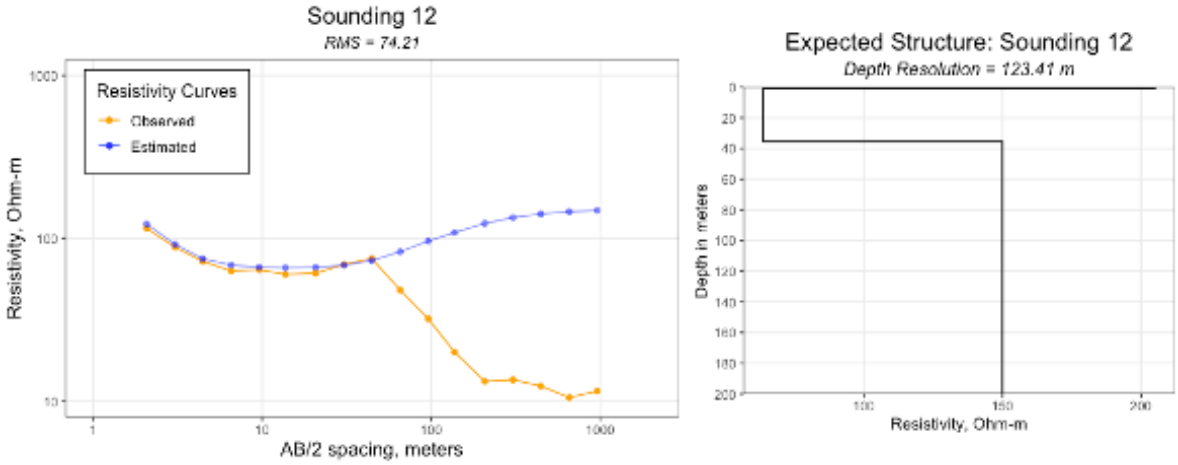

Figure 28. Sounding 12 (left) with Resistivity-Depth Structure (right).

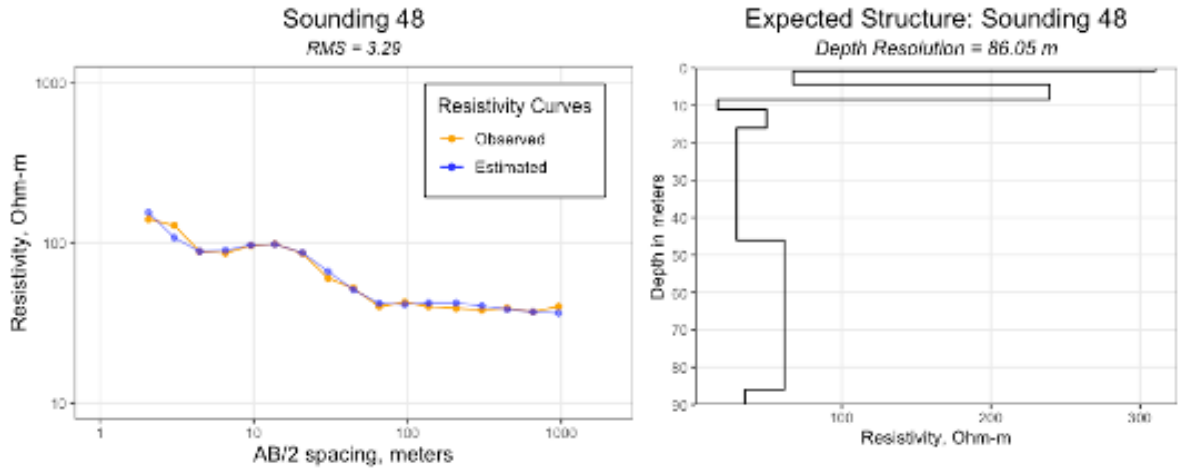

Figure 29. Sounding 48 (left) with Resistivity-Depth Structure (right).

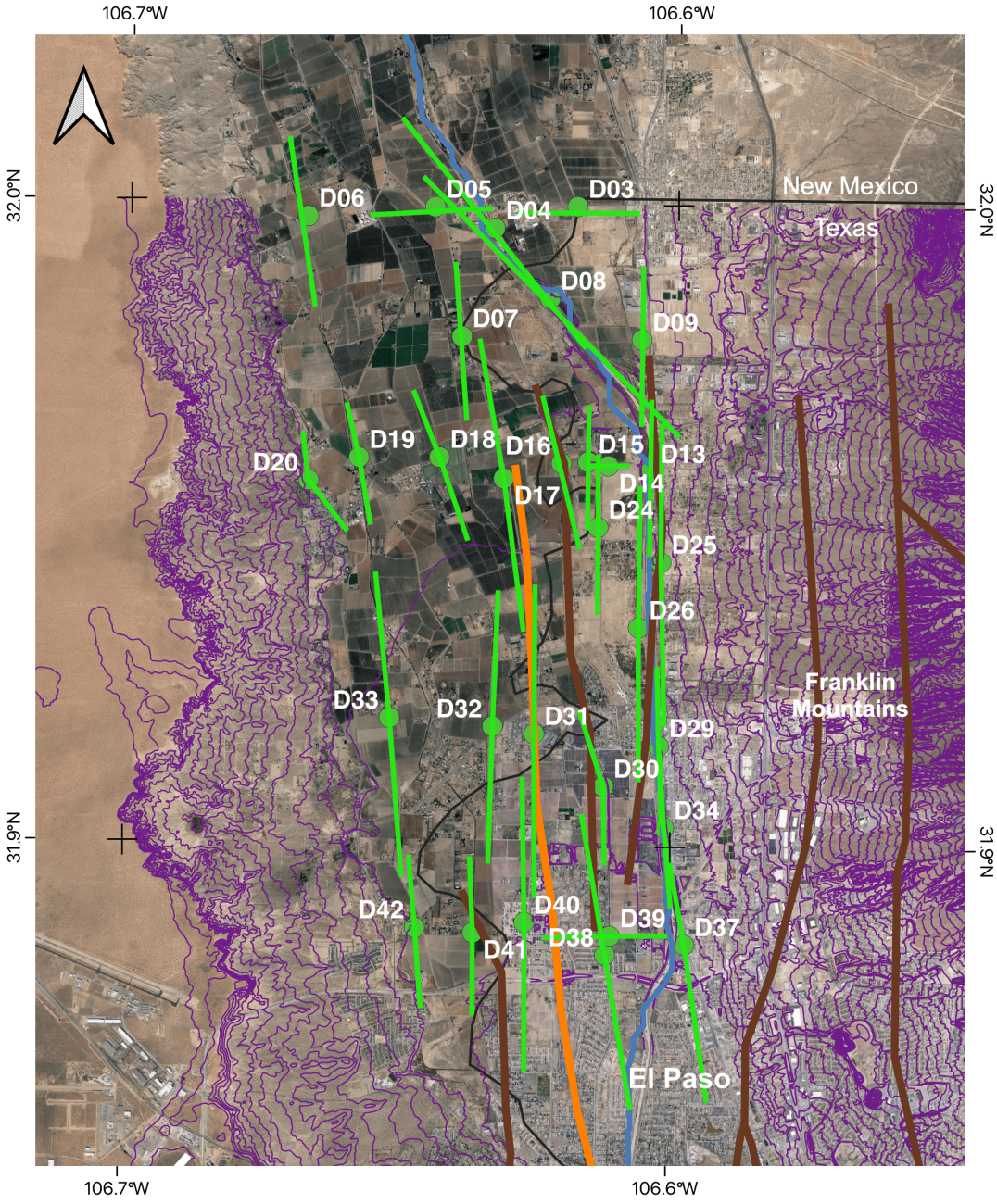

Region 2. River Valley

Figure 30. Region 2 - River Valley.

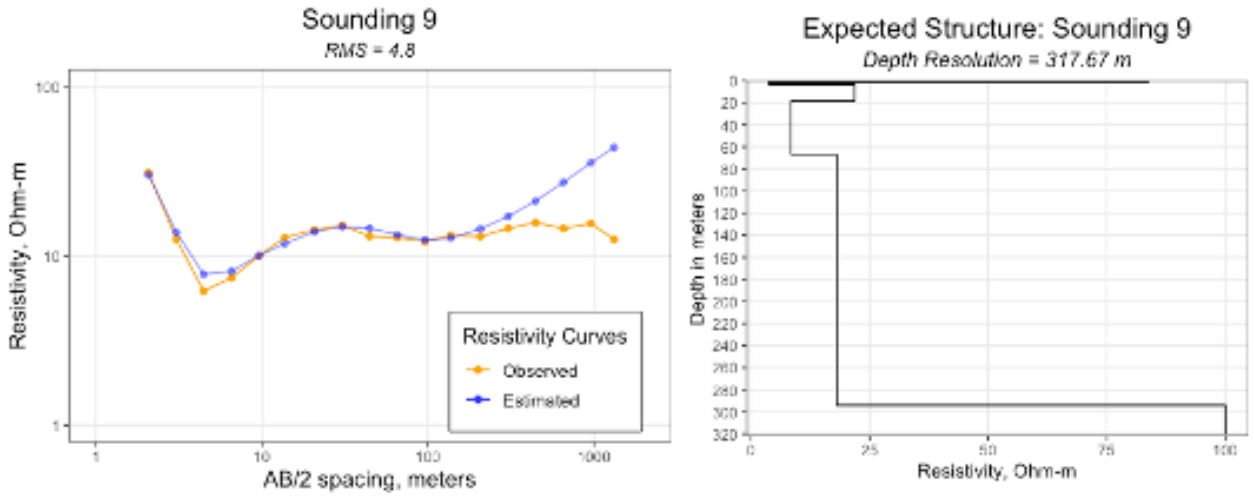

Figure 31. Sounding 9 (left) with Resistivity-Depth Structure (right).

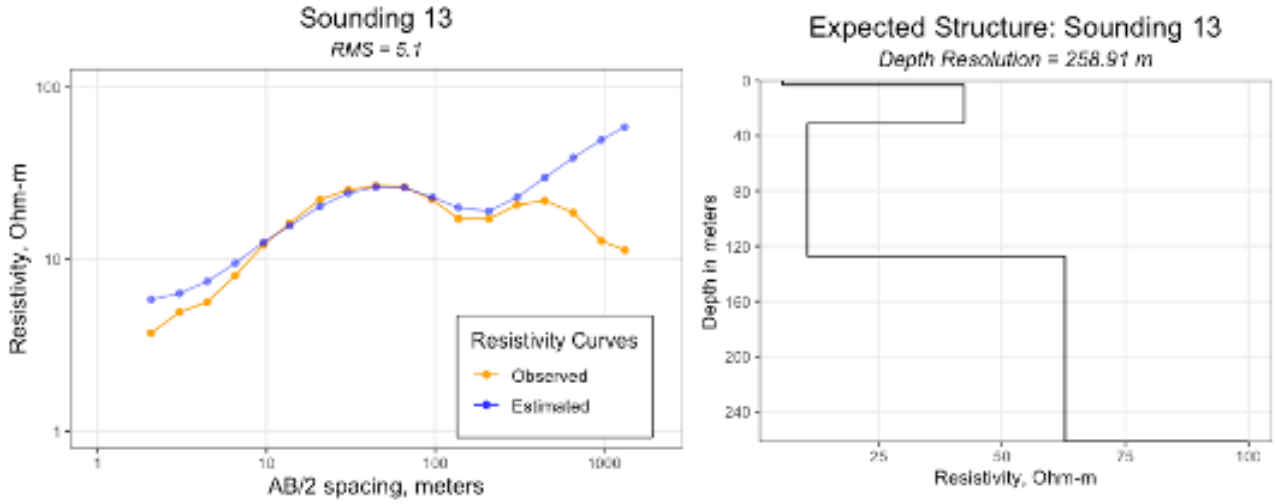

Figure 32. Sounding 13 (left) with Resistivity-Depth Structure (right).

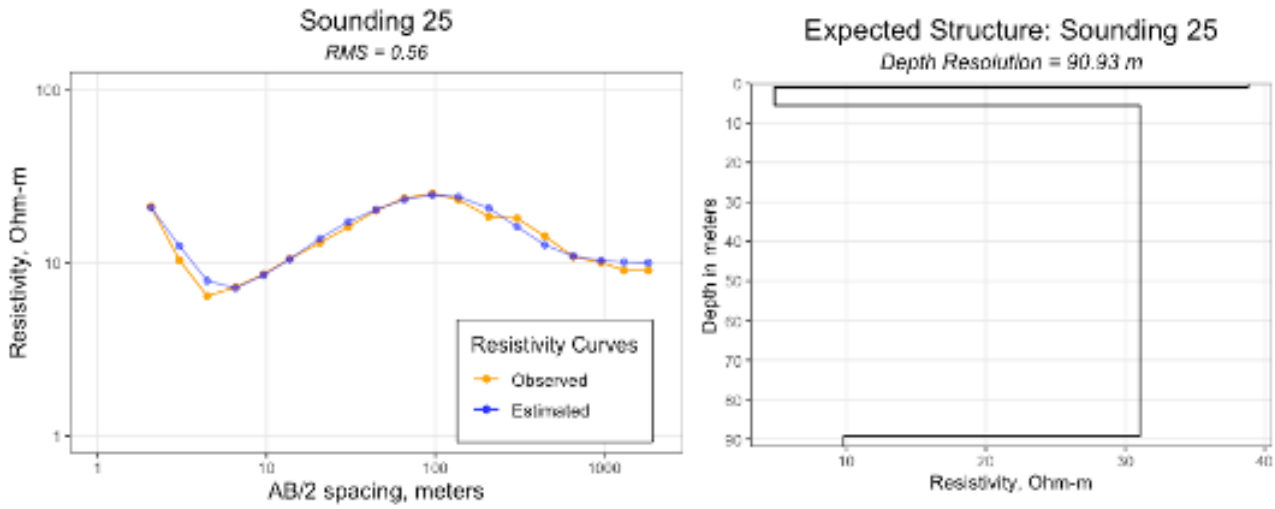

Figure 33. Sounding 25 (left) with Resistivity-Depth Structure (right).

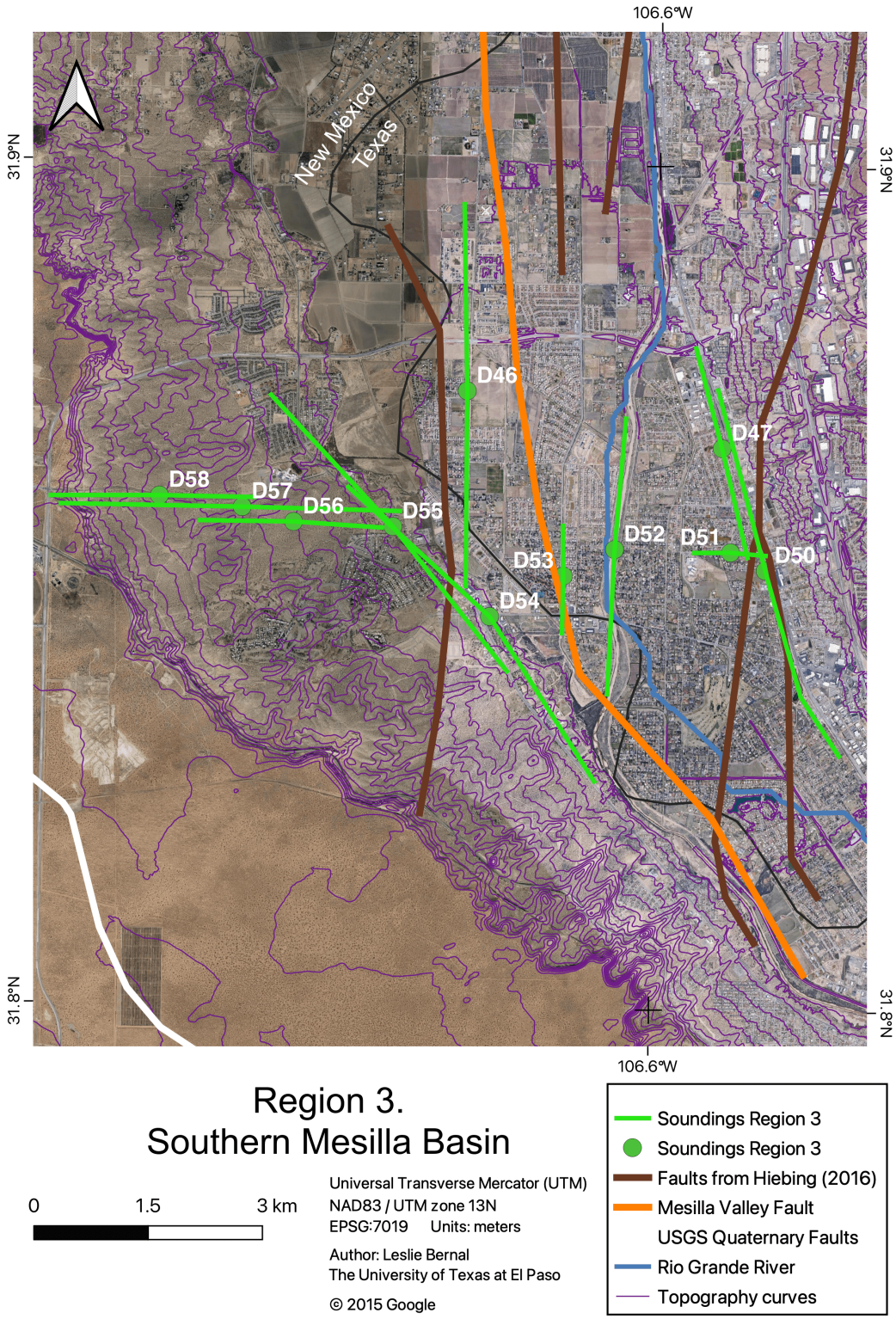

Figure 34. Region 3 - Southern Mesilla Basin.
The white line on the figure is a Quaternary fault mapped by the USGS.

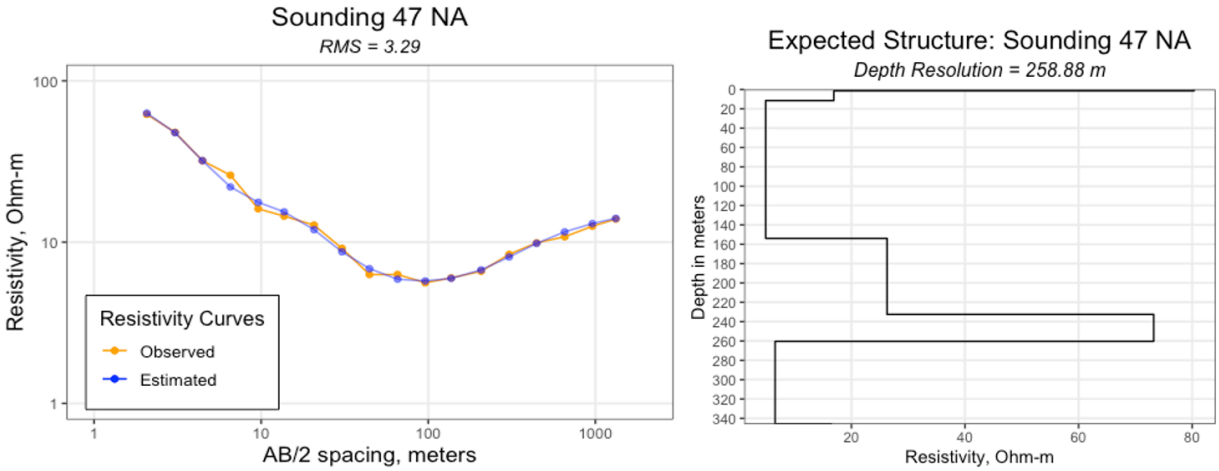

Figure 35. Sounding 47 (left) with Resistivity-Depth Structure (right).

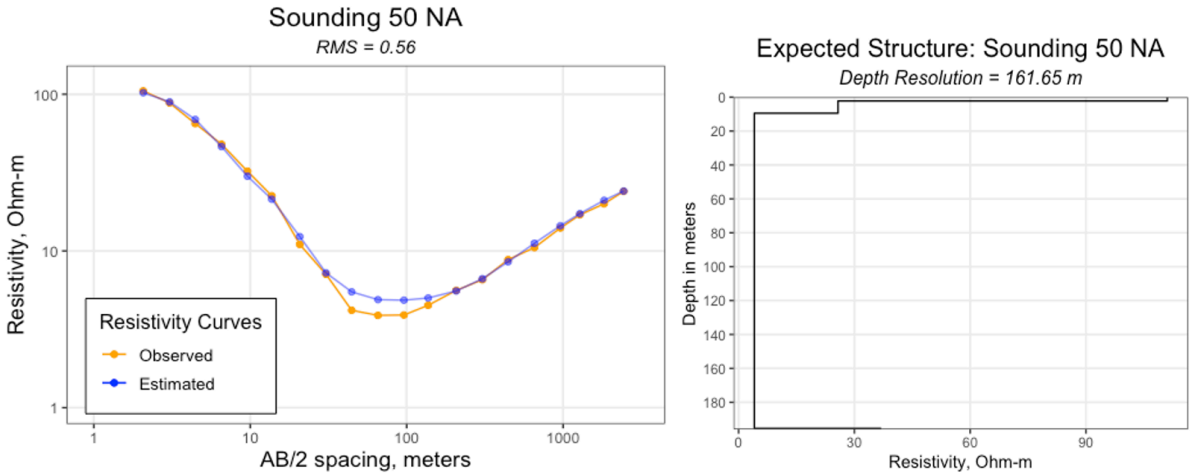

Figure 36. Sounding 50 (left) with Resistivity-Depth Structure (right).

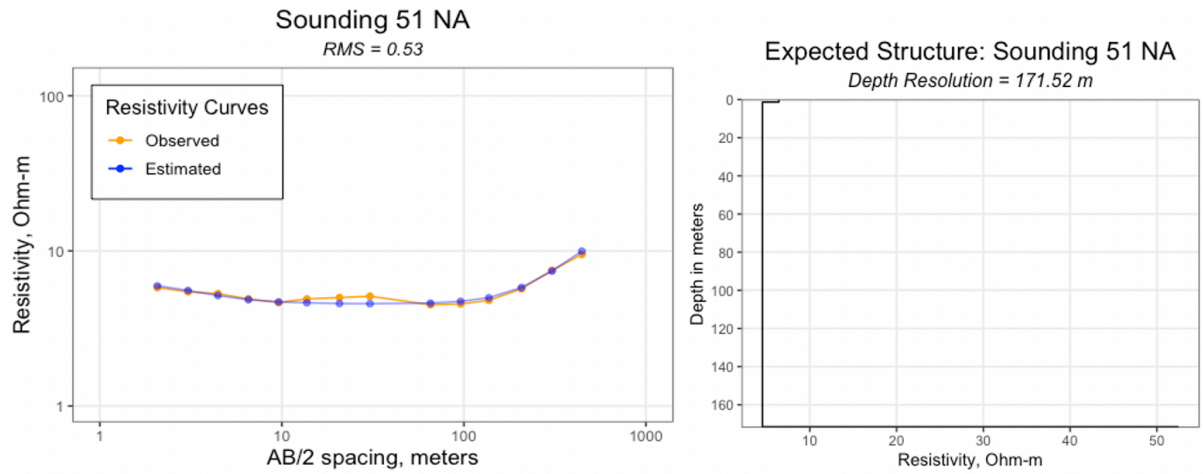

Figure 37. Sounding 51 (left) with Resistivity-Depth Structure (right).

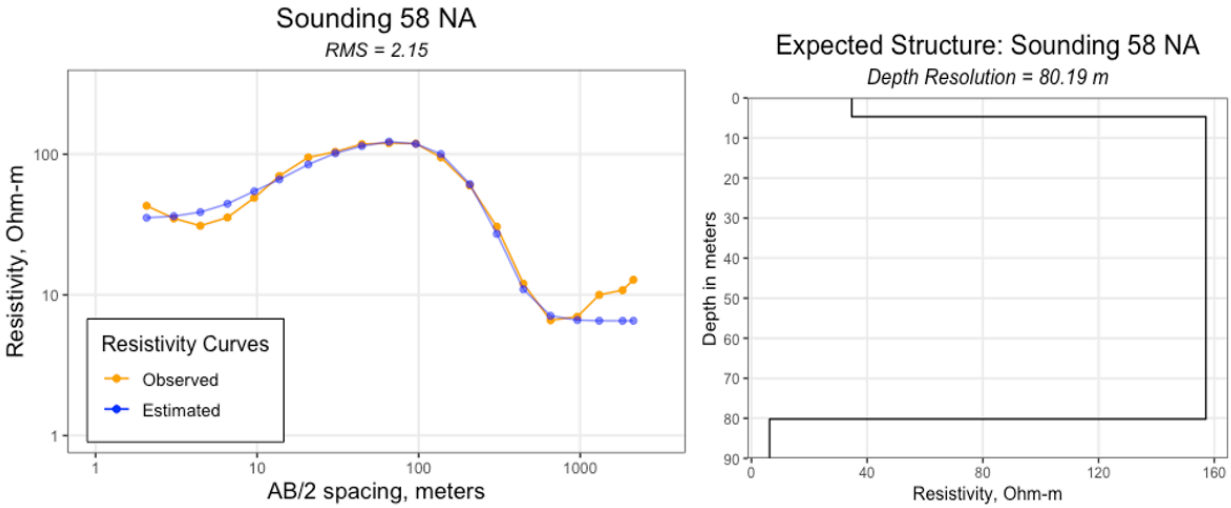

Figure 38. Sounding 58 (left) with Resistivity-Depth Structure (right).

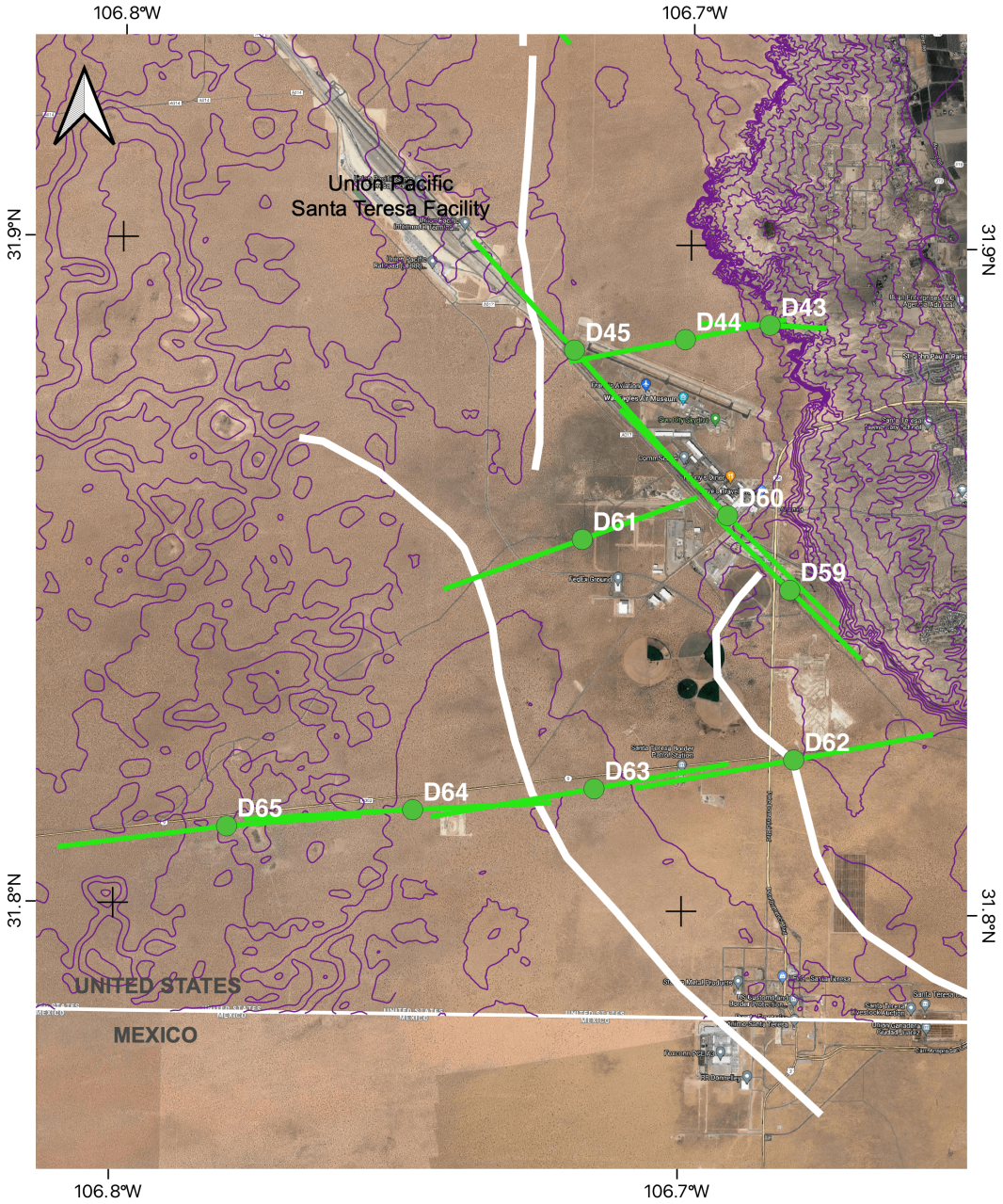

Figure 39. Region 4 - La Mesa.
The white lines represent Quaternary faults mapped by the USGS.

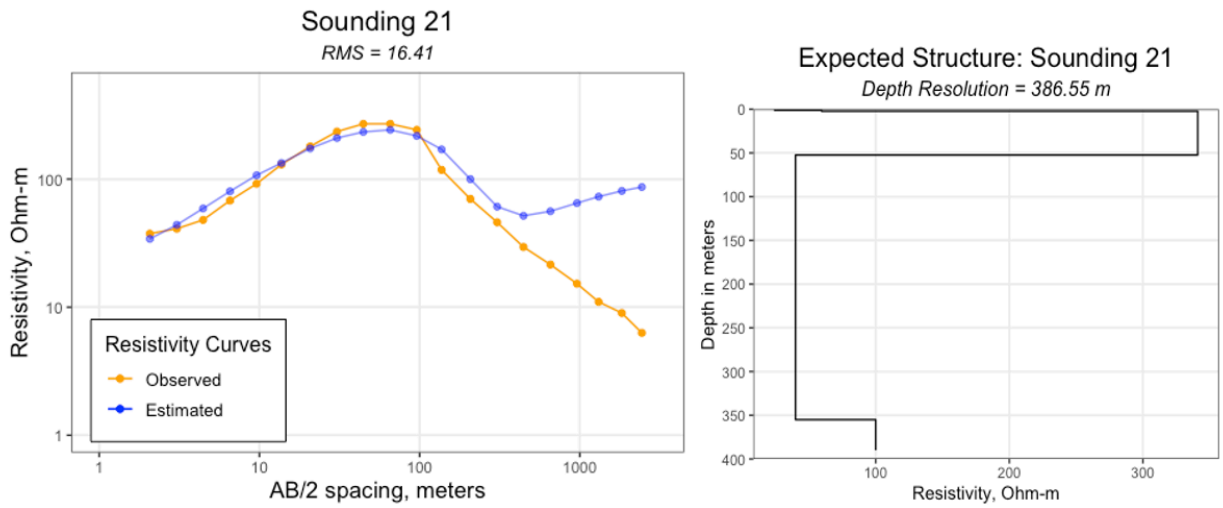

Figure 40. Sounding 21 (left) with Resistivity-Depth Structure (right).

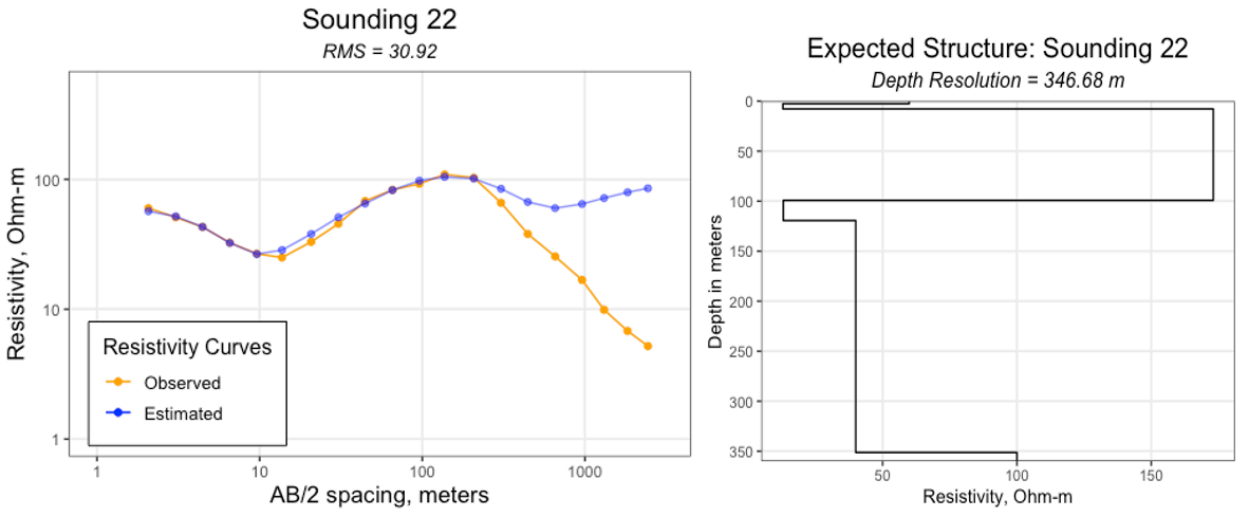

Figure 41. Sounding 22 (left) with Resistivity-Depth Structure (right).

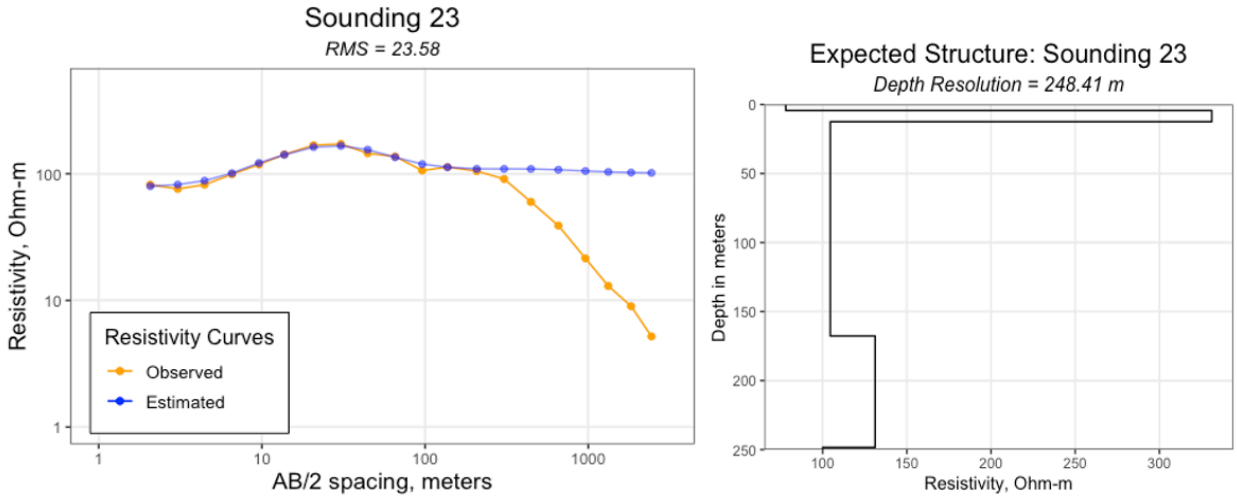

Figure 42. Sounding 23 (left) with Resistivity-Depth Structure (right).

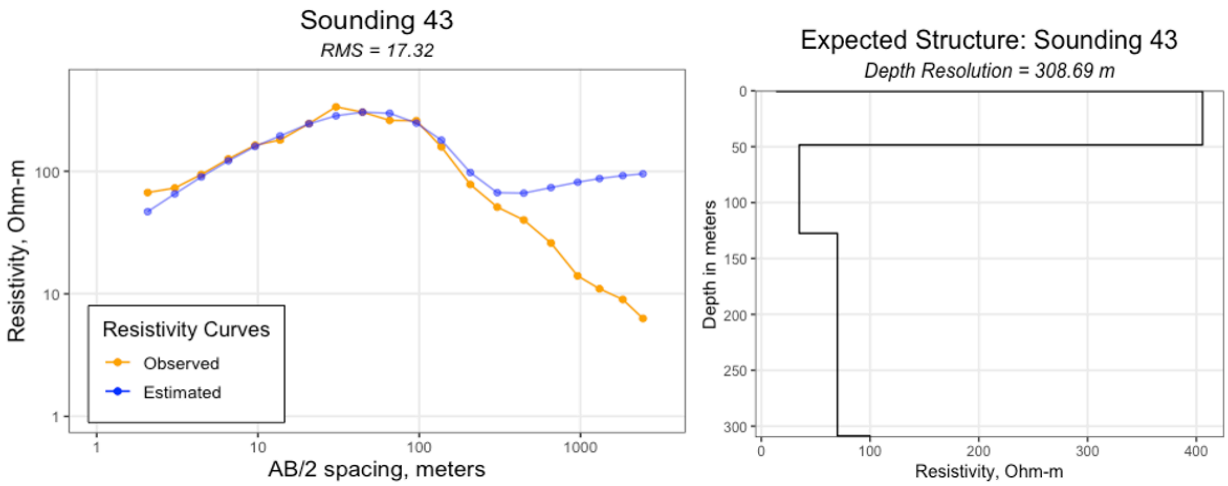

Figure 43. Sounding 43 (left) with Resistivity-Depth Structure (right).

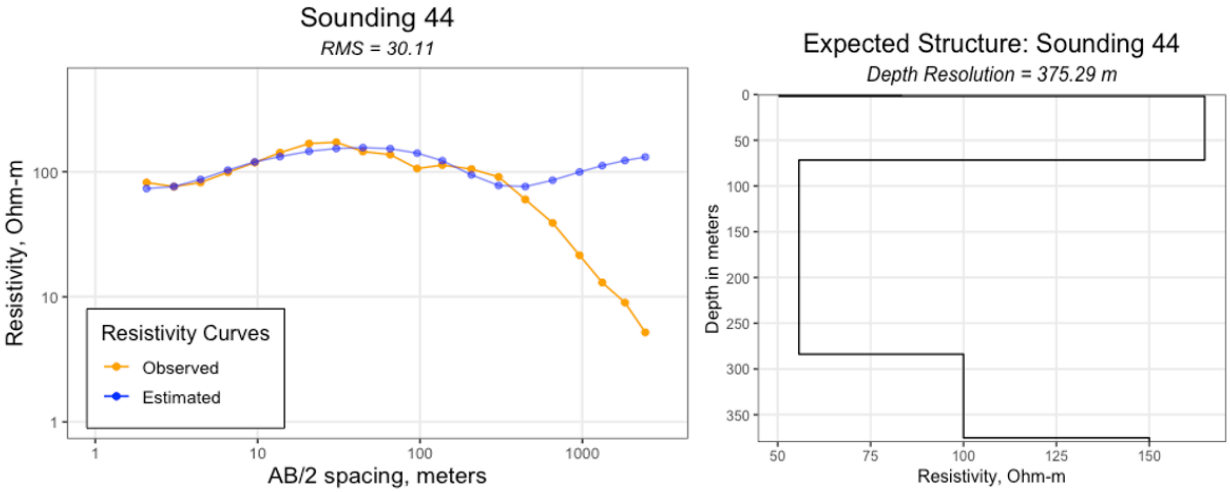

Figure 44. Sounding 44 (left) with Resistivity-Depth Structure (right).

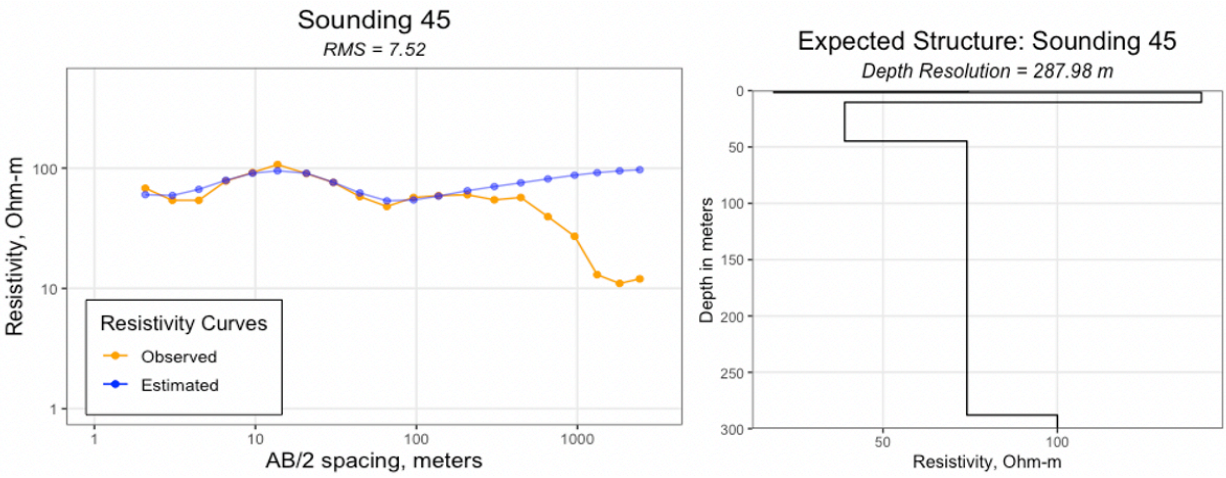

Figure 45. Sounding 45 (left) with Resistivity-Depth Structure (right).

Chapter 4: Discussion

This thesis has focused on reprocessing resistivity soundings to obtain results that are consistent with the known geology of the Mesilla Valley. As with all geophysical data, resistivity interpretations are non-unique, with multiple models capable of fitting the observed soundings.

In order to better classify how well my resistivity models (based on known geology) fit the observed soundings I classified them according to their Root Mean Square error (RMS) (Figure 46), and the difficulty I had when I was modeling them (Figure 47). The difficulty classification considers which soundings I had troubles processing because of issues like the absence of wells or geological profiles near soundings to help constrain the subsurface geology or the presence of known fault systems intersecting the sounding locations.

Sounding 27 is an example of a difficult modeling. Figure 48 shows how the electric current dissipates after finding a resistive layer (limestone). The RMS map (Figure 46) indicates a high percentage of error because a reasonable geologic model could not be fit to the sounding curve, and the difficulty map (Figure 47) classifies the model as a partial fitting. In contrast, sounding 51 is an example of a good result that was easy to model (Figure 49). The resistivity values reflected the known characteristics of the area such as high contents of clays and salts in the top layers. Figure 49 shows near surface low resistivity values that then increase with depth. The RMS map indicates a low error, and the difficulty map shows a good fit.

While many models determined by Al-Garni (1996) fit the data better than my final models (see Appendix 2), Al-Garni's results often were not geological plausible; here are some of the geologic features that may be causing the mismatches:

- Surface topography – The largest changes in topography are seen in La Mesa area, going from 20 to 110 m.

- Crossing Fault Zones – Mesilla Valley Fault, Quaternary faults, and other faults detected by different authors (Figure 24).
- Bedrock topography – This mainly affected the soundings from Group 1 (Foothills of the Franklin Mountains).
- Extremely high resistivities causing current to flow sideways rather than deeper into the ground as sounding spacing is increased – This effect was only seen in soundings from Group 1.
- The time of the year when the soundings were taken - Near surface moisture can influence the estimated values for deeper layers (Arunshankar, 1993). All soundings were affected by this.

Another example is unacceptably low values of resistivity at depths within the bedrock. Al-Garni's models go to depths that are not likely resolved using the rule of thumb (maximum depth of penetration is 1/3 to 1/5 maximum current electrode spacing). For example, Al-Garni's cross-section that covers soundings 62, 63, 64, and 65 (Figure 50) noted a resistivity of 3 ohm-m at 500 m depth. Well information (or geologic profiles) in this region indicate limestone bedrock occurs at a depth of 500 m. Using the Indonesia equation, first introduced by Poupon and Leveaux (1971), we can estimate the porosity of limestone at 500 m depth based on Al-Garni's model:

$$\frac{1}{\sqrt{R_t}} = \sum_i \frac{V_i^{\left(1-\frac{V_i}{2}\right)}}{\sqrt{R_i}} = \frac{V_w}{\sqrt{R_w}} + \frac{V_{hc}}{\sqrt{R_{hc}}} + \sum_i \frac{V_i^{\left(1-\frac{V_i}{2}\right)}}{\sqrt{R_i}}$$

Where R_t is the total resistivity, R_w is the resistivity of water, R_{hc} is the resistivity of any hydrocarbons, R_i is the resistivity of minerals in the rock matrix, V_w is the volume fraction of the water formation, V_{hc} is the volume of hydrocarbons and V_i is the volume fraction of minerals in the rock matrix.

When the volume of hydrocarbons is zero and the rock is pure limestone (lm) the above equation reduces to:

$$\frac{1}{\sqrt{R_t}} = \frac{V_w}{\sqrt{R_w}} + \frac{V_{lm}^{\left(1-\frac{V_{lm}}{2}\right)}}{\sqrt{R_{lm}}}$$

In the lowermost Mesilla Valley, the saline groundwater has a resistivity of about 0.5 ohm-m and limestone has a resistivity of around 3000 ohm-m (see Table 4). Thus:

R_t = 3 ohm-m (from Al-Garni's model)

R_w = 0.5 ohm-m

Rlm = 3000 ohm-m Standard resistivity for limestone

Solving for V_w (the volume fraction of water – i.e., porosity) we obtain a volume fraction of 41%. It is geologically implausible for rocks at 500 m depth would have these great of porosities, suggesting the low apparent resistivity values (< 5 ohm-m) observed at large spacings (> 100 m) for some soundings are erroneous. Given the extremely high resistivity values for bedrock (limestones or volcanics) it is likely that the current at these large spacings could not easily penetrate into the deep subsurface but rather flowed into other, lower, shallower resistivity units located out of the plane of the sounding line.

Soundings that crossed faults or major changes in topography (> 10 m) also would violate the assumption that the current flowed through a simple 1-D, layered Earth. Some shifts in the modeled resistivity layering observed between soundings in the La Mesa region could be related to the presence of faults.

Figure 52 shows a groundwater flow map for the Mesilla Basin, but as most flow maps available, no one has considered how faults control the flow. Budhathoki et al. (2018), established that the location of freshwater and saline water in the Hueco Bolson is controlled by

structural changes. Upwelling of saline water, despite its location close to the mountains recharge zones, occurs because a fault fractured and uplifted deeper basin sediments containing higher salinity water (Budhathoki, 2018). If this is the case in the Hueco Bolson, it would not be unreasonable to assume that the same process happens in the Mesilla Basin area, considering that it is an active rift zone.

I also estimated depths of penetration during the modeling process. When I was modifying the parameters for the model (thickness of layers and their correspondent resistivity values), I had to adjust the curve of predicted data to the observed data points. This curve moved up and down until I was able to fit it to the observed data with the least RMS error. When I tried to use models extending to depths greater than 300 to 400 m, the model stopped responding to these deeper changes. After trying different scenarios, I concluded that any modifications made below those depths were not affecting the model at all, so I took that limit as the depth of resolution. Figure 53 as well as Appendix 1 show the depths of resolution of each sounding. I have a maximum resolution of ~ 400 m, and a couple cases with just ~ 2 m of resolution. The average lies between 100 to 300 m.

If we take into consideration that the average sounding length is ~ 2 km then our maximum depth of resolution should be 400 to 666 m (which is 1/3 to 1/5 the maximum electrode spacing). However, my modeling results suggest depths of resolution (100 to 300 m) that are considerably less than the "rule of thumb" estimates. Different factors could be responsible for this diminished depth of penetration, such as lack of sufficiently strong electrical currents during field operations,

but we cannot determine this, because the equipment specifications and similar details from when the survey was taken are unknown.

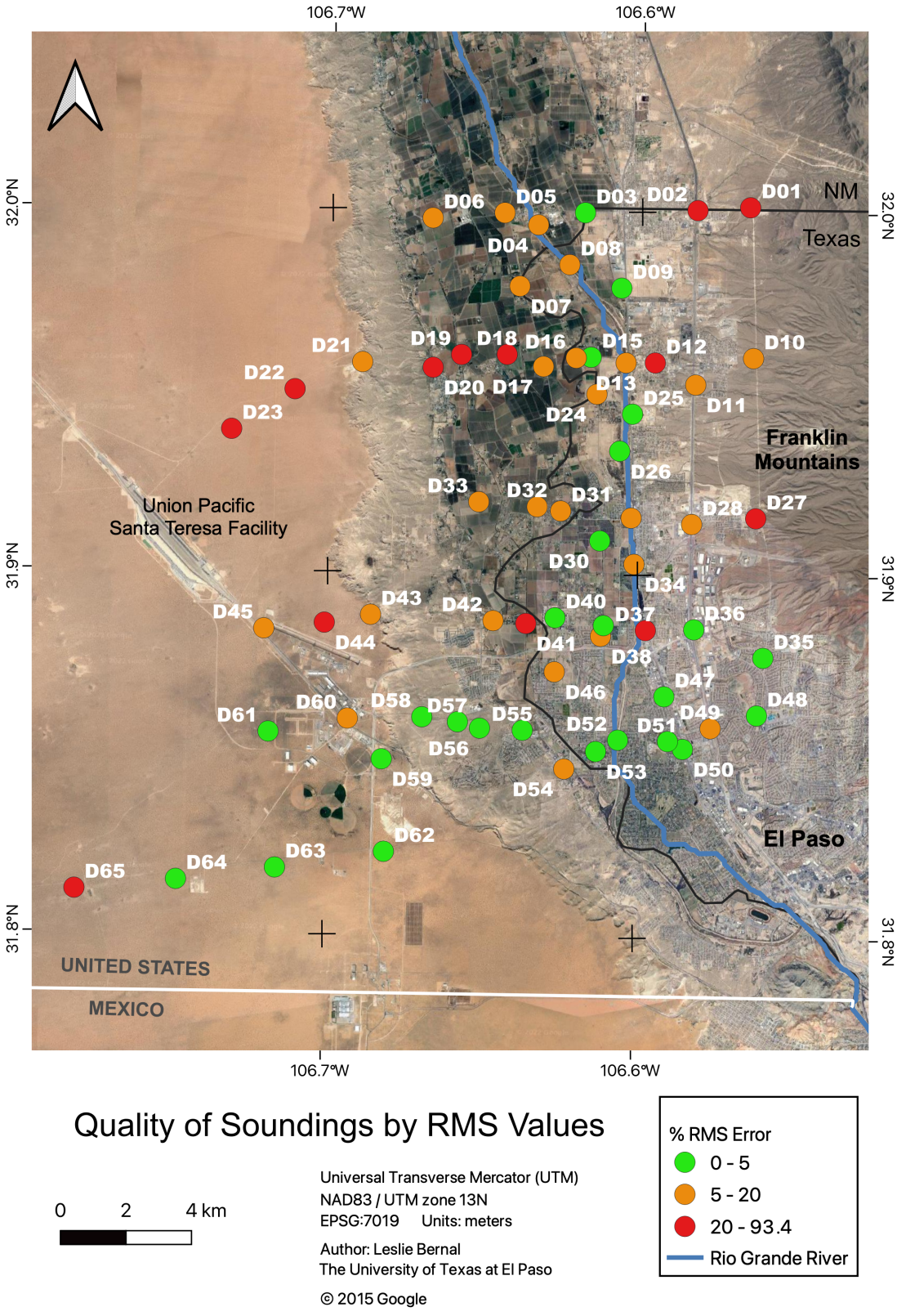

Figure 46. RMS Classification.
This map shows the resistivity soundings classified according to their RMS (error) values.

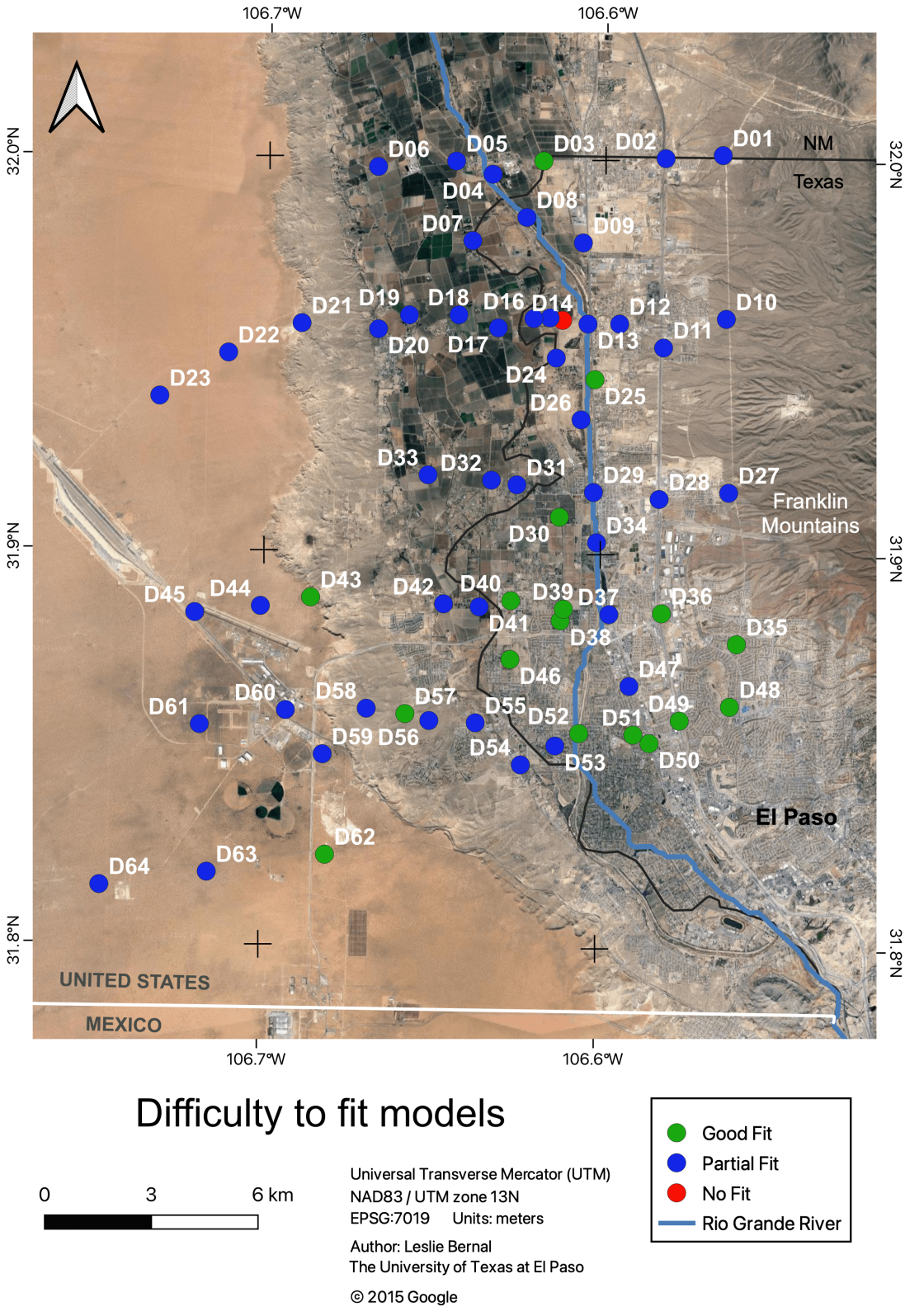

Figure 47. Difficulty Classification.
This map shows the resistivity soundings classified according to the level of difficulty I had when processing them. See text for further details.

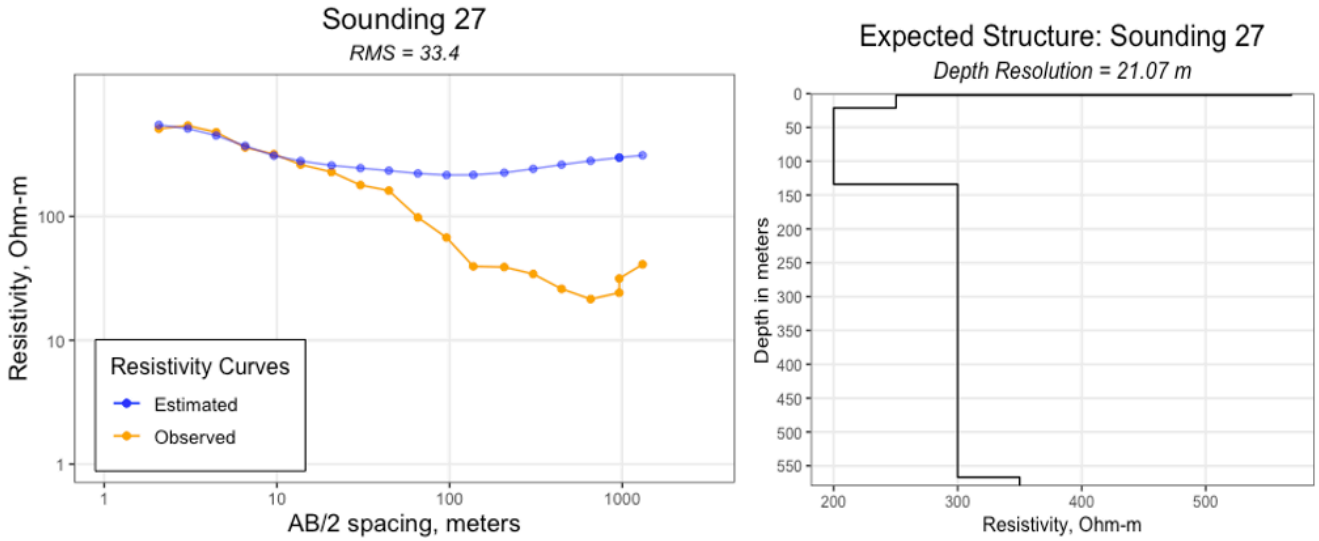

Figure 48. Sounding 27.
Example of a difficult model.

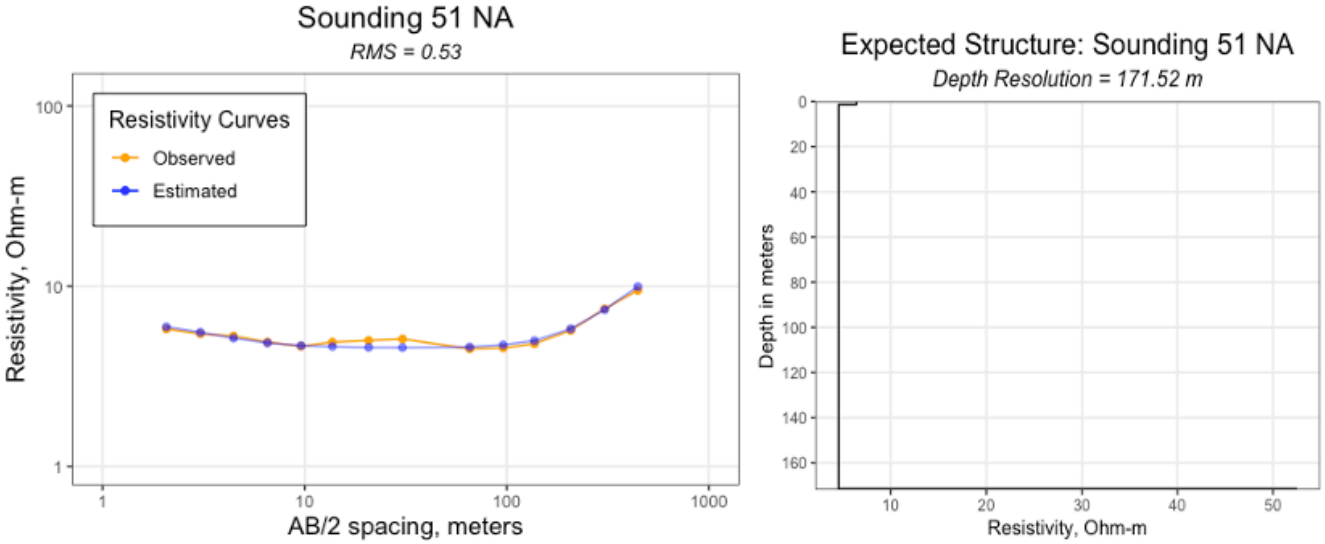

Figure 49. Sounding 51.
Example of an easy model.

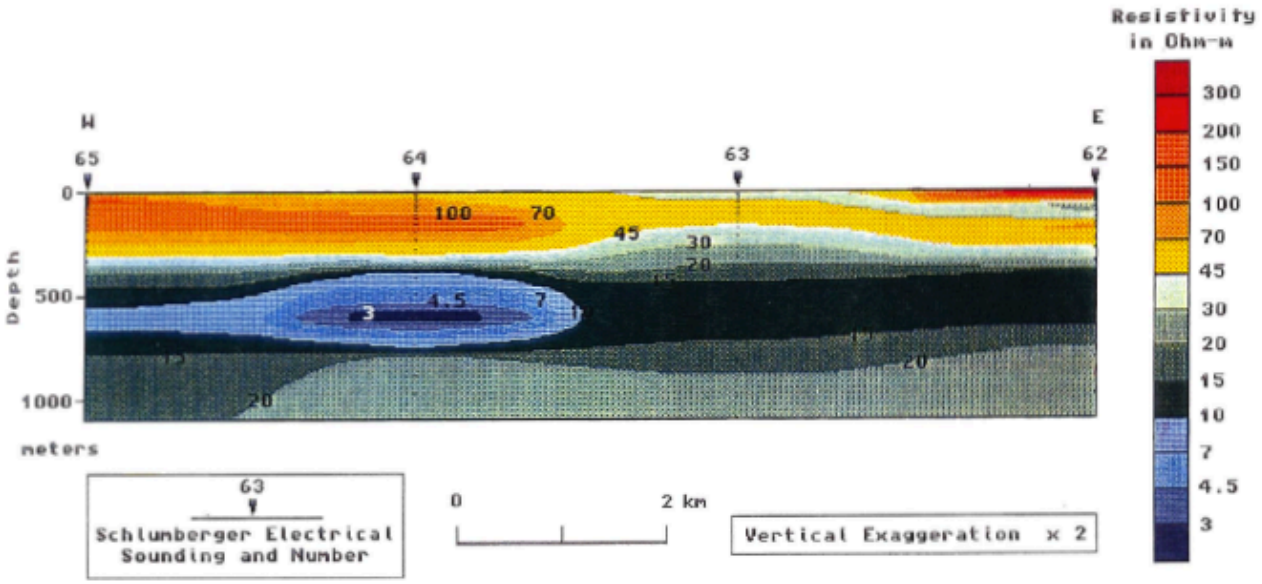

Figure 50. Al-Garni's Cross-Section.
This cross-section shows very low resistivity values at depths of 500 m and more.

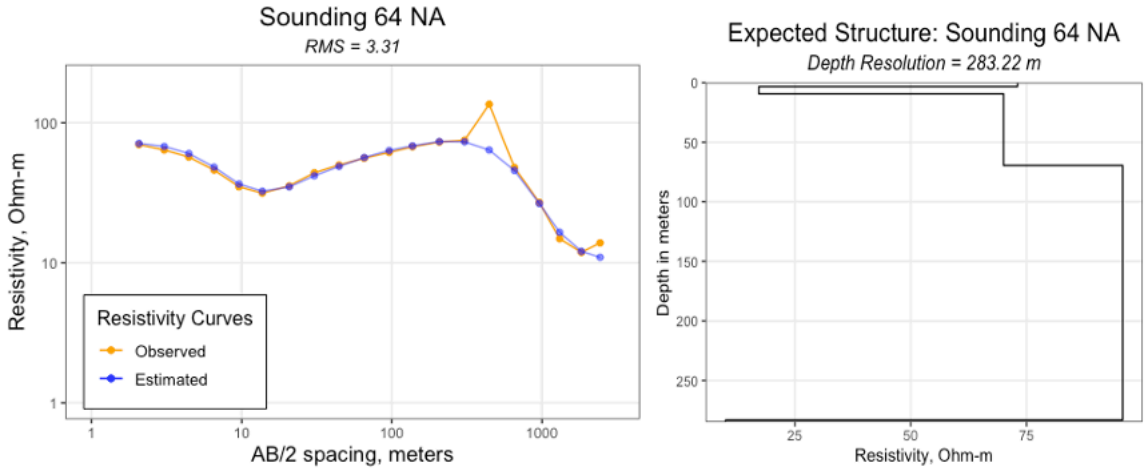

Figure 51. Sounding 64.
Sounding 64 modeled in this thesis; we can see that the depth of resolution does not go further than 300 m, in comparison with Figure 50.

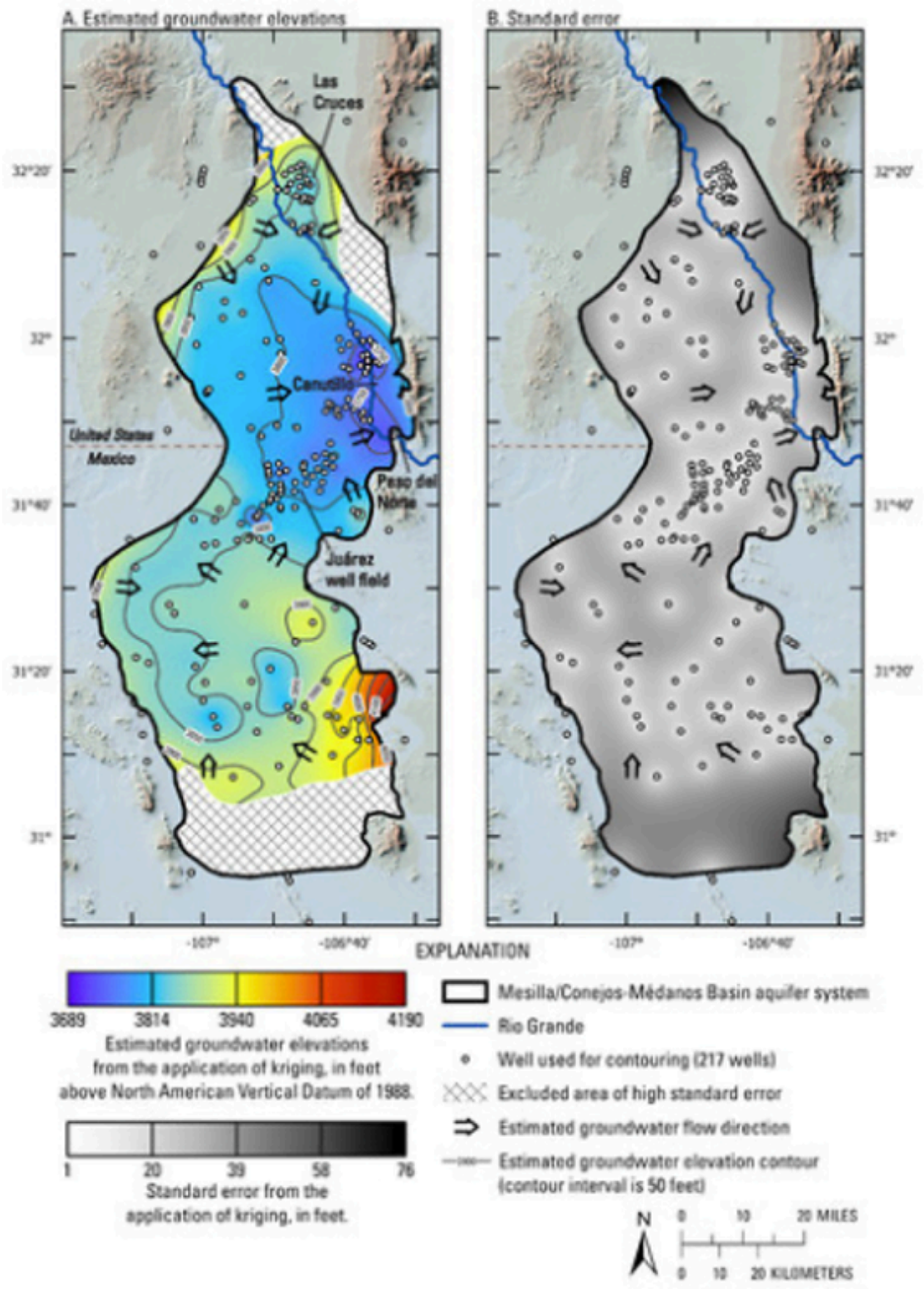

Figure 52. Groundwater flow from the Mesilla Basin.
This map shows the flow directions in the Mesilla Basin. Source: Robertson et al. (2022).

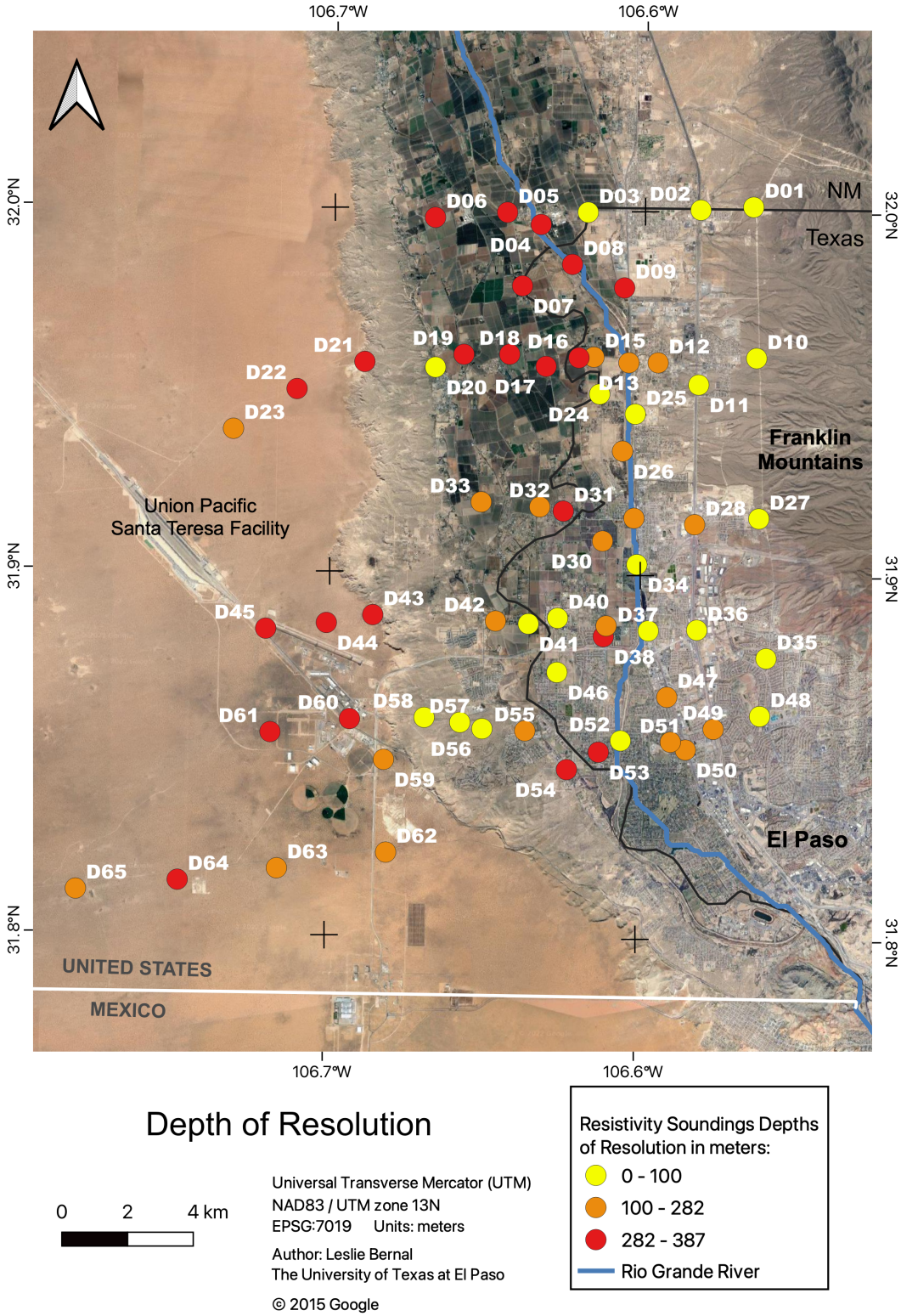

Figure 53. Depth of Resolution.
This map classifies the different depths of resolution of all soundings into 3 different ranges.

Chapter 5: Conclusion

A resistivity survey from 1973 was reprocessed using current methods to provide better fits of the soundings with known geological models and other geophysical information. A new set of models was then generated. Due to the non-unique nature of the data these models were constrained by geological information. We determined the quality of the soundings based on their RMS fit to known geology and the difficulty in determining models due to a lack of geological information, or soundings collected in regions where the assumption of a 1-D layered Earth model broke down (e.g., profiles crossing faults). These re-interpreted profiles provide a valuable new tool for continuing geophysical, geochemical, and hydrological studies of the basin.

Soundings were arranged into four different groups according to the characteristics they had in common, such as modeling patterns and location. Group 1, on the Franklin Mountains, offered us an insight on how shallow bedrock affected the resistivity soundings. In some cases the extremely high bedrock resistivities caused current to flow sideways at shallow depths rather than deeper into the ground as sounding spacing was increased. As the current strength was not great enough to penetrate the limestone bedrock, we only obtained resolutions of about 2 to 20 m depth, instead of the desired 400 m of resolution. In addition, it appears that the soundings were collected in the late fall and early winter (Hawley, personal communication, 2022) during the driest months of the year, leading to very dry layers within the upper 1-2 m also hampering the flow of electricity.

Group 2, in the north part of the river valley, presented extremely low apparent resistivity values that met the expectations of the geological structures along the Rio Grande River. Soundings yielded interpreted resistivity values of around 4-8 ohm-m, typical of interbedded layers of sand and clay, as well as saturated river channels. The issue for this region was the attempt by previous investigators to match soundings at depths beyond the resolution of

electrode spacings. While they determined models to depths of ~ 800 m, our modeling suggests maximum resolutions of 300 to 400 m.

Group 3 represents the soundings measured in the southernmost part of the river valley on the U.S. side of the border. In this particular area, outcrops and shallow intrusive bodies are found, along with a thick salty-clay surface soil layer, that causes roads to flood every time it rains due to the poor drainage of the area. This leads to deposition of saline runoff, decreasing resistivity values. Most of the terrain here consists of layers of silty clay and sand, with high salinity levels found in water samples. Soundings in the area present low apparent resistivity values that could be associated with clays, or salty groundwater; some also present high apparent resistivity values likely related to intrusions.

The last group, number 4, represents the soundings located on La Mesa surface. This group was the most challenging to model. The lack of water wells and geologic reports in the area made the process difficult, coupled with the fault systems running perpendicular to the soundings and intersecting them. A few soundings were affected by large changes in surface topography and bedrock topography as well.

Finally, these soundings will form the basis of an improved model of the Mesilla Basin. Studies like this are important to other groundwater basins as climate change decreases snowpack and stream flow, increasing demand for groundwater.

FUTURE WORK

For future work, some soundings will be selected according to their location and orientation to create 2D cross-sections, especially those that lie close to the 2-D geologic cross-sections of Hawley and Kennedy (2004). One example would be the soundings from La Mesa region (Figure 39). Although few wells are found within the region many soundings are located near Hawley and Kennedy's geologic cross-section K-K' (Figure 19). The soundings also intersect each other, helping to identify lateral variations in geology. Another good example is

the soundings located in the foothills of the Franklin Mountains area (Figure 26) that fall near Hawley and Kennedy's geologic cross section J-J' (Figure 18).

A different analysis will be developed to understand how igneous intrusions influence groundwater flow and quality in the southernmost Mesilla Basin. Hiebing (2016) and Hiebing et al. (2018) observed local bedrock structures and andesite intrusions in the area reflected in their gravity data and affecting groundwater quality. In addition, some of the groundwater samples from Teeple (2017) had higher concentrations of As, which indicates dissolution of volcanic rocks. Only a few resistivity soundings lie within the region of suspected igneous structures, therefore additional seismic and gravity data will be used to create a model of the area in a follow-up study.

Finally, the resistivity soundings provide an important snapshot of groundwater conditions in the early 1970's. A comparison of the resistivity structure to water well information (water levels, geochemistry) obtained before and after the resistivity surveys, may help indicate how water levels and water quality has changed over the past ~ 50-80 years.

References

Al-Garni, M. A. (1996). Direct current resistivity investigation of groundwater in the lower Mesilla Valley, New Mexico, and Texas. Doctoral dissertation, Colorado School of Mines.

Arunshankar, B. N. (1993). Use of earth resistivity method for monitoring saline groundwater movement in aquifers: MS Thesis. The University of Texas at El Paso.

Baker, Mark (2019). DcRes 1.1.3 [Computer software].

Bernard, J. (2003). Multi-electrode, D. O. I. O. Short note on the depth of investigation of electrical methods. http://www.iris-instruments.com/Pdf_file/Resistivity_Imaging/methods_depth_investigation.pdf

Bruun, B., Jackson, K., Lake, P., & Walker, J. (2016). Texas Aquifers Study Groundwater Quantity, Quality, Flow, and Contributions to Surface Water.

Budhathoki, P., Doser, D. I., Thapalia, A., Langford, R. P., & Avila, V. M. (2018). Geological and geophysical studies of the structure and stratigraphy of the northwestern Hueco Bolson Aquifer, El Paso, Texas. *Geosphere*, *14*(2), 731-748.

Cervantes, J. P. (2018). Gravitational Analysis and Fault Identification Within an Active Rift Basin: The Mesilla Valley Bolson in Western Texas-Southern New Mexico. The University of Texas at El Paso.

Chavez, Octavio E. (2000). Mining of internationally shared aquifers: the El Paso-Juárez case. Natural Resources Journal: 237-260.

Chenoweth, D. (2015). Sequence stratigraphy and depositional environment of the Cambro-Ordovician bliss sandstone, Franklin mountains of El Paso, Texas. The University of Texas at El Paso.

Cliett, T. (1969). Groundwater occurrence of the El Paso area and its related geology. Guidebook of the border region, Chihuahua and the United States: New Mexico Geological Society Twentieth Field Conference (Vol. 209, p. 214).

Cornell, William C., (1996). Geology of El Paso. Unpublished manuscript.

El Paso Water (2018a). Desalination. Retrieved from: https://www.epwater.org/our_water/water_resources/desalination

El Paso Water (2018b). Water Resources. Retrieved from: https://www.epwater.org/our_water/water_resources

El Paso Water (2019). Water Conservation Plan 2019. Prepared in collaboration with Alan Plummer Associates, Inc. Last accessed Nov/2022 at: https://cdn5-hosted.civiclive.com/UserFiles/Servers/Server_6843404/File/Conservation/Water%20Conservation%20Plan%202019.pdf

Garcia, S., Louvat, P., Gaillardet, J., Nyachoti, S., & Ma, L. (2020). Combining uranium, boron, and strontium isotope ratios (234U/238U,δ 11B, 87Sr/86Sr) to trace and quantify salinity contributions to Rio Grande River in Southwestern United States. Frontiers in Water, 2, 82.

Hawley, J. W., & Lozinsky, R. P. (1992). Hydrogeologic framework of the Mesilla Basin in New Mexico and western Texas. New Mexico Bureau of Mines and Mineral Resources.

Hawley, J. W., & Kennedy, J. F. (2004). Creation of a digital hydrogeologic framework model of the Mesilla Basin and southern Jornada del Muerto Basin (p. 105). New Mexico Water Resources Research Institute, New Mexico State University.

Hawley, J. W. (2016). Challenges and Opportunities for Brackish Groundwater-Resource Development in New Mexico—Prediction Hydro-Science from an Octogenarian Hydrogeologist's Perspective.

Hiebing, M. S. (2016). Using geochemistry and gravity data to pinpoint sources of salinity in the Rio Grande and fault networks of the Mesilla Basin. The University of Texas at El Paso.

Hiebing, M., Doser, D. I., Avila, V. M., & Ma, L. (2018). Geophysical studies of fault and bedrock control on groundwater geochemistry within the southern Mesilla Basin, western Texas and southern New Mexico. Geosphere, 14(4), 1912-1934.

Hoffer, J.M. (1970). Petrology and mineralogy of the Campus Andesite Pluton, El Paso, Texas. Geol. Soc. Amer. Bull. 81, 2129-2136.

Ikard, S., Teeple, A., & Humberson, D. (2021). Gradient Self-Potential Logging in the Rio Grande to Identify Gaining and Losing Reaches across the Mesilla Valley. Water, 13(10), 1331.

Imana, E. C. (2002). The Mesilla bolson: An integrated geophysical, hydrological, and structural analysis utilizing Free Air Anomalies (Unpublished master's thesis). The University of Texas at El Paso.

International Boundary & Water Commission. (n.d.). About the Rio Grande. Retrieved from https://www.ibwc.gov/CRP/riogrande.htm in February 2022.

Karlstrom, K. E., Amato, J. M., Williams, M. L., Heizler, M., Shaw, C. A., Read, A. S., & P., Bauer (2004). Proterozoic tectonic evolution of the New Mexico region: A synthesis. The Geology of New Mexico: A Geologic History: New Mexico Geological Society Special Publication, 11, 1-34.

Keller, G.V., and Frischknecht, F.C. (1966). Electrical methods in geophysical prospecting: Pergamon Press, Oxford, England, 519 pp.

Khatun, S., Ekal, M. I., & Doser, D. I. (2003). Gravity studies to detect faults controlling ground water movement within the lower Mesilla basin, west Texas. In *Symposium on the Application of Geophysics to Engineering and Environmental Problems 2003* (pp. 1184-1193). Society of Exploration Geophysicists.

Kubicki, C., Carroll, K.C., Witcher, J.C., and Robertson, A. (2021). An Integrated Geochemical Approach for Defining Sources of Groundwater Salinity in the Southern Rio Grande Valley of the Mesilla Basin, New Mexico and West Texas, USA: Desalination and Water Purification Research Program. Research and Development Office Report No. NMSU005, Prepared for the Bureau of Reclamation under Agreement No. R16AC00002; New Mexico Water Resources Research Institute Report No. 388, 40 p., 3 Appendices.

Leveaux, J., & Poupon, A. (1971). Evaluation of water saturation in shaly formations. *The Log Analyst*, *12*(04).

Morgan, P., Seager, W. R., & Golombek, M. P. (1986). Cenozoic thermal, mechanical and tectonic evolution of the Rio Grande rift. Journal of Geophysical Research: Solid Earth, 91(B6), 6263-6276.

New Mexico Water Rights Reporting System. New Mexico Office of the State Engineer, 2010. Last accessed Jun/27/2022 at: http://nmwrrs.ose.state.nm.us/nmwrrs/meterReport.html

Pskowski, M. (2022). Rio Grande water returns to El Paso this weekend, quenching arid border region. El Paso Times. Last accessed: Nov/21/2022 at: https://eu.elpasotimes.com/story/news/2022/06/05/rio-grande-water-el-paso-irrigation-farming/7485424001/

Ricketts, J. W., Amato, J. M., & Gavel, M. M. (2021). The Origin and Tectonic Significance of the Basin and Range–Rio Grande Rift Boundary in Southern New Mexico, USA. GSA Today, 31(10).

Robertson, A. J., Matherne, A. M., Pepin, J. D., Ritchie, A. B., Sweetkind, D. S., Teeple, A. P., Granados-Olivas A., García-Vásquez, A.C., Carroll, K.C., Fuchs, E.H., & Galanter, A. E. (2022). Mesilla/Conejos-Médanos Basin: US-Mexico Transboundary Water Resources. *Water*, *14*(2), 134.

Saad, R., Nawawi, M. N. M., & Mohamad, E. T. (2012). Groundwater detection in alluvium using 2-D electrical resistivity tomography (ERT). *Electronic Journal of Geotechnical Engineering*, *17*, 369-376.

Sistema de Consulta de Integración Territorial SCITEL, Instituto Nacional de Estadística y Geografía INEGI (2020). Censo de Población y Vivienda 2020. Last accessed Nov/2022 at: https://www.inegi.org.mx/app/scitel/consultas/index

Sheng, Z. (2013). Impacts of groundwater pumping and climate variability on groundwater availability in the Rio Grande Basin. Ecosphere 4(1):5. http://dx.doi.org/10.1890/ES12-00270.1

Stuart, C. J., & Willingham, D. L. (1984). Late Tertiary and Quaternary fluvial deposits in the Mesilla and Hueco bolsons, El Paso area, Texas. Sedimentary Geology, 38(1-4), 1-20.

Swift, D. B. (1973). Lithofacies of the Cuchillo Formation, Southern Sierra de Juárez, Chihuahua, Mexico. The University of Texas at El Paso.

Teeple, A. P. (2017). Geophysics-and geochemistry-based assessment of the geochemical characteristics and groundwater-flow system of the US part of the Mesilla Basin/Conejos-Médanos aquifer system in Doña Ana County, New Mexico, and El Paso County, Texas, 2010–12 (No. 2017-5028). US Geological Survey.

Telford, W. M., Geldart, L. P., Sheriff, R. E., & Sheriff, R. E. (1990). Applied geophysics. Cambridge University Press.

Texas Commission on Environmental Quality, Water Well Report Viewer. Last accessed Oct/04/2022 at: https://tceq.maps.arcgis.com/apps/webappviewer/index.html?id=aed10178f0434f2781dafaf19eb326fe2

Texas Water Development Board (2022). Groundwater Data Viewer, last accessed Oct/04/2022 at:

https://www3.twdb.texas.gov/apps/WaterDataInteractive/GroundwaterDataViewer/?map=sdr

Thomann, W. F. (1980). Petrology and geochemistry of the Precambrian Thunderbird Formation. Franklin Mountains, El Paso County, Texas. [unpublished Ph. D. thesis]: University of Texas at El Paso, El Paso, Texas.

U.S. Census Bureau (2020). 2020 Decennial Census. Last accessed Nov/2022 at: https://www.census.gov/quickfacts/fact/table/elpasocitytexas/POP010220

Villagran, Lauren (2017a). Two nations, one aquifer: 'I am going to be out of water'. Albuquerque Journal. Las Cruces Bureau. Retrieved February 23, 2021, from https://www.abqjournal.com/1028133/nm-rancher-fears-deep-mexican-wells-will-leave-him-high-and-dry.html#foogallery-0/p:2.

Villagran, Lauren (2017b). Two nations, one aquifer: 'The Biggest Pump Wins'. Albuquerque Journal. Las Cruces Bureau. Retrieved February 23, 2021, from https://www.abqjournal.com/1026922/as-mexico-pumps-water-quality-questioned.html.

Witcher, J. C., King, J. P., Hawley, J. W., Kennedy, J. F., Williams, J., Cleary, M., & Bothern, L. R. (2004). Sources of salinity in the Rio Grande and Mesilla Basin groundwater. *New Mexico Water Resources Research Institute Technical Completion Report*, *330*, 168p.

Zohdy, A. A. (1973). A computer program for the automatic interpretation of Schlumberger sounding curves over horizontally layered media: National Technical Information Survey, PB-323-703, 27 p.

Zohdy, A. A., & Bisdorf, R. J. (1989). Programs for the automatic processing and interpretation of Schlumberger sounding curves in QuickBASIC 4.0 (No. 89-137-A). United States Department of the Interior, Geological Survey.

Zohdy, A. A., Bisdorf, R. J., & Gates, J. S. (1994). A direct-current resistivity survey of the Beaver Dam Wash drainage in southwest Utah, southeast Nevada, and northwest Arizona. U.S. Geological Survey Open-File Report 94-676.

Zohdy, A.A., Bisdorf, R. J., and Gates, J.S. (1976). Schlumberger Soundings in the Lower Mesilla Valley of the Rio Grande, Texas, and New Mexico. U.S. Geological Survey Open-File Report 76-324,77 p.

Zohdy, A. A., Eaton, G. P., & Mabey, D. R. (1974). Application of surface geophysics to ground-water investigations. U.S. Geological Survey Techniques of Water-Resources Investigations, Book 2, Chapter D1.

Appendix 1. Location of Resistivity Soundings

Latitude and Longitude are expressed in decimal degrees. Height above mean sea level (ASL) is expressed in meters. Length of sounding is expressed in meters. RMS is expressed as a percentage. Depth represents the depth of resolution of each sounding and is expressed in meters.

ID	Latitude	Longitude	ASL in m	Length in m	Orientation	RMS %	Depth in m
D01	32.00167	106.56518	1,231.9	2,463.9	N-S	93.4	2.22
D02	32.00068	106.58218	1,192.3	2,384.6	N-S	31.3	70
D03	31.99963	106.61851	1,155.7	2,311.5	E-W	0.5	94.76
D04	31.9961	106.63359	1,153.3	2,306.6	NW-SE	6.36	314
D05	31.9993	106.6445	1,156.4	2,312.7	E-W	9.7	318.63
D06	31.99762	106.6677	1,155.4	2,310.9	N-S	13.55	288.46
D07	31.97917	106.63931	1,154.5	2,309.1	N-S	10.7	371.33
D08	31.98526	106.62332	1,154.8	2,309.7	NW-SE	15.42	339.52
D09	31.97901	106.60642	1,157.0	2,313.9	N-S	4.8	317.67
D10	31.96014	106.56355	1,253.0	2,505.9	N-S	6.61	362.13
D11	31.95264	106.5821	1,198.7	2,397.4	N-S	12.74	84.87
D12	31.95856	106.59526	1,165.5	2,331.0	E-W	74.21	123.41
D13	31.95845	106.60468	1,152.7	2,305.4	N-S	5.1	258.91
D14	31.95929	106.61224	1,152.4	2,304.8	E-W	NA	NA
D15	31.95987	106.61597	1,152.4	2,304.8	N-S	3.21	175.7
D16	31.95961	106.6208	1,152.7	2,305.4	N-S	13.55	307.6
D17	31.95713	106.63133	1,153.0	2,306.0	N-S	11.19	326.07
D18	31.96031	106.64311	1,153.3	2,306.6	NW-SE	21.6	287.13
D19	31.96011	106.65783	1,154.2	2,308.4	N-S	23.12	313.15
D20	31.95647	106.66696	1,155.7	2,311.5	NW-SE	21.05	65
D21	31.95773	106.68974	1,233.8	2,467.5	SW-NE	16.41	386.55
D22	31.94999	106.71144	1,251.4	2,502.9	SW-NE	30.92	346.68
D23	31.93879	106.73171	1,256.9	2,513.9	NW-SE	23.58	248.41
D24	31.9497	106.61396	1,151.5	2,303.0	N-S	6.03	7.81
D25	31.94436	106.60237	1,154.5	2,309.1	N-S	0.56	90.93
D26	31.93412	106.60633	1,150.0	2,299.9	N-S	3.25	252.62
D27	31.91605	106.56212	1,245.0	2,490.1	N-S	33.4	21.07
D28	31.91422	106.58277	1,185.6	2,371.2	N-S	15.65	102.16
D29	31.91574	106.60233	1,149.3	2,298.7	N-S	5.21	143.79
D30	31.90934	106.61233	1,147.8	2,295.6	N-S	0.94	149.15
D31	31.91741	106.62511	1,148.7	2,297.5	N-S	7.79	336.4

D32	31.91849	106.63272	1,150.0	2,299.9	N-S	5.75	223.44
D33	31.91962	106.65158	1,150.9	2,301.7	N-S	7.98	223.55
D34	31.90301	106.60119	1,146.6	2,293.2	N-S	15.08	45.52
D35	31.87766	106.55917	1,233.8	2,467.5	N-S	2.37	54.73
D36	31.88523	106.58159	1,174.3	2,348.7	N-S	4.11	68.46
D37	31.88483	106.5972	1,148.4	2,296.9	N-S	22.49	80.02
D38	31.88308	106.61164	1,146.0	2,292.0	N-S	11.98	329.6
D39	31.88604	106.61078	1,146.3	2,292.6	E-W	0.87	266.33
D40	31.88799	106.62643	1,146.3	2,292.6	N-S	1.8	85.83
D41	31.8863	106.63582	1,146.9	2,293.8	N-S	25.87	74.3
D42	31.88695	106.6464	1,149.3	2,298.7	N-S	15.86	106.44
D43	31.8882	106.68594	1,239.6	2,479.1	E-W	17.32	308.69
D44	31.88584	106.70083	1,252.4	2,504.7	SW-NE	30.11	375.29
D45	31.88401	106.72033	1,253.0	2,505.9	NW-SE	7.52	287.98
D46	31.87309	106.6264	1,145.7	2,291.4	N-S	5.78	46.36
D47	31.86668	106.59092	1,145.7	2,291.4	NW-SE	3.29	258.88
D48	31.86176	106.56097	1,235.0	2,470.0	N-S	3.29	86.05
D49	31.85805	106.57584	1,168.9	2,337.7	N-S	19.22	178.35
D50	31.85225	106.5847	1,144.8	2,289.5	NW-SE	0.56	161.65
D51	31.85435	106.58956	1,144.5	2,288.9	E-W	0.53	171.52
D52	31.85454	106.60564	1,143.6	2,287.1	N-S	4.71	40.44
D53	31.85131	106.6127	1,143.6	2,287.1	N-S	0.24	284.52
D54	31.84639	106.62285	1,145.1	2,290.2	NW-SE	5.22	359.06
D55	31.85689	106.63645	1,150.9	2,301.7	NW-SE	1.53	127.09
D56	31.8573	106.65024	1,170.1	2,340.1	E-W	1.03	49.07
D57	31.85897	106.65739	1,178.6	2,357.2	E-W	2	80.83
D58	31.86019	106.6689	1,189.9	2,379.8	E-W	2.15	80.19
D59	31.84846	106.68177	1,244.7	2,489.5	NW-SE	1.98	229.09
D60	31.85953	106.69292	1,252.1	2,504.1	NW-SE	14.4	347.72
D61	31.85561	106.71842	1,253.3	2,506.6	SW-NE	0.73	295.5
D62	31.82299	106.68062	1,253.6	2,507.2	SW-NE	2.41	226.69
D63	31.81821	106.71566	1,247.5	2,495.0	SW-NE	1.03	252.73
D64	31.81464	106.74751	1,248.4	2,496.8	E-W	3.31	283.22
D65	31.81176	106.7802	1,253.0	2,505.9	E-W	25.84	278.17

Appendix 2. Sounding Plots and Interpretations

See Chapter 3 for an explanation of these soundings and their interpretations.

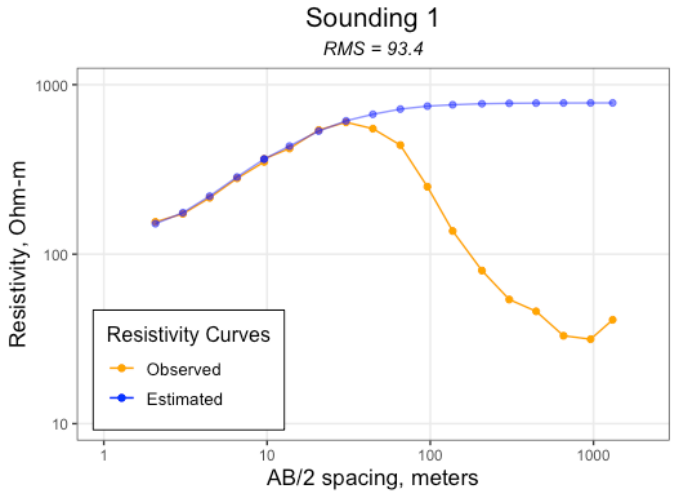

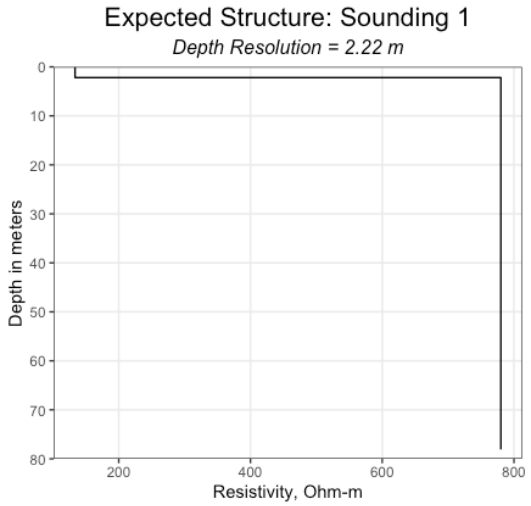

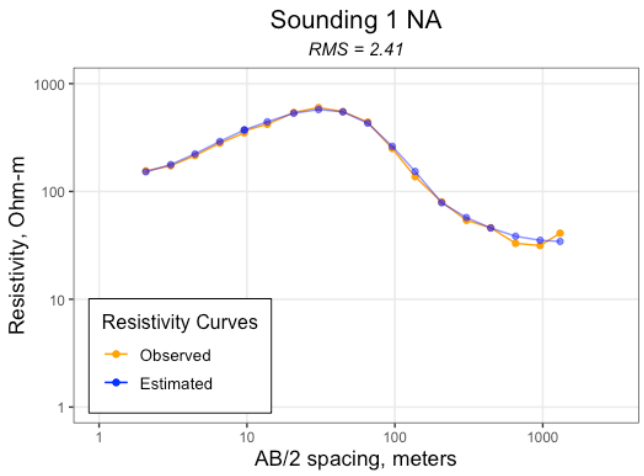

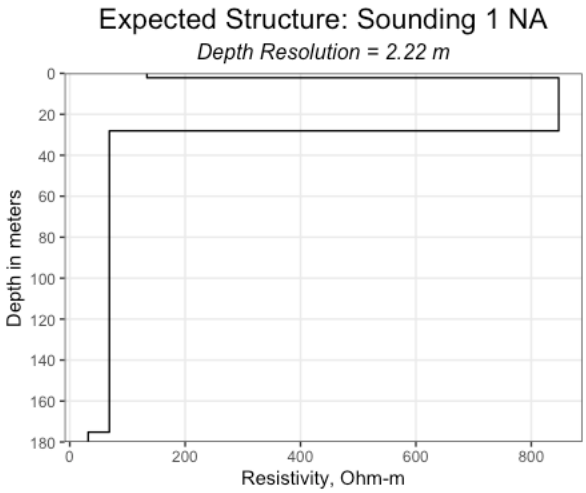

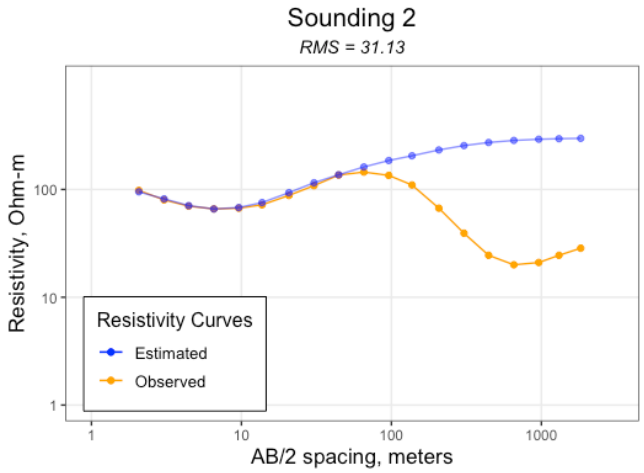

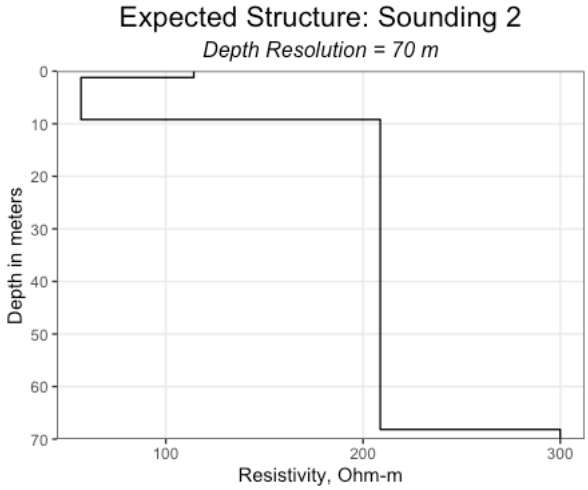

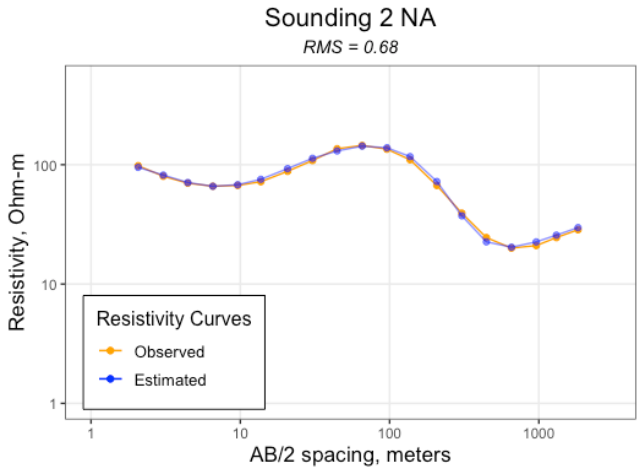
Sounding 2 NA
RMS = 0.68
Resistivity, Ohm-m
AB/2 spacing, meters
Resistivity Curves
Observed
Estimated

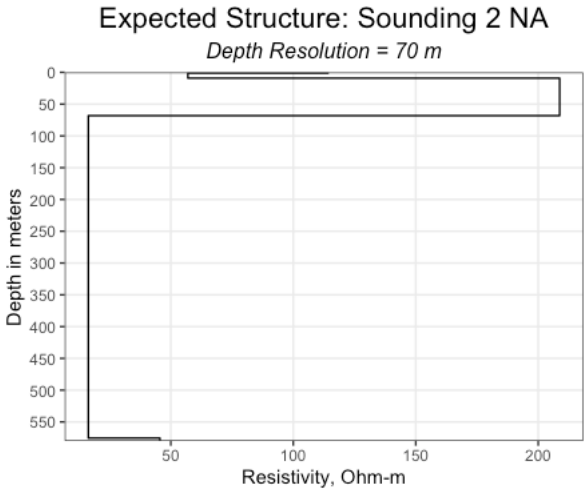
Expected Structure: Sounding 2 NA
Depth Resolution = 70 m
Depth in meters
Resistivity, Ohm-m

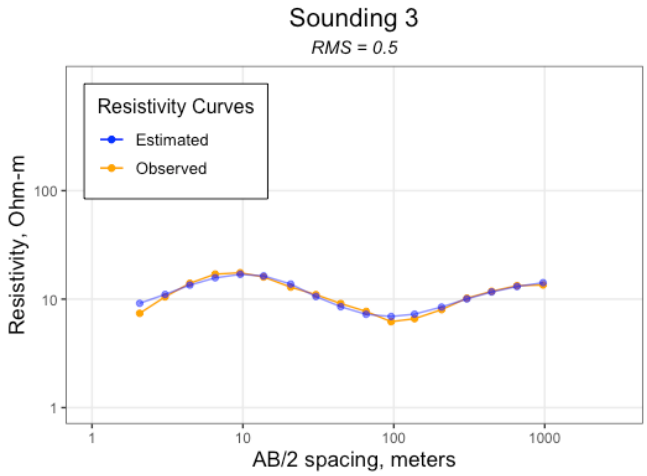
Sounding 3
RMS = 0.5
Resistivity, Ohm-m
AB/2 spacing, meters
Resistivity Curves
Estimated
Observed

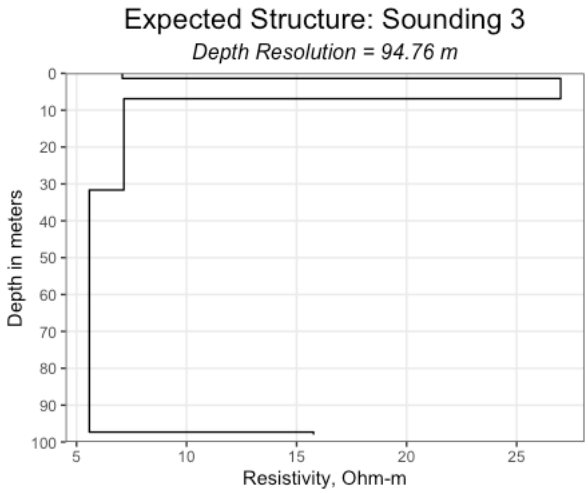
Expected Structure: Sounding 3
Depth Resolution = 94.76 m
Depth in meters
Resistivity, Ohm-m

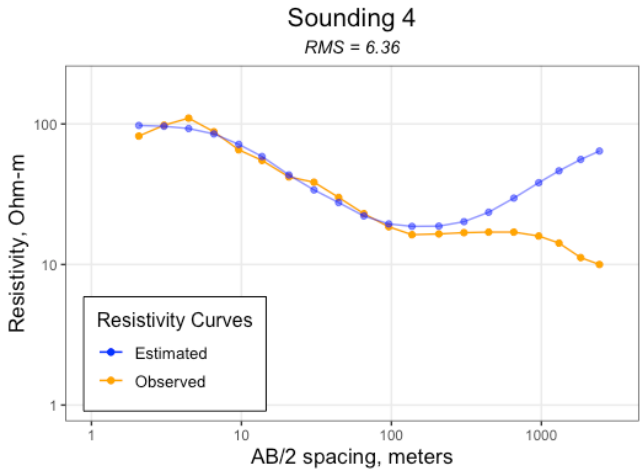
Sounding 4
RMS = 6.36
Resistivity, Ohm-m
AB/2 spacing, meters
Resistivity Curves
Estimated
Observed

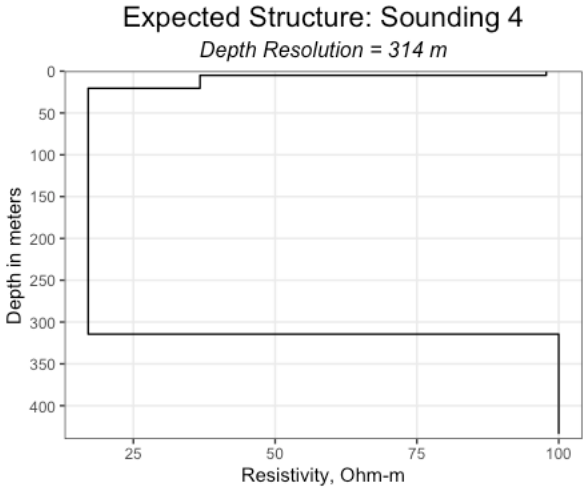
Expected Structure: Sounding 4
Depth Resolution = 314 m
Depth in meters
Resistivity, Ohm-m

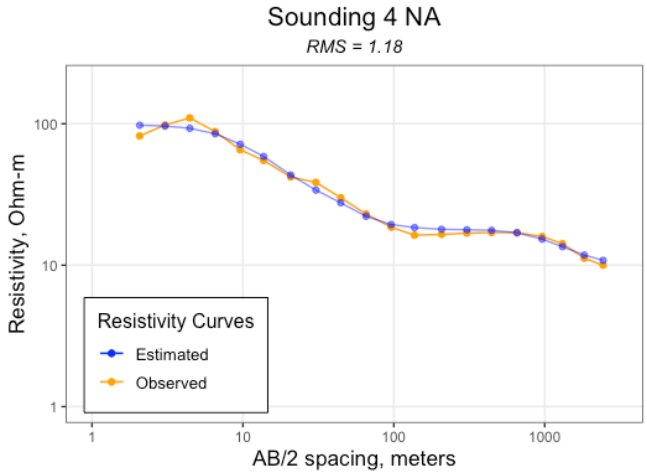
Sounding 4 NA
RMS = 1.18
Resistivity, Ohm-m
AB/2 spacing, meters
Resistivity Curves
Estimated
Observed

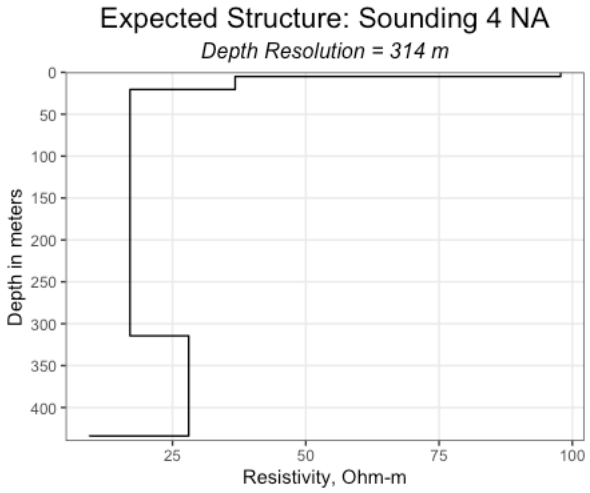
Expected Structure: Sounding 4 NA
Depth Resolution = 314 m
Depth in meters
Resistivity, Ohm-m

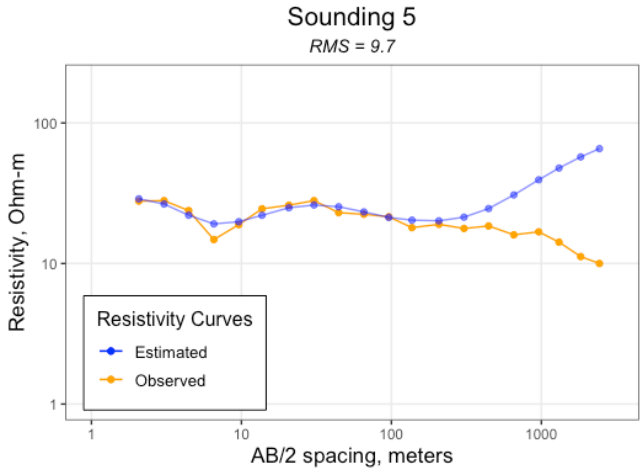
Sounding 5
RMS = 9.7
Resistivity, Ohm-m
AB/2 spacing, meters
Resistivity Curves
Estimated
Observed

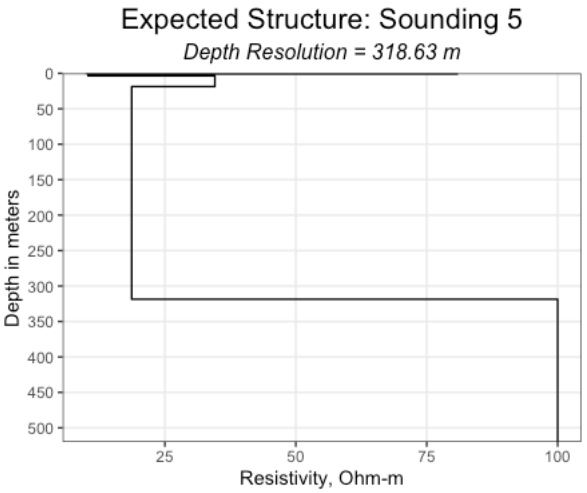
Expected Structure: Sounding 5
Depth Resolution = 318.63 m
Depth in meters
Resistivity, Ohm-m

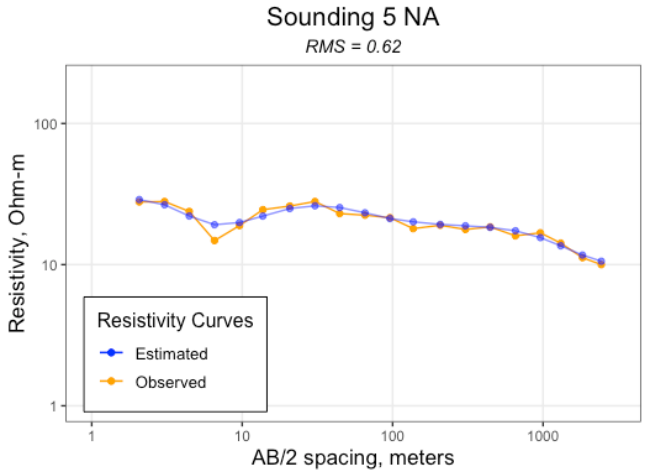
Sounding 5 NA
RMS = 0.62
Resistivity, Ohm-m
AB/2 spacing, meters
Resistivity Curves
Estimated
Observed

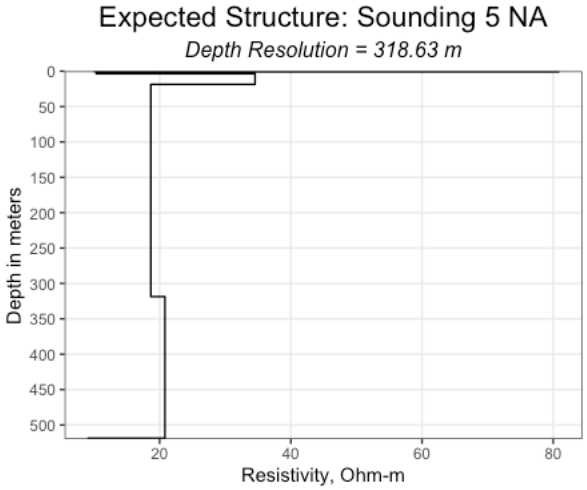
Expected Structure: Sounding 5 NA
Depth Resolution = 318.63 m
Depth in meters
Resistivity, Ohm-m

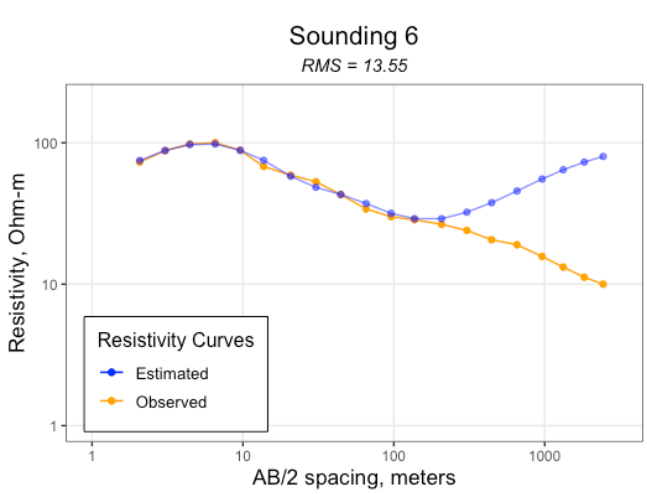
Sounding 6
RMS = 13.55
Resistivity, Ohm-m
AB/2 spacing, meters
Resistivity Curves
Estimated
Observed

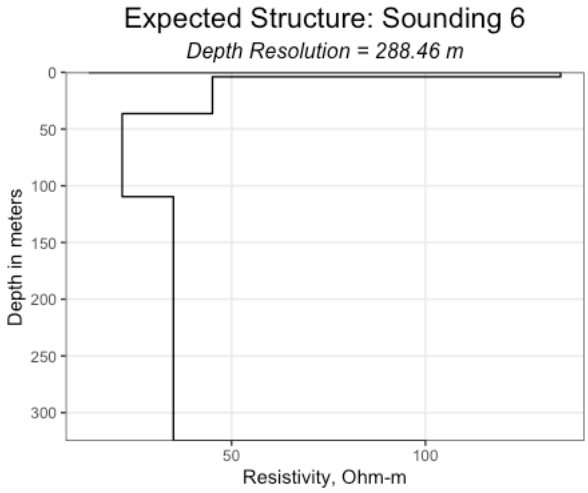
Expected Structure: Sounding 6
Depth Resolution = 288.46 m
Depth in meters
Resistivity, Ohm-m

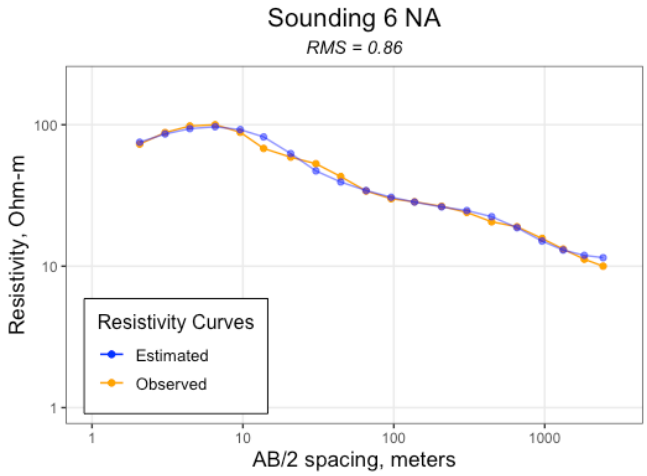
Sounding 6 NA
RMS = 0.86
Resistivity, Ohm-m
AB/2 spacing, meters
Resistivity Curves
Estimated
Observed

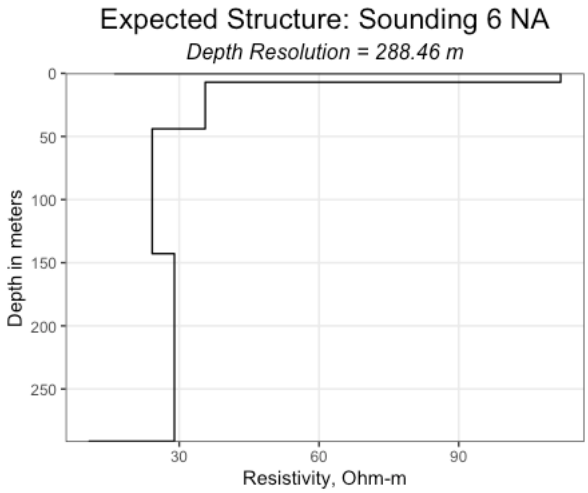
Expected Structure: Sounding 6 NA
Depth Resolution = 288.46 m
Depth in meters
Resistivity, Ohm-m

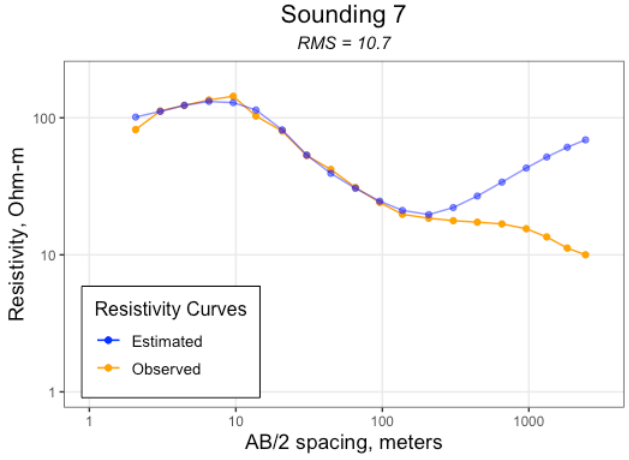
Sounding 7
RMS = 10.7
Resistivity, Ohm-m
AB/2 spacing, meters
Resistivity Curves
Estimated
Observed

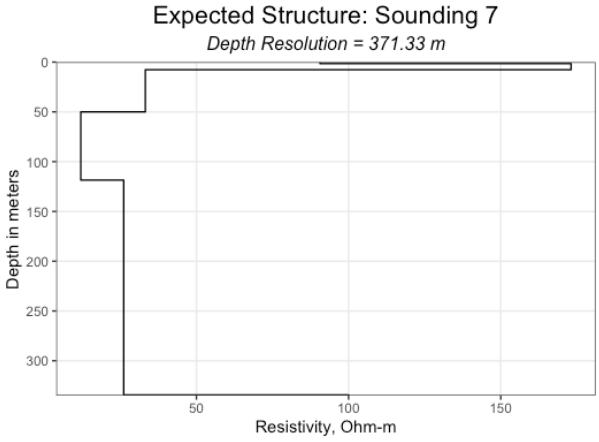
Expected Structure: Sounding 7
Depth Resolution = 371.33 m
Depth in meters
Resistivity, Ohm-m

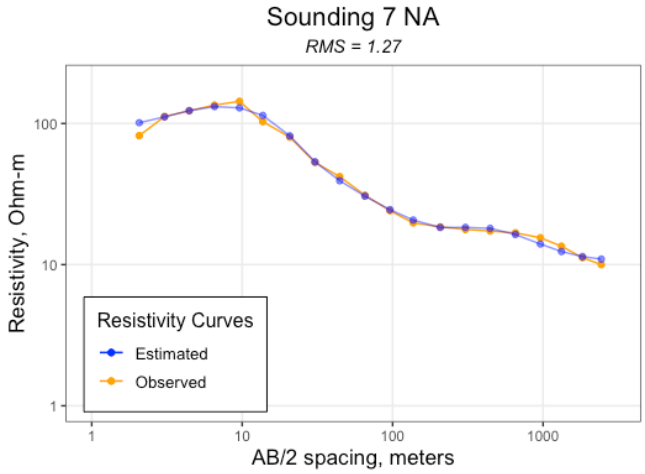
Sounding 7 NA
RMS = 1.27
Resistivity, Ohm-m
AB/2 spacing, meters
Resistivity Curves
Estimated
Observed

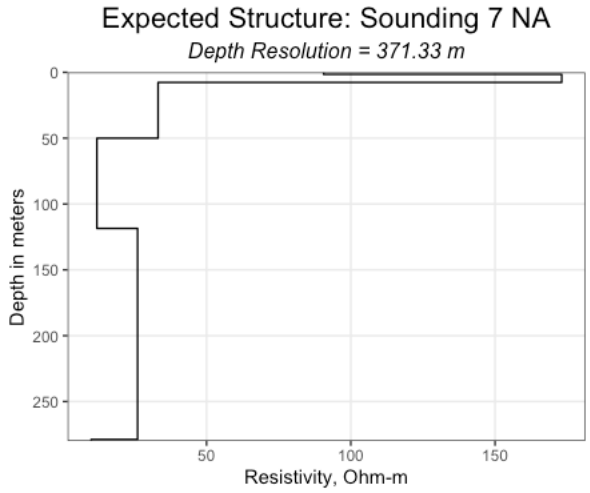
Expected Structure: Sounding 7 NA
Depth Resolution = 371.33 m
Depth in meters
Resistivity, Ohm-m

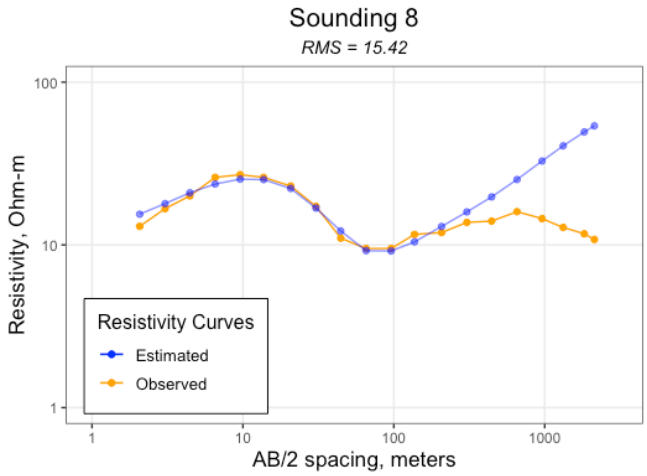
Sounding 8
RMS = 15.42
Resistivity, Ohm-m
AB/2 spacing, meters
Resistivity Curves
Estimated
Observed

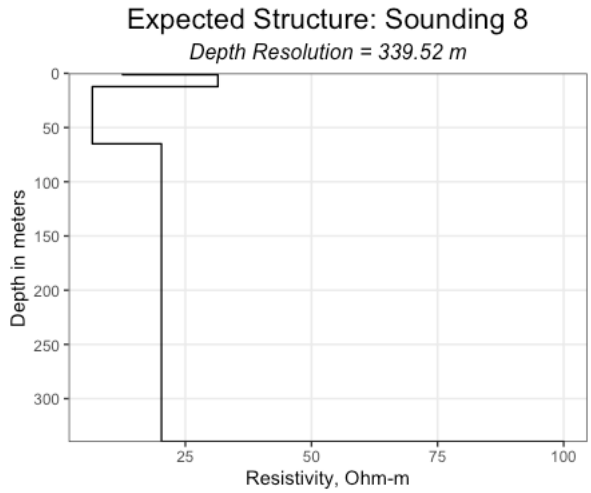
Expected Structure: Sounding 8
Depth Resolution = 339.52 m
Depth in meters
Resistivity, Ohm-m

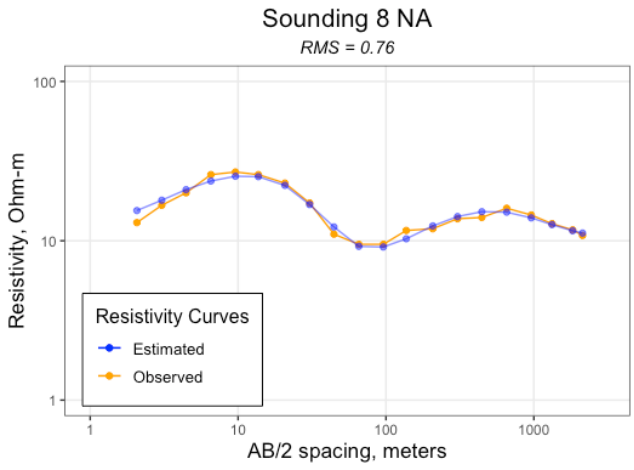
Sounding 8 NA
RMS = 0.76
Resistivity, Ohm-m
AB/2 spacing, meters
Resistivity Curves
Estimated
Observed

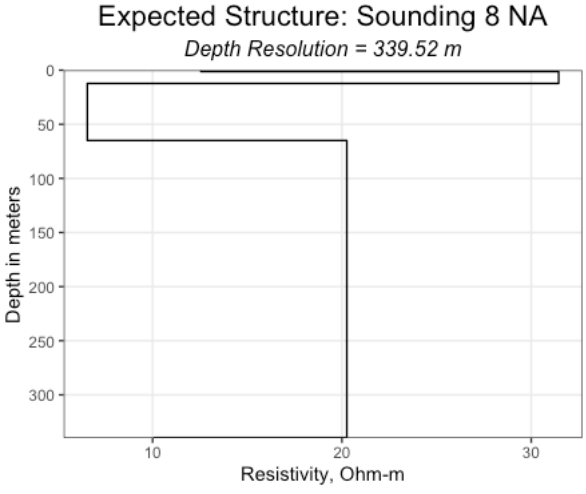
Expected Structure: Sounding 8 NA
Depth Resolution = 339.52 m
Depth in meters
Resistivity, Ohm-m

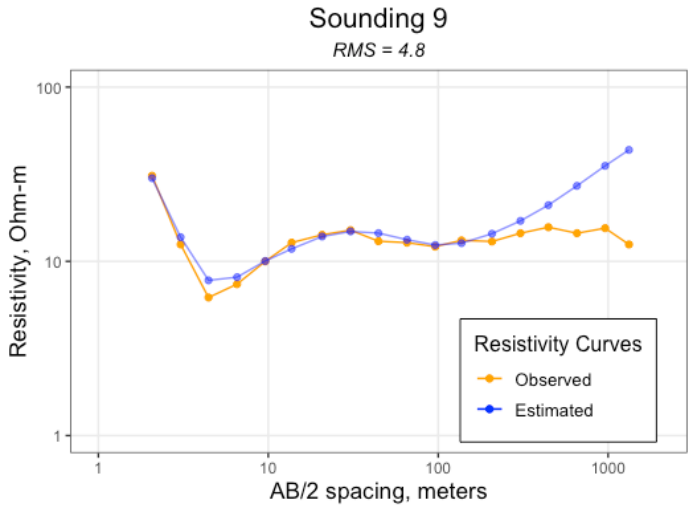
Sounding 9
RMS = 4.8
Resistivity, Ohm-m
AB/2 spacing, meters
Resistivity Curves
Observed
Estimated

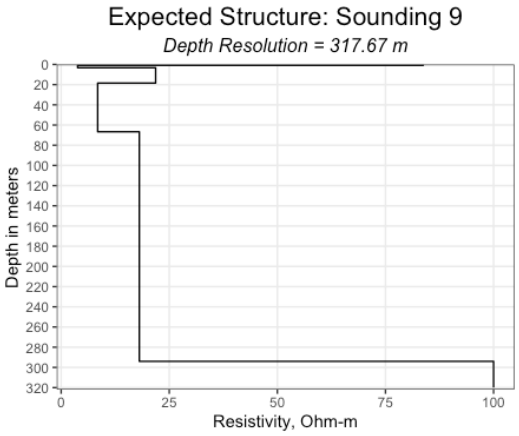
Expected Structure: Sounding 9
Depth Resolution = 317.67 m
Depth in meters
Resistivity, Ohm-m

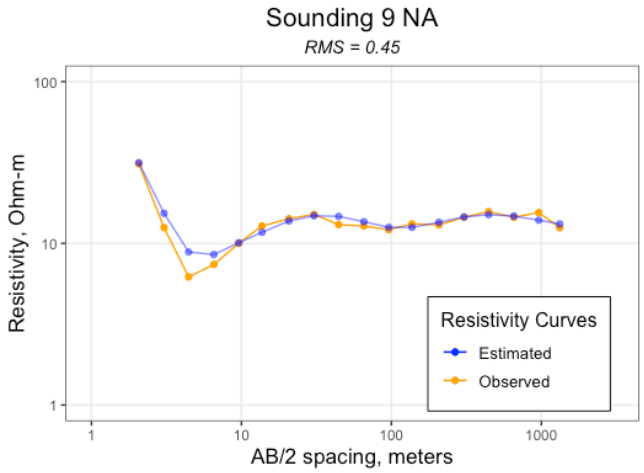
Sounding 9 NA
RMS = 0.45
Resistivity, Ohm-m
AB/2 spacing, meters
Resistivity Curves
Estimated
Observed

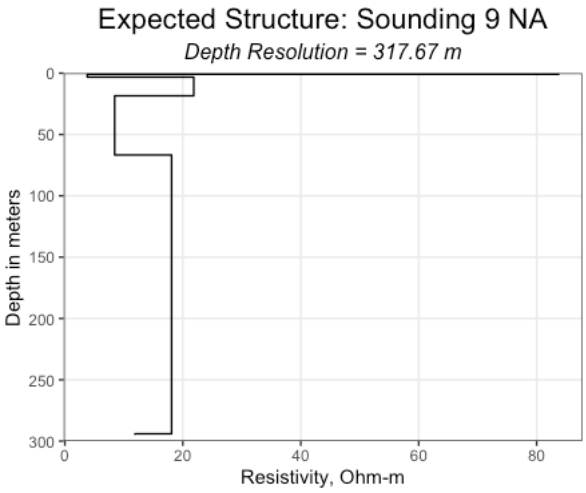
Expected Structure: Sounding 9 NA
Depth Resolution = 317.67 m
Depth in meters
Resistivity, Ohm-m

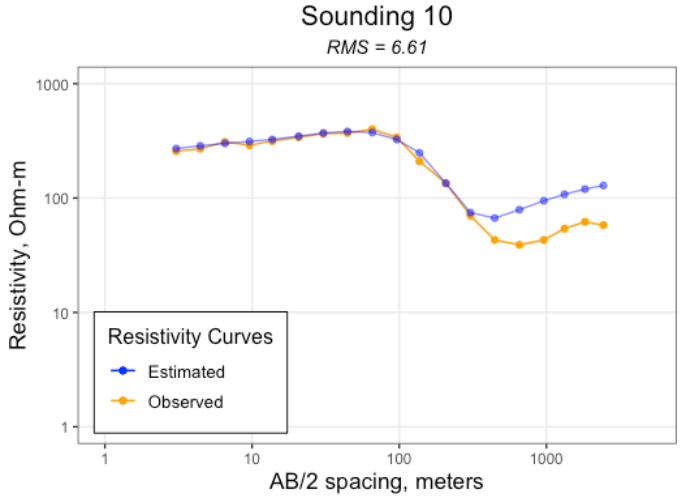
Sounding 10
RMS = 6.61
Resistivity, Ohm-m
AB/2 spacing, meters
Resistivity Curves
Estimated
Observed

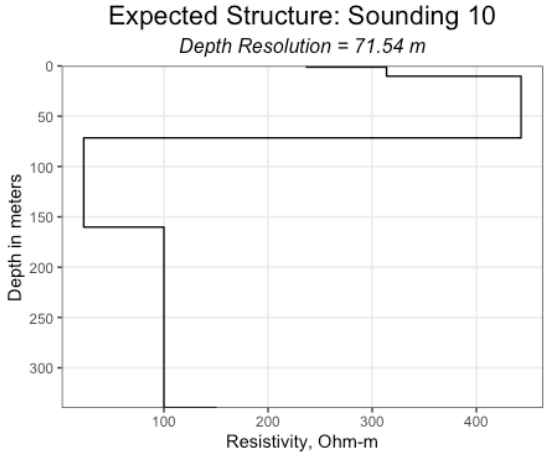
Expected Structure: Sounding 10
Depth Resolution = 71.54 m
Depth in meters
Resistivity, Ohm-m

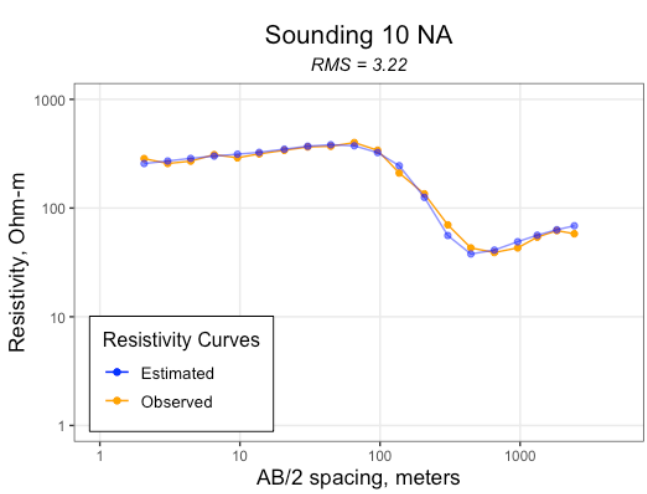
Sounding 10 NA
RMS = 3.22
Resistivity, Ohm-m
AB/2 spacing, meters
Resistivity Curves
Estimated
Observed

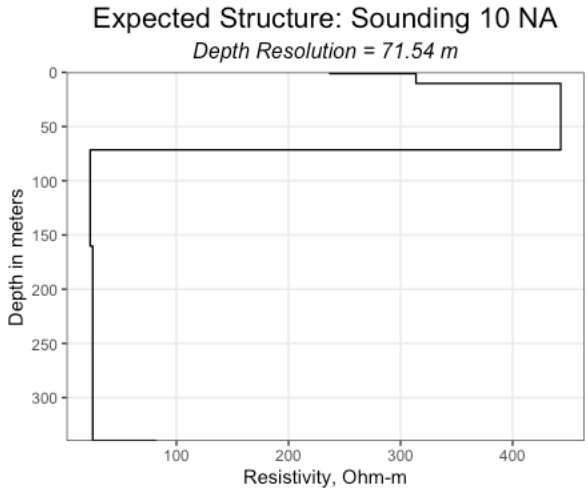
Expected Structure: Sounding 10 NA
Depth Resolution = 71.54 m
Depth in meters
Resistivity, Ohm-m

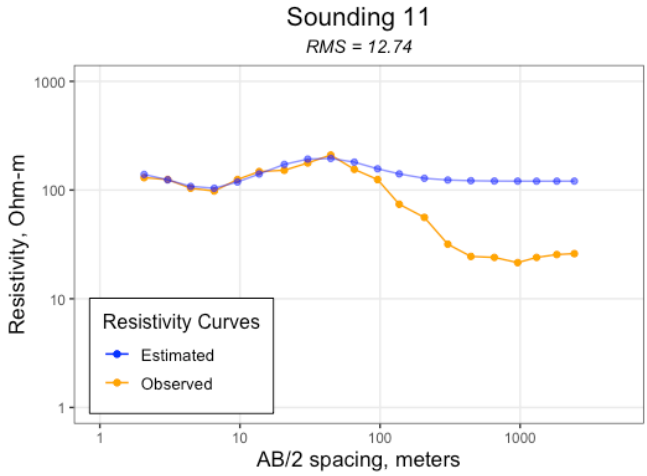
Sounding 11
RMS = 12.74
Resistivity, Ohm-m
AB/2 spacing, meters
Resistivity Curves
Estimated
Observed

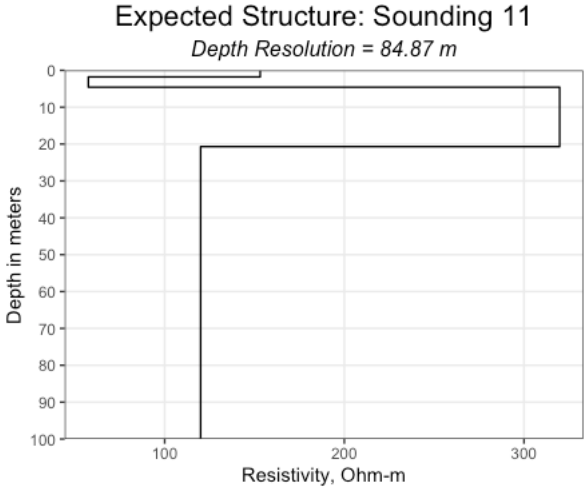
Expected Structure: Sounding 11
Depth Resolution = 84.87 m
Depth in meters
Resistivity, Ohm-m

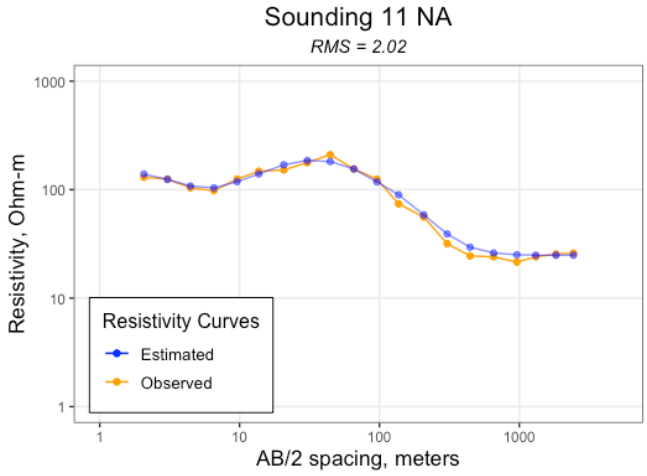
Sounding 11 NA
RMS = 2.02
Resistivity, Ohm-m
AB/2 spacing, meters
Resistivity Curves
Estimated
Observed

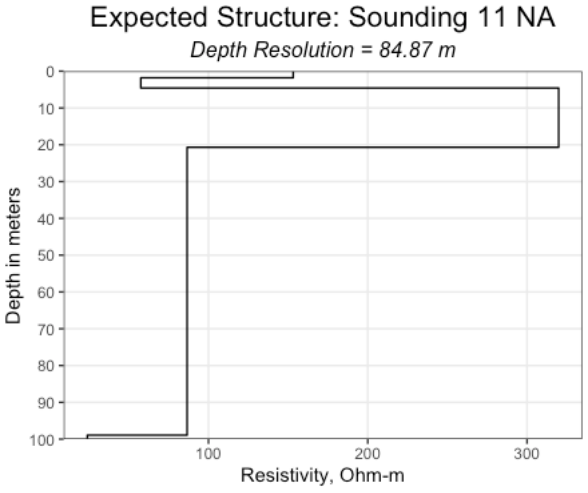
Expected Structure: Sounding 11 NA
Depth Resolution = 84.87 m
Depth in meters
Resistivity, Ohm-m

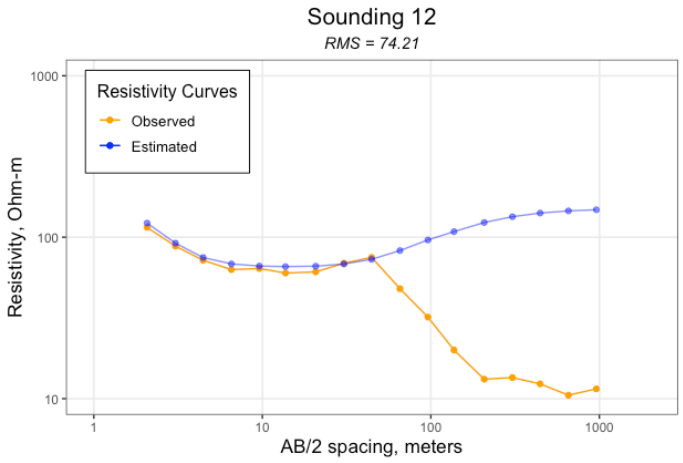
Sounding 12
RMS = 74.21
Resistivity Curves
Observed
Estimated
Resistivity, Ohm-m
1000
100
10
1
10
100
1000
AB/2 spacing, meters

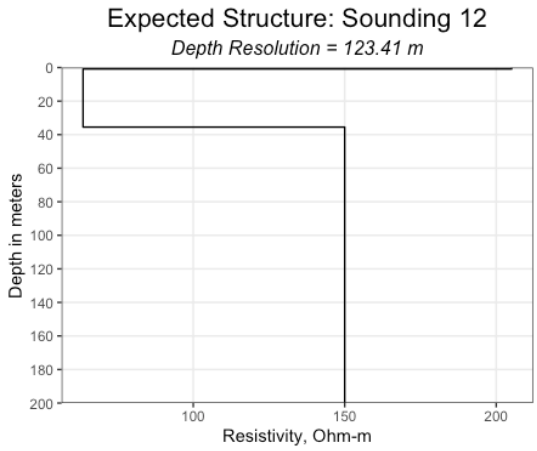
Expected Structure: Sounding 12
Depth Resolution = 123.41 m
Depth in meters
0
20
40
60
80
100
120
140
160
180
200
100
150
200
Resistivity, Ohm-m

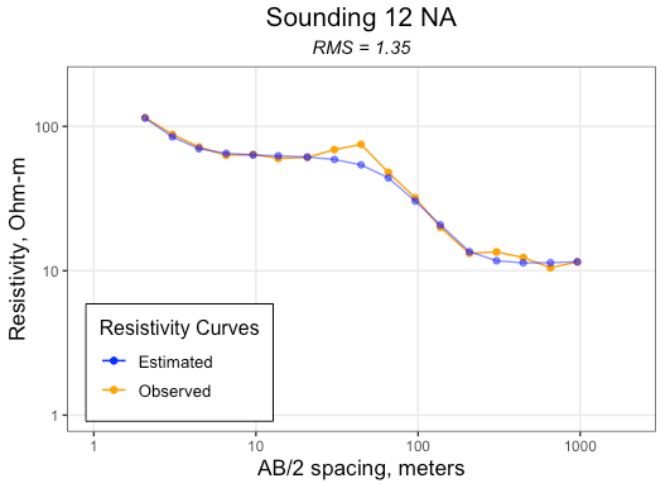
Sounding 12 NA
RMS = 1.35
Resistivity, Ohm-m
100
10
1
Resistivity Curves
Estimated
Observed
1
10
100
1000
AB/2 spacing, meters

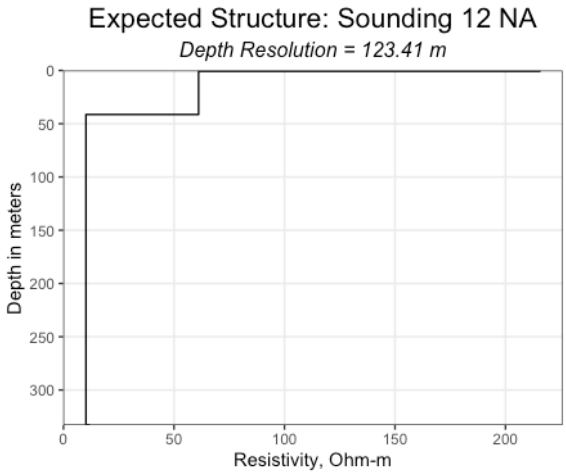
Expected Structure: Sounding 12 NA
Depth Resolution = 123.41 m
Depth in meters
0
50
100
150
200
250
300
0
50
100
150
200
Resistivity, Ohm-m

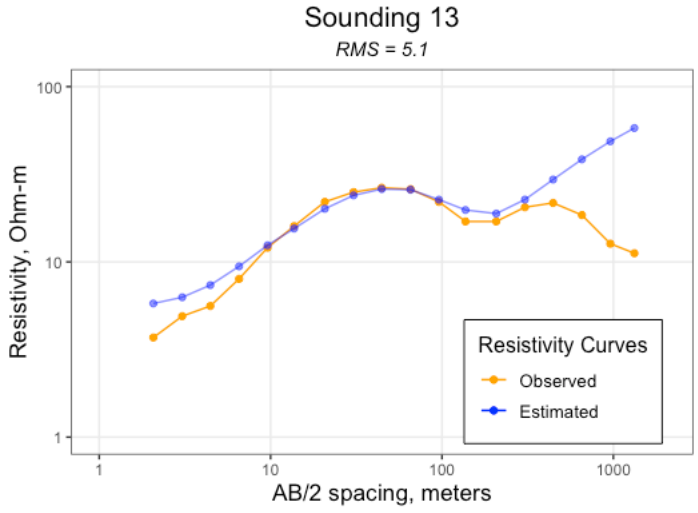
Sounding 13
RMS = 5.1
Resistivity, Ohm-m
100
10
1
Resistivity Curves
Observed
Estimated
1
10
100
1000
AB/2 spacing, meters

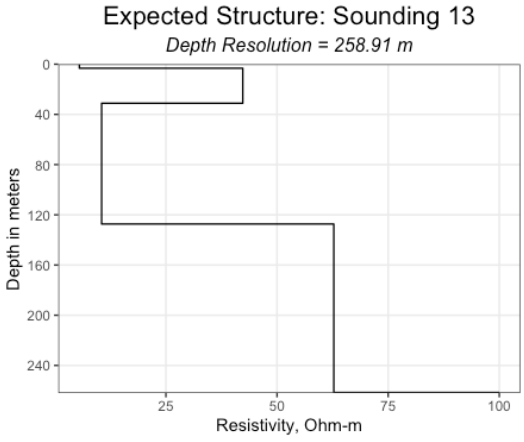
Expected Structure: Sounding 13
Depth Resolution = 258.91 m
Depth in meters
0
40
80
120
160
200
240
25
50
75
100
Resistivity, Ohm-m

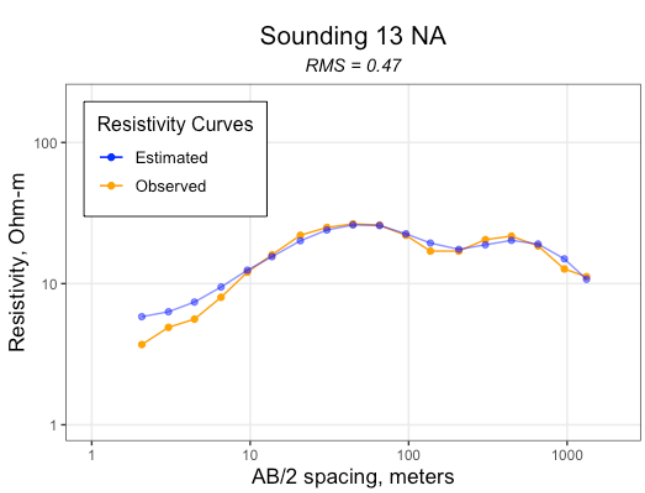
Sounding 13 NA
RMS = 0.47
Resistivity Curves
Estimated
Observed
Resistivity, Ohm-m
AB/2 spacing, meters

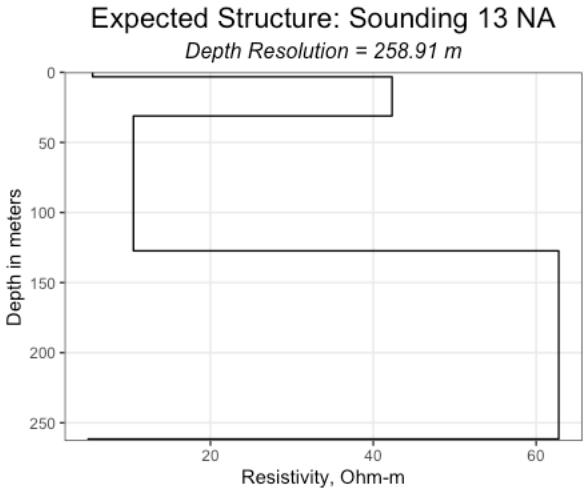
Expected Structure: Sounding 13 NA
Depth Resolution = 258.91 m
Depth in meters
Resistivity, Ohm-m

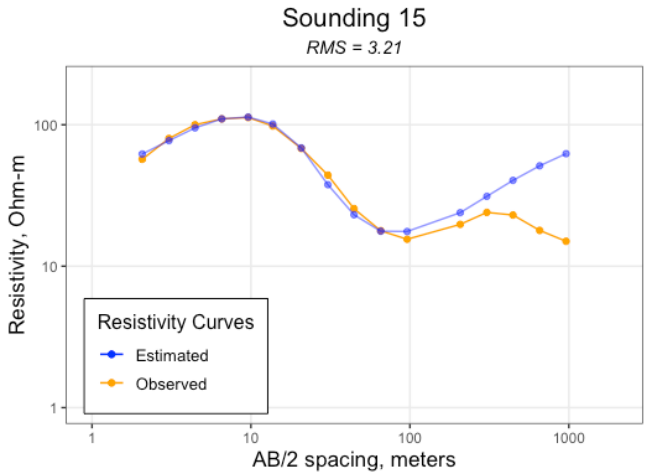
Sounding 15
RMS = 3.21
Resistivity Curves
Estimated
Observed
Resistivity, Ohm-m
AB/2 spacing, meters

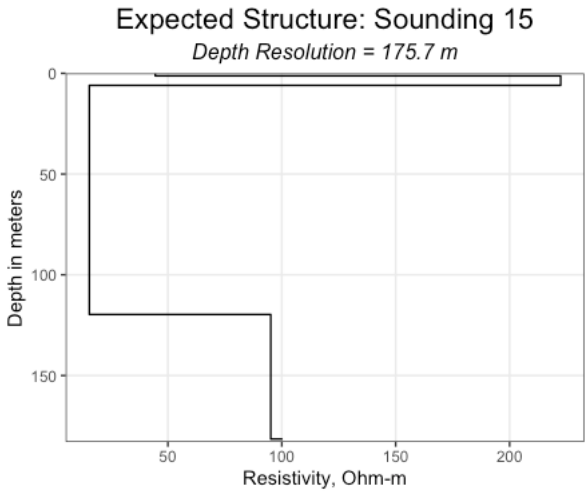
Expected Structure: Sounding 15
Depth Resolution = 175.7 m
Depth in meters
Resistivity, Ohm-m

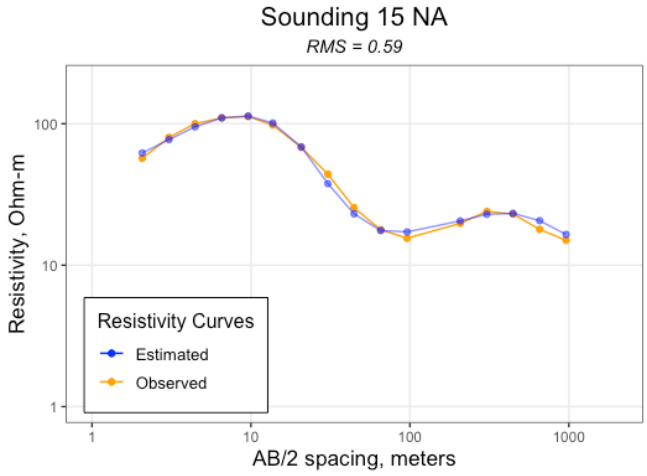
Sounding 15 NA
RMS = 0.59
Resistivity Curves
Estimated
Observed
Resistivity, Ohm-m
AB/2 spacing, meters

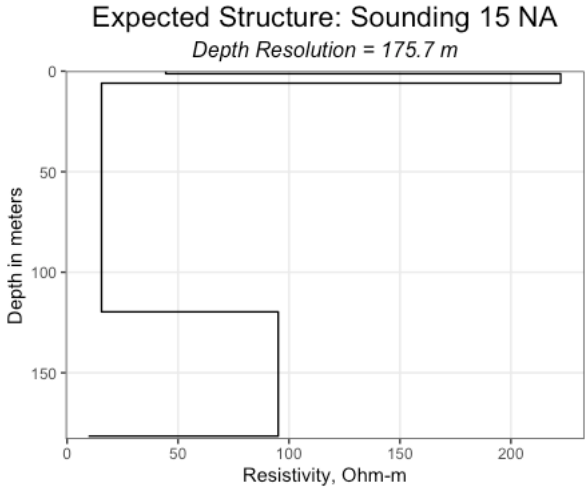
Expected Structure: Sounding 15 NA
Depth Resolution = 175.7 m
Depth in meters
Resistivity, Ohm-m

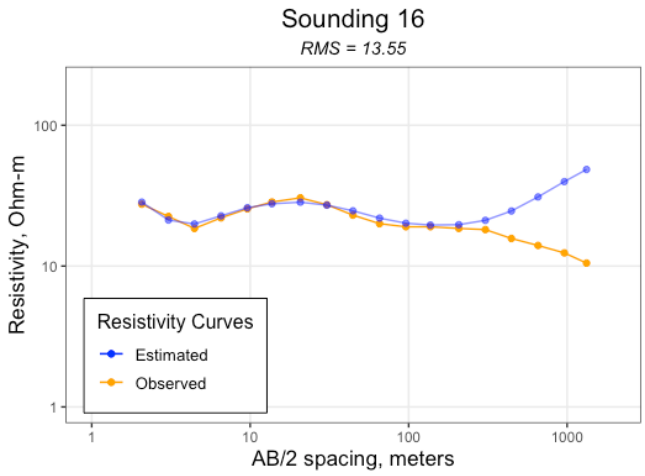
Sounding 16
RMS = 13.55
Resistivity, Ohm-m
AB/2 spacing, meters
Resistivity Curves
Estimated
Observed

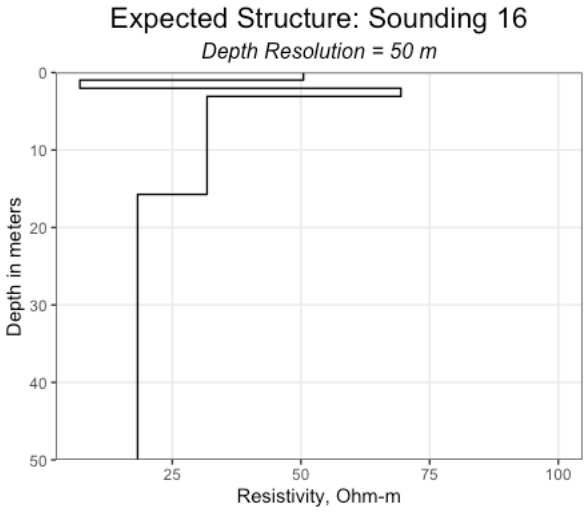
Expected Structure: Sounding 16
Depth Resolution = 50 m
Depth in meters
Resistivity, Ohm-m

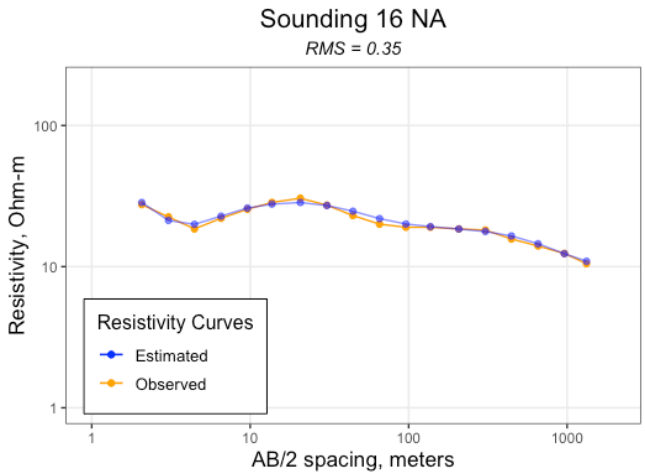
Sounding 16 NA
RMS = 0.35
Resistivity, Ohm-m
AB/2 spacing, meters
Resistivity Curves
Estimated
Observed

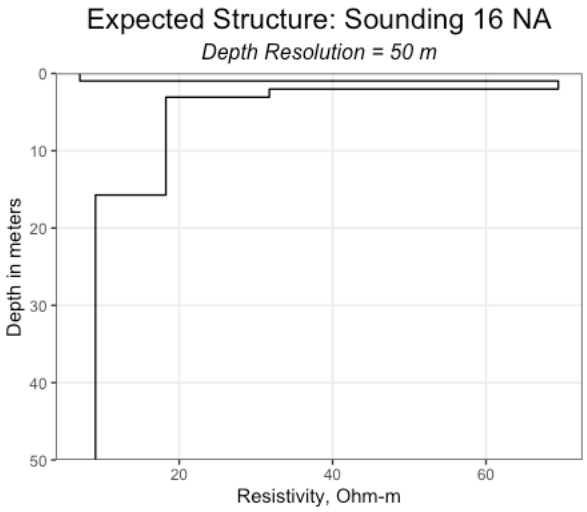
Expected Structure: Sounding 16 NA
Depth Resolution = 50 m
Depth in meters
Resistivity, Ohm-m

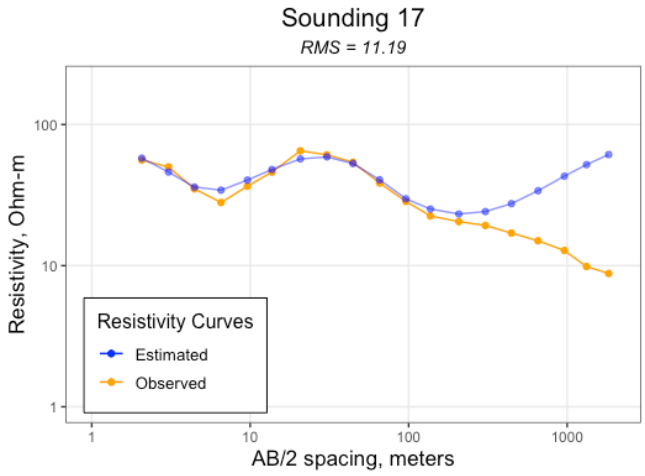
Sounding 17
RMS = 11.19
Resistivity, Ohm-m
AB/2 spacing, meters
Resistivity Curves
Estimated
Observed

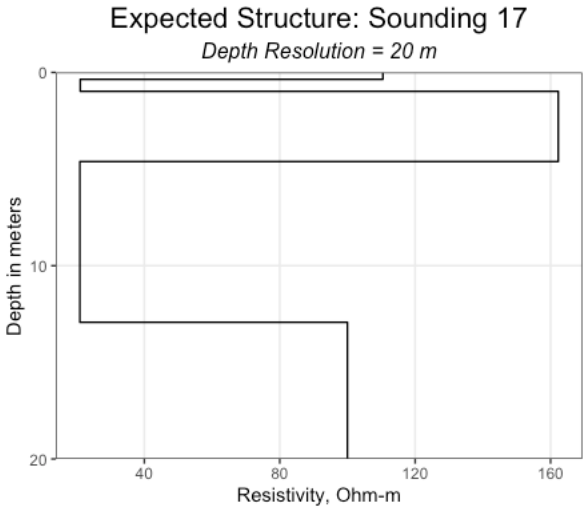
Expected Structure: Sounding 17
Depth Resolution = 20 m
Depth in meters
Resistivity, Ohm-m

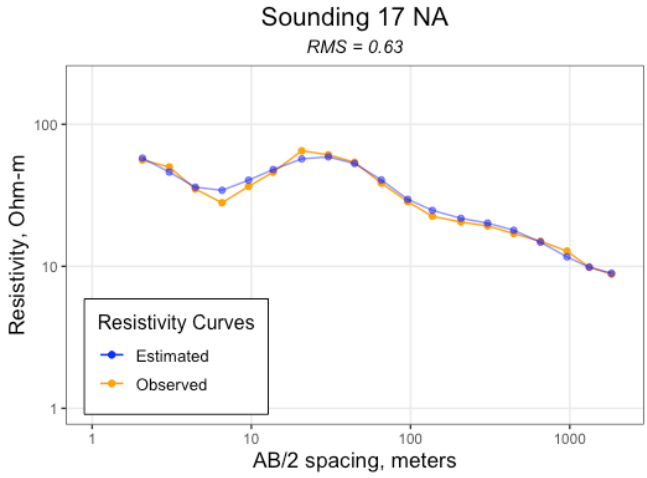
Sounding 17 NA
RMS = 0.63
Resistivity, Ohm-m
AB/2 spacing, meters
Resistivity Curves
Estimated
Observed

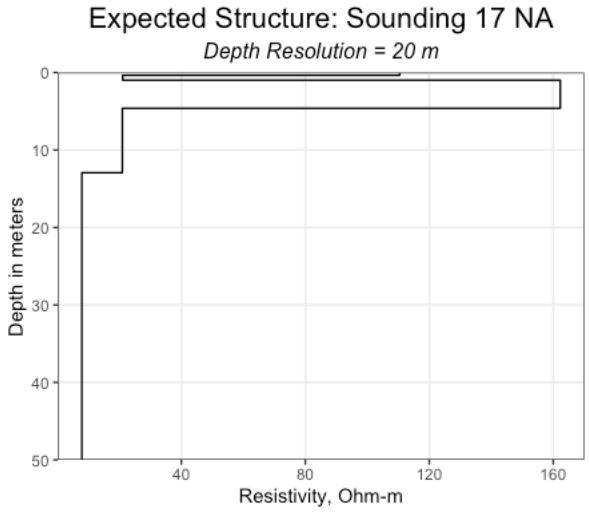
Expected Structure: Sounding 17 NA
Depth Resolution = 20 m
Depth in meters
Resistivity, Ohm-m

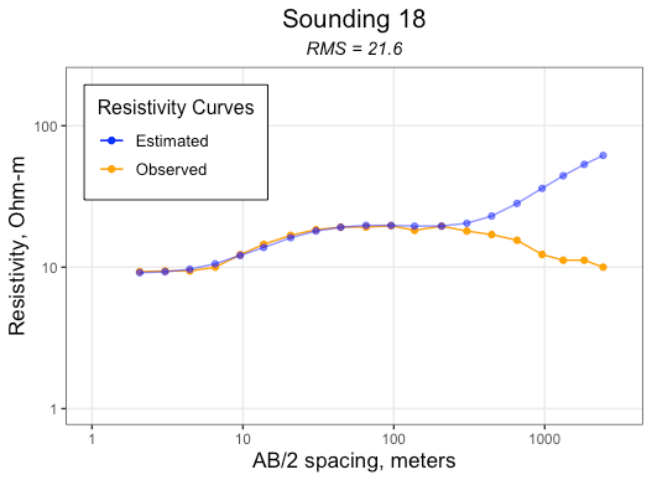
Sounding 18
RMS = 21.6
Resistivity, Ohm-m
AB/2 spacing, meters
Resistivity Curves
Estimated
Observed

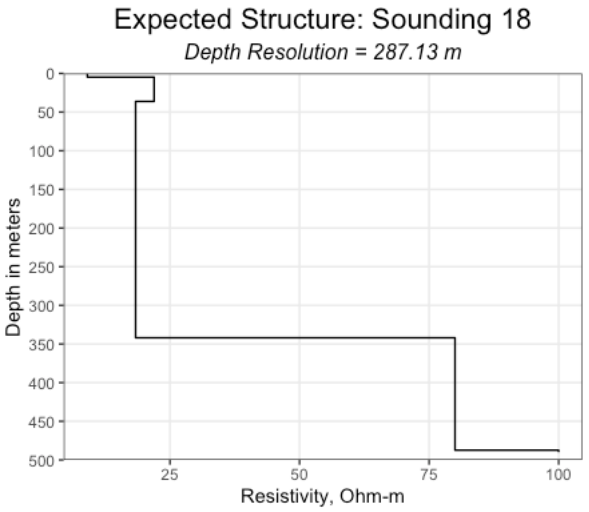
Expected Structure: Sounding 18
Depth Resolution = 287.13 m
Depth in meters
Resistivity, Ohm-m

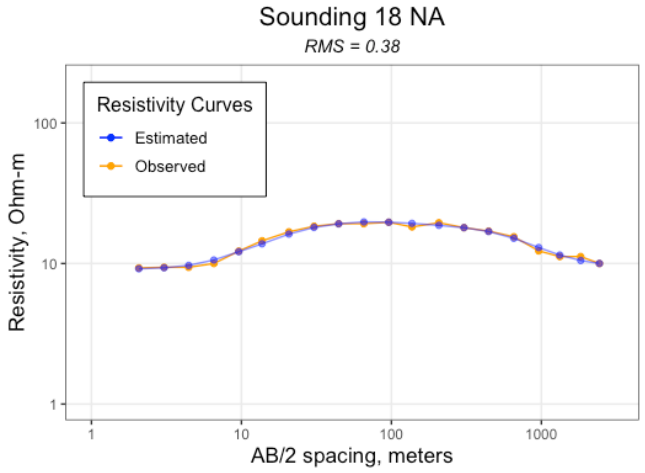
Sounding 18 NA
RMS = 0.38
Resistivity, Ohm-m
AB/2 spacing, meters
Resistivity Curves
Estimated
Observed

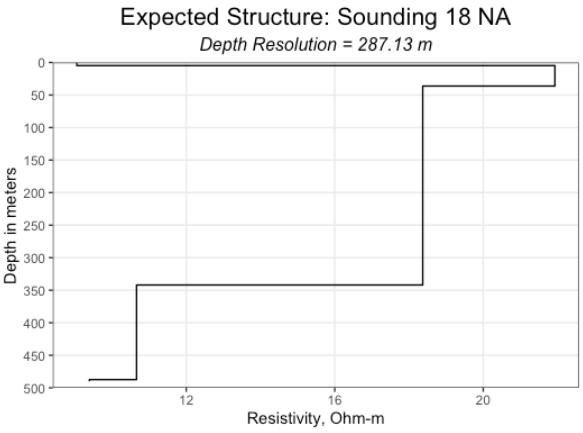
Expected Structure: Sounding 18 NA
Depth Resolution = 287.13 m
Depth in meters
Resistivity, Ohm-m

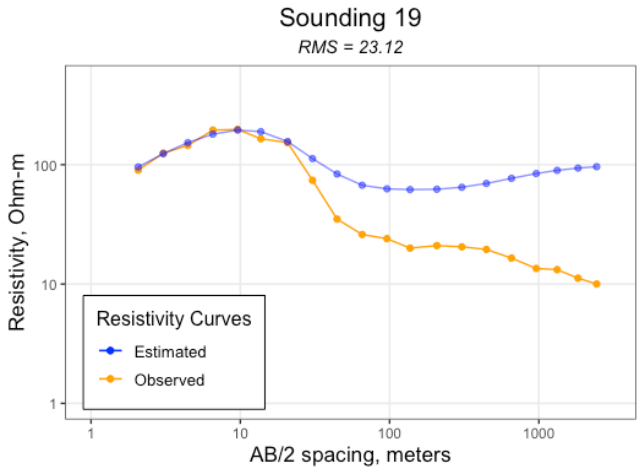
Sounding 19
RMS = 23.12
Resistivity, Ohm-m
AB/2 spacing, meters
Resistivity Curves
Estimated
Observed

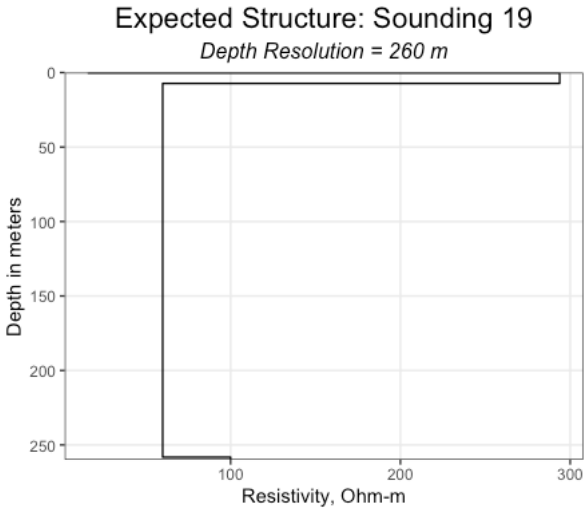
Expected Structure: Sounding 19
Depth Resolution = 260 m
Depth in meters
Resistivity, Ohm-m

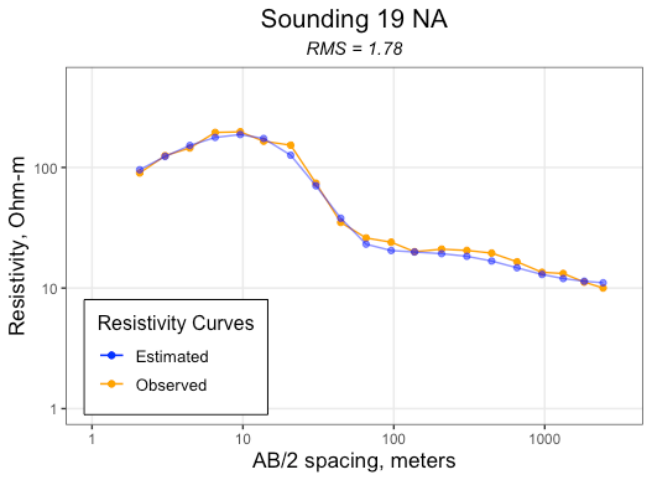
Sounding 19 NA
RMS = 1.78
Resistivity, Ohm-m
AB/2 spacing, meters
Resistivity Curves
Estimated
Observed

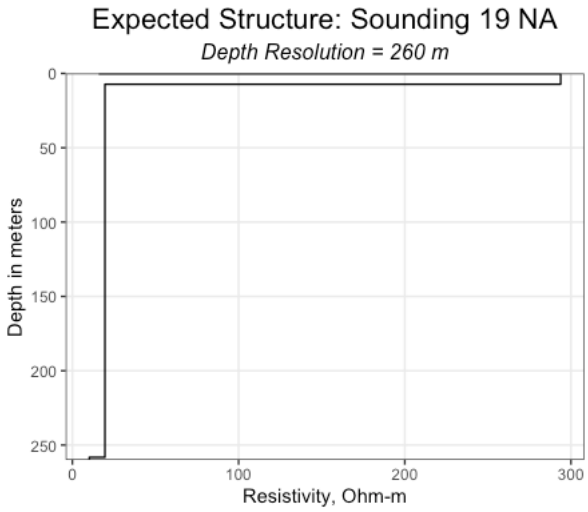
Expected Structure: Sounding 19 NA
Depth Resolution = 260 m
Depth in meters
Resistivity, Ohm-m

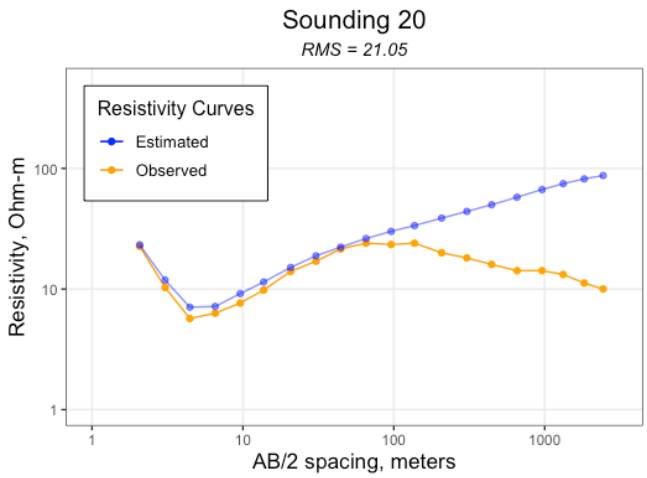
Sounding 20
RMS = 21.05
Resistivity, Ohm-m
AB/2 spacing, meters
Resistivity Curves
Estimated
Observed

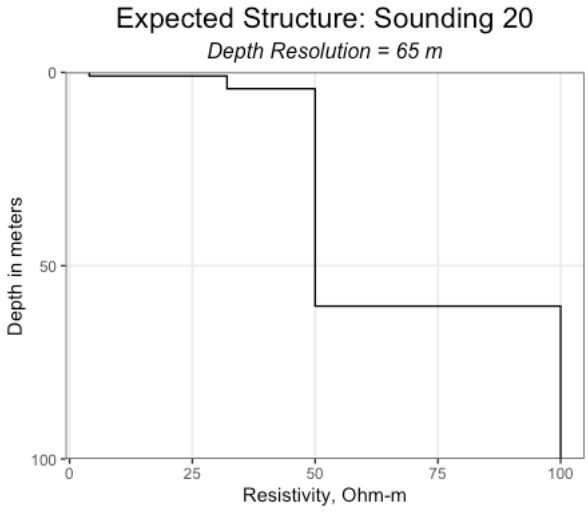
Expected Structure: Sounding 20
Depth Resolution = 65 m
Depth in meters
Resistivity, Ohm-m

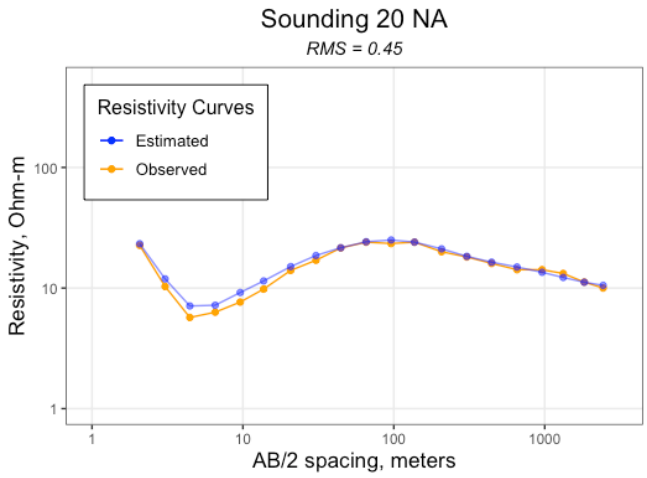
Sounding 20 NA
RMS = 0.45
Resistivity Curves
Estimated
Observed
Resistivity, Ohm-m
AB/2 spacing, meters

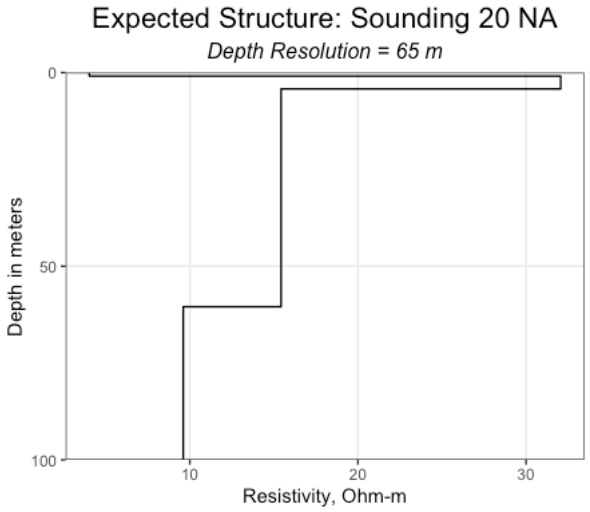
Expected Structure: Sounding 20 NA
Depth Resolution = 65 m
Depth in meters
Resistivity, Ohm-m

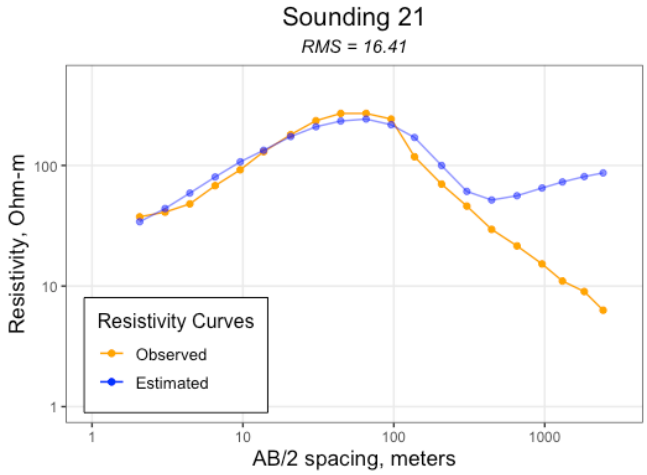
Sounding 21
RMS = 16.41
Resistivity Curves
Observed
Estimated
Resistivity, Ohm-m
AB/2 spacing, meters

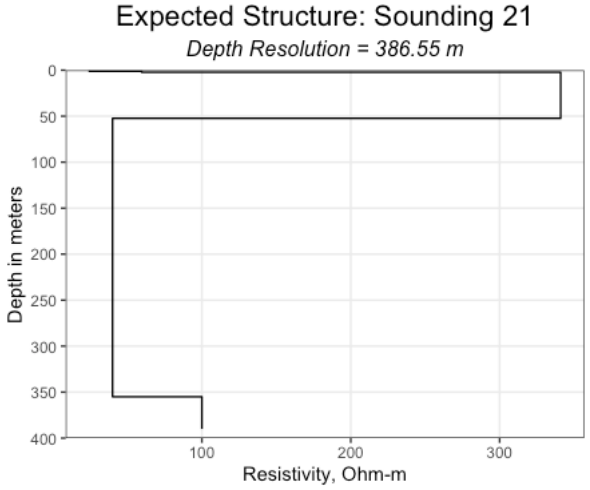
Expected Structure: Sounding 21
Depth Resolution = 386.55 m
Depth in meters
Resistivity, Ohm-m

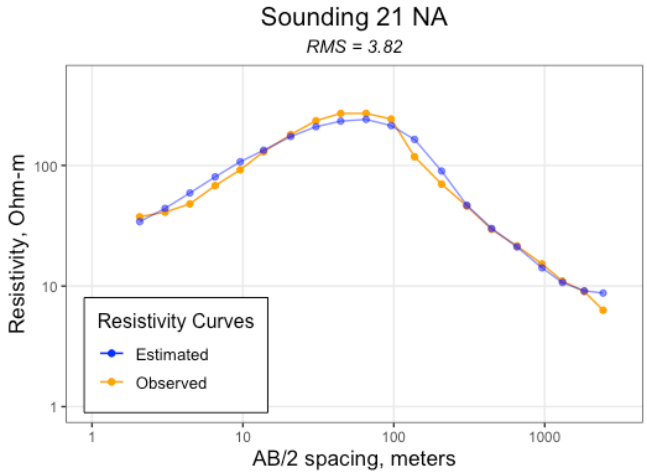
Sounding 21 NA
RMS = 3.82
Resistivity Curves
Estimated
Observed
Resistivity, Ohm-m
AB/2 spacing, meters

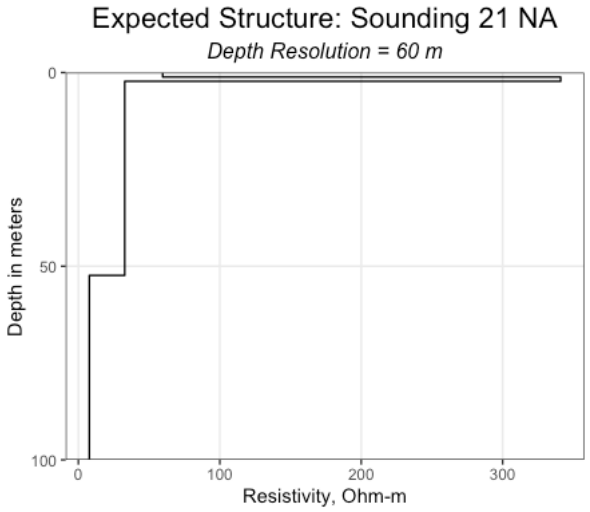
Expected Structure: Sounding 21 NA
Depth Resolution = 60 m
Depth in meters
Resistivity, Ohm-m

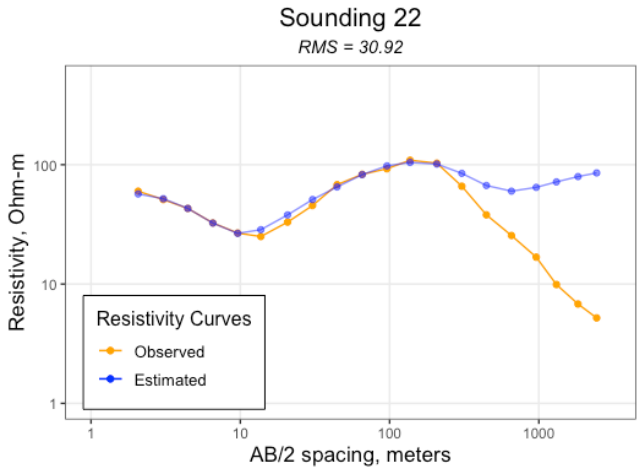
Sounding 22
RMS = 30.92
Resistivity, Ohm-m
AB/2 spacing, meters
Resistivity Curves
Observed
Estimated

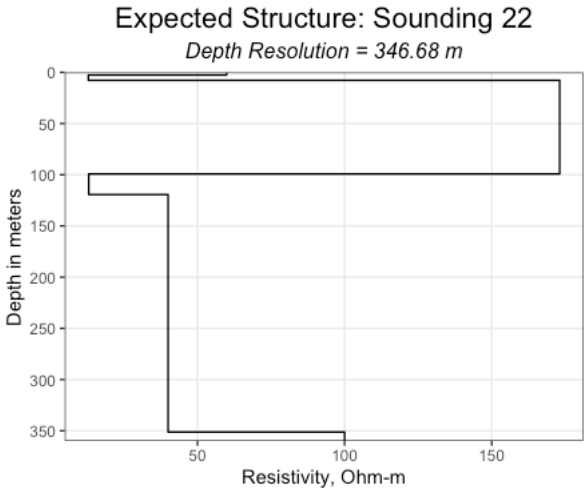
Expected Structure: Sounding 22
Depth Resolution = 346.68 m
Depth in meters
Resistivity, Ohm-m

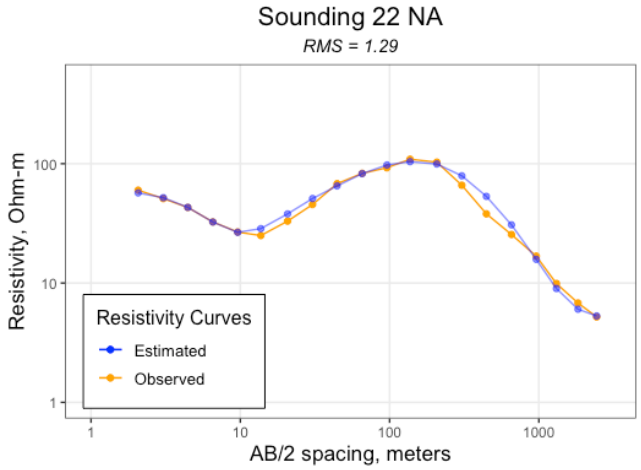
Sounding 22 NA
RMS = 1.29
Resistivity, Ohm-m
AB/2 spacing, meters
Resistivity Curves
Estimated
Observed

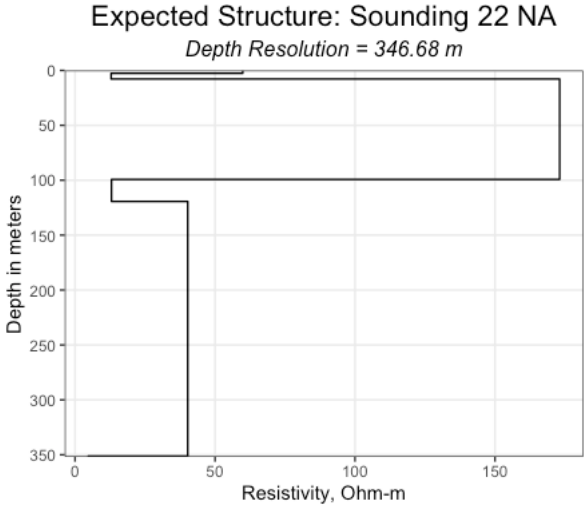
Expected Structure: Sounding 22 NA
Depth Resolution = 346.68 m
Depth in meters
Resistivity, Ohm-m

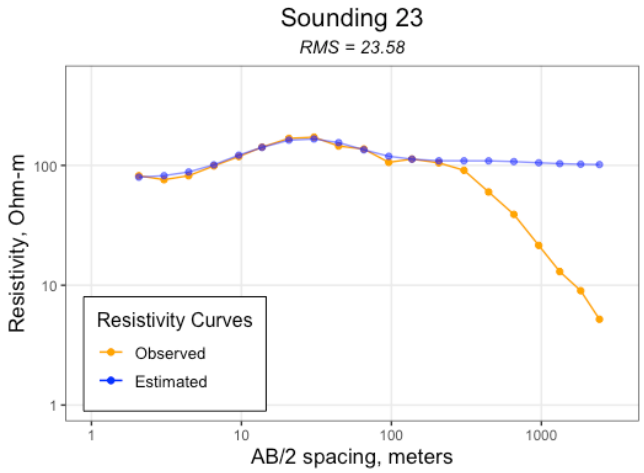
Sounding 23
RMS = 23.58
Resistivity, Ohm-m
AB/2 spacing, meters
Resistivity Curves
Observed
Estimated

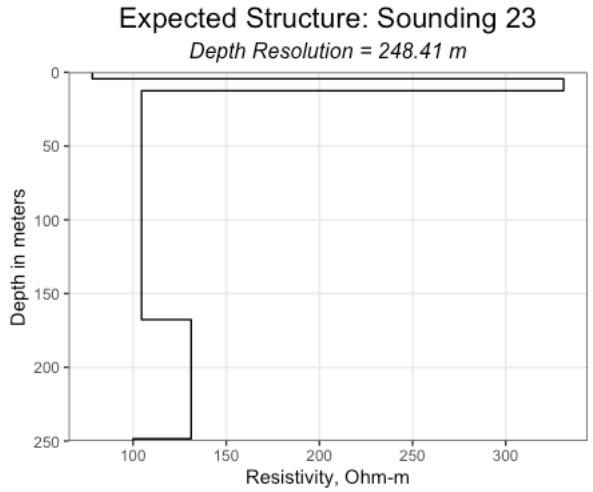
Expected Structure: Sounding 23
Depth Resolution = 248.41 m
Depth in meters
Resistivity, Ohm-m

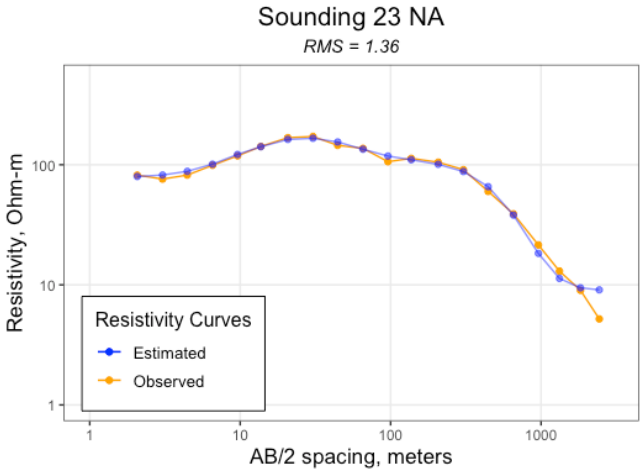
Sounding 23 NA
RMS = 1.36
Resistivity, Ohm-m
AB/2 spacing, meters
Resistivity Curves
Estimated
Observed

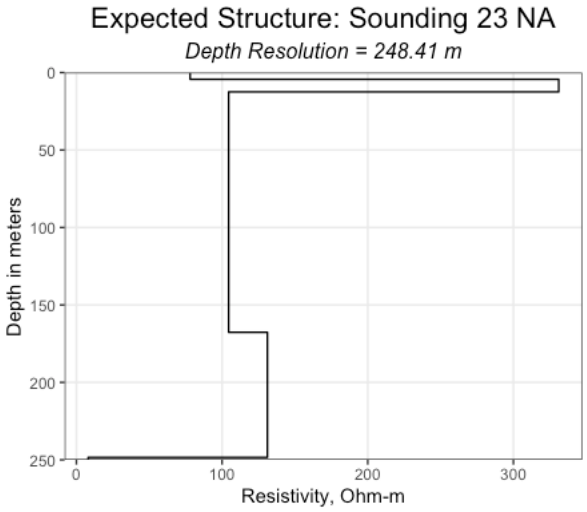
Expected Structure: Sounding 23 NA
Depth Resolution = 248.41 m
Depth in meters
Resistivity, Ohm-m

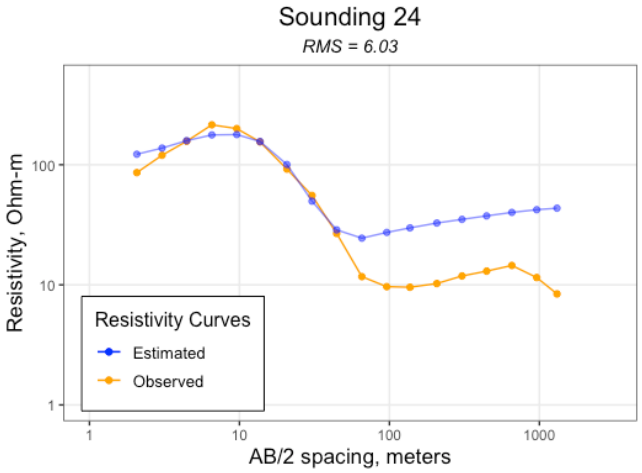
Sounding 24
RMS = 6.03
Resistivity, Ohm-m
AB/2 spacing, meters
Resistivity Curves
Estimated
Observed

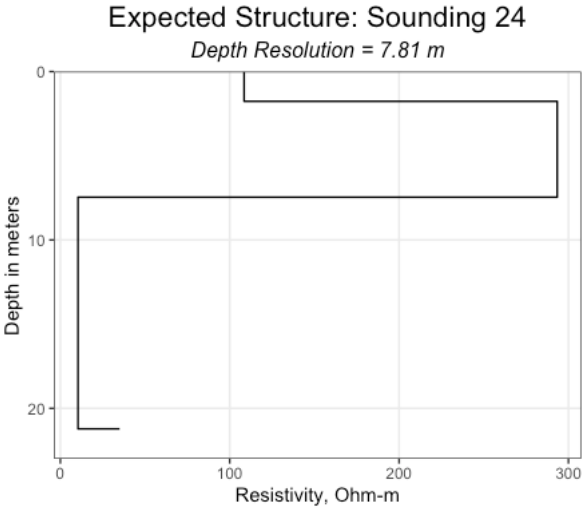
Expected Structure: Sounding 24
Depth Resolution = 7.81 m
Depth in meters
Resistivity, Ohm-m

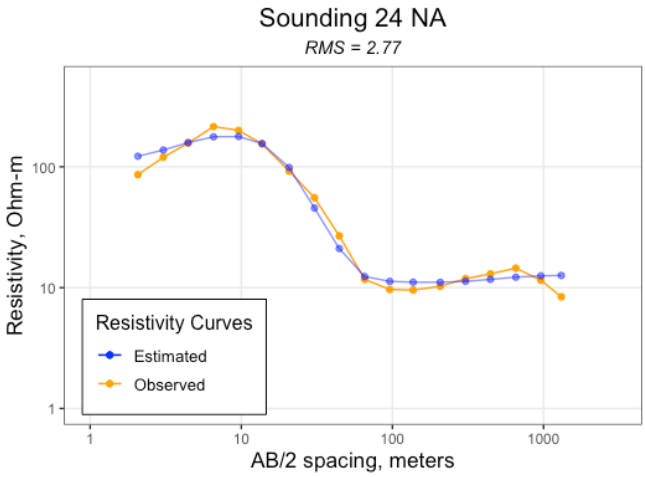
Sounding 24 NA
RMS = 2.77
Resistivity, Ohm-m
AB/2 spacing, meters
Resistivity Curves
Estimated
Observed

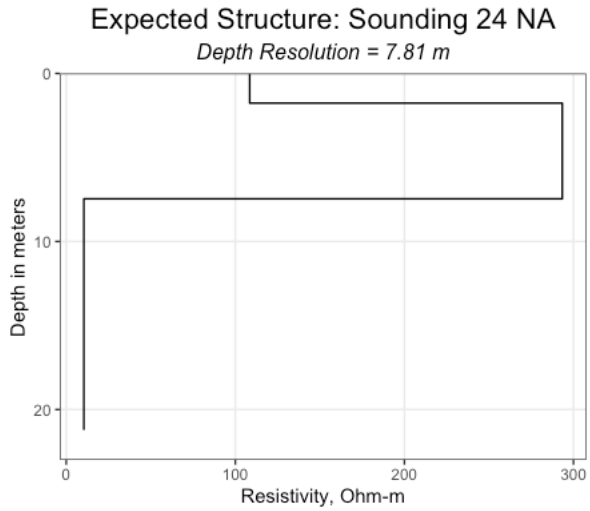
Expected Structure: Sounding 24 NA
Depth Resolution = 7.81 m
Depth in meters
Resistivity, Ohm-m

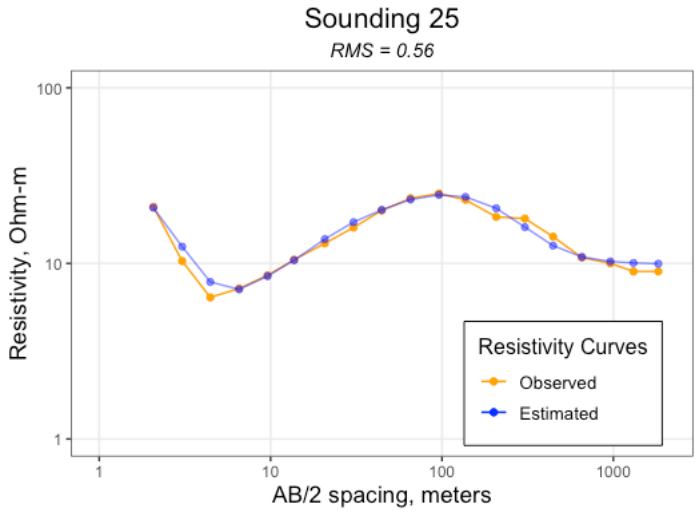
Sounding 25
RMS = 0.56
Resistivity, Ohm-m
AB/2 spacing, meters
Resistivity Curves
Observed
Estimated

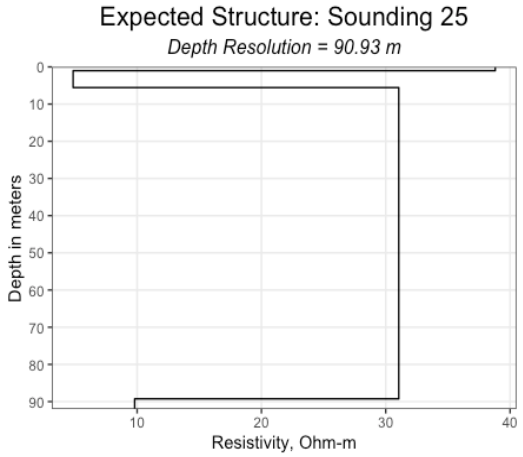
Expected Structure: Sounding 25
Depth Resolution = 90.93 m
Depth in meters
Resistivity, Ohm-m

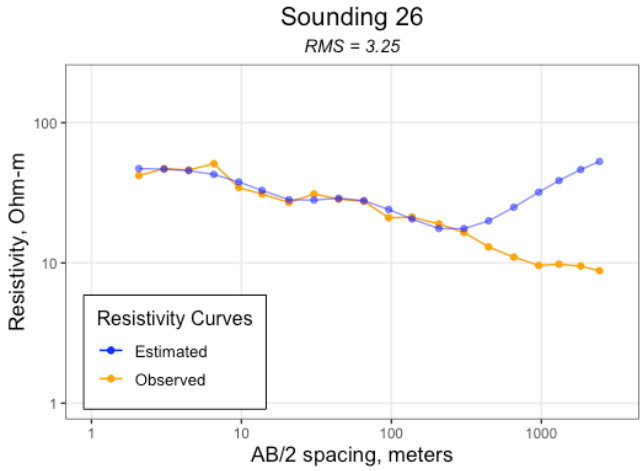
Sounding 26
RMS = 3.25
Resistivity, Ohm-m
AB/2 spacing, meters
Resistivity Curves
Estimated
Observed

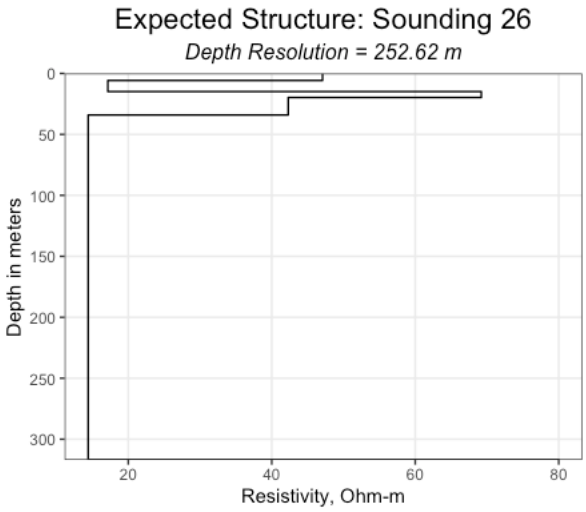
Expected Structure: Sounding 26
Depth Resolution = 252.62 m
Depth in meters
Resistivity, Ohm-m

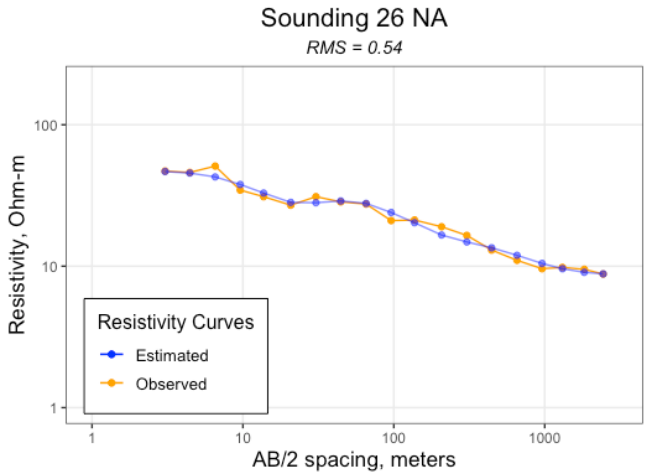
Sounding 26 NA
RMS = 0.54
Resistivity, Ohm-m
AB/2 spacing, meters
Resistivity Curves
Estimated
Observed

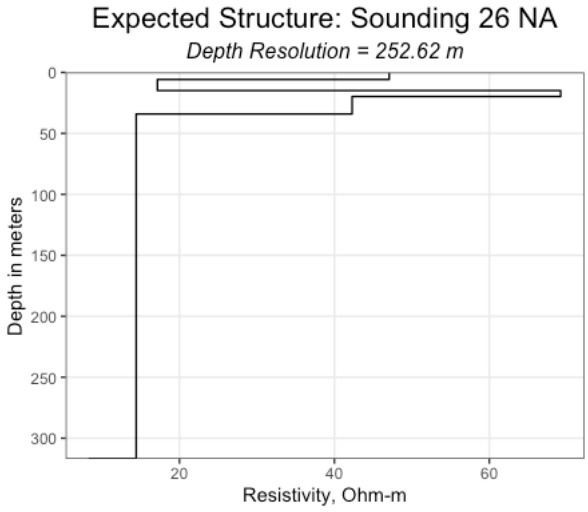
Expected Structure: Sounding 26 NA
Depth Resolution = 252.62 m
Depth in meters
Resistivity, Ohm-m

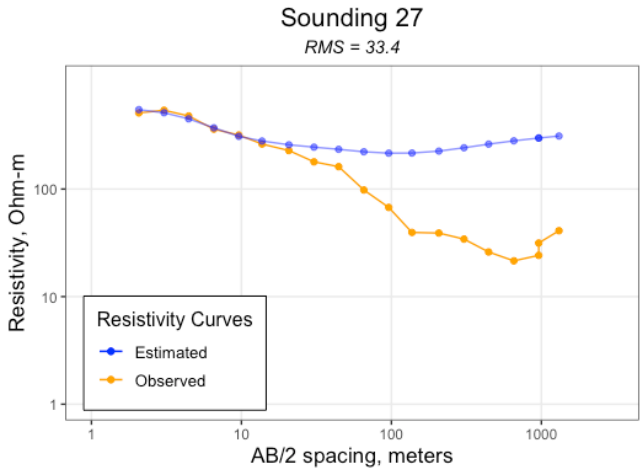
Sounding 27
RMS = 33.4
Resistivity, Ohm-m
AB/2 spacing, meters
Resistivity Curves
Estimated
Observed

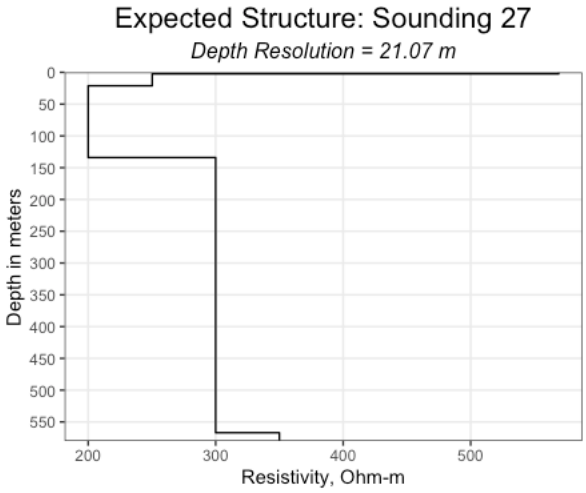
Expected Structure: Sounding 27
Depth Resolution = 21.07 m
Depth in meters
Resistivity, Ohm-m

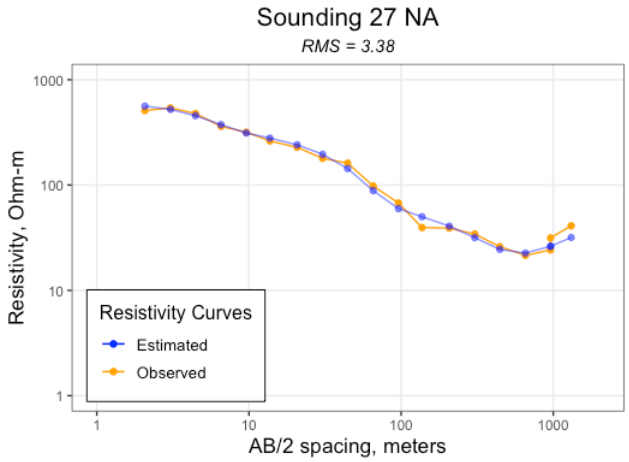
Sounding 27 NA
RMS = 3.38
Resistivity, Ohm-m
AB/2 spacing, meters
Resistivity Curves
Estimated
Observed

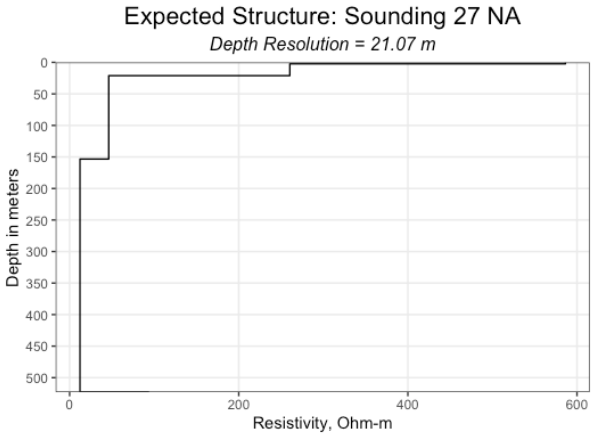
Expected Structure: Sounding 27 NA
Depth Resolution = 21.07 m
Depth in meters
Resistivity, Ohm-m

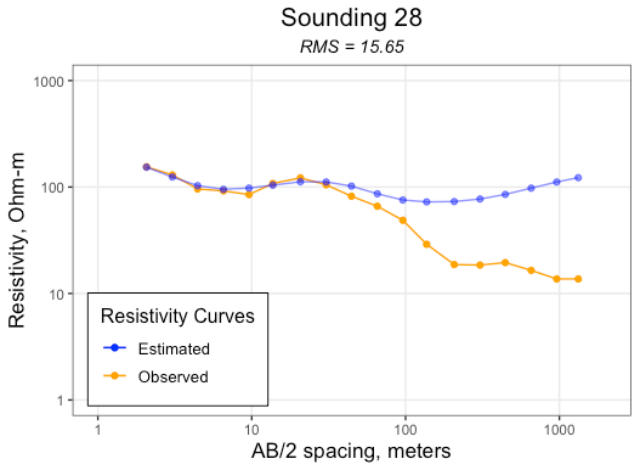
Sounding 28
RMS = 15.65
Resistivity, Ohm-m
AB/2 spacing, meters
Resistivity Curves
Estimated
Observed

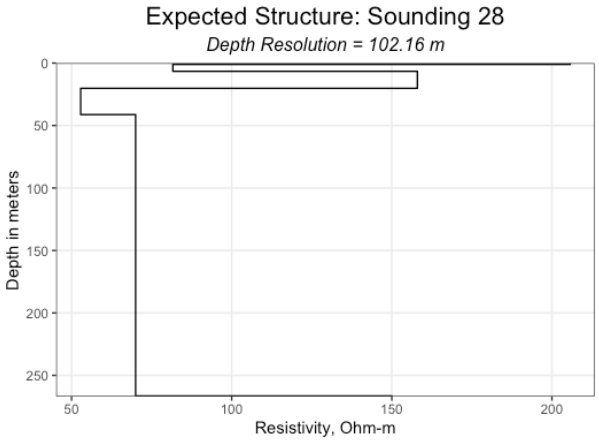
Expected Structure: Sounding 28
Depth Resolution = 102.16 m
Depth in meters
Resistivity, Ohm-m

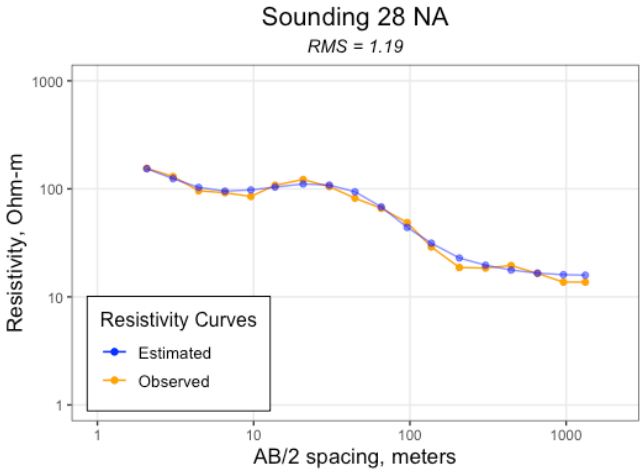
Sounding 28 NA
RMS = 1.19
Resistivity, Ohm-m
AB/2 spacing, meters
Resistivity Curves
Estimated
Observed

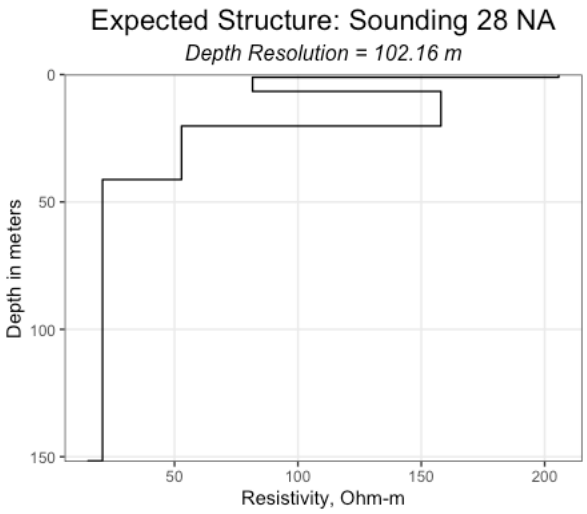
Expected Structure: Sounding 28 NA
Depth Resolution = 102.16 m
Depth in meters
Resistivity, Ohm-m

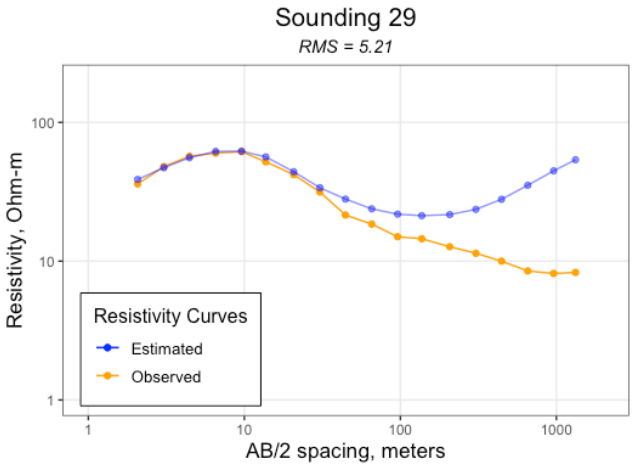
Sounding 29
RMS = 5.21
Resistivity, Ohm-m
AB/2 spacing, meters
Resistivity Curves
Estimated
Observed

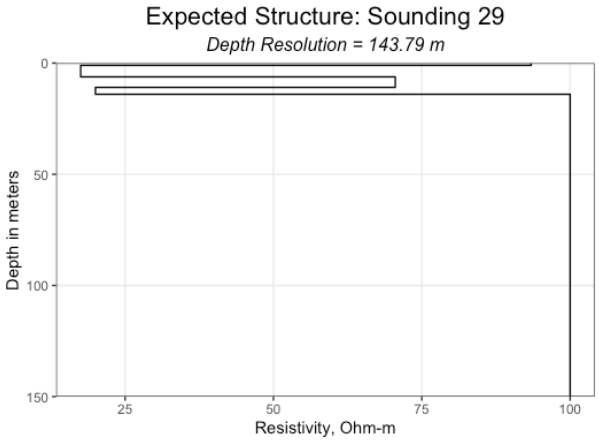
Expected Structure: Sounding 29
Depth Resolution = 143.79 m
Depth in meters
Resistivity, Ohm-m

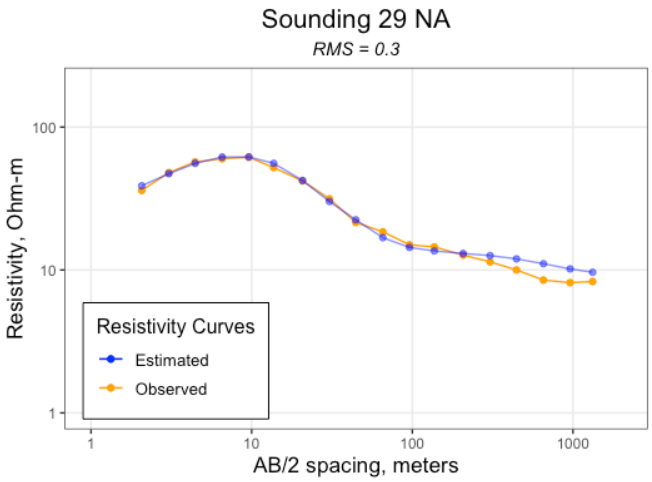
Sounding 29 NA
RMS = 0.3
Resistivity, Ohm-m
AB/2 spacing, meters
Resistivity Curves
Estimated
Observed

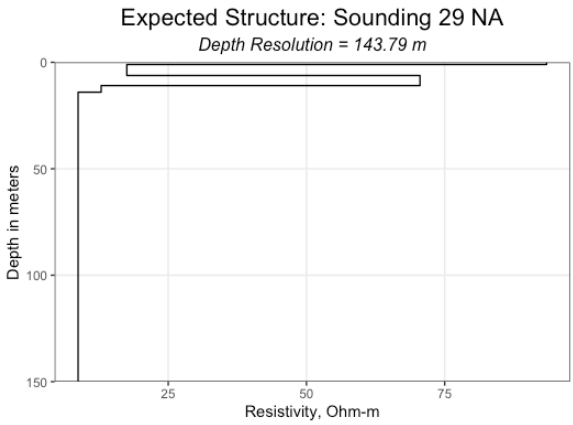
Expected Structure: Sounding 29 NA
Depth Resolution = 143.79 m
Depth in meters
Resistivity, Ohm-m

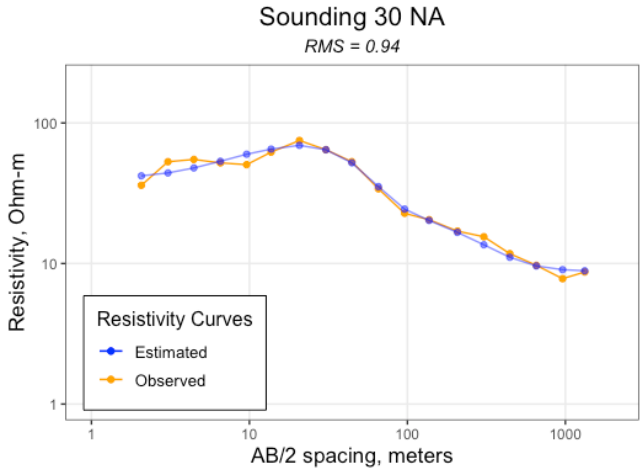
Sounding 30 NA
RMS = 0.94
Resistivity, Ohm-m
AB/2 spacing, meters
Resistivity Curves
Estimated
Observed

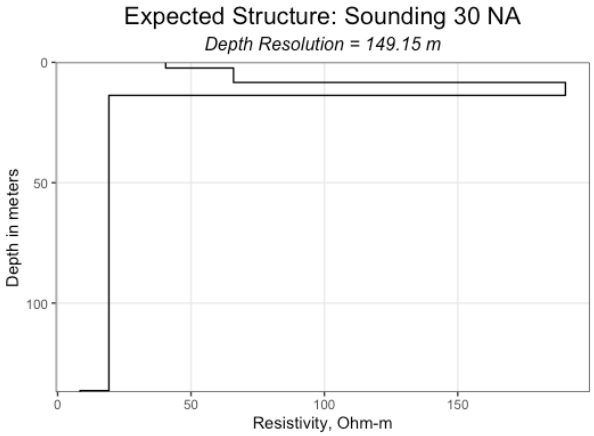
Expected Structure: Sounding 30 NA
Depth Resolution = 149.15 m
Depth in meters
Resistivity, Ohm-m

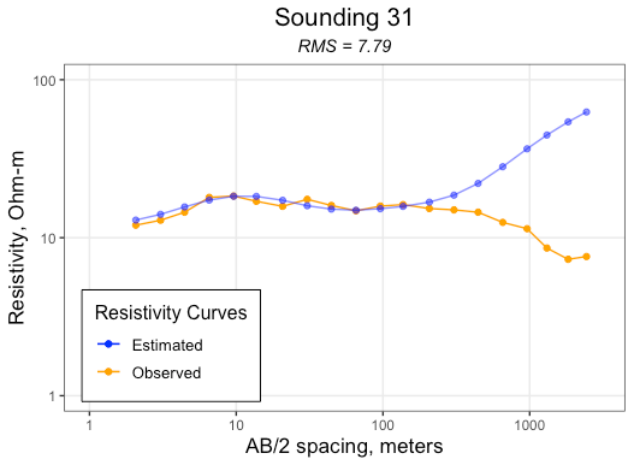
Sounding 31
RMS = 7.79
Resistivity, Ohm-m
AB/2 spacing, meters
Resistivity Curves
Estimated
Observed

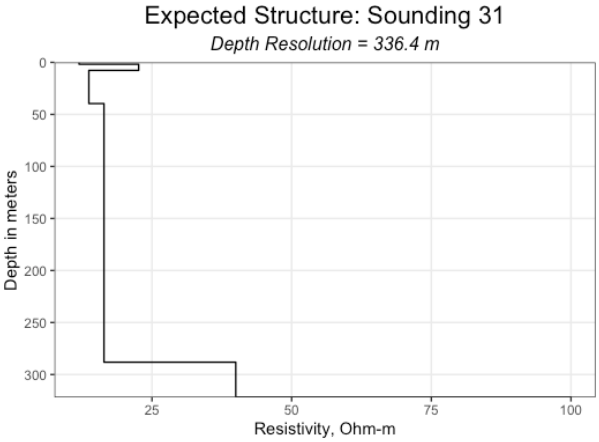
Expected Structure: Sounding 31
Depth Resolution = 336.4 m
Depth in meters
Resistivity, Ohm-m

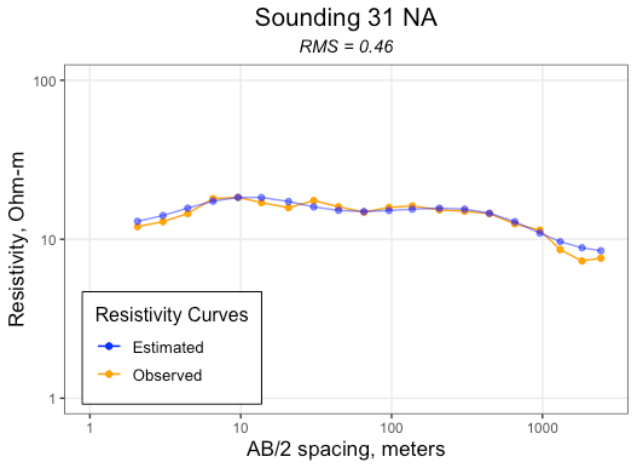
Sounding 31 NA
RMS = 0.46
Resistivity, Ohm-m
AB/2 spacing, meters
Resistivity Curves
Estimated
Observed

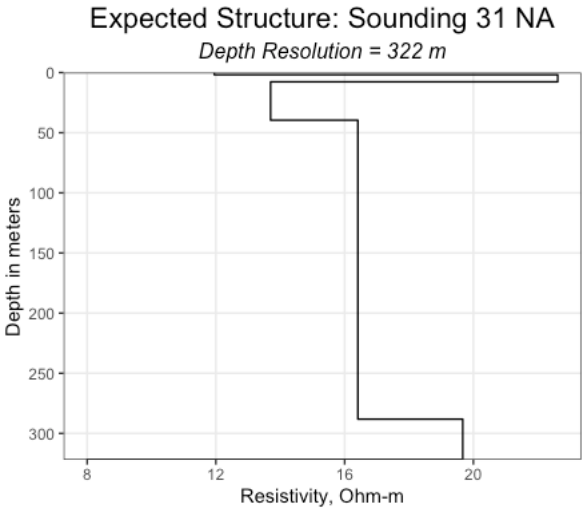
Expected Structure: Sounding 31 NA
Depth Resolution = 322 m
Depth in meters
Resistivity, Ohm-m

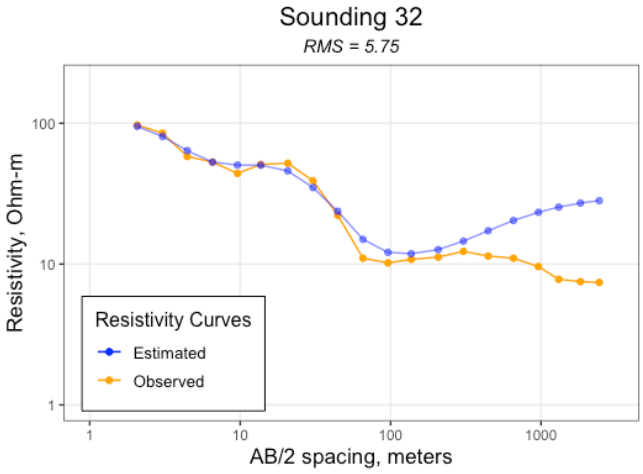
Sounding 32
RMS = 5.75
Resistivity, Ohm-m
AB/2 spacing, meters
Resistivity Curves
Estimated
Observed

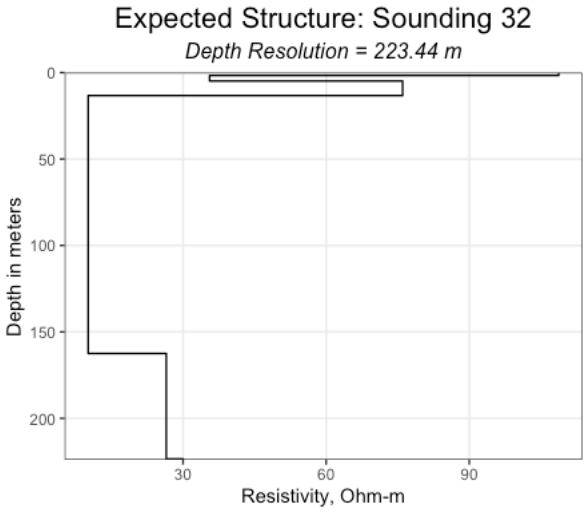
Expected Structure: Sounding 32
Depth Resolution = 223.44 m
Depth in meters
Resistivity, Ohm-m

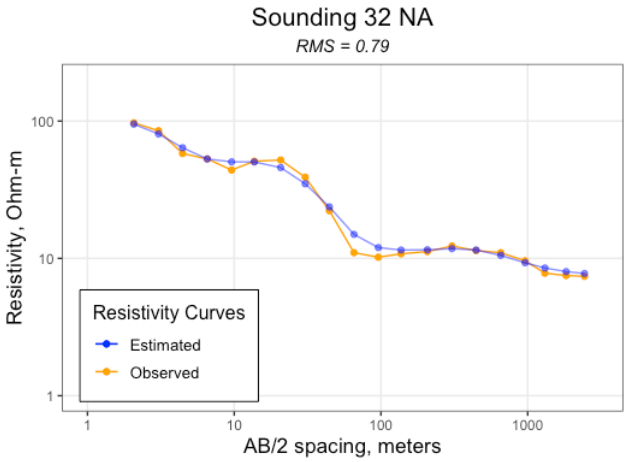
Sounding 32 NA
RMS = 0.79
Resistivity, Ohm-m
AB/2 spacing, meters
Resistivity Curves
Estimated
Observed

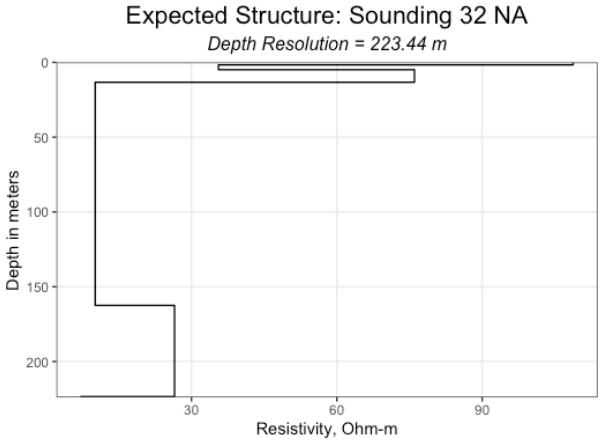
Expected Structure: Sounding 32 NA
Depth Resolution = 223.44 m
Depth in meters
Resistivity, Ohm-m

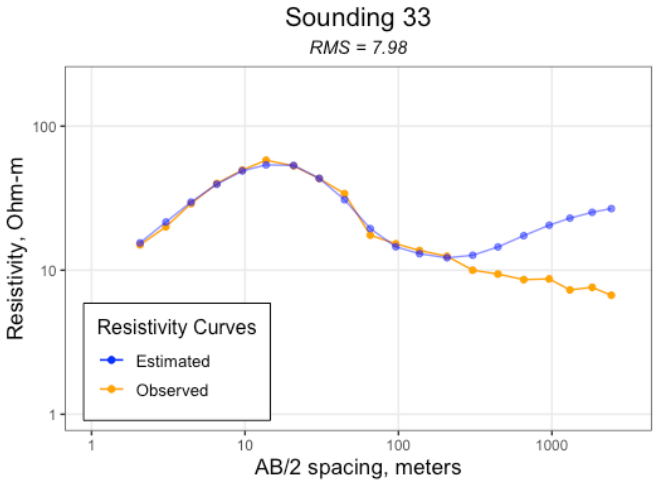
Sounding 33
RMS = 7.98
Resistivity, Ohm-m
AB/2 spacing, meters
Resistivity Curves
Estimated
Observed

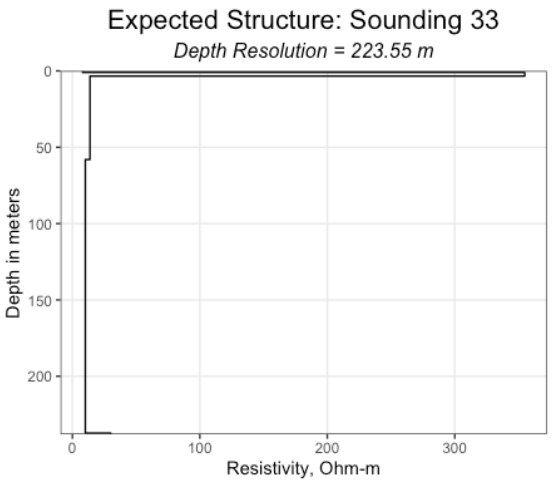
Expected Structure: Sounding 33
Depth Resolution = 223.55 m
Depth in meters
Resistivity, Ohm-m

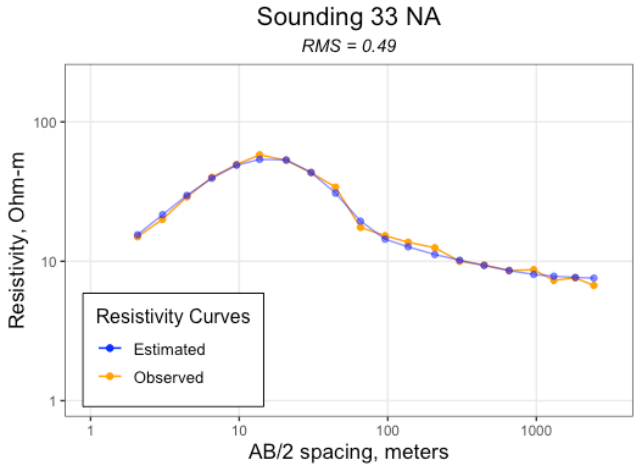
Sounding 33 NA
RMS = 0.49
Resistivity, Ohm-m
AB/2 spacing, meters
Resistivity Curves
Estimated
Observed

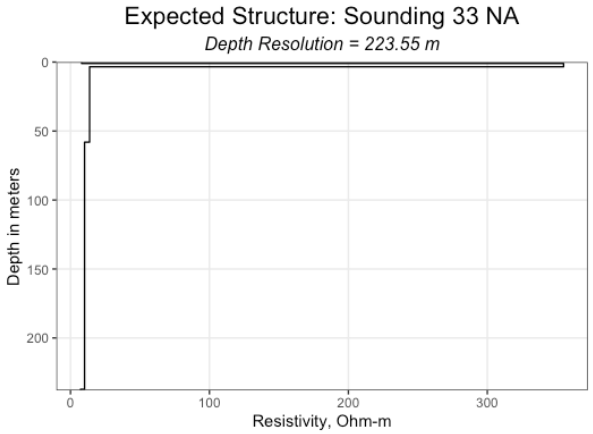
Expected Structure: Sounding 33 NA
Depth Resolution = 223.55 m
Depth in meters
Resistivity, Ohm-m

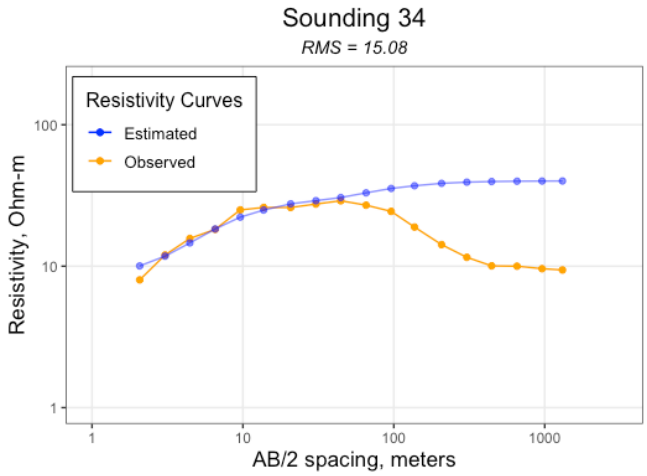
Sounding 34
RMS = 15.08
Resistivity, Ohm-m
AB/2 spacing, meters
Resistivity Curves
Estimated
Observed

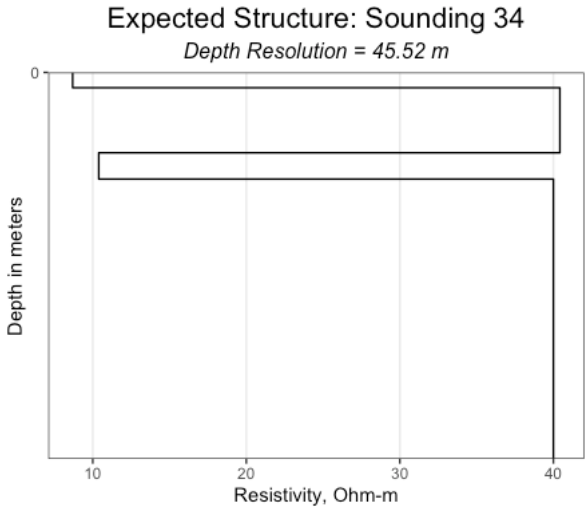
Expected Structure: Sounding 34
Depth Resolution = 45.52 m
Depth in meters
Resistivity, Ohm-m

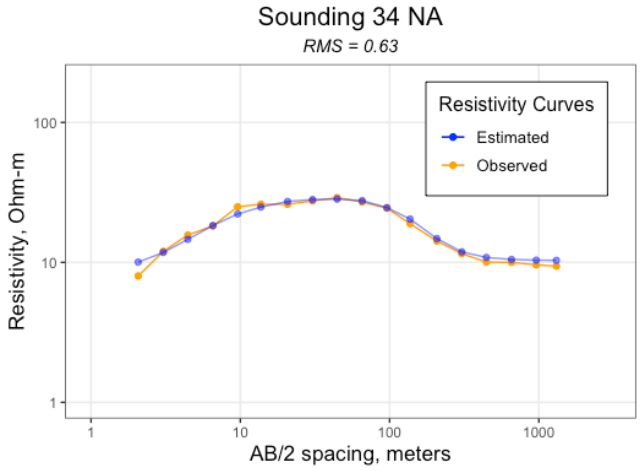
Sounding 34 NA
RMS = 0.63
Resistivity, Ohm-m
AB/2 spacing, meters
Resistivity Curves
Estimated
Observed

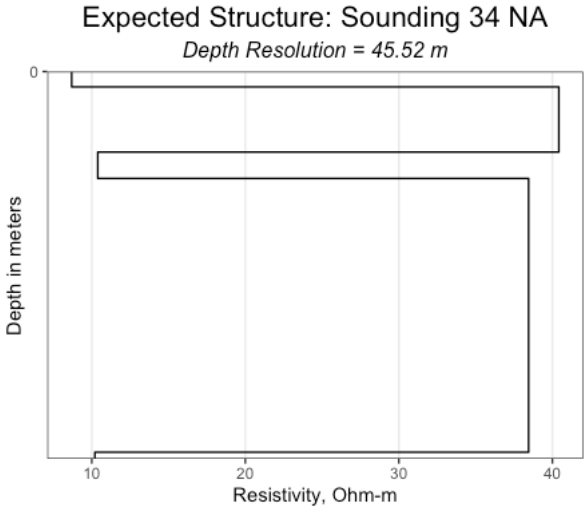
Expected Structure: Sounding 34 NA
Depth Resolution = 45.52 m
Depth in meters
Resistivity, Ohm-m

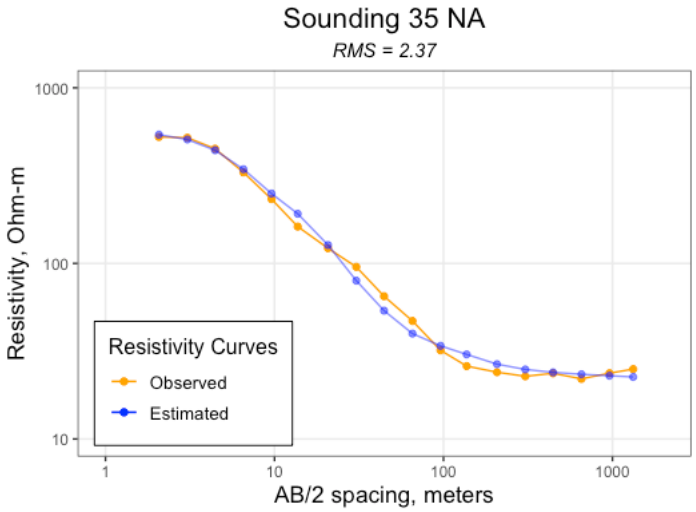
Sounding 35 NA
RMS = 2.37
Resistivity, Ohm-m
AB/2 spacing, meters
Resistivity Curves
Observed
Estimated

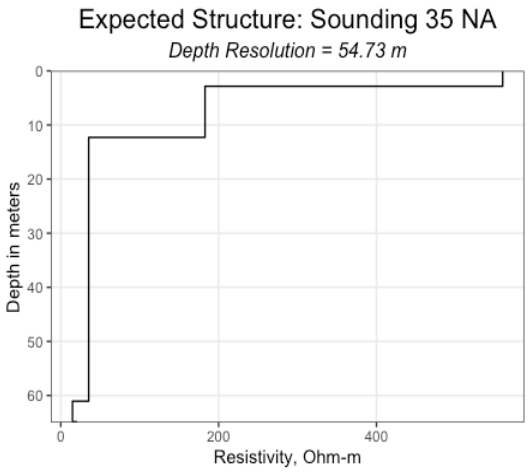
Expected Structure: Sounding 35 NA
Depth Resolution = 54.73 m
Depth in meters
Resistivity, Ohm-m

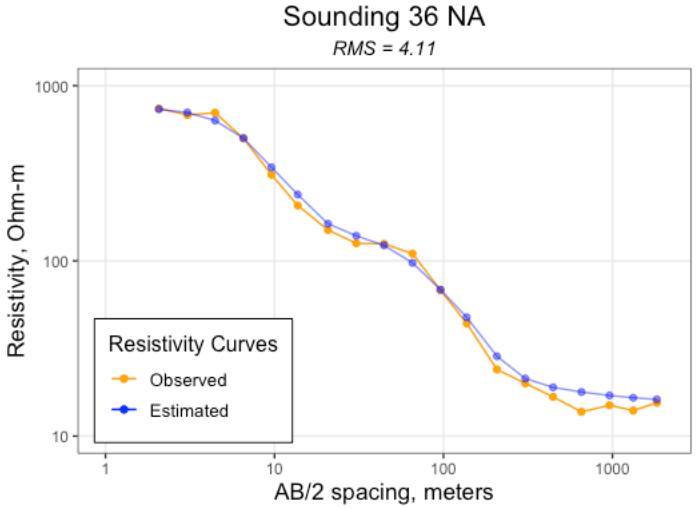
Sounding 36 NA
RMS = 4.11
Resistivity, Ohm-m
AB/2 spacing, meters
Resistivity Curves
Observed
Estimated

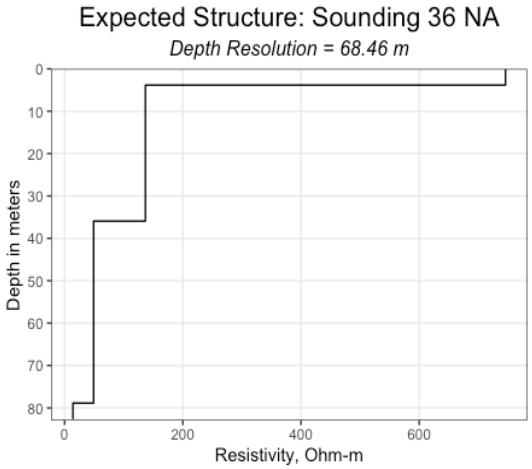
Expected Structure: Sounding 36 NA
Depth Resolution = 68.46 m
Depth in meters
Resistivity, Ohm-m

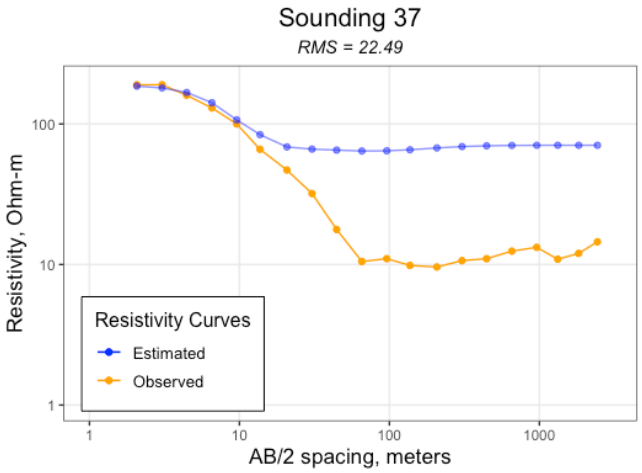
Sounding 37
RMS = 22.49
Resistivity, Ohm-m
AB/2 spacing, meters
Resistivity Curves
Estimated
Observed

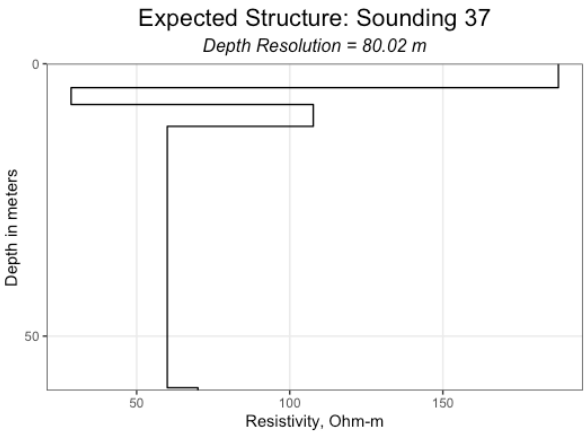
Expected Structure: Sounding 37
Depth Resolution = 80.02 m
Depth in meters
Resistivity, Ohm-m

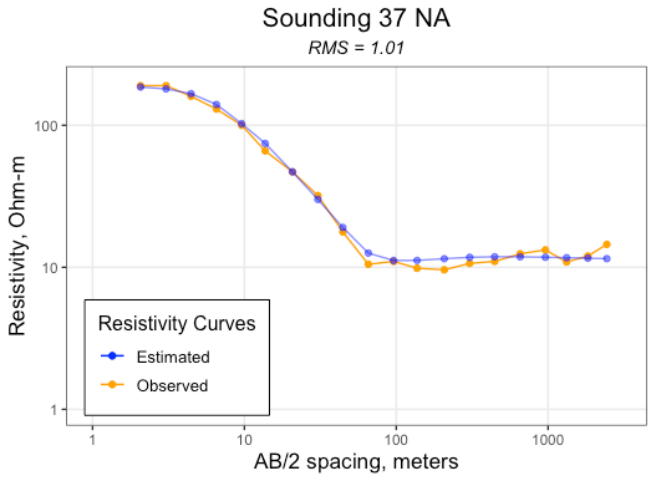
Sounding 37 NA
RMS = 1.01
Resistivity, Ohm-m
AB/2 spacing, meters
Resistivity Curves
Estimated
Observed

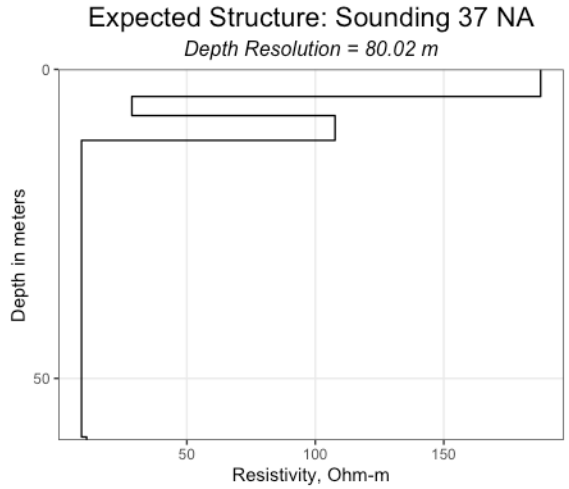
Expected Structure: Sounding 37 NA
Depth Resolution = 80.02 m
Depth in meters
Resistivity, Ohm-m

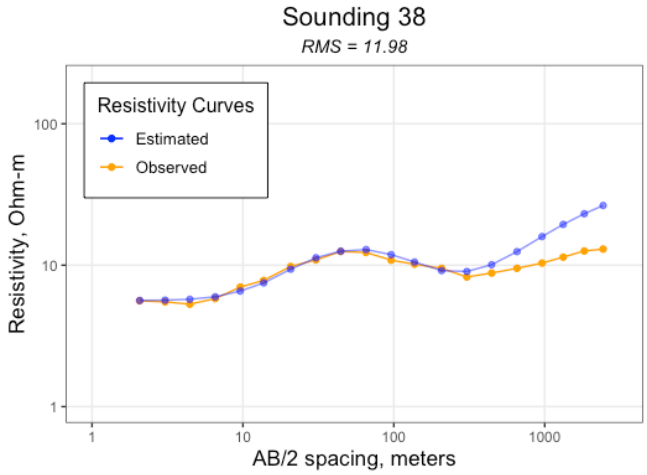
Sounding 38
RMS = 11.98
Resistivity, Ohm-m
AB/2 spacing, meters
Resistivity Curves
Estimated
Observed

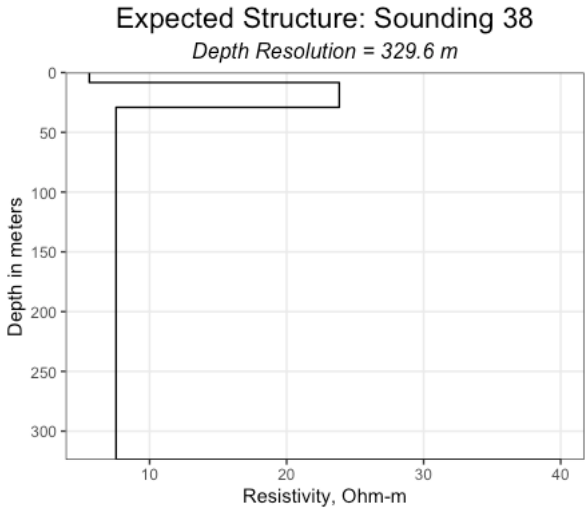
Expected Structure: Sounding 38
Depth Resolution = 329.6 m
Depth in meters
Resistivity, Ohm-m

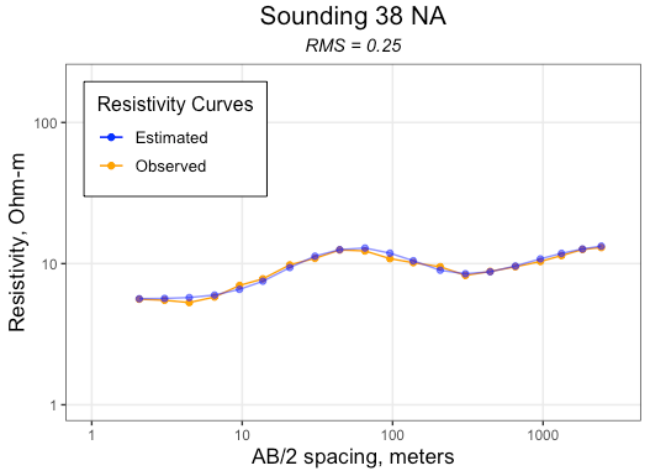
Sounding 38 NA
RMS = 0.25
Resistivity, Ohm-m
AB/2 spacing, meters
Resistivity Curves
Estimated
Observed

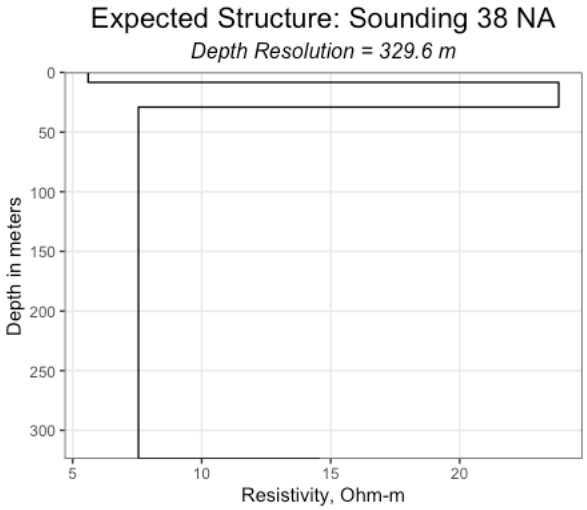
Expected Structure: Sounding 38 NA
Depth Resolution = 329.6 m
Depth in meters
Resistivity, Ohm-m

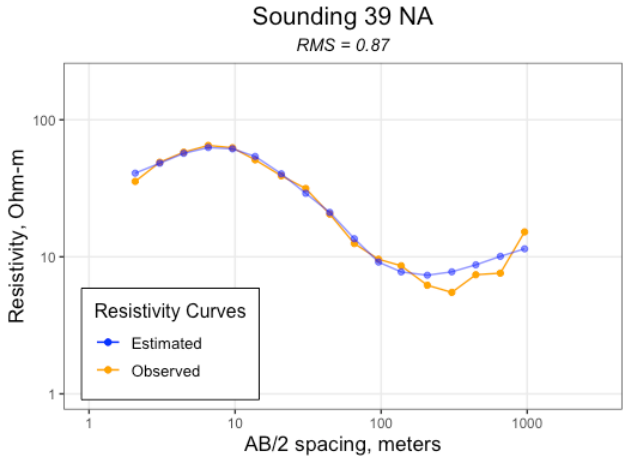
Sounding 39 NA
RMS = 0.87
Resistivity, Ohm-m
AB/2 spacing, meters
Resistivity Curves
Estimated
Observed

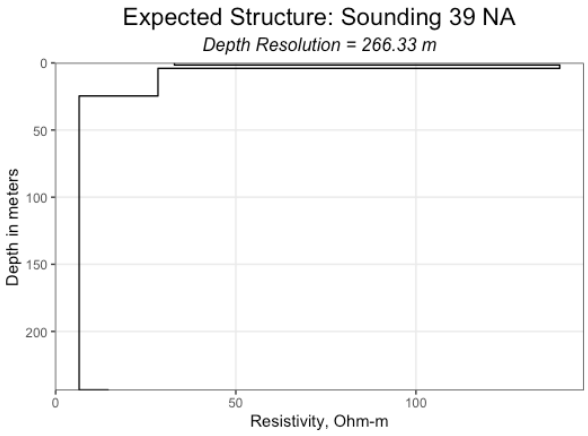
Expected Structure: Sounding 39 NA
Depth Resolution = 266.33 m
Depth in meters
Resistivity, Ohm-m

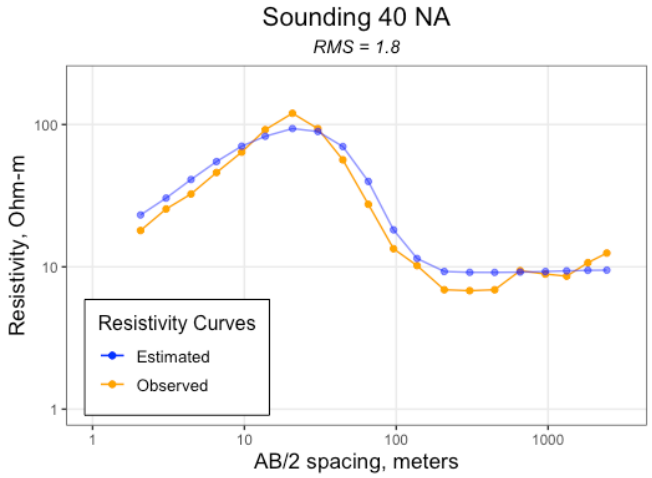
Sounding 40 NA
RMS = 1.8
Resistivity, Ohm-m
AB/2 spacing, meters
Resistivity Curves
Estimated
Observed

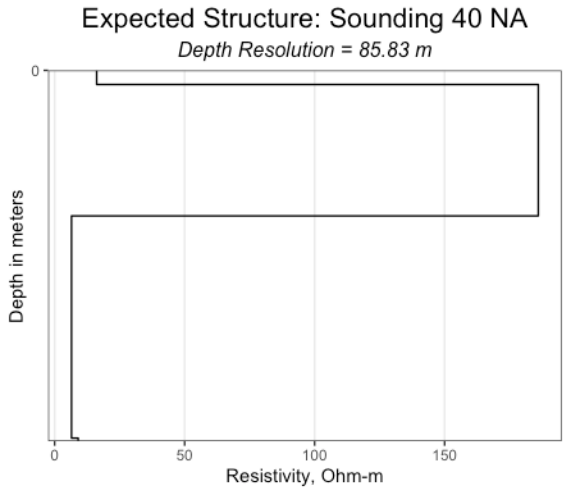
Expected Structure: Sounding 40 NA
Depth Resolution = 85.83 m
Depth in meters
Resistivity, Ohm-m

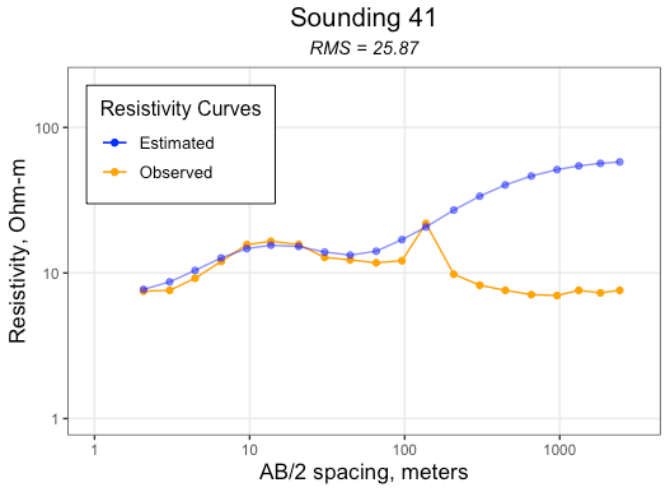
Sounding 41
RMS = 25.87
Resistivity, Ohm-m
AB/2 spacing, meters
Resistivity Curves
Estimated
Observed

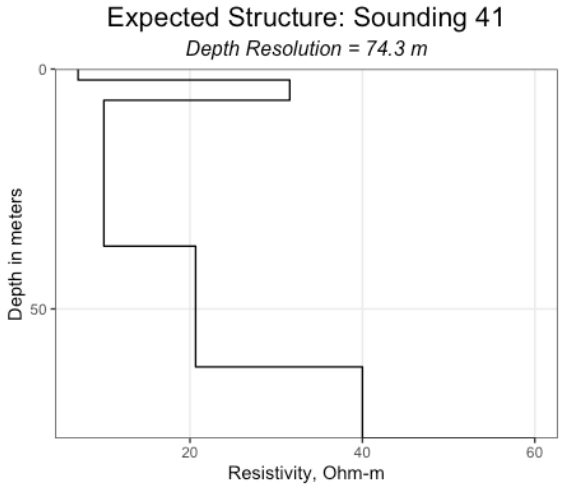
Expected Structure: Sounding 41
Depth Resolution = 74.3 m
Depth in meters
Resistivity, Ohm-m

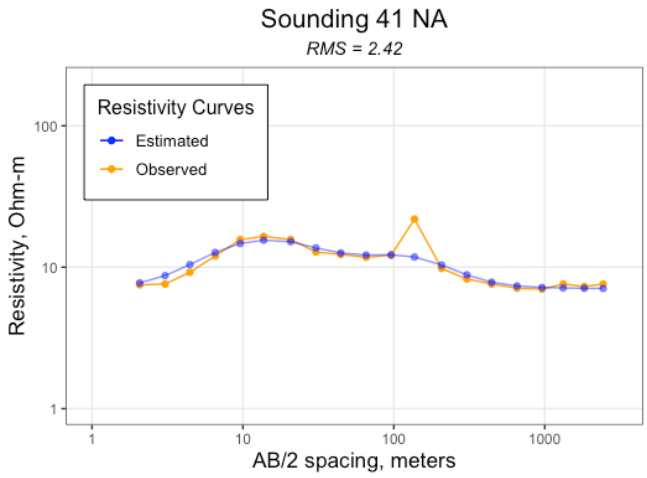
Sounding 41 NA
RMS = 2.42
Resistivity Curves
Estimated
Observed
Resistivity, Ohm-m
AB/2 spacing, meters

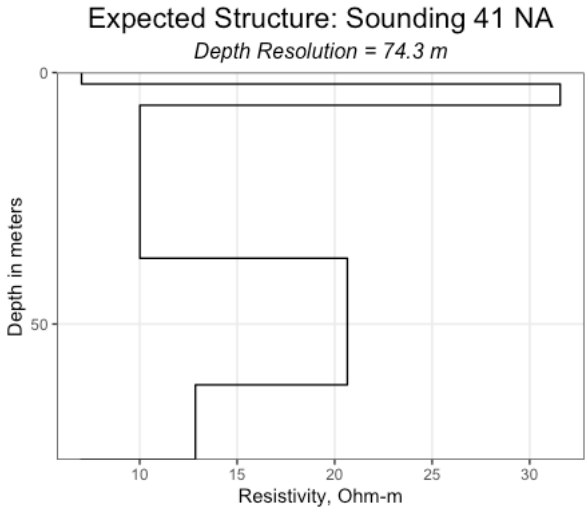
Expected Structure: Sounding 41 NA
Depth Resolution = 74.3 m
Depth in meters
Resistivity, Ohm-m

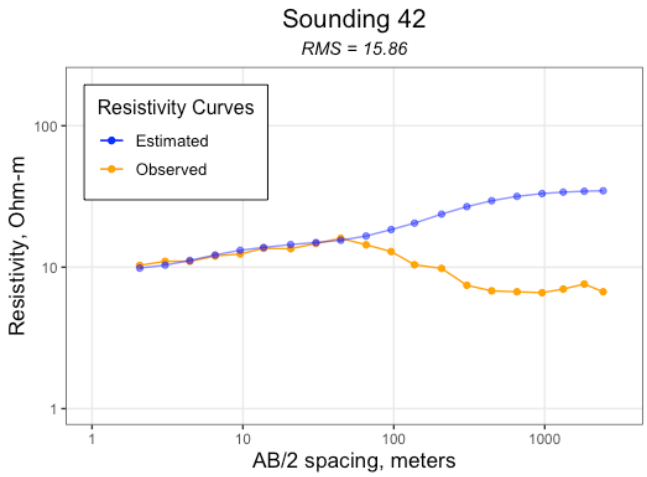
Sounding 42
RMS = 15.86
Resistivity Curves
Estimated
Observed
Resistivity, Ohm-m
AB/2 spacing, meters

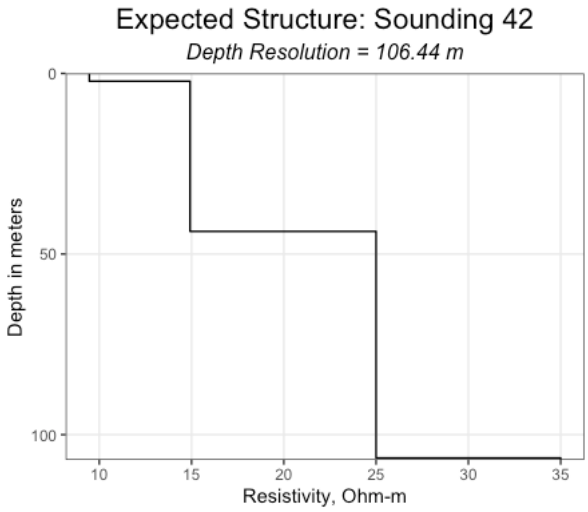
Expected Structure: Sounding 42
Depth Resolution = 106.44 m
Depth in meters
Resistivity, Ohm-m

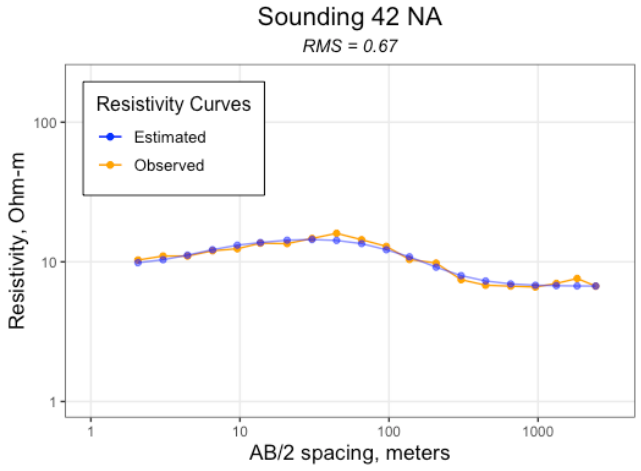
Sounding 42 NA
RMS = 0.67
Resistivity Curves
Estimated
Observed
Resistivity, Ohm-m
AB/2 spacing, meters

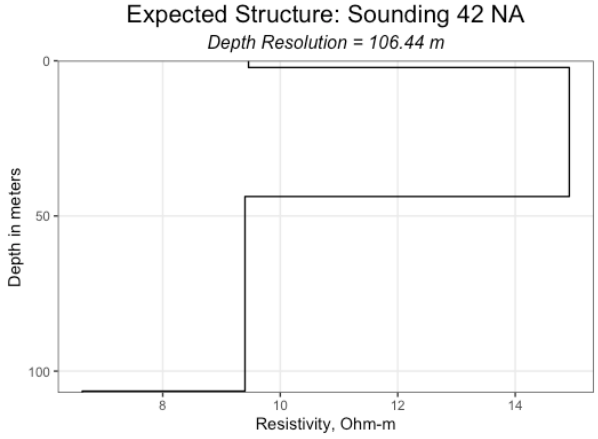
Expected Structure: Sounding 42 NA
Depth Resolution = 106.44 m
Depth in meters
Resistivity, Ohm-m

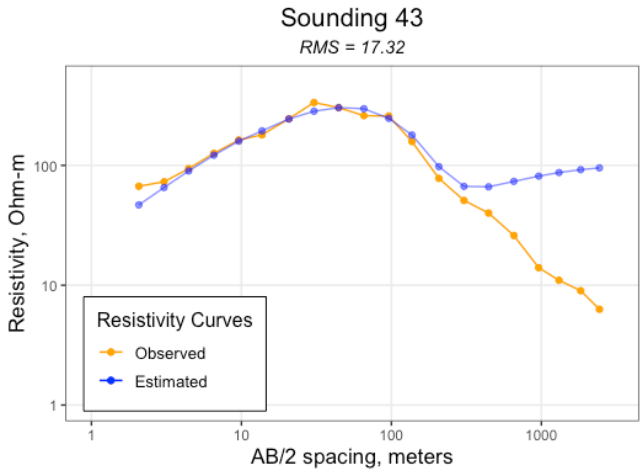
Sounding 43
RMS = 17.32
Resistivity, Ohm-m
AB/2 spacing, meters
Resistivity Curves
Observed
Estimated

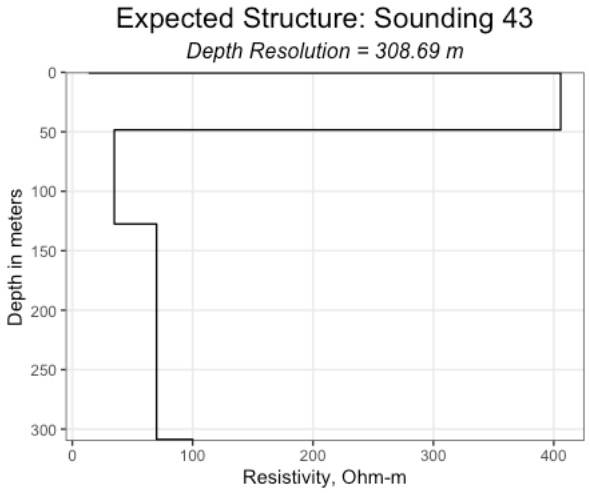
Expected Structure: Sounding 43
Depth Resolution = 308.69 m
Depth in meters
Resistivity, Ohm-m

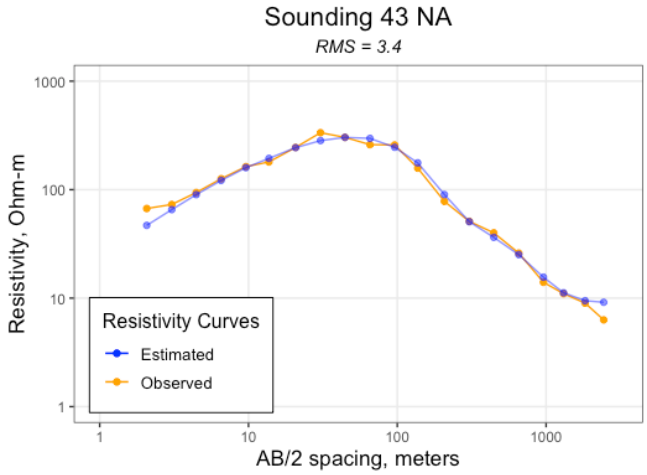
Sounding 43 NA
RMS = 3.4
Resistivity, Ohm-m
AB/2 spacing, meters
Resistivity Curves
Estimated
Observed

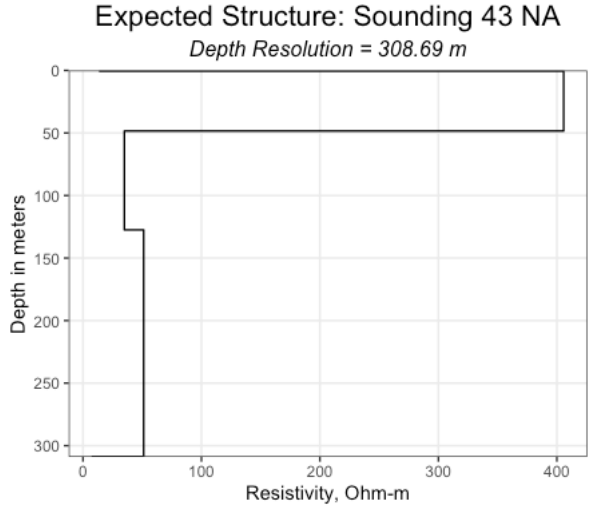
Expected Structure: Sounding 43 NA
Depth Resolution = 308.69 m
Depth in meters
Resistivity, Ohm-m

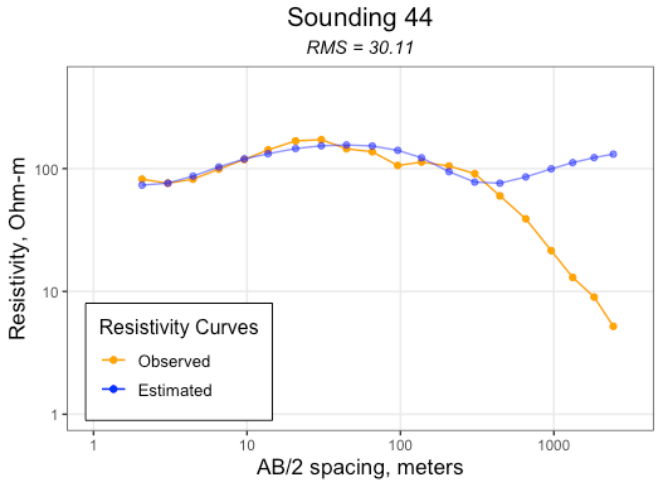
Sounding 44
RMS = 30.11
Resistivity, Ohm-m
AB/2 spacing, meters
Resistivity Curves
Observed
Estimated

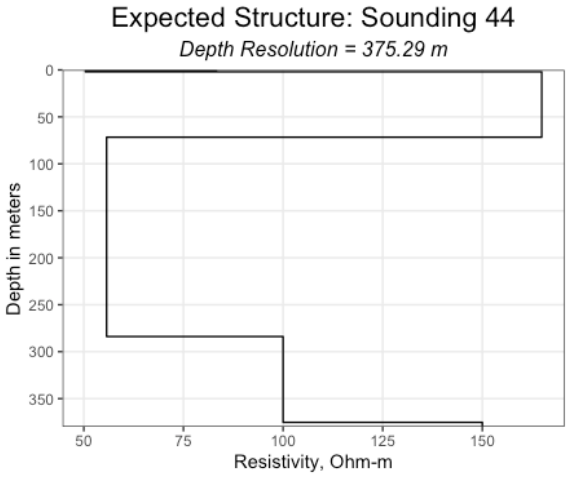
Expected Structure: Sounding 44
Depth Resolution = 375.29 m
Depth in meters
Resistivity, Ohm-m

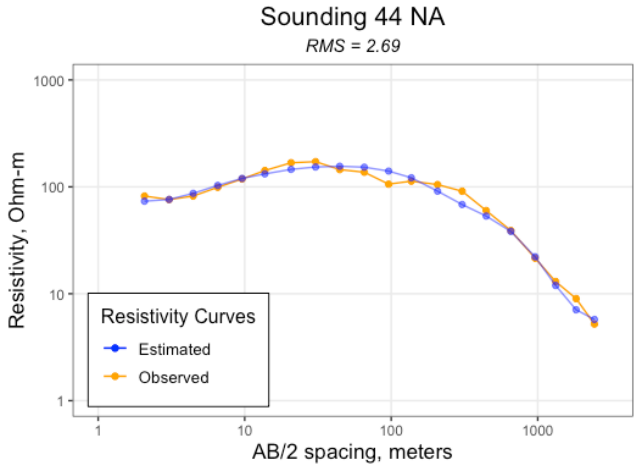
Sounding 44 NA
RMS = 2.69
Resistivity, Ohm-m
AB/2 spacing, meters
Resistivity Curves
Estimated
Observed

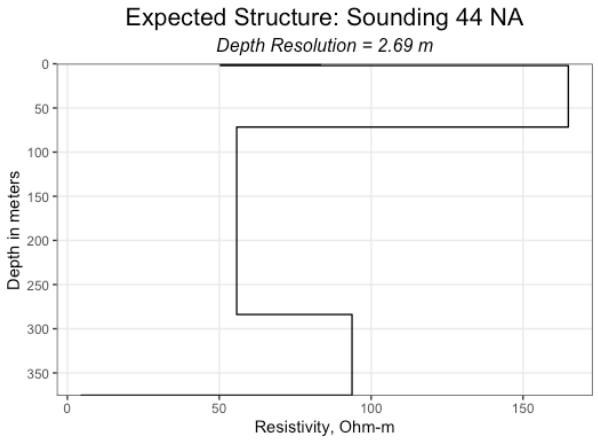
Expected Structure: Sounding 44 NA
Depth Resolution = 2.69 m
Depth in meters
Resistivity, Ohm-m

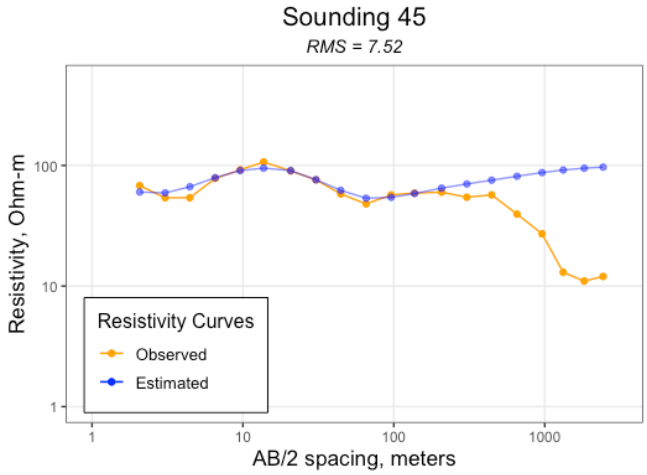
Sounding 45
RMS = 7.52
Resistivity, Ohm-m
AB/2 spacing, meters
Resistivity Curves
Observed
Estimated

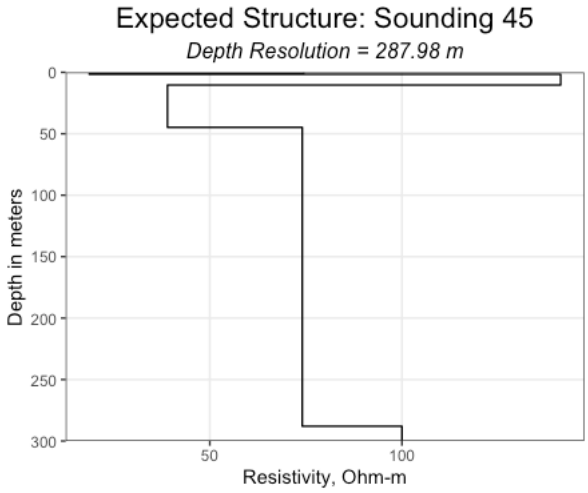
Expected Structure: Sounding 45
Depth Resolution = 287.98 m
Depth in meters
Resistivity, Ohm-m

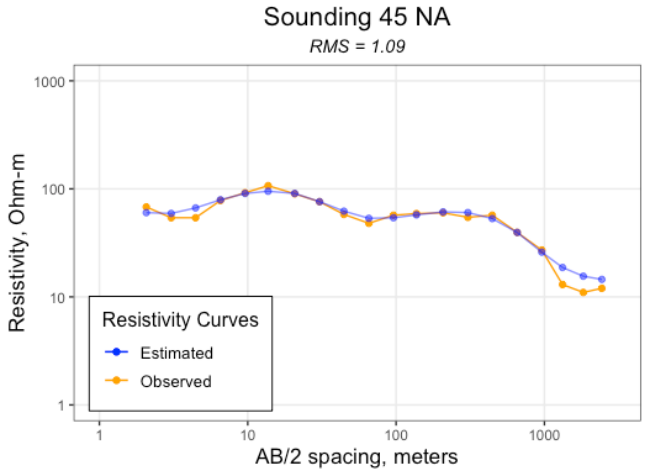
Sounding 45 NA
RMS = 1.09
Resistivity, Ohm-m
AB/2 spacing, meters
Resistivity Curves
Estimated
Observed

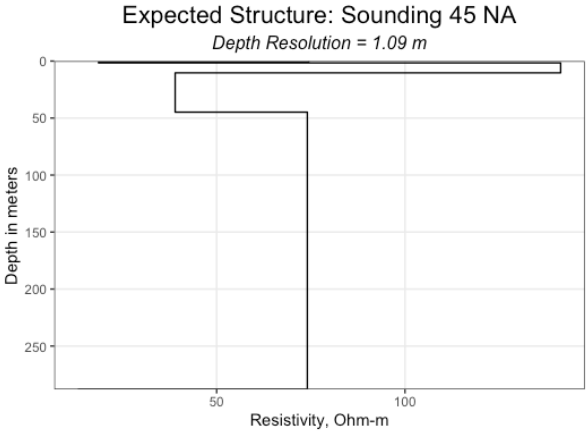
Expected Structure: Sounding 45 NA
Depth Resolution = 1.09 m
Depth in meters
Resistivity, Ohm-m

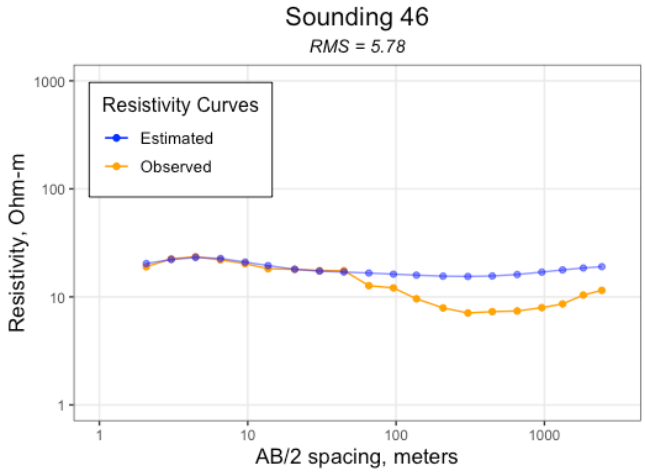
Sounding 46
RMS = 5.78
Resistivity Curves
Estimated
Observed
Resistivity, Ohm-m
AB/2 spacing, meters

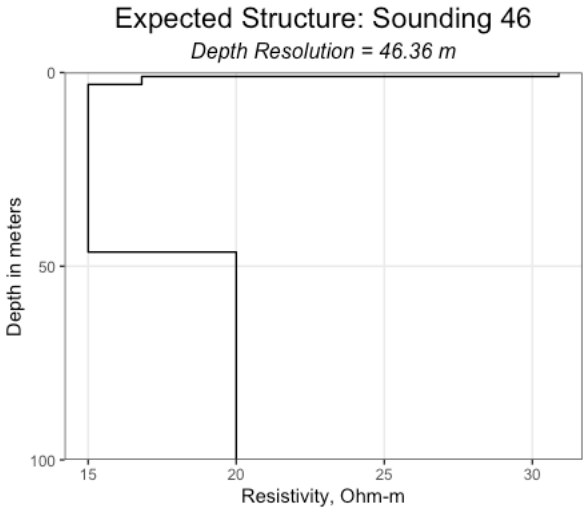
Expected Structure: Sounding 46
Depth Resolution = 46.36 m
Depth in meters
Resistivity, Ohm-m

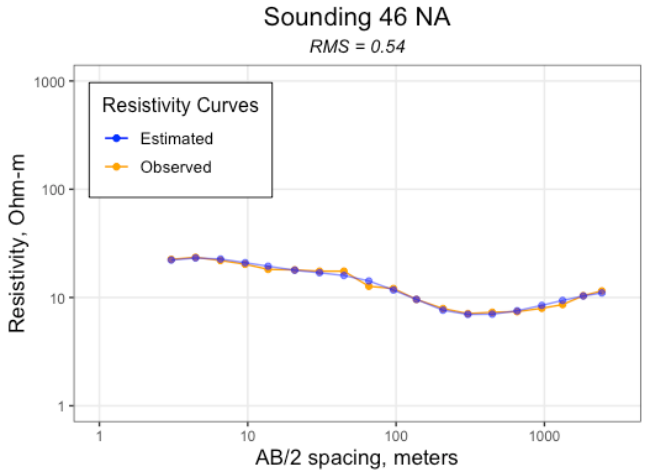
Sounding 46 NA
RMS = 0.54
Resistivity Curves
Estimated
Observed
Resistivity, Ohm-m
AB/2 spacing, meters

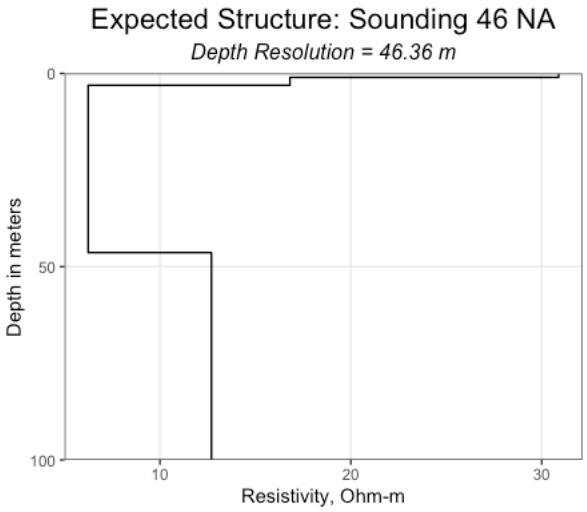
Expected Structure: Sounding 46 NA
Depth Resolution = 46.36 m
Depth in meters
Resistivity, Ohm-m

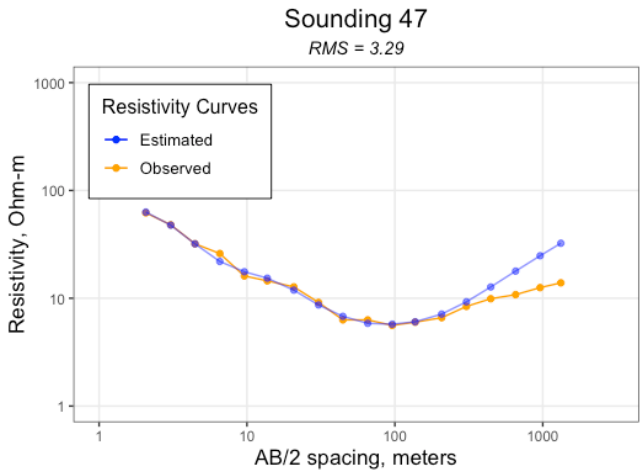
Sounding 47
RMS = 3.29
Resistivity Curves
Estimated
Observed
Resistivity, Ohm-m
AB/2 spacing, meters

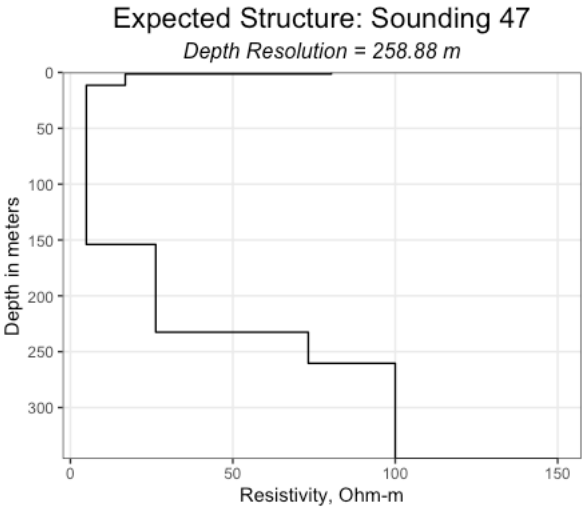
Expected Structure: Sounding 47
Depth Resolution = 258.88 m
Depth in meters
Resistivity, Ohm-m

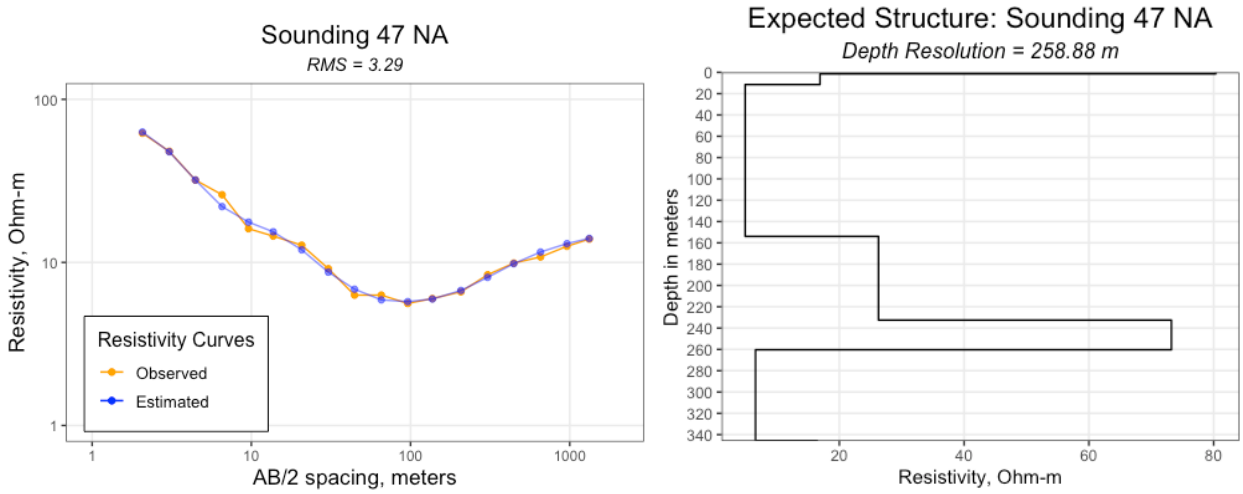
Sounding 47 NA
RMS = 3.29
Resistivity, Ohm-m
AB/2 spacing, meters
Resistivity Curves
Observed
Estimated
Expected Structure: Sounding 47 NA
Depth Resolution = 258.88 m
Depth in meters
Resistivity, Ohm-m

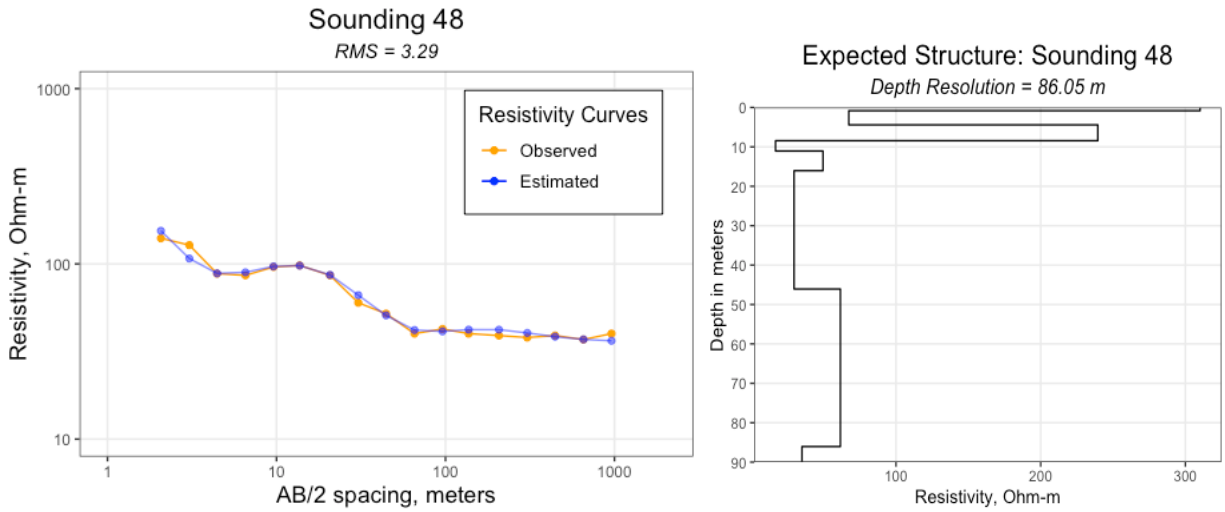
Sounding 48
RMS = 3.29
Resistivity, Ohm-m
AB/2 spacing, meters
Resistivity Curves
Observed
Estimated
Expected Structure: Sounding 48
Depth Resolution = 86.05 m
Depth in meters
Resistivity, Ohm-m

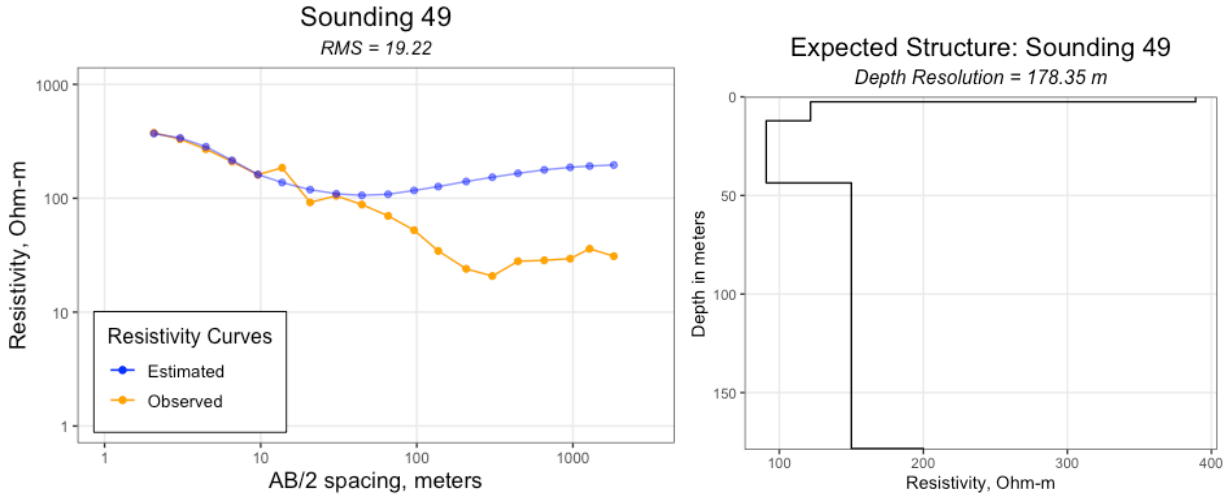
Sounding 49
RMS = 19.22
Resistivity, Ohm-m
AB/2 spacing, meters
Resistivity Curves
Estimated
Observed
Expected Structure: Sounding 49
Depth Resolution = 178.35 m
Depth in meters
Resistivity, Ohm-m

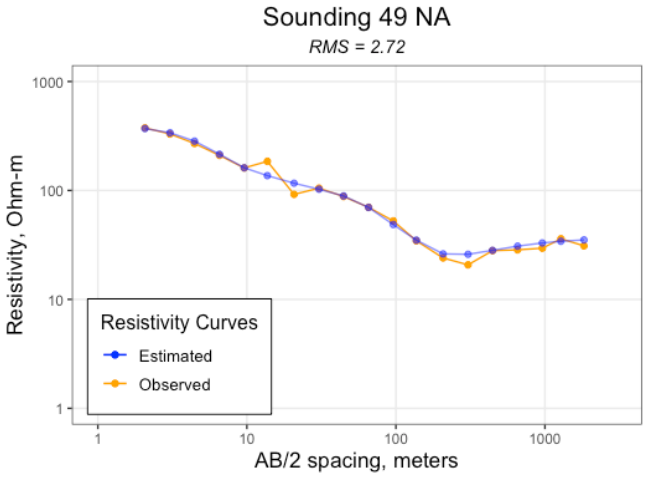
Sounding 49 NA
RMS = 2.72
Resistivity, Ohm-m
AB/2 spacing, meters
Resistivity Curves
Estimated
Observed

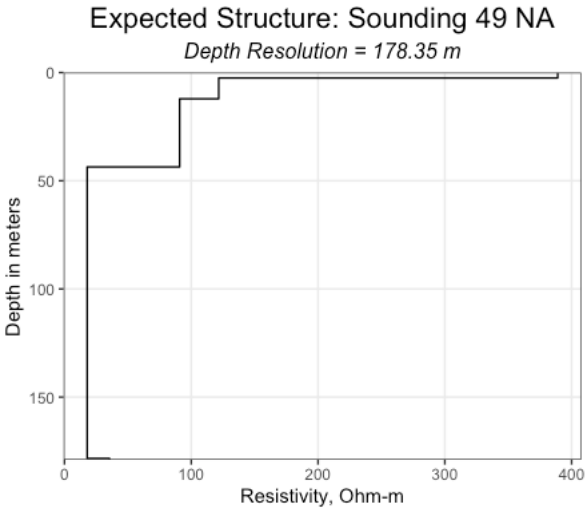
Expected Structure: Sounding 49 NA
Depth Resolution = 178.35 m
Depth in meters
Resistivity, Ohm-m

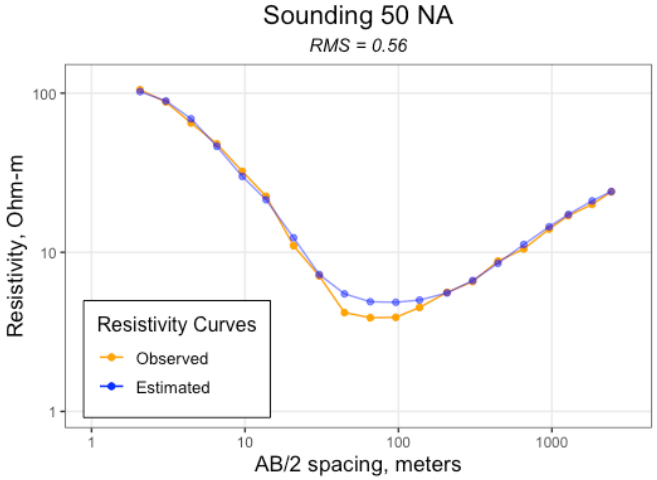
Sounding 50 NA
RMS = 0.56
Resistivity, Ohm-m
AB/2 spacing, meters
Resistivity Curves
Observed
Estimated

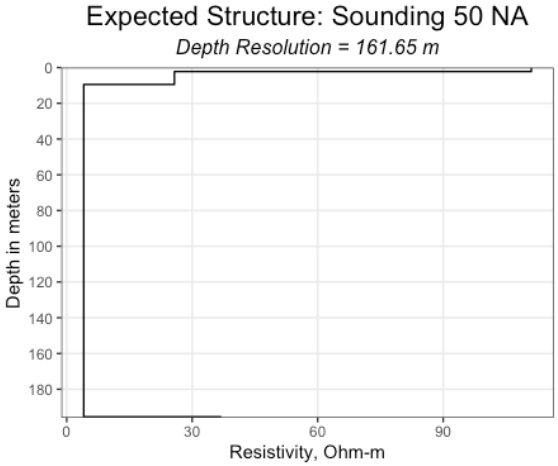
Expected Structure: Sounding 50 NA
Depth Resolution = 161.65 m
Depth in meters
Resistivity, Ohm-m

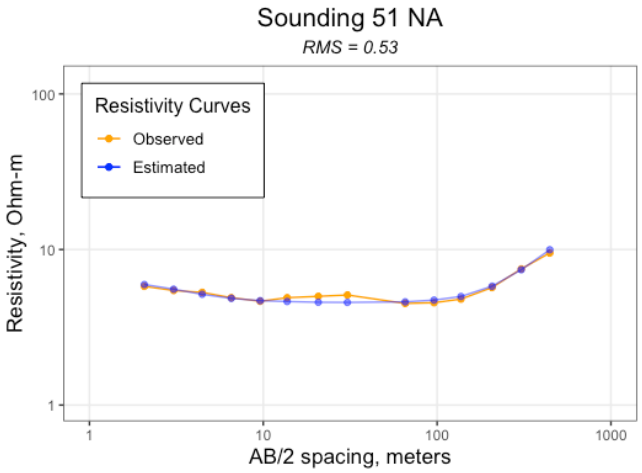
Sounding 51 NA
RMS = 0.53
Resistivity, Ohm-m
AB/2 spacing, meters
Resistivity Curves
Observed
Estimated

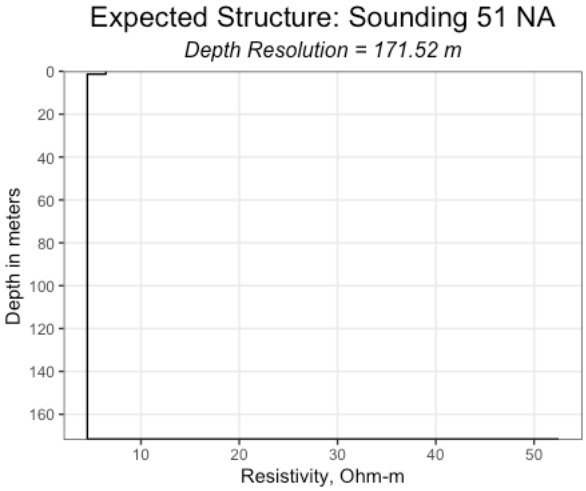
Expected Structure: Sounding 51 NA
Depth Resolution = 171.52 m
Depth in meters
Resistivity, Ohm-m

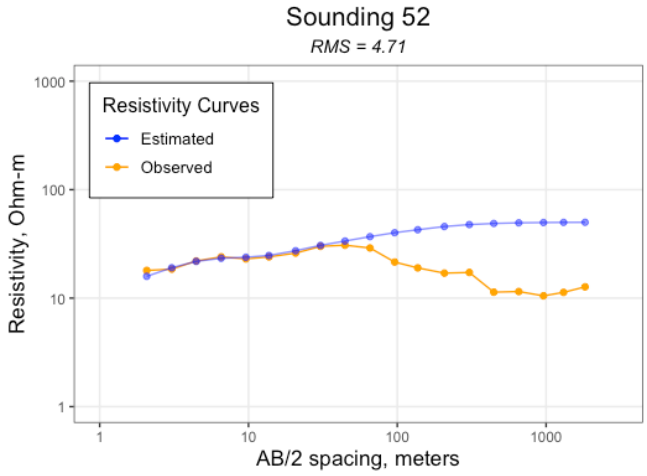
Sounding 52
RMS = 4.71
Resistivity Curves
Estimated
Observed
Resistivity, Ohm-m
AB/2 spacing, meters

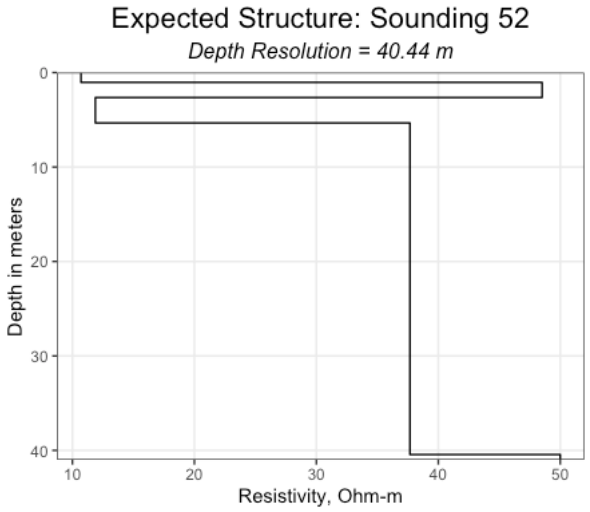
Expected Structure: Sounding 52
Depth Resolution = 40.44 m
Depth in meters
Resistivity, Ohm-m

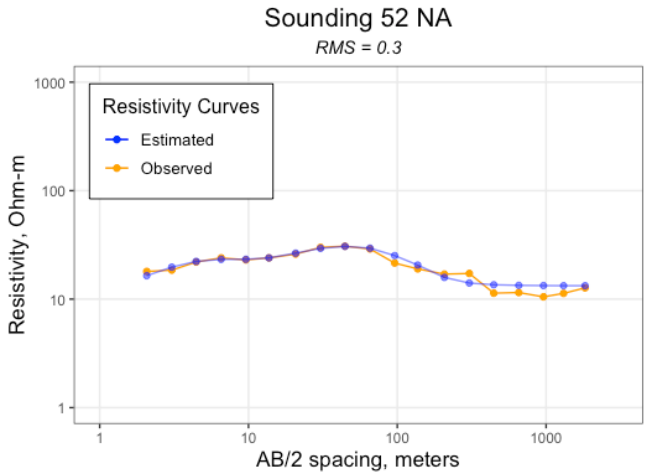
Sounding 52 NA
RMS = 0.3
Resistivity Curves
Estimated
Observed
Resistivity, Ohm-m
AB/2 spacing, meters

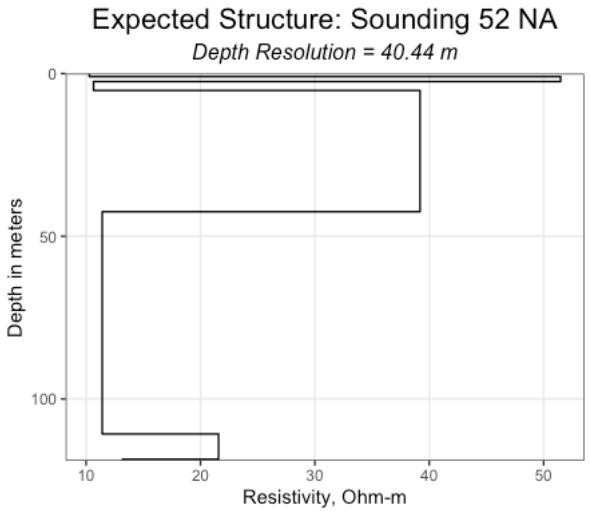
Expected Structure: Sounding 52 NA
Depth Resolution = 40.44 m
Depth in meters
Resistivity, Ohm-m

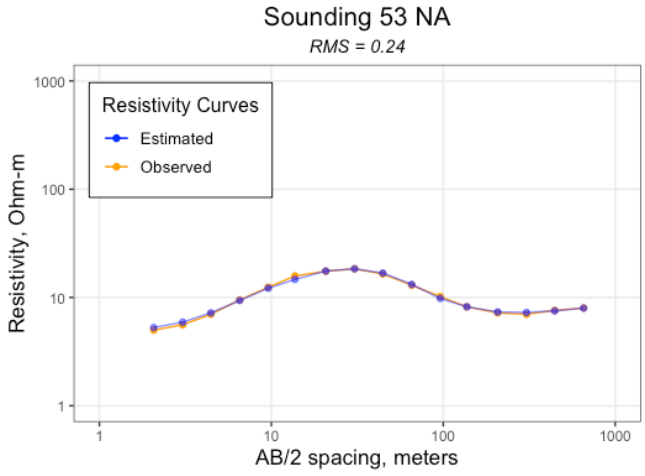
Sounding 53 NA
RMS = 0.24
Resistivity Curves
Estimated
Observed
Resistivity, Ohm-m
AB/2 spacing, meters

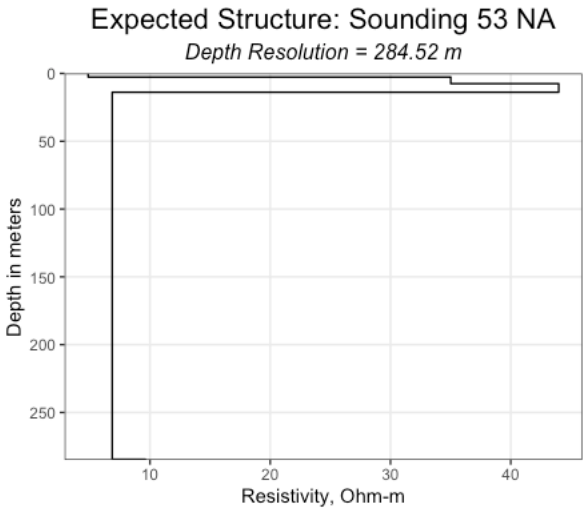
Expected Structure: Sounding 53 NA
Depth Resolution = 284.52 m
Depth in meters
Resistivity, Ohm-m

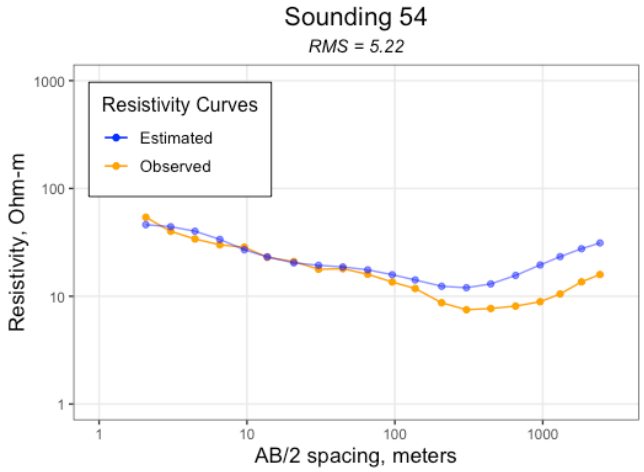
Sounding 54
RMS = 5.22
Resistivity Curves
Estimated
Observed
Resistivity, Ohm-m
AB/2 spacing, meters

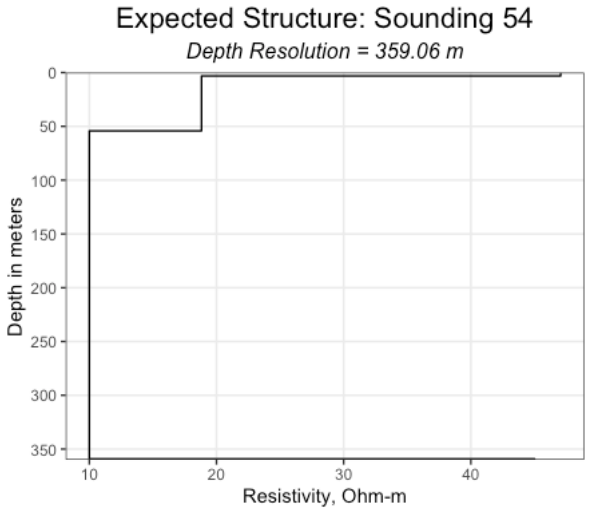
Expected Structure: Sounding 54
Depth Resolution = 359.06 m
Depth in meters
Resistivity, Ohm-m

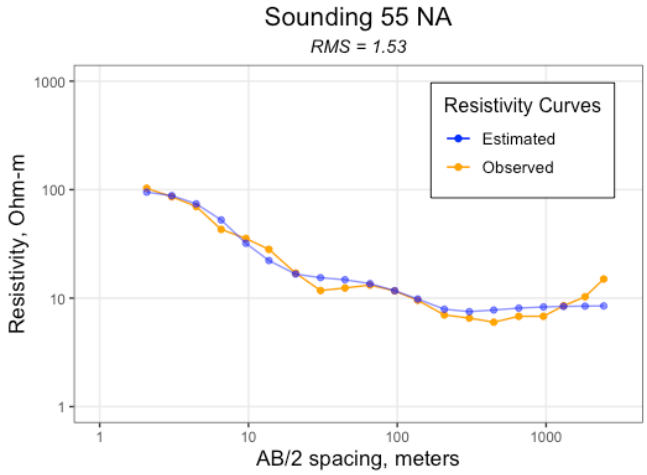
Sounding 55 NA
RMS = 1.53
Resistivity Curves
Estimated
Observed
Resistivity, Ohm-m
AB/2 spacing, meters

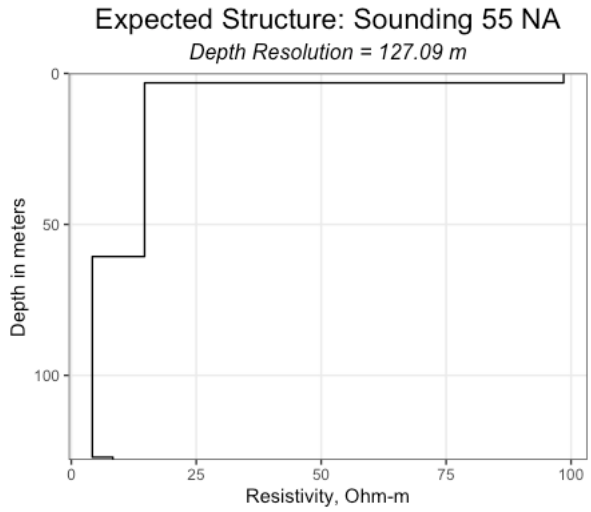
Expected Structure: Sounding 55 NA
Depth Resolution = 127.09 m
Depth in meters
Resistivity, Ohm-m

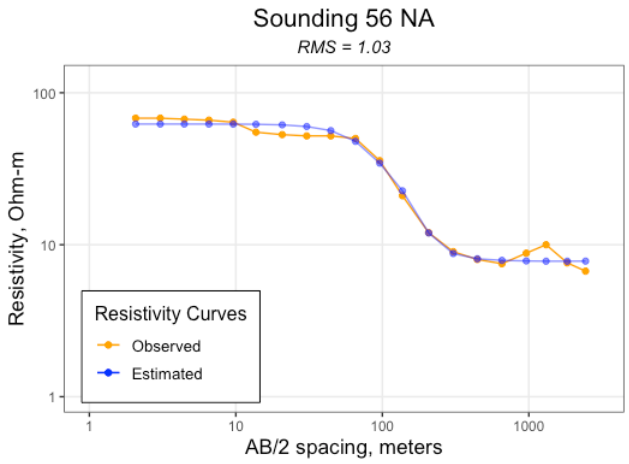
Sounding 56 NA
RMS = 1.03
Resistivity Curves
Observed
Estimated
Resistivity, Ohm-m
AB/2 spacing, meters

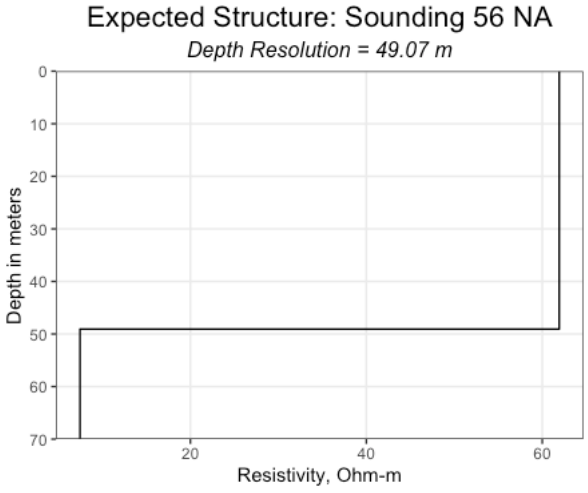
Expected Structure: Sounding 56 NA
Depth Resolution = 49.07 m
Depth in meters
Resistivity, Ohm-m

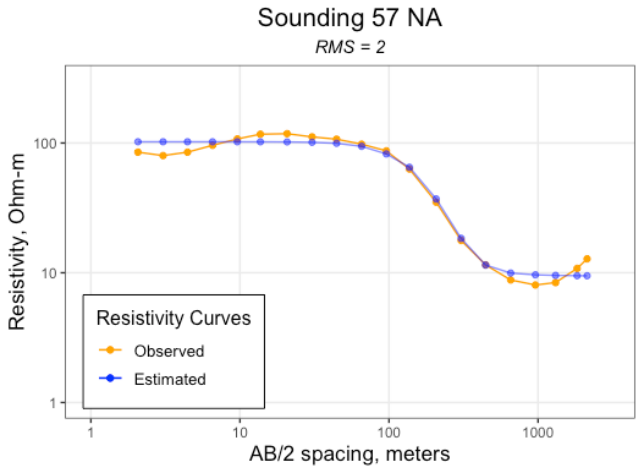
Sounding 57 NA
RMS = 2
Resistivity, Ohm-m
AB/2 spacing, meters
Resistivity Curves
Observed
Estimated

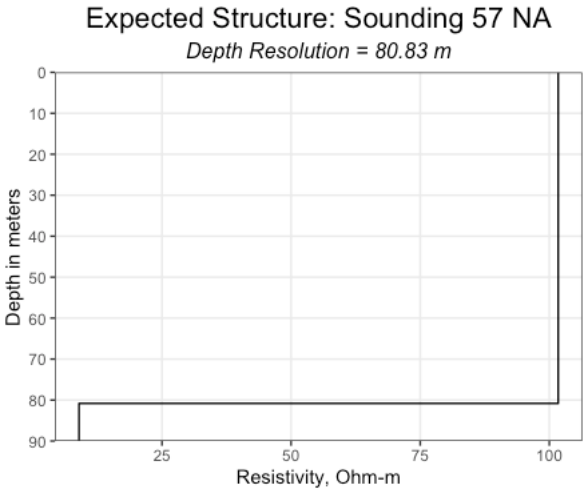
Expected Structure: Sounding 57 NA
Depth Resolution = 80.83 m
Depth in meters
Resistivity, Ohm-m

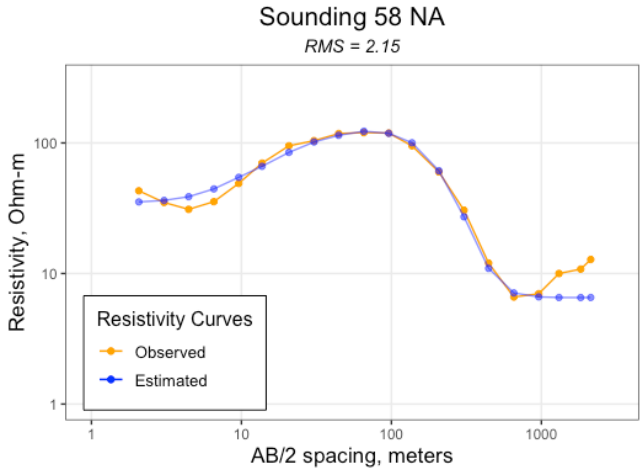
Sounding 58 NA
RMS = 2.15
Resistivity, Ohm-m
AB/2 spacing, meters
Resistivity Curves
Observed
Estimated

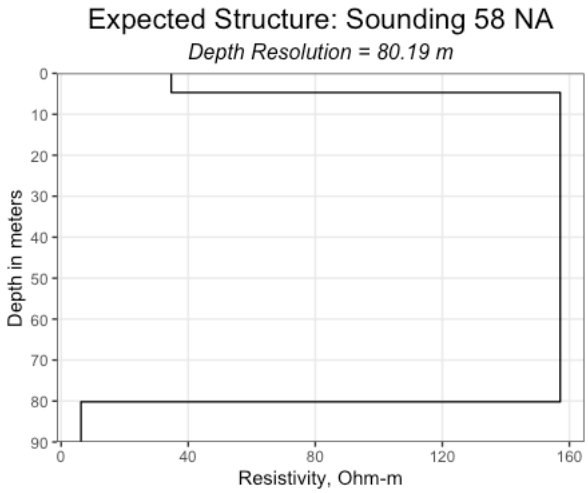
Expected Structure: Sounding 58 NA
Depth Resolution = 80.19 m
Depth in meters
Resistivity, Ohm-m

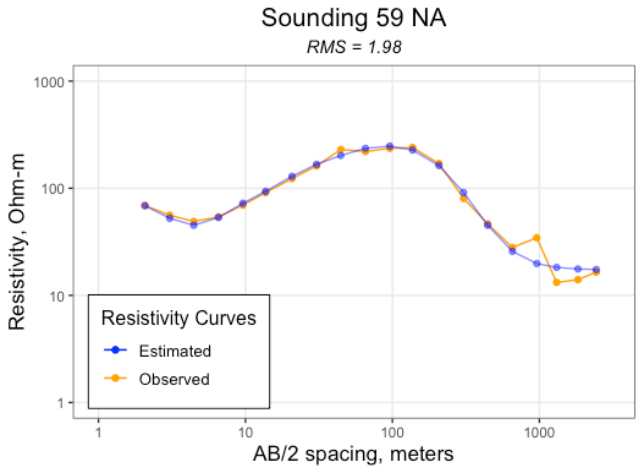
Sounding 59 NA
RMS = 1.98
Resistivity, Ohm-m
AB/2 spacing, meters
Resistivity Curves
Estimated
Observed

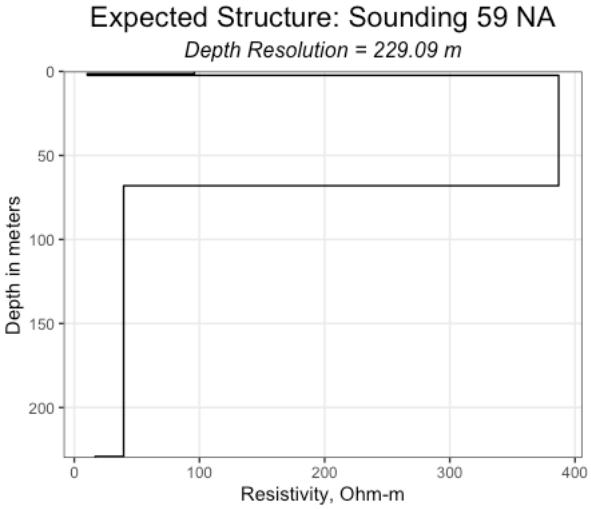
Expected Structure: Sounding 59 NA
Depth Resolution = 229.09 m
Depth in meters
Resistivity, Ohm-m

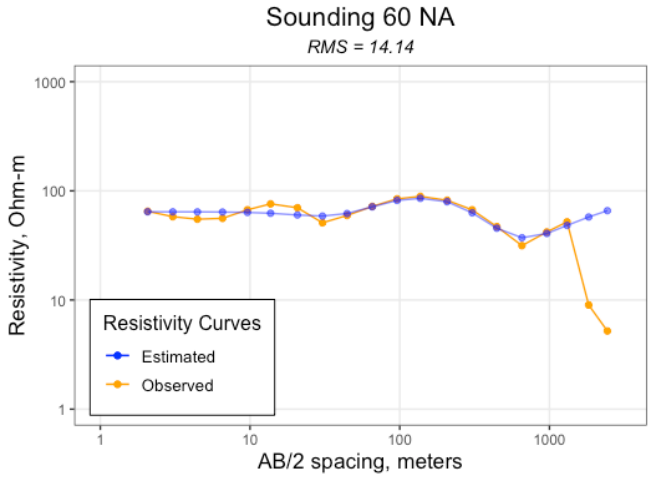
Sounding 60 NA
RMS = 14.14
Resistivity, Ohm-m
AB/2 spacing, meters
Resistivity Curves
Estimated
Observed

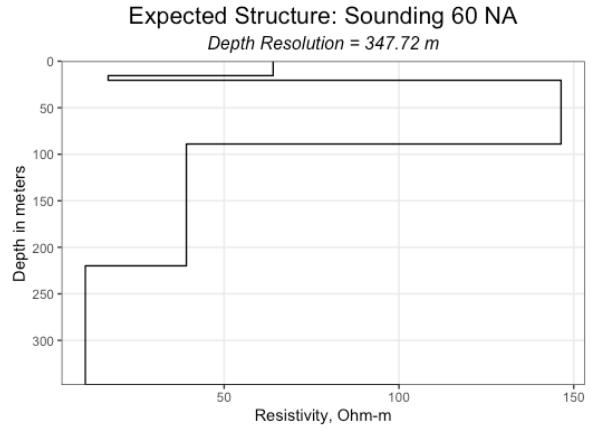
Expected Structure: Sounding 60 NA
Depth Resolution = 347.72 m
Depth in meters
Resistivity, Ohm-m

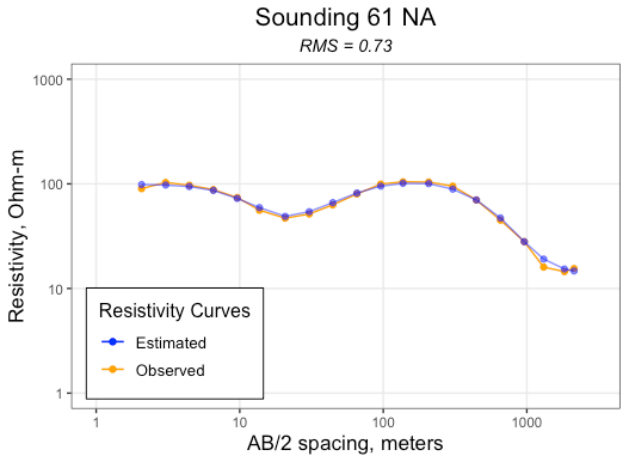
Sounding 61 NA
RMS = 0.73
Resistivity, Ohm-m
AB/2 spacing, meters
Resistivity Curves
Estimated
Observed

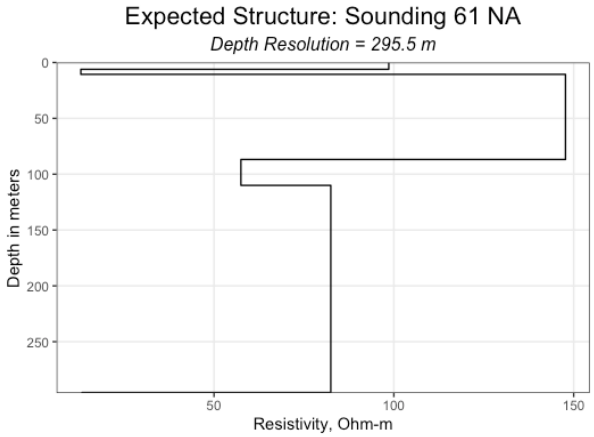
Expected Structure: Sounding 61 NA
Depth Resolution = 295.5 m
Depth in meters
Resistivity, Ohm-m

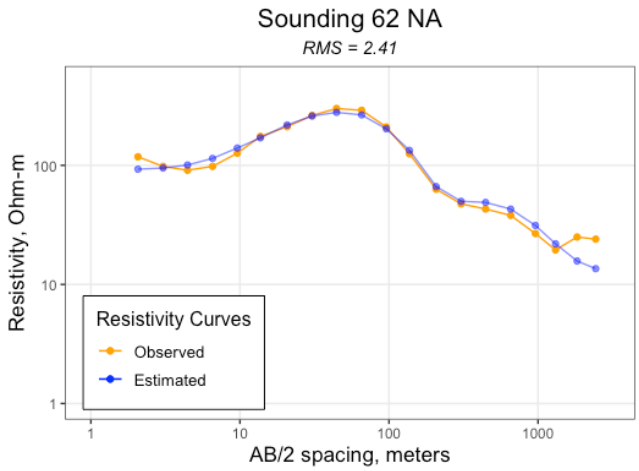
Sounding 62 NA
RMS = 2.41
Resistivity, Ohm-m
AB/2 spacing, meters
Resistivity Curves
Observed
Estimated

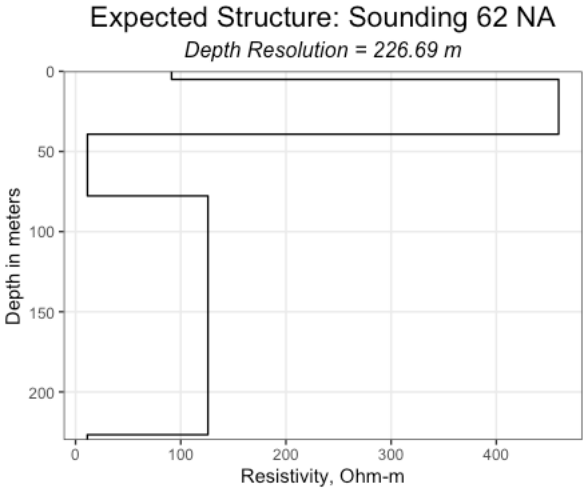
Expected Structure: Sounding 62 NA
Depth Resolution = 226.69 m
Depth in meters
Resistivity, Ohm-m

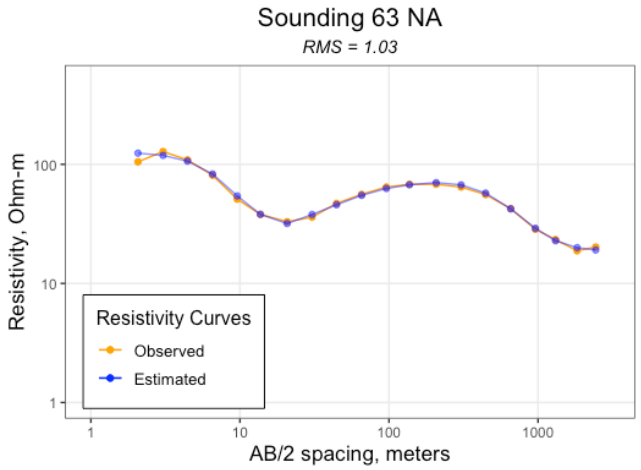
Sounding 63 NA
RMS = 1.03
Resistivity, Ohm-m
AB/2 spacing, meters
Resistivity Curves
Observed
Estimated

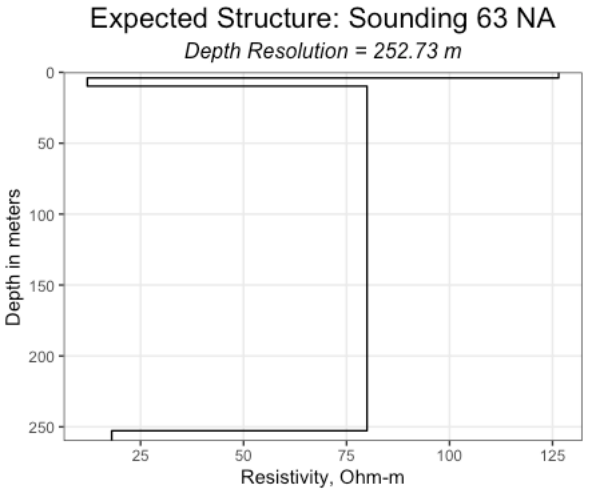
Expected Structure: Sounding 63 NA
Depth Resolution = 252.73 m
Depth in meters
Resistivity, Ohm-m

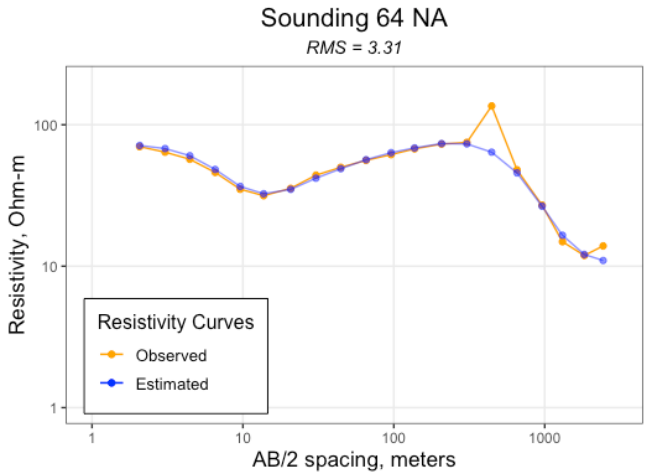
Sounding 64 NA
RMS = 3.31
Resistivity, Ohm-m
AB/2 spacing, meters
Resistivity Curves
Observed
Estimated

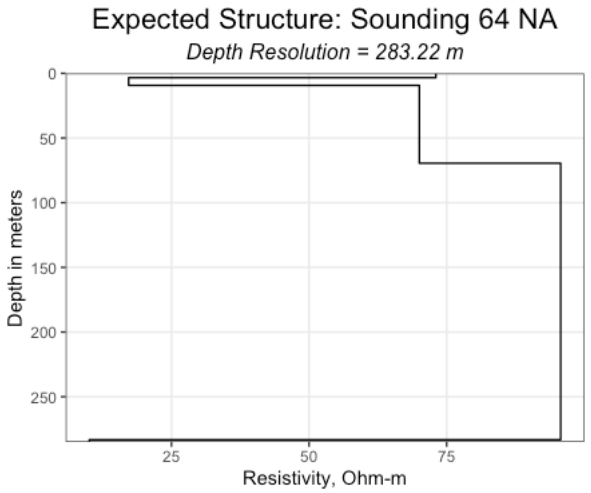
Expected Structure: Sounding 64 NA
Depth Resolution = 283.22 m
Depth in meters
Resistivity, Ohm-m

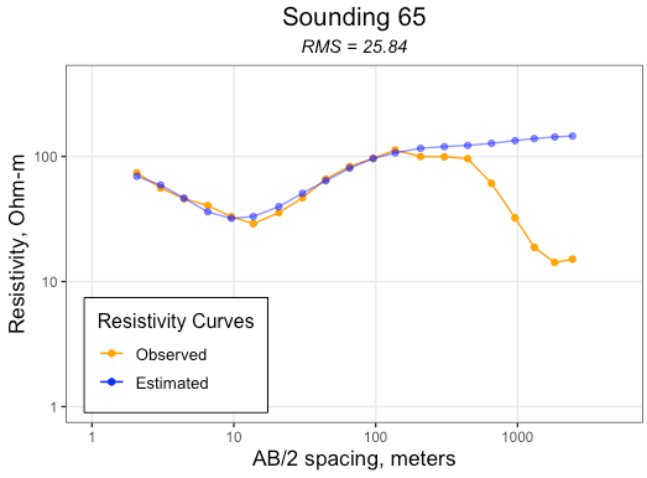
Sounding 65
RMS = 25.84
Resistivity, Ohm-m
AB/2 spacing, meters
Resistivity Curves
Observed
Estimated

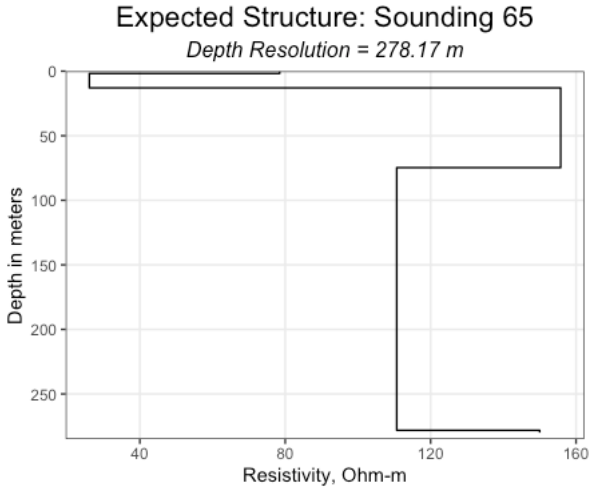
Expected Structure: Sounding 65
Depth Resolution = 278.17 m
Depth in meters
Resistivity, Ohm-m

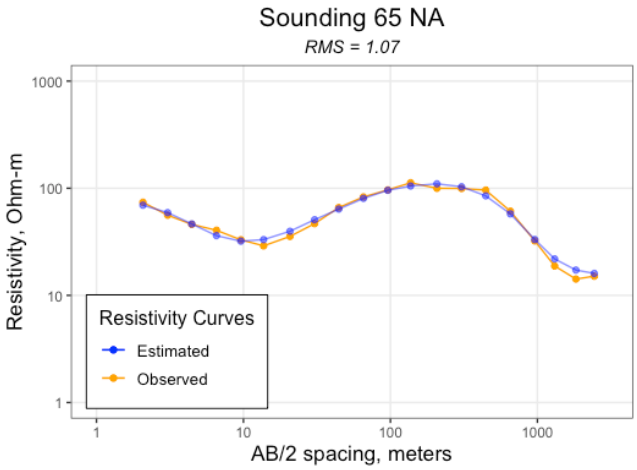
Sounding 65 NA
RMS = 1.07
Resistivity, Ohm-m
1000
100
10
1
Resistivity Curves
Estimated
Observed
1
10
100
1000
AB/2 spacing, meters

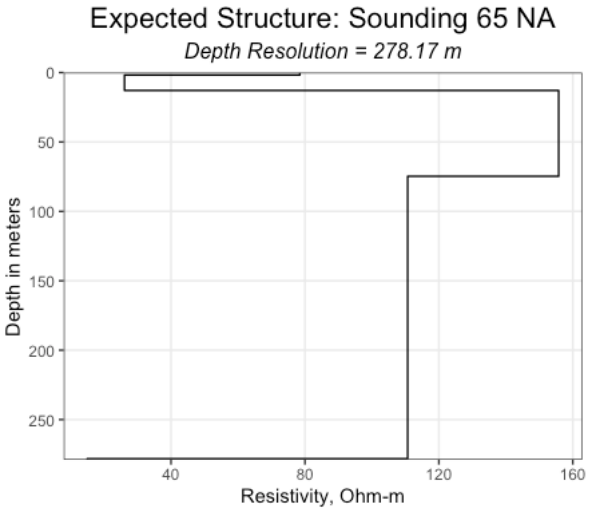
Expected Structure: Sounding 65 NA
Depth Resolution = 278.17 m
Depth in meters
0
50
100
150
200
250
40
80
120
160
Resistivity, Ohm-m

Appendix 3. Notes on Soundings

- Sounding 1. No wells or information available near sounding. Topography: ~ 1,228 m (4,030 ft) ASL, 80 m higher than Sounding 10. Shallow limestone, first 10 m depth. According to Hawley's profiles (comparison between I-I' and J-J'), Sounding 1 has ~ 40 m less sediments than Sounding 10.
- Sounding 2. Close to the mountains, located on I-10, on the border between Texas and New Mexico. High resistivities because of limestone, but they drop after 60 m. Current couldn't travel further in depth than that.
- Sounding 3. Sounding is located on agricultural fields close to the river. Presents low resistivity values. Basement at ~ 265 m, not visible in model. 2 km sounding can only see about ~100 m depth. Water can be found at 2.4 m, 10.6 m, 24.4 m, and 36 m according to wells.
- Sounding 4. Sounding 4 crosses agricultural fields for its first half and falls along the river for the second half. Water is found at 1.8, 2.1, and 3.6 m. It is 2 km and can see around 300 m depth, SD changed due to low values.
- Sounding 5. Model is 2 km long and good to 300 m, probably not seeing below that depth. Bedrock at approximately 320 to 340 m depth, not visible. Water can be found at 1.8, 2.1, 3, 3.6, and 33 m. Sounding along agricultural fields. Well report describes shallow/alluvium basin fill. Sounding hard to model.
- Sounding 6. 2 km length can see about 300 m depth, water can be found at 1.8, 2.7, 3.6, and 7.3 m. Located 1 km east of la mesa (alluvial terrace). Easy to model.
- Sounding 7. Lies within agricultural fields, is 2 km and can see ~300 m. Water can be found at 2.1, 2.7, 3, 3.6, 4.9, 5.8, and 6.7 m. Topsoil with high resistivities, very resistive layer in the first 2 m. After that there is alluvium. Once I modeled the accurate version (increased resistivity at bedrock), it shows exactly where the bedrock should be (~ 300 m).
- Sounding 8. Water can be found at 1.2, 2.4, 6, 13, and 18.3 m. It lays on top of the river. It is 2 km wide and can see ~ 300 m. Thin layers of 1.5 m of clay and sand, mostly clay. Conglomerate is found at 402 m.
- Sounding 9. Lies on agricultural fields and what looks like a river channel. Water can be found at 16.7 and 19.7 m. Last half of the sounding located parallel 100 to 200 meters from one of Hiebing's faults. Conglomerate and limestone found at 300-305 m depth. There is a layer of clay on the well report (see below) that was observed in the first few meters of the sounding:

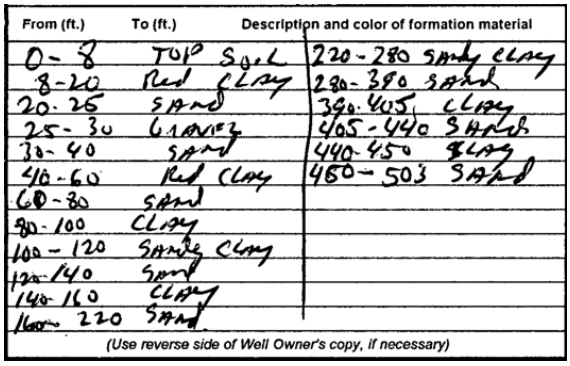

From (ft.)	To (ft.)	Description and color of formation material
0-8	Top Soil	220-280 Sandy clay
8-20	Red clay	280-390 Sand
20-25	Sand	390-405 Clay
25-30	Gravel	405-440 Sand
30-40	Sand	440-450 Clay
40-60	Red clay	480-503 Sand
60-80	Sand	
80-100	Clay	
100-120	Sandy clay	
120-140	Sand	
140-160	Clay	
160-220	Sand	

(Use reverse side of Well Owner's copy, if necessary)

- Sounding 10. Closest to the mountains (same proximity as Sounding 1), it is 2.4 km. After 70 m depth nothing can be seen. Located 300 m parallel to one of Hiebing's faults. Located at 1,252.7

m of elevation. Water table is at about 60 to 77 m here. Sand carrying water found from 93.9 to 94.5 m, limestone found at 94.5 m and from 100 to 182 m.

- Sounding 11. Located 500 m parallel to one of Hiebing's faults. Limestone found at 124 m. Conglomerate found from 103 - 131 m and 185 - 205 m, shale found at 250 m. Parallel to sounding 10, also close to the mountains. The unsaturated sand is likely making it hard to see beneath it.
- Sounding 12. Sounding starts exactly where another of Hiebing's faults is. Maybe this is the reason why it was very hard to model. It runs East to West, so the topography affects it. Water can be found at 28.6, 30, and 36 m.
- Sounding 13. It runs North to South, the same as one of Hiebing's faults whose it intersects. Water can be found at 6.7, 18.2, and 19.5 m. Well report describes layers of sand and clays. Well report indicates that from 5 to 15 m there is a layer of gravel.
- Sounding 14. Could not make it work. Cultural effects.
- Sounding 15. Water can be found at 1.8, 3.35, 8.8 and 16.5 m. It runs North to South. It has a resistive layer; the well report (below) indicates that it is sand and coarse gravel.

From (ft.)	To (ft.)	Description and color of formation material
0	3	Addobe Top Soil
3	7	Red Clay
7	22	Sandy Clay
22	27	Red Clay
27	50	Sand & Course Gravel
50	55	Sandy Clay
55	76	Sand & Gravel
76	83	Red Clay
83	90	Sand
90	95	Red Clay
95	123	Sand
123	127	Brown Clay
127	140	Sand
140	143	Brown Clay
143	178	Sand
178	181	Grey Clay
181	212	Sand
212	215	Grey Clay
215	220	Sand

- Sounding 16. It can't get to bedrock here (current doesn't go deep enough). The resistivities seem low for bedrock. It sits on top of one of Hiebing's faults. Water can be found at 3.35, 4.87, and 6 m. Located on top of agricultural fields, on the west side of the river. Sounding 15 has higher resistivity values, even though is closer to the river.
- Sounding 17. This sounding was very hard to model. Looks like there are some strong lateral variations in the upper 20 m that are hard to model. These things affect the deeper modeling. It runs parallel but extremely close to the Mesilla Valley Fault (< 200 m). Sits on top of agricultural fields. Water can be found at 4.2, 4.9, 5.9, 9.8, and 13.7 m. Soundings 16 and 17 have the same variation at the beginning but I was able to fix it with very thin layers.
- Sounding 18. Has very low resistivity values but it is located on an orchard. A good reason could be some flooding crops like peaches. Water can be found at 2.4, 3, 3.6, and 6.7 m.

- Sounding 19. Sits on top of agricultural fields, along an irrigation canal. Water can be found at 2.4, 3.6, 4.2, 5.8, and 7 m. According to Hawley's profiles (J-J'), it falls into the Mesilla Valley Fault Zone.
- Sounding 20. Located in the town of La Union, right by the mesa. Close to the Mesilla Valley fault here. It is really different from sounding 6. It could be because it is getting saltier water from the Mesilla Valley fault. Water is located at 2.4, 2.7, 6, 7, and 9 m. Sounding is > 2 km in length and can't see anything after 50 m.
- Sounding 21. Located on the side of Aviation Road, right by La Mesa. This sounding goes from the valley floor to the mesa surface, so a lot of topography is probably influencing the flow of electricity. Water can be found at 65, 96 and 97.5 m. There is a high resistive layer on the surface (2 m depth) that doesn't allow further penetration.
- Sounding 22. Water can be found at 97.5 m. This sounding suggests the water table is at ~90 m but there appears to be no further penetration. On top of the Mesa, bedrock is found at ~ 1,000 m depth, so the sounding does not detect it.
  → 10 m Loose sand, maybe some water (USF)
  → 100 m MSF according to Hawley
  → 100 m Aquifer (matches well records)

  After the aquifer, the sounding is not able to see further.
- Sounding 23. Modeling does not respond for the first 8 points. Model starts responding in the last part of the curve. I tried adding more layers, but it did not work. The very shallow layers can have a huge amount of variability; one electrode could be near a bush or clump of grass versus another on bare soil. It is very close to one of the USGS Quaternary faults and runs perpendicular to Sounding 22. It also has high resistivity values and cannot detect the water table.
- Sounding 24. I was able to detect the water table at ~ 8 m, just as a well report nearby describes. Once you reach that low value, you can't detect anything deeper. Boulders and coarse gravel are described in the surface parts as well, so it matches the high resistivity values.
- Sounding 25. This sounding is located parallel to Doniphan Drive, and it is oriented from north to south. There is a lot of near surface clay along this road, which doesn't drain well after it rains. The water table is < 5 m from the surface. The sounding sits on top of one of Hiebing's faults, almost on top of the river. There is a well report nearby (below) that describes the materials around the area. It fits my model, but the layer thicknesses vary a little bit. Cannot resolve more than 100 m depth.

From (ft.)	To (ft.)	Description and color of formation material
0	8	Top Soil
8	18	Red Clay
18	33	Red Sandy Clay
33	41	Sand and gravel
41	58	Red Sandy Clay
58	62	Red Sand/some clay
62	63	Red Sand

- Sounding 26. Conglomerate or limestone at 290 m depth. Water level is 2.4 and 9.1 m. It is next to the river and close to two of Hiebing's faults. It was a sounding difficult to model.

- Sounding 27. The resistivities at the bottom of the model are too low but shows high resistivities (indicating limestone). This might be a case where the high resistivities near the surface are masking the resistivities of the lower layers. This is very close to the mountains, similar to Soundings 1, and 10. No well information around.
- Sounding 28. This looks like a strange sounding. The resistivities seem far too low, maybe because they were close to a pipeline. This makes sense as the sounding sits on top of I-10. The closest well (500 m) marks the water level at 26, 45, and 53 m. A different well (1.5 km) indicates the presence of conglomerate from 328 to 420 m and from 467 to 550 m. Used sounding 11 as reference.
- Sounding 29. This sounding is located next to the river. Bedrock should be around 200 to 300 m here. In the northern part of the sounding, according to Imana there are resistivities of 17 ohm-m, in the middle area they go down to 8 ohm-m and at the southern part they fall to 6 ohm-m. This sounding is only able to detect the first 80 m. Used sounding 25 as reference.
- Sounding 30. This sounding is located in the river valley and probably bedrock is deep. Water levels in the northern part of the sounding are 6, 6.7, and 7 m. It intersects one of Hiebing's faults. Only the upper 50 m are detected for this sounding (until the second resistive layer).

  → 0 to 9 m Brown clay topsoil
  → 9 to 30 m Grey medium sand
  → 30 to 32 m Gray soft clay
  →32 to 50 m Sand and gravel

- Sounding 31. Located in the valley. Looking at Hiebing's J-J' cross section the depth to bedrock could be up to 400 m here. Water depth is 3 to 3.6 m in several wells along the sounding. Located on top of agricultural fields. Sits on the Mesilla Valley fault and has very low resistivity values.
- Sounding 32. This sounding likely crosses faults, and it is not detecting bedrock. Water is located at 3, 4.5, 5.1, and 5.5 m. It was easy to model, detecting different layers (resistive and non-resistive).
- Sounding 33. This is at the very edge of the valley and could be within the Mesilla Valley fault zone. The high resistivity is suspect. At times the river did flow on this side of the valley. Water is located at 2.1, 2.7, 3.6, and 4.26 m. Used sounding 19 as a reference.
- Sounding 34. Well records indicate a layer of sand and gravel near the surface. Water level at 1.2 m. It has a resolution of only 50 m depth. Topsoil layer is where people are producing water from (according to well reports).
- Sounding 35. Cuts across the Three Sisters igneous intrusion. We know there is bedrock at or near the surface here. The really high resistivities of the limestone and andesite don't allow the electricity to penetrate very deeply. It has a resolution of only 80 m depth. No well information around.
- Sounding 36. Parallels I-10. The lower layers of the model seem to be very insensitive to fairly large changes in resistivity. Conglomerate is found in the area from 100 to 128 m, and from 142 to 167.64 m. The same happened with sounding 35. A very resistive layer doesn't let the current to travel along. One of Hiebing's faults intersects the sounding perpendicularly. Cannot detect anything after 80 m. Conglomerate observed at 300 m but cannot confirm.
- Sounding 37. Located parallel to Doniphan Drive. Water level is between 3 and 4 m, and bedrock is deep. South of the sounding there is a well that indicates salty water. Covers part of the river. Used sounding 35 as reference. Cannot detect anything after 20 m.

- Sounding 38. Located close to the river on the west side of it, water level is 1.8 m. One of Hiebing's faults intersects it. Well report indicates clays, and gravels.
- Sounding 39. Located in the valley, possibly perpendicular to a fault. Barely intersects the Mesilla Valley fault. Water table is at 2.4 to 3 m. Cannot detect below 50 m.
- Sounding 40. This sounding runs parallel to Upper Valley Road. Water table is ~ 10 m. Hiebings's cross sections suggest bedrock is 480 m deep here. This model can't detect further than 50 m depth. Mostly saturated material or clays.
- Sounding 41. This sounding is near Westside Road and the Mesilla Valley fault. Basement is probably at 500 m here according to Hiebing's cross section. Cannot resolve to this depth. Gravel/conglomerate found at 67 to 73 m. Water at 2.4, 3.6 and 5.5 m. Sandstone/gravel/conglomerate found at 5.8 to 67 m. Located on top of a canal and next to agricultural fields, top layer appears to be saturated, very low resistivity values.
- Sounding 42. This sounding is located at the edge of the Mesa. Extremely low resistivity values with water depths at 2.1, 3, 6, 9 and 7.6 m.
- Sounding 43. Cuts across the edge of the Mesa and there is some topographic variation. Based on sounding 21 because of location. Water levels at 9, 21 and 30 m. The high resistivity layer on top is thick. Bedrock in the Mesa is over 1,000 m down (see Cervantes' A-A' cross section) so we cannot resolve.
- Sounding 44. This sounding has an east – west orientation. It also nearly touches a Quaternary fault that is just at the west edge of the Santa Teresa airport runway. Cervantes (2018) calls the fault the East La Mesa fault (USGS didn't give it a name). According to the figures of the water table elevation from Cervantes (2018), the water table is sloping very gradually, but the Mesa is about 100 m higher than the valley. The sounding presents resistive layers, and the values for the aquifer are very high (~ 50 ohm-m). Values increase at the end of the curve. There are no wells around the area.
- Sounding 45. This sounding definitely crosses the East La Mesa fault and depth to bedrock is about 1600 m here. Based on sounding 23 and there are no wells around the area. Resistive layer on top.
- Sounding 46. This sounding is located at the edge of the valley. It has low resistivities, and this sounding was hard to model. Water depths are at 3, 3.6 and 55 m.
- Sounding 47. This sounding appears to be along Doniphan Drive near Keystone Park. This area is very wet and salty. The park encloses wetlands that are quite large when it is rainy. Anything they try to build around the area (including the road) fails because there is a lot of clay in the soil, and it is hard to compact. I don't have much depth of penetration because of the salty, wet, clay rich soil. Water depth is 2.4 m. Conglomerate starts at 350 to 400 m and bedrock is at 400 m but cannot be detected.
- Sounding 48. This sounding crosses the Westside Open Reserve, where the Three Sisters Andesite is located. There are no wells around this area, but this sounding was easy to model. It shows different layers that reflect the topographic features of the area.
- Sounding 49. Sounding 49 is located on I-10. There are no wells around the area. It presents some inconsistencies that make it hard to model plus a very resistive layer on top.
- Sounding 50. This sounding runs parallel to Doniphan Drive. Water depth is 2.4 m and used sounding 47 as reference. It was easy to model.
- Sounding 51. This sounding runs perpendicular to sounding 50 and Doniphan Drive. There is a small water reservoir close to it and water depth varies from 2.5 to 3.5 m. It was hard to model due to its low resistivity values.

- Sounding 52. This sounding runs along the Rio Grande. It presents low resistivity values and water depths of 0.9, 1.2, 2.4 and 17.6 m. It was hard to model.
- Sounding 53. This sounding is located in the Santa Teresa paleovalley. It has low resistivity values and the water depth here is 3.6 m. Depth to bedrock should be about 100 m.
- Sounding 54. This sounding orientation is NW-SE and could cross the Mesilla Valley fault. Low resistivities, based on sounding 46 and the water depth goes from 3 to 10 m. Soundings 54, 55, 56, 57 and 58 are located from the base to the top of La Mesa, experiencing changes in topography.
- Sounding 55. Strikes NW-SE. May be on west side of Mesilla Valley fault. A 350 m depth to bedrock seems reasonable. The values suggest the aquifer is saltier here. It does not have more than 200 m of depth resolution and there is a low resistivity layer (partially saturated?) that extends from 3 to 10 m.
- Sounding 56. Crosses the edge of the mesa. It has topographic changes along the sounding (18 m). Strikes NW-SE. Bedrock at 350 m and water table at ~ 100 m. Based on sounding 42.
- Sounding 57. No wells around the area, based on sounding 56. This sounding was easy to model, with water table at ~ 80 m, and is the one experiencing the largest change in topography (109.7 m).
- Sounding 58. Water table around 80 m and no bedrock. Topographic change of 67 m. No wells around the area. This sounding was easy to model, using sounding 57 as reference.
- Sounding 59. Based on sounding 43 because of location respect to the Mesa. It was easy to model but there are no wells around the area. This sounding crosses the East Mesa Fault. It is probably 500 m to bedrock here and it could have some 2-D structure due to the fault.
- Sounding 60. This sounding is based on sounding 44. Water depths go from 90 to 140 m.
- Sounding 61. This sounding may cross a fault. It is near a region of irrigation wells and there might be a cone of depression in the water table due to the significant pumping. Water depths are 100 and 106 m. This sounding was easy to model and is based on sounding 45.
- Sounding 62. Soundings 62 to 65 are all on La Mesa surface. At sounding 62 it is probably 400 m to bedrock and cannot detect the basement here. Water depth is 100 to 107 m. It is based on sounding 45 and was easy to model. Also it appears the water is a bit fresher.
- Sounding 63. This sounding crosses the Mastodon fault. The depth to basement here is around 500 m according to Hawley and Kennedy's K-K' but cannot be detected. The low resistivity layer near the surface could be a thick clay layer (perhaps accumulation of wind-blown silt or lake clays). It seems to show up on soundings 63 through 65. Water depths go from 90 to 107 m, and it was an easy model to fit.
- Sounding 64. Based on sounding 63, probably west of the Mastodon fault. Bedrock is now greater than 500 m depth. No well information available.
- Sounding 65. Based on sounding 64, very easy to model. Bedrock at ~ 500 m so cannot be detected. No well information available.

Appendix 4. Input Format for Software

This is an example (Sounding 1) of the format that data needs to have to be imported into the software. This should be saved as a .CSV document.
Column 1: MN Spacing in meters
Column 2: Measured Resistivity in ohm-m
Column 3: Standard Deviation
Column 4: Calculated Resistivity (Fill up with ones for initial run)
Column 5: Array (In this case is S for Schlumberger)
Column 6: AB/2 Spacing in meters

0.15	155	5	1	S	2.07
0.61	173	5	1	S	3.05
0.61	215	5	1	S	4.45
0.61	280	5	1	S	6.55
0.61	350	5	1	S	9.6
0.61	365	5	1	S	9.6
6.1	420	5	1	S	13.72
6.1	540	5	1	S	20.73
6.1	600	5	1	S	30.48
18.29	550	5	1	S	44.5
18.29	440	5	1	S	65.53
18.29	250	5	1	S	96.01
60.96	137	5	1	S	137.16
60.96	80	5	1	S	207.26
60.96	54	5	1	S	304.8
60.96	46	5	1	S	445.01
60.96	33	5	1	S	655.32
60.96	31.5	5	1	S	960.12
60.96	41	5	1	S	1310.64

Appendix 5. R Plotting Codes

```
################################################################################
# Code to plot both curves and depths from resistivity soundings
# Files need to be saved as .CSV
# Code written by Leslie Bernal
# Last updated October 28, 2022
################################################################################

###### Clean CSV File for Resistivity Curves ###########################################
library(dplyr)
Sounding <- read .csv
("/Users/lesliebernal/Documents/UTEP/Research/Masters_thesis/Exit/Sound
ing_1.csv", header=FALSE)
View (Sounding)

###### CHECK ########
#Delete rows not needed for depth plot
Sounding <- Sounding [-c (1, 2, 3, 4, 5, 6), ]

###### CHECK ######
#Delete columns not needed for depth plot
Sounding = select (Sounding, -c (7:13))

#Change column names
colnames (Sounding) <- c ("MN_sp", "R_Meas", "R_SD", "R_Est", "Array",
"AB")

#Ordering row names
rownames (Sounding) <- 1:nrow(Sounding)

# Convert one variable to numeric
Sounding$MN_sp <- as.numeric(as.character(Sounding$MN_sp))
Sounding$R_Meas <- as.numeric(as.character(Sounding$R_Meas))
Sounding$R_SD <- as.numeric(as.character(Sounding$R_SD))
Sounding$R_Est <- as.numeric(as.character(Sounding$R_Est))
Sounding$AB <- as.numeric(as.character(Sounding$AB))
################################################################################

######### Resistivity Curves Plots ###################################################
library(tidyverse)
library(ggplot2)
library(grid)
library(gtable)

#Sounding <- read .csv
```

```
("/Users/lesliebernal/Documents/UTEP/Research/Masters_thesis/Exit/Sound
ing_25.csv",
# header=FALSE)
#View(Sounding)

ggplot(Sounding, aes(AB))+
geom_point(aes(y = R_Meas, colour = "Observed"))+
geom_line(aes(y = R_Meas, color = "Observed"))+
geom_point(aes(y = R_Est, colour = "Estimated"), alpha = 0.5)+
geom_line(aes(y = R_Est, color="Estimated"), alpha = 0.5)+
labs(colour = "Resistivity Curves",
x = "AB/2 spacing, meters",
y = "Resistivity, Ohm-m",
tag = "RMS = 0.8")+
scale_colour_manual(values = c("Observed"="orange",
"Estimated"="blue"))+

##### CHANGE #####
ggtitle("Sounding 1") +
theme_bw()+
theme(plot.title = element_text(hjust = 0.5),
legend.title = element_text(size=12),
legend.text = element_text(size=10),

#CHANGE RMS LOCATION
plot.tag.position = c(.22, .15),
plot.tag = element_text(hjust = 0.5, size = 11))+
scale_x_continuous(trans = 'log10',
limits = c(1, 2000),
breaks = c(1, 10, 100, 1000))+
scale_y_continuous(trans = 'log10',
limits = c(10, 1000),
breaks = c(10,100, 1000))+
theme(panel.grid.minor.x = element_blank(),
panel.grid.minor.y = element_blank(),
title = element_text(size = 13),
plot.title = element_text(hjust = 0.5),

#CHANGE POSITION OF BOX
legend.position = c(0.3, 0.35),
legend.justification = c("right","top"),
legend.box.just = "right",
legend.margin = margin(6, 6, 6, 6),
legend.box.background = element_rect(color = "black"),

#CHANGE BOX SIZE
```

```
legend.box.margin = margin(t = 2, l = 2, b = 16, r = 2))
################################################################################

########## Clean Data for Depth Plot ############################################
library(dplyr)
Sounding <- read .csv
("/Users/lesliebernal/Documents/UTEP/Research/Masters_thesis/Exit/Sound
ing_1.csv",
header=FALSE)
View(Sounding)

###### CHECK ##########
#Delete rows not needed for depth plot
Sounding <- Sounding[-c(1, 2, 6:25), ]

###### CHECK ##########
#Delete columns not needed for depth plot
SDepth = select(Sounding, -c(1,2,4,5, 7:13))

#Change column names
colnames(SDepth) <- c("Thickness1", "Resistivity")

#Change order of columns
SDepth <- Sdepth[, c("Resistivity", "Thickness1")]

#Add up Thickness values (cumulative sum)
SDepth$Thickness <- cumsum(SDepth$Thickness1)
head(SDepth)

#Delete column
SDepth = subset(SDepth, select = -c(Thickness1) )

#Repeat values for Resistivity
SDepth <- SDepth[rep(seq_len(nrow(SDepth)), each = 2), ]

#Convert all to character
SDepth$Thickness <- as.character(SDepth$Thickness)

#Add a zero at the beginning of depth
SDepth <- add_row(SDepth, Thickness="0", Resistivity="0",
.before = 1)

#Separating columns into individual files
Res <- SDepth[, 1, drop=FALSE]
Thick <- SDepth[, 2, drop=FALSE]
```

```
#Ordering row names
rownames(Res) <- 1:nrow(Res)
rownames(Thick) <- 1:nrow(Thick)

#Deleting first zero row in Resistivity column
Res <- Res[-c(1), ]

#Convert list to dataframe
Res <- as.data.frame(Res)

####### MAKE A CHANGE #######
#Add missing value to Thick and ADD that value to the last one
#For example, if I just want to add 100, I will add 100 + last number, in this case is 175.19, so
#the total would be 275.19. Also check the rows, in this case, there are 6 rows in Thick.
Thick[6, 1] = 78.09

#Bind Res and Thick columns
library(plyr)
SDepth <- rbind.fill(Res, Thick)

###### MAKE A CHANGE ######
#Shift Thickness values up CHANGE VALUE THICKNESS
shift2 <- function(x, n) `length<-`(tail(x, -n), length(x))
SDepth <- transform(SDepth, Thickness = shift2(Thickness, 6))

#Delete NA values from S3depth
SDepth <- na.omit(SDepth)

##### CHANGE ##########
#Save as CSV
Write .csv (SDepth,"~/Documents/UTEP/Research/Masters_thesis/Exit_depths/S1
.csv", row.names = FALSE)
################################################################################

################## Depth Plots ##################################################
library(tidyverse)

##### CHANGE #######
SDepth <- read.csv ("~/Documents/UTEP/Research/Masters_thesis/Exit_depths/S1.csv",
header=TRUE)
SDepth
ggplot(SDepth, aes(x=Res, y=Thickness))+
#geom_point(size = 3, color = "orange")+
geom_path()+
#geom_line(color = "orange")+
labs(colour = "Expected Structure",
```

```
x = "Resistivity, Ohm-m",
y = "Depth in meters")+
scale_y_reverse(limits = c(80, 0),
breaks = seq(0, 80, 10),
expand = c(0, 0))+
ggtitle("Expected Structure") +
theme_bw()+
theme(plot.title = element_text(hjust = 0.5, size = 20))
##############################################################################
```

Vita

Leslie Alejandra Bernal Lopez received a Bachelor of Science in Physics Engineering from Universidad Autónoma de Ciudad Juárez in 2011. She received the Academic Excellence award from the Confederación Patronal de la República Mexicana (COPARMEX) in 2011. After completing her bachelor's degree, she started working as a lecturer at Universidad Autónoma de Ciudad Juárez and Universidad Interamericana del Norte in Ciudad Juárez, Mexico.

She then completed a Master of Science in Geophysics from Universidad de Guadalajara in 2015. Leslie worked as an engineer for Regal Rexnord, and Lear Corporation until she was accepted to the Geological Sciences program at the University of Texas at El Paso, to pursue her Doctoral Degree. She then acquired a scholarship from ConTEX and CONACYT to continue with her studies, as well as two scholarships from the Geological Society of America. She obtained the GIST certificate from UTEP in 2021, and as of 2022, she was admitted into a summer internship program at the Environmental Policy Innovation Center. She is planning on defending her Ph.D. dissertation in 2023.

Contact Information: bernal.leslie1@gmail.com